COMPARATIVE STUDY OF SEEPAGE THROUGH AN EARTH DAM

A

THESIS

Submitted for partial fulfilment of the requirement of the award of degree

of

DOCTOR OF PHILOSOPHY

In

CIVIL ENGINEERING

Submitted By

SUSHANT KUMAR

Roll No: 2K17/PHD/CE/04

Under the Guidance of

Prof. A. K. Sahu
Professor, DTU Delhi
Supervisor

Prof. Munendra Kumar
Professor, DTU Delhi
Joint-Supervisor

DEPARTMENT OF CIVIL ENGINEERING
DELHI TECHNOLOGICAL UNIVERSITY
SHAHBAD DAULATPUR, BAWANA ROAD, DELHI- 110042,
INDIA

DEC 2022

CANDIDATE'S DECLARATION

I hereby declare that the work which is being presented in the dissertation entitled **"COMPARATIVE STUDY OF SEEPAGE THROUGH AN EARTH DAM"** for the partial fulfilment of the requirement for the award of the degree of Doctor of Philosophy in Civil Engineering, Delhi Technological University, Delhi is an authentic record of my own work carried out under the supervision of **Prof. Anil Kumar Sahu**, Professor, Department of Civil Engineering, DTU, Delhi and **Prof. Munendra Kumar**, Professor, Department of Civil Engineering, DTU, Delhi. I have not submitted the matter embodied in this thesis for the award of any other degree or diploma.

(SUSHANT KUMAR)

Registration No. 2K17/Ph.D./CE/04

Department of Civil Engineering

DTU, Delhi

This is to certify that the above statements made by the candidate is true to the best of our knowledge.

(Prof. A. K. Sahu)
Professor
Supervisor
Department of Civil Engineering
DTU, Delhi

(Prof. Munendra Kumar)
Professor
Joint-Supervisor
Department of Civil Engineering
DTU, Delhi

दिल्ली प्रौद्योगिकी विश्वविद्यालय, दिल्ली, भारत, 110042
Delhi Technological University, Delhi, India, 110042

CERTIFICATE

This is to certify that the Thesis dissertation entitled '**COMPARATIVE STUDY OF SEEPAGE THROUGH AN EARTH DAM**' submitted by **Sushant Kumar** in the partial fulfilment of the requirements for the award degree of **Doctor of Philosophy** in the **Department of Civil Engineering, Delhi Technological University, Delhi** is a bonafide work carried out by him out under our supervision and guidance. The matter presented in this report has not been presented elsewhere for any other degree or diploma.

To the best of our knowledge, project work embodies the work of the candidate; the project work is of standard both in the report of contents and language being presented to the external examiners.

(Prof. A.K. Sahu)
Professor
Supervisor
Dept. of Civil Engineering
DTU, Delhi

(Prof. Munendra Kumar)
Professor
Joint-Supervisor
Dept. of Civil Engineering
DTU, Delhi

.

(Prof. V.K. Minocha)
Professor and Head of the Department
Dept. of Civil Engineering
DTU, Delhi

ACKNOWLEDGEMENTS

It is my proud privilege to express my heartfelt indebtedness to my research supervisors Prof. Anil Kumar Sahu, Professor, Department of Civil Engineering, DTU Delhi and Prof. Munendra Kumar, Professor, Department of Civil Engineering, DTU Delhi, for their excellent guidance, valuable suggestions and encouragement in the course of the study and preparation of this thesis. Indeed, I am greatly honoured to be their research student and greatly influenced by their penchant for excellence. Their unwavering support and help in the face of all kinds of odds and uncertainties are humbly acknowledged. I avail this opportunity to express my deep sense of gratitude and sincere thanks to my research supervisors for their inspiration, expert guidance, moral support and continuous encouragement, which were vital factors in the successful completion of the present work.

Sincere thanks are due to Hon'ble Shri Vinai Kumar Saxena, Chancellor, Delhi Technological University, Delhi and Prof. Jai Prakash Saini, Hon'ble Vice-Chancellor, Delhi Technological University, Delhi.

I would like to thank Prof. V.K. Minocha, Professor and Head, Department of Civil Engineering, Delhi Technological University, Delhi.

I would also like to thank Prof. K.C. Tiwari, DRC (Departmental Research Committee) Chairman, to be head of my research committee and SRC (Student Research Committee) member, Prof. A.K. Gupta, Professor in the Department of Civil Engineering, to spend valuable time reviewing and critically examining the work.

I am thankful to Prof. A.K. Shrivastava, Professor and Geotechnical Lab incharge, Department of Civil Engineering, DTU Delhi, and Dr. Ritu Raj, Assistant Professor, CAD Lab incharge, Department of Civil Engineering, for their co-operation. I would also like to thank all the professors of the Geotechnical Department and the Hydraulics Department.

I am thankful to Prof. D.R. Kaushal, Professor, Department of Civil Engineering, IIT Delhi, and Late Prof. Anupam Mittal, Professor, NIT Kurukshetra, for giving valuable suggestions as external experts of my SRC.

I am thankful to the Delhi Technological University for providing an opportunity for research through its research fund and sponsoring me to pursue my research. I would also like to thank the DTU Library for providing me with the literature of research content and online journals.

I am thankful to Prof. Rinku Sharma, Professor and Head of the Department of Applied Physics, to support lab tests.

I am thankful to all the lab staff and other staff for helping me through my research work.

The co-operation and encouragement of my colleagues at Delhi Technological University, Delhi, are gratefully acknowledged. I express my special thanks to my friends for their help and valuable support.

I express my warm regards and profound gratitude to my esteemed father, Mr. Raghuvir Singh, and my family members for their moral support, encouragement and blessings.

I want to express my highest appreciation for the strong moral and emotional support and deep understanding shown by my wife, Mrs. Deepika Singh, during my endeavour to complete this research work.

I humbly thank all those who, in any manner, directly or indirectly, put a helping hand to complete this research work.

(SUSHANT KUMAR)

ABSTRACT

Earth dams are commonly used in many nations because of their ease of building and maintenance. This study aims to determine the seepage discharge in an earth dam by building twenty-four models in a hydraulic flume and altering various input parameters. A dam with a central impermeable core and a homogeneous earth dam has been built in a hydraulic flume in the lab. The earth dam also has a filter to prevent the phreatic line from cutting the downstream slope of the dam, which might cause damage. Some of the characteristics studied in this study include upstream slope, downstream slope, longitudinal slope, upstream slope, downstream slope, changing the top and bottom widths of the dam while keeping the upstream and downstream slopes the same, changing the height and length of the earth dam, central core width, filter length, and filter height; and their impact on seepage and the phreatic line. A fluorescent dye was used to identify a phreatic line in the experimental model, then compared to the phreatic line developed from Seep/w in Geostudio software. The numerical analysis results were found to be consistent with the experimental findings. Dupuit's equation, Casagrande's, Schaffernak's, and Pavlovsky's solutions were used to validate homogenous physical experimental and numerical models. The stability of the upstream and downstream slopes of the earth dam was also examined using Slope/w in Geostudio software, which was confirmed to be safe under full reservoir conditions.

The temperature measurement was used to investigate the seepage fluctuation in the earth dam. In a hydraulic flume, seventeen models of earth dams were built by altering geometrical and flow input parameters. Temperature measurement along the phreatic line was done using a digital thermometer and compared to the phreatic line produced by Seep/w. The phreatic line derived from the experimental models was identified using a fluorescent dye. Temp/w was used to model temperature variation inside an earth dam due to the convective flow of water. Temperature variation in an earth dam by the experimental model was compared with the contours of temperature obtained using temp/w and were in good agreement. It was discovered that as the longitudinal slope, downstream slope, and dam height are increased, the water flow accelerates, which leads to a rise in temperature variation of the earth dam due to increased convection and vice versa for the upstream slope. With the introduction of an impervious central core in the earth dam, the dam’s temperature reduced significantly due to the reduced flow

rate of water. The inclusion of a downstream filter stopped the phreatic line from cutting the earth dam's downstream face. The temperature was increased drastically due to an increased water flow rate due to the filter's increased length and thickness. Temperature measurement proved to be a cost-effective method of detecting seepage in an earth dam.

The water flux in an earth dam was simulated in a hydraulic flume by altering geometrical and flow input parameters to determine heat and water flux. A Homogeneous, as well as earth dam with a clay core, was built-in a hydraulic flume. Heat flux was calculated in the experimental model using temperature observations. Seep/w was used to calculate water flux, and temp/w was used to calculate heat flux in a finite element model of the earth dam. When comparing homogeneous models to central impermeable core models, a considerable decrease in heat and water flux was observed. When the length and longitudinal slope of the downstream filter was increased, the heat and water flow increased, and vice versa when the upstream slope and clay core thickness were increased. Heat flux measurements proved to be a cost-effective option for measuring water flux and seepage in an earth dam.

Keywords: Convection; Earth dam; Heat flux; Horizontal filter; Pore water-pressure; Porous medium; Seepage; Seepage discharge; Temperature; Water flow; Water flux; Water pressure head.

CONTENTS

LIST OF TABLES

LIST OF FIGURES

NOTATIONS

a_v	Coefficient of compression
c	Cohesion
C_c	Coefficient of curvature
C_u	Uniformity coefficient
C_v	Coefficient of consolidation
d	spacing between planes
D_{10}	Particle size such that 10% of soil is finer than this size
D_{30}	Particle size such that 30% of soil is finer than this size
D_{60}	Particle size such that 60% of soil is finer than this size
G	Specific gravity of soil
G_1	Specific gravity of water
i	Hydraulic gradient
H	Pressure function
k	Hydraulic conductivity
m_v	Coefficient of volume change
V	Darcy's velocity
ϕ	Friction angle
μ	Soil water yield factor
Θ	angle of incidence

ABBREVIATION

IS	Indian standards
M1	Model 1
M2	Model 2
M3	Model 3
M4	Model 4
M5	Model 5
M6	Model 6
M7	Model 7
M8	Model 8
M9	Model 9
M10	Model 10
M11	Model 11
M12	Model 12
M13	Model 13
M14	Model 14
M15	Model 15
M16	Model 16
M17	Model 17
M18	Model 18
M19	Model 19
M20	Model 20
M21	Model 21
M22	MODEL 22
M23	MODEL 23

M24	MODEL 24
XRD	X-ray diffraction

UNITS

cm	Centimetre
^{o}C	Degree Celsius
m^3/sec	Discharge
g/cm^3	Dry density
kN/m^3	Dry density
g	Grams
$kJ/sec/m^2$	Heat flux
hrs	hours.
kg	Kilogram
mm	Millimetres
kg/cm^2	Pressure
strokes/min	Rolling rate
Sec	Seconds
J/kg	Specific heat
W/(m. K)	Thermal conductivity
$J/(m^3.K)$	Volumetric heat capacity
$m^3/sec/m^2$	Water flux

CHAPTER 1

INTRODUCTION

Earth dams are basic constructions that resist slippage and flipping by standing on their own weight. In areas where concrete manufacture and shipping costs are high, they can be quite cost-effective. These are the most prevalent dams in use across the world. The earthen dams were built to redirect large amounts of water and safeguard the community during a previous time. Because of their ease of construction and maintenance, they are widely employed in many nations. The widespread usage of earthen dams is due to the fact that they may be built with materials found on-site or nearby. They're made up of natural materials. Up until 1930, the construction of an earth dam was mostly dependent on trial and error. However, because of advances in geotechnical engineering, these dams are now designed and built in a more engineered manner. They may be built on almost any sort of foundation (except strongly liquescent muddy soil). These dams have a trapezoidal or roughly trapezoidal cross-section and are made of earth and rock.

Seepage is a concern with earth dams, and inadequate seepage may lead to stability issues when high water pressure and saturation develop in the embankment and foundation soils, reducing the dam's shear strength and potentially leading to failure. The shape of the embankment, the soil composition, the construction method used, the slope protective cover, the upstream head, and other factors all influence seepage. Rodent holes, rooted tree roots, fissures or splits in rocks at the dam site, incorrect filter or drain design, earthquakes, and trapped groundwater can all cause seepage. Filters, drains, clay blankets, flatter side slopes, and the use of geosynthetics in the dam are some of the countermeasures that may be utilised to prevent massive seepage loss (Omofunmi et al., 2017).

An alternative method to detect seepage losses in an earth dam is temperature measurements, as temperature measurements can detect leakage and seepage velocity without costly equipment. Temperature measurements are easy to do with sensors available such as distributed temperature sensing, vibrating wire temperature sensor, Greisinger PT 100, etc. Several researchers, including some of the following, have done extensive work on seepage and temperature modelling in porous media. Similarly,

water flux can be predicted using the heat flux value evaluated using temperature measurements.

Various researchers have developed analytical solutions for evaluating the seepage discharge in an earth dam through its body. Still, these analytical solutions don't hold for the practical case and have significantly less accuracy. There arises a need to model earth dams, such as a finite element model using software or due by experimental model. Many software commercially available includes Seep/w (Geostudio), Plaxis, Ansys, Abaqus, etc.

1.1 SEEPAGE

The flow of water in soils is referred to as seepage in soil engineering. The permeability of the soil and the pressure gradient, which is simply the sum of forces acting on water through gravity and other variables, are both important elements in seepage. However, if seepage becomes too concentrated or uncontrolled, it will cause water loss, weaken shear strength, and eventually cause the dam to fail. One of the kinds of seepage failure is piping. Piping occurs when reservoir water moving through the pores of the soil (seepage) exerts a tractive force on the soil particles it passes through, causing them to be removed at an unprotected seepage exit point. A boil, a cone-shaped mound of dirt, or a torrent of muddy water escaping from the slope is frequently the first outward manifestations of piping.

The difference in water levels between the upstream and downstream faces of the earth dam causes seepage through the earth dam. Darcy experimented with the flow of water through a porous medium. As seen in equation (i), the flow velocity is directly proportional to the head loss and inversely proportional to the length of the flow route (Das, 2014):

$$V = Ki \qquad \text{(i)}$$

Where V is Darcy's velocity, K is the porous medium's hydraulic conductivity, and i is the hydraulic gradient. Darcy's law only applies to laminar flow and cannot be used in a turbulent flow. Darcy's experiment had additional drawbacks, such as maintaining isothermal equilibrium and keeping the fluid's material characteristics unchanged (Narasimhan, 2016).

Several strategies have been offered for determining seepage through the earth dam body resting on an impermeable base. The following are some of the most prominent and commonly recognised theories:

A) Dupuit's Solution

"The hydraulic gradient i , according to Dupuit, is equal to the slope of the free surface and is constant with depth, i=dz/dx. Darcy's law states that the quantity of seepage through a unit length at right angles to the cross-section is q=KiA. Which can alternatively be expressed as an equation (ii)." (Das, 2014)

$$q = \frac{k\,(H_1^2 - H_2^2)}{2d} \qquad \text{(ii)}$$

Figure 1.1 shows the phreatic line as ab of the earth dam section. But in equation (ii), no entrance and exit conditions were considered.

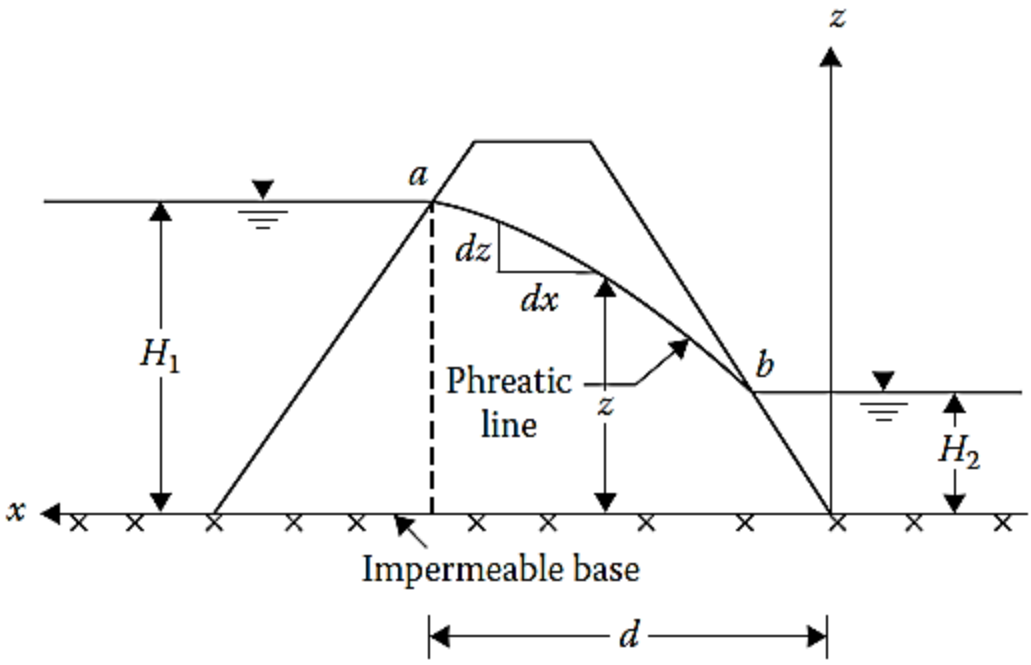

Figure 1.1: Dupuit's solution for flow through an earth dam (Das, 2014)

B) Schaffernak's solution

"Schaffernak postulated that the phreatic surface will meet the downstream slope at a distance from the impervious base", as ab in figure 1.2. The triangle bcd, as illustrated in figure 1.2, may be used to calculate the seepage per unit length of the dam as given in equation (iii). (Das, 2014)

$$Q = K\, l \sin\beta \tan\beta \qquad \text{(iii)}$$

$$l = \frac{d}{\cos\beta} - \sqrt{\frac{d^2}{\cos^2\beta} - \frac{H^2}{\sin^2\beta}} \qquad \text{(iv)}$$

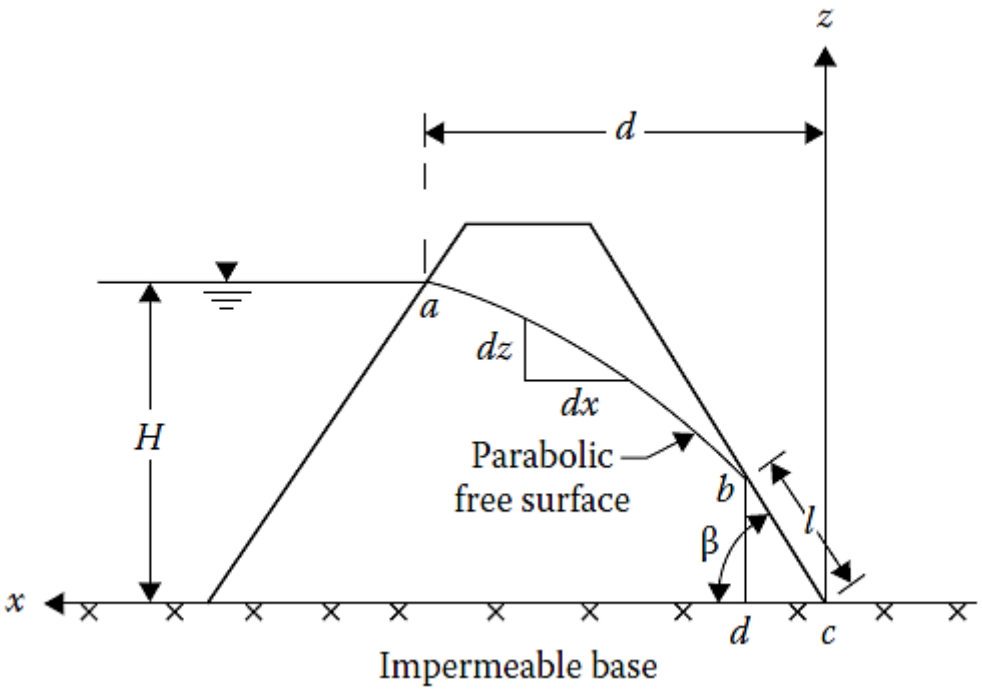

Figure 1.2: Schaffernak's solution for flow through an earth dam (Das, 2014)

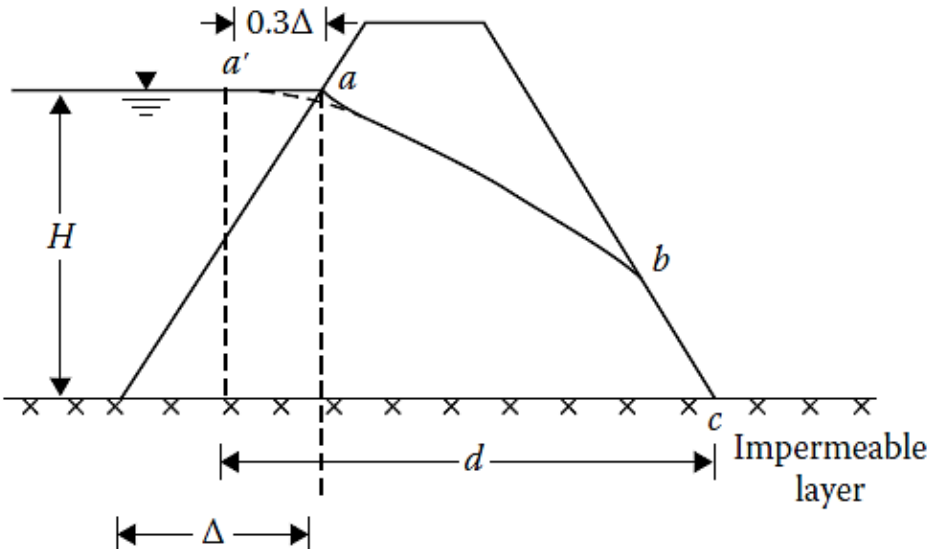

Figure 1.3: Modified distance d as per USBR recommendation. (Das, 2014)

Casagrande showed experimentally that the phreatic line ab, which is parabolic in nature as starts from a' as shown in the figure. So with the modification aa'= 0.3 Δ, The horizontal distance between a' and c equals the value of d.

C) L. Casagrande's equation

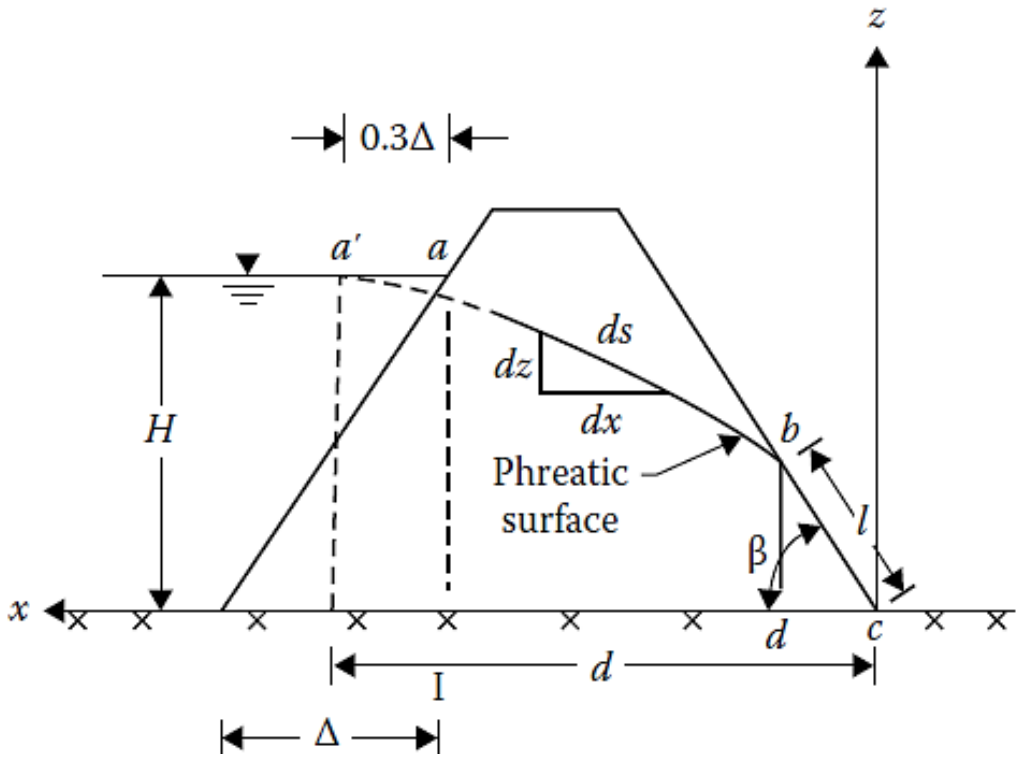

Figure 1.4: Casagrande's solution for flow through an earth dam (Das, 2014)

Casagrande proposed equation (v) for rate of seepage as shown in figure 1.4 as (Das, 2014):

$$q = K\, l \sin^2\beta \qquad (v)$$

Where l, can be computed as:

$$l = s - \sqrt{s^2 - \frac{H^2}{\sin^2\beta}} \qquad (vi)$$

Equation vii may be used to compute s as the length of a straight line a'c with a 4-5% inaccuracy.

$$s = \sqrt{d^2 + H^2} \qquad (vii)$$

D) Pavlovsky's solutions

Pavlovsky divided the earth dam into three zones to calculate the rate of seepage, as shown in figure 1.5 (Das, 2014).

Zone 1

Pavlovksy assumed that the curved seepage line could be replaced using horizontal lines and proposed a formula for zone 1 as equation (viii).

$$q = \frac{K\,(H-h_1)}{\cot\beta_1}\,\ln\frac{H_d}{H_d-h_1} \quad \text{(viii)}$$

Zone 2

The Dupuit's equation may be used to calculate the rate of seepage in zone 2.

$$q = \frac{K\,(h_1^2-h_2^2)}{2L} \quad \text{(ix)}$$

Where, $L = B + (H_d\text{-}h_2)\cot\beta_2$ (x)

Zone 3

In zone 3, streamlines are assumed to be horizontal. The rate of seepage of zone 3 is given as equation (xi)

$$q = \frac{Kh_2}{cot\beta_2} \quad \text{(xi)}$$

where, h_1 and h_2 which can be solved using equations (xii) and (xiii)

$$h_2 = \frac{\beta}{\cot\beta_2} + H_d - \sqrt{\left(\frac{\beta}{Cot\beta_2} + H_d\right)^2 - h_1^2} \quad \text{(xii)}$$

$$\frac{H-h_1}{\cot\beta_1}\ln\frac{H_d}{H_{d-h_1}} = \frac{h_2}{\cot\beta_2} \quad \text{(xiii)}$$

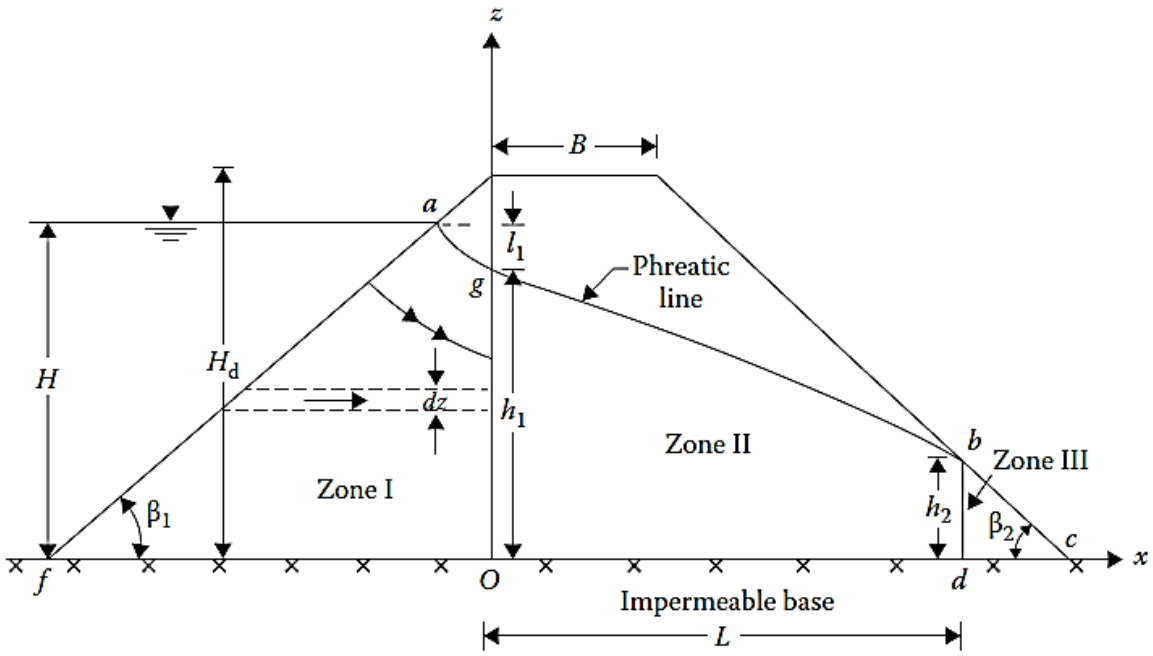

Figure 1.5: Pavlovsky's solution for flow through an earth dam (Das, 2014)

1.2 PHREATIC LINE

The phreatic line is the top flow line of a saturated soil mass below which seepage occurs. Above the phreatic line, hydrostatic pressure acts, but atmospheric pressure acts below the phreatic line. A saturated soil mass is separated from an unsaturated soil mass by this line. It's a flow line, not an equipotential line. The phreatic line for an earthen dam approximates the form of a parabola.

• It establishes a boundary between dry (or moist) and submerged soil. For the purposes of determining soil shear strength, the soil above the seepage line will be considered dry, and the soil below the seepage line will be considered submerged.

• It depicts the top streamline and so aids in the construction of the flow net.

• The seepage line determination assists us in ensuring that it does not cut the dam's downstream face, which is critical for keeping the dam from weakening or sloughing.

1.3 EQUATION FOR DETERMINATION OF SEEPAGE

In general, the seepage issue, which includes seepage in the core of an earthen dam, may be reduced to a solution of the differential Poisson's equation (xiv)

$$\frac{\partial}{\partial x}\left(K_x \frac{\partial H}{\partial x}\right) + \frac{\partial}{\partial y}\left(K_y \frac{\partial H}{\partial y}\right) + \frac{\partial}{\partial z}\left(K_z \frac{\partial H}{\partial z}\right) - \mu \frac{\partial H}{\partial t} = 0 \qquad \text{(xiv)}$$

where H = f (x, y, z, t) is the desired pressure function in the computational domain, measured over time t; K_x, K_y, and K_z are seepage factors (hydraulic conductivity) for the coordinate axes X, Y, and Z, respectively; and is the soil water yield factor The final term is zero in the most popular and widely accepted steady-state seepage situations, and the equation becomes the Laplace equation. There are several ways to solve this equation (Aniskin et al., 2016).

1.4 CAUSES OF SEEPAGE

The followings are the few key factors that cause seepage in earth dams:-

(i) Inadequate soil compaction in the environment.
(ii) Inadequate foundation and abutment preparation
(iii) Rodent burrows
(iv) Tree roots and timber that are firmly rooted
(v) Cracks, joints, and open spaces in dam rocks
(vi) Sand or coarse gravel in the foundation or abutment
(vii) Coarse drain clogging
(viii) Inadequate design of porous filters or drains
(ix) Frost action.
(x) Environmental soil shrinkage cracking
(xi) Environmental soil settlement; uprooted trees
(xii) Earthquakes
(xiii) Inadequate drainage in the structure
(xiv) Trapped Groundwater.
(xv) An excessive amount of lifting pressure.

1.5 EFFECTS OF SEEPAGE

Seepage causing problems that can lead to dam failure are classified as follows:

(i) Piping.
(ii) Internal erosion
(iii) Soluble rock solutioning
(iv) Internal pressures and saturation that are too high
(v) Uplift, heave, or blowout in excess.

1.6 DAM MONITORING INSTRUMENTS

Dam monitoring's goal is to provide data for analysing dam performance while it's in use. Deformation, movement, stress, strain, seepage flow rate, turbidity, groundwater level, pore water pressure, reservoir and tailwater levels, precipitation, temperature, and seismic observations are all common control variables. The variations of flow rate, pore water pressure, relative humidity, precipitation, and water quality, among other factors impacting the mechanical stability and operation of the system, may be monitored.

Pore pressure, settlement, the formation of strains, and the response to an earthquake are all important factors to consider. Following are the instruments:

(i) Pore pressure measurements: basic stand pipe, Casagrade's porous tube, closed hydraulic type such as Pneumatic type, and electrical type piezometers. A closed hydraulic system is usually preferable. Instruments like Piezometers should be deployed at numerous layers throughout the foundation and dam.

(ii) Settling gauges or vertical movement devices are used to track the dam's consolidation and foundation settlement. Cross arms, fluid level devices, and surface monuments are among the tools utilised.

(iii) Internal strain or relative motions are measured using horizontal movement instruments. Extensometers and inclinometers are two examples.

(iv) Seismic activity measurements- strong-motion accelograph, structural response recorder, Seismoscope, pressure cells.

1.7 OBJECTIVE OF THE STUDY

To investigate seepage through an earthen dam, which might pose a serious threat to the integrity and operation of the dam in the future. Various parameters of the earthen dam will be changed to examine how they affect seepage, as indicated below:

1. Properties of the soil used for shell and core of the earthen dam.
2. Effect of viscosity of fluid flowing.
3. Effect of dam’s geometry on seepage.
4. The filter of the dam.
5. The location of the phreatic line.

1.8 THE APPROACH, METHODOLOGY AND THE OUTCOME OF THE STUDY

Seepage through a homogeneous earth dam constructed on an impervious foundation is studied using the experimental and Seep/w 2D finite element numerical models, as well as earth dam models with a central impervious core. The research work presents experimental modelling developed for obtaining seepage flow via homogeneous earth dams with a horizontal downstream filter and earth dams with a central impermeable clay core. Different scenarios for fluid parameters i.e. viscosity of the fluid, upstream head, and geometrical parameters i.e. upstream slope, downstream slope, longitudinal slope, top width and bottom width of dam, height and length of earth dam, and length and height of horizontal filter were included in experimental and numerical modelling programmes. The cases have not carried out seepage modelling utilising experiments and seep/w by modifying geometrical and fluid parameters (particularly the fluid's viscosity effect) in earth dam models, as described previously in the literature studies.

The comparison of a homogeneous earth dam to a dam with a central impermeable clay core, as well as the comparison of a homogeneous earth dam to an earth dam with a horizontal downstream filter, were not widely considered. Few researchers did not include slope stability modelling on the upstream and downstream slopes of the earth dam during full reservoir conditions while analysing seepage models. All of the findings in this study are related to detecting inadequate seepage in order to determine the most effective geometrical parameter of the central clay core and downstream filter on seepage characteristics, as well as the upstream head and viscosity influence of fluid upstream of the reservoir. Analytical solutions obtained by Casagrande's, Dupuit's, Pavlovsky's, and Schaffernak's solutions were also used to compare seepage achieved with experimental and computational modelling of homogeneous earth dam models. These analytical solutions were shown to be ineffective. As a result, experimental and numerical modelling are considered necessary.

1.9 FLOWCHART OF WORK

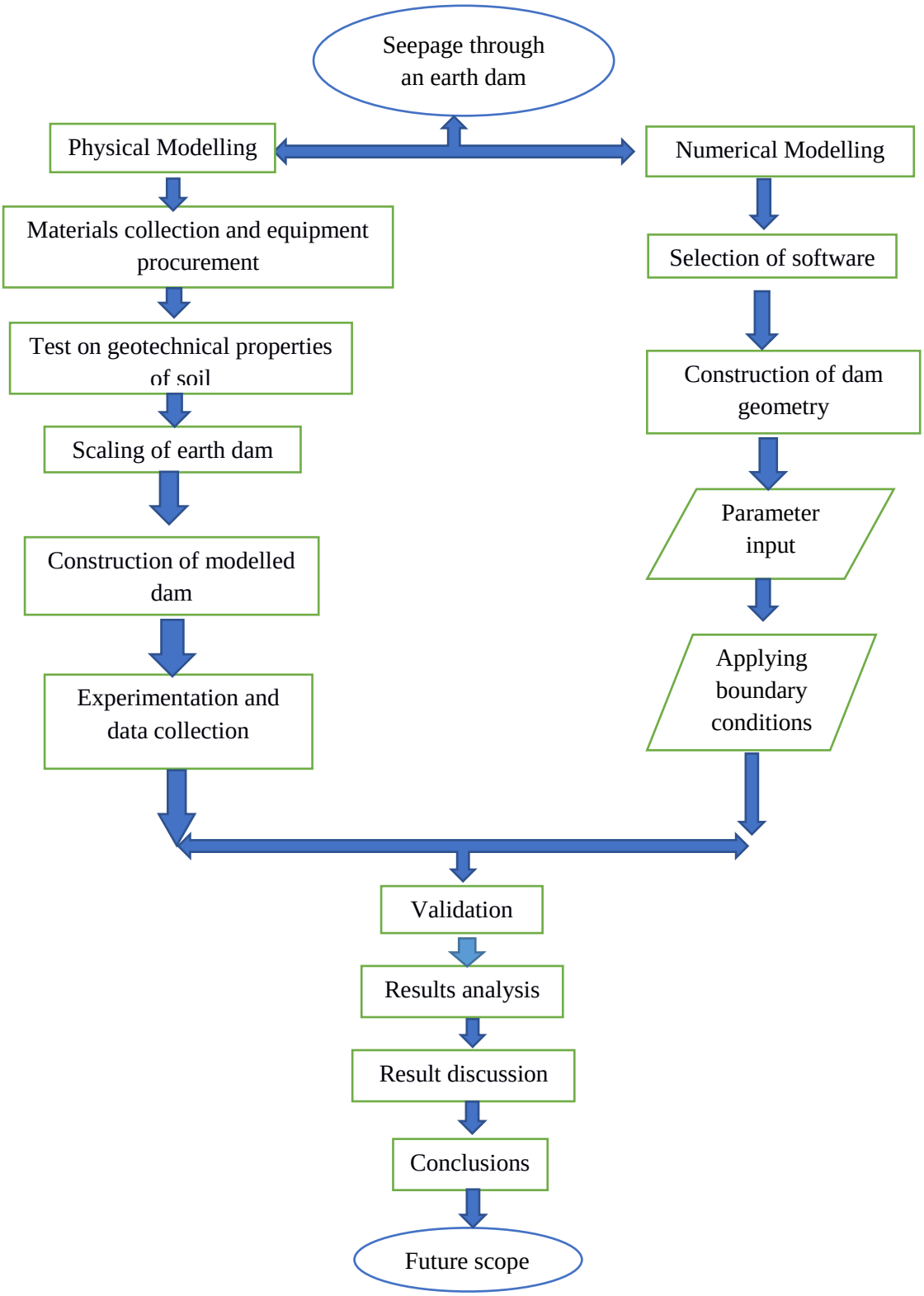

1.10 COMPOSITION OF THESIS

Chapter 1 describes the general introduction of the research work area related to the aim of works and the research work scope in the field; at the start of the introduction, generalized information about research using the raw materials in the production.

Chapter 2 introduces a large comprehensive survey of the literature about the seepage through earth dams and heat transfer through porous media such as earth dams. The comprehensive survey is based on the factors that directly affect the seepage behaviour of the earth dams.

Chapter 3 describes the materials used in the construction of the earth dam models with detailed properties. The test carried out on the soil used to construct the core of the earth dam and the shell to determine its composition was mentioned. The experimental setup was mentioned in detail regarding the construction of the earth dam and instrumentations, along with the specification of different models constructed as per various Indian standard codes. Details of numerical model carried out using finite element method, was also mentioned.

Chapter 4 describes the results and discussion section of the various experimental tests conducted on the material used to construct dams, such include the geotechnical characteristics of the soil employed in the dam's shell and core, XRD of soils, and viscosity measurement of upstream water. Natural moisture content, specific gravity, particle size analysis, liquid limit, plastic limit, compaction test, direct shear test, triaxial test, consolidation test, and permeability test are all determined by various soil tests conducted in the geotechnical laboratory. The thermal properties of soil were also mentioned. Seepage analysis result of the different experimental models was mentioned, along with a comparison with their numerical models using Seep/w software. Temperature modelling of the earth dam was also carried out in the experimentally as well as using Temp/w software to evaluate seepage using temperature measurements and comparing it with the water flux-heat flux.

Chapter 5 describes the detailed conclusions of the experimental modelling and numerical simulations. It also describes the alternative technique to identify seepage using temperature measurement.

Chapter 6 consists of the conclusion of the thesis and the scope for further study.

CHAPTER- 2

LITERATURE REVIEW

Several researchers have made significant contributions to the field of seepage, including the following.

Abdul Alim et al. (2017) analysed the earth dam model using seep/w software to calculate seepage discharge for a homogeneous earth dam built entirely on impermeable foundations with no filter or clay core. Additionally, the dimensional analysis of the model was also carried out. An equation for seepage through a homogeneous earth dam built on an impermeable foundation was presented based on the findings obtained using Seep/w.

Abu-Hamdeh (2014) studied in a lab setting the influence of water content and bulk density on the specific heat and volumetric heat capacity of sand and loam. Both types of soils had their specific heat measured using the calorimeter method. It was discovered that as the moisture content of the soil rises, so does the specific heat. Conversely, when the density and moisture content of the soil grew, so did the volumetric heat capacity. Loamy soil showed greater specific heat and volumetric heat capacity than sandy soil when moisture content and soil density were equivalents.

Abu-Hamdeh (2003) investigated the influence of water content and bulk density on specific heat, volumetric heat capacity, and thermal diffusivity in sandy and clayey soils. The calorimetric approach was used in laboratory studies. The specific heat of the soil increased as the moisture content increased, and the volumetric heat capacity increased as the moisture content and soil density increased. Clayey soil has higher specific heat and volumetric heat capacity than sandy soil, according to the findings.

Ahmed (2009) developed a fixed mesh finite element analysis to compute seepage discharge. Based on a probabilistic approach, the free surface flow through the earth dam was evaluated. It was discovered that seepage flow through the dam was lower than predicted by computational models for a homogenous soil formation. It was also discovered that the conventional deterministic solution's exit point was higher than the real location. According to the findings, it may not be required to build a core of smaller

hydraulic conductivity soil within the dam to limit seepage flow if the soil has a higher degree of variability.

Akyüz and Merdun (2003) established a Hele-Shaw viscous flow model to quantify seepage discharge via an impervious foundation earth dam. The results of the physical model were compared to those of Dupuit, Schaffernak and Van Iterson, Casagrande, and Pavlovsky. The Pavlovsky equation was determined to be the least consistent with a model for seepage computations. Schaffernak and Van Iterson and L. Casagrande's equation, on the other hand, did not yield a satisfactory result. Dupuit's equation was most suitable for seepage calculation as it has shown high compatibility with the model.

Aniskin et al. (2016) estimated seepage through the core of an earth and rockfill dam under non-steady-state conditions using numerical methods for an anisotropic seepage situation in an earth dam. Even after 30 years of operation, the seepage water enters the core at a minimal distance, according to the analysis.

Alekseevich and Sergeevich (2017) developed a thermal-seepage regime numerical model based on the finite element method (FEM) for earth dam foundations operated in permafrost conditions. The impact of heat and mass transmission, as well as liquid phase change, were estimated for the earth dam's soil interstices.

Al-Mansori et al. (2020) investigated the influence of seepage in an earth-fill dam using the SEEP2D programme and a finite element approach to quantify the quantity of seepage through the dam in a case study in Iraq. The important parameters taken for the study were the total head measurements, core permeability, and anisotropy ratio (k_x/k_y). The impact of the reservoir's various water heads on seepage was investigated. The quantity of seepage rises as the water heads increase. Output variables and input variables have been linked by the ANN model that governs seepage quantity through zoned earth dams. The findings revealed that both models provide a decent estimate of the coefficient R^2: 0.9003, 0.933.

Amanifard et al. (2007) examined how an electrical double layer (EDL) along the solid/liquid interface affected a three-dimensional heat transfer profile. There was also a numerical examination of the pressure decreases of water flow via a rectangular microchannel. Fluid velocity distribution and temperature were also examined for various boundary conditions and geometric instances in the presence and absence of

the electrical double layer effect. The EDL was found to have a considerable impact on the liquid flow in a rectangular microchannel, especially at high electric potentials.

Andreea (2015) examined slope stability and seepage analysis in unsaturated regimes in the earth dam for steady-state and transient flow analysis. Along with the ISO surface of the pressure head, there was a seepage study of full water level and flow following a rapid drawdown. Shear stress and shear forces were also computed to determine the slope failure safety.

Badruddin et al. (2020) reviewed heat transport in porous media with different geometrical shapes, such as a vertical plate, a cylindrical shape, a cavity, and so on. Heat transfer in free convection, mixed convection, thermal equilibrium, and thermal non-equilibrium was also covered in the review study.

Bardet and Tobita (2002) developed a FEM for the unconfined seepage concept that was based on the extended pressure and flux conservation theory. For large issues, it was discovered that the proposed technique eliminates the formation of matrix systems at the cost of a delayed convergence rate.

Bobkob (1973) used temperature measurements in an earth dam for its maintenance using an electro-thermometer. It was recommended that existing methods like fluorescein or radioactive isotopes detect leakage in an earth dam. Measurements obtained using temperature techniques were economical.

Buntebarth (2020) calculated heat transfer between the source and the study media to evaluate the thermal conductivity and thermal diffusivity of dry granular material. The thermal conductivity and the diffusivity of porous media were found to have an empirical relationship.

Chahar (2004) established formulae for determining seepage discharge in an earth dam by varying upstream slope, downstream slope, horizontal drains, freeboard, and top width. The downstream filter's minimum and maximum effective lengths were also determined. The desired length decreases for a given value of downstream slope cover when upstream slope, top width, or freeboard rises, while it increases as downstream slope increases.

Chen et al. (2009) established a fully coupled multiphase flow, thermal, and stress/deformation model in a porous geological media using a Finite element approach. "THYME3D," a three-dimensional software programme, was also developed.

Chen et al. (2010) investigated seepage control methods in geotechnical engineering. Seepage flow physical mechanisms were categorised based on their functions in mathematical models. A process for assessing performance was proposed, and a seepage control optimisation design was carried out.

Cho (2012) analysed seepage through a dam on a soil foundation using probabilistic analysis for the hydraulic conductivity of a layered soil profile's uncertainty and spatial variation utilising Karhunen-Loéve expansion; two-dimensional random fields were generated. Using the random fields generated data of seepage analysis of embankment-foundation, the influence of uncertainty in hydraulic conductivity attributed to spatial heterogeneity on seepage flow was investigated. Based on the findings, it was discovered that the probabilistic framework could well be utilized successfully in seepage evaluation for diverse flow patterns produced by geographical heterogeneity of hydraulic conductivity.

Chuvilin and Bukhanov (2019) employed a KD-2 needle probe in an experiment to assess the thermal conductivity of frozen soil at gas pressures below equilibrium, which had no effect on the soil samples in the research region.

Cuong et al. (2017) examined temperature measurements to determine seepage in an earth dam. The downstream toe was identified as the most crucial area for deploying fibre optic sensors to detect seepage. Short-term temperature analysis proved effective for estimating localised leakage and lowering repair costs. It was also reviewed to calculate seepage velocity using temperature sensors.

Del Piero (2020) contrasted classical thermodynamic theories to a heat conduction theory in rigid heat conductors based on mechanical principles. The suggested mechanical technique was shown to produce the same equation as the thermodynamic approach but in a more straightforward manner.

Djehiche et al. (2014) studied a homogeneous earth dam model based on the pervious and impervious foundations with a vertical drain on a pervious foundation and also compared the discharge attained using experimental and Seep/w models. In order to

compute the head, fourteen piezometers were fitted inside the dam body. The results of an empirical formula generated through experiments and the results acquired using Seep/w software were found to be in good agreement.

Dvinoff (1987) proposed an equation to describe the transient phreatic surface in the dam with an arbitrary upstream slope.

El Molla (2019) designed a new 2D finite element numerical model to assess the impact of sheet pile height and location on total seepage discharge and velocities across the dam's cross-section. The height of the sheet pile, rather than its location, was shown to have a greater impact on the overall seepage flow.

Fakhari and Ghanbari (2013) developed an equation for predicting seepage discharge in an earth dam with vertical and oblique central clay cores of different thicknesses by altering the upstream head in the reservoir, the width of the dam's crest, and the central angle of the core. It was the seepage discharge rate of an embankment dam having an oblique core is a function of core angle, and an equation has been proposed to compute seepage from the body of the embankment dam with an oblique core.

Farzampour et al. (2014) simulated the dam's seepage and slope stability using numerical modelling via the Geostudio bundle. Eleven dam models with various core sizes were examined to determine the ideal core thickness. It was concluded that, in the design of earth dams, using optimization techniques while considering hydraulic and geo-technique criteria, economic improvement in the plans was noticed.

Fazelabdolabadi and Golestan (2020) designed a Bayesian framework to calculate the absolute permeability of water in a porous structure using the geometry and clustering characteristics of the underlying pore-throat network. A Micro Network Database for micro-scale porous structures was established.

Fu and Jin (2009) developed an experimental model and tested it against analytical solutions. When comparing analytical solutions to experimental findings, it was discovered that the model accurately simulates the fluctuation of the seepage surface over time. The model accurately replicates the temporal development of an unsteady seepage flow field in a dam when pressures are compared between computation and experiments.

Indraratna et al. (2008) reviewed the evolution of granular dam filter behaviour from empirical and mathematical investigations and geometrical-probabilistic methods. The authors developed granular filter retention criteria based on constriction. Extensive experimental data from small-scale and large-scale filtering experiments conducted by several authors were used to verify the suggested retention requirements.

Irzooki and Jamel (2012) performed the Hele-Shaw experimental model to compute discharge via an earth dam body by varying the upstream slope, filter length, and upstream reservoir head, as well as utilising three different viscous oils to present three distinct soil permeabilities. An empirical equation was developed using dimensional analysis and experimental findings to identify the best efficient filter length. The findings showed that when the upstream and downstream slope angles decrease, the unit discharge through the earthen dam body rises. It rises as the horizontal filter length, upstream reservoir head, and hydraulic conductivity increase.

Ivolt and Dobe (2014) investigated the effect of a change in the calorimetry test procedure on the observed value of three different building materials' specific heat and thermal conductivity.

Jhanwar et al. (2016) established an experimental model to calculate seepage discharge and compared its result using Geostudio software. He also phreatic line and stability of slopes using Geostudio software. It was found that the dam was safe against seepage failure.

Jiang et al. (2010) programmed 3DS-NMM, a finite-element-based 3D tool for unconfined seepage analysis in homogeneous earth dams. For determining the free surface, a tetrahedral finite element mesh was employed. By using Simplex integration, the seepage force formula was determined.

Johansson and Sjödahl (2004) utilized temperature data to evaluate a downstream toe of roughly ten embankment dams to determine seepage. PT-100 sensors were used to measure temperature in the downstream toe, and long-term monitoring was done using optic fibres in embankment dams.

Kacimov (1996) developed a two-dimensional seepage model using a homogenous trapezoidal dam with conformal mapping and boundary value problem technique. Conformal mappings and the boundary value problem approach were used to

investigate steady two-dimensional gravity-driven seepage in homogeneous porous lumps. A trapezoidal dam exposed to a strong rainfall was studied using the Terzaghi flow behaviour. The impact of impervious bed tilting on a semi-circular massif was investigated. The total flow rate indicating the unit's water-bearing capacity, as well as the recharge-discharge distributions, hinge points, and gradients along the lump contour, were all obtained in explicit form. Non-isobaric boundary conditions were also addressed in general.

Kamanbedast and Delvari (2012) compared stability and seepage discharge in earth dams using Ansys software and Geostudio (Seep/w). It was found that Ansys software yields a better result than Geostudio while evaluating the stability of the earth dam.

Kamanbedast and Shahosseini (2011) investigated seepage behaviour using seep/w software and compared its result with the actual field data. It was recommended that for the Karkheh earth dam, another underground water gallery must be built. It was concluded that the seep/w is a reliable seepage software and thus, leakage and seepage can be determined successfully using it.

Kanarskii (1987) structured a flow net to investigate seepage via a homogeneous earth dam. According to the calculations, the stress-strain condition of an earth's structures varies in accordance with seepage and saturation regimes.

Kanchana (2015) applied Darcy's equation to compute seepage discharge for a dam with a central impervious core. By altering the effective length of the horizontal drain filter, the behaviour of the phreatic line was also studied. It was found that seepage doesn’t depend on the thickness of the filter, and the provision of a horizontal filter 75% from downstream toe was avoided because the phreatic line falls entirely within the dam’s core.

Kappelmeyer (1956) used temperature data made at shallow depths to detect subsurface characteristics. The thermal conductivity of the soil, the microclimate, and the vegetation in the region all influenced the temperature readings. It was discovered that calculating the quantity of heat energy transported to the surface can determine the amount of water rising.

Kazemzadeh-Parsi and Daneshmand (2011) created a non-boundary fitting mesh known as a smooth fixed grid finite element technique (SFGFEM) to handle the dam's

unconfined seepage problem. This approach was devised to iterate in order to determine a more precise position of the phreatic surface. The necessity for mesh modification (or re-meshing) in SFGFEM was abolished with this technique, and the phreatic surface could be created precisely even with coarse material.

Kodeová et al. (2013) used a KD2 PRO device with TR-1 and SH-1 sensors to assess thermal conductivity and heat capacity. The highest thermal conductivities were found in soils on quartz and substrates, according to the findings.

Kratochvil and Bachoree (2004) established a finite-element based model using ANSYS software. Due to an analogy between heat diffusion and seepage, ANSYS thermal was used to evaluate the problem of the free-surface flow of an earth dam.

Kumar et al. (2020) reviewed the effect of solute transport due to pollutants upstream in an earth dam. The harmful effect of chemical pollutants on various crops and plants due to water travelling downstream the earth dam due to seepage was also discussed. The maximum level of concentration of the various chemical in upstream of the earth dam was also discussed in the review.

Kumar et al. (2021a) developed a finite element model using Geostudio 2020 to study the seepage flow in an earth dam by varying various geometrical and fluid parameters. Numerical modelling was carried out using seep/w software, compared with experimental models. It was found that numerical models agreed with each other.

Kumar et al. (2021b) developed a finite element model using Temp/w software in Geostudio 2020 to estimate seepage discharge using heat-flux measurements. He observed that variation in heat-flux at a section in a dam is correlated with water-flux at the same section.

Kumar et al. (2021c) developed a solute transport model using arsenic at various concentrations. The chemical concentration in the earth dam body and downstream of the dam due to seepage was studied.

Kumar et al. (2022) developed a finite element model using Temp/w to study the temperature variation inside an earth dam body due to seepage. It was found that temperature variation can detect any leakage from the earth dam body and also able to estimate seepage discharge by recording the temperature variation.

Kumar and Mohan et al. (2017) compared experimental results for seepage discharge in a homogeneous earth dam with Casagrande's and Dupuit's analytical solutions. It was which was found that experimental and analytical results were in good agreement.

Kurz et al. (2017) reported experimental laboratory data on the thermal conductivity of frozen and unfrozen clay, silt, and peat soil samples subjected to seasonal freezing and thawing at the research site area. The values of thermal conductivity collected using empirical methods were compared to those acquired using a thermal probe in the lab.

Lam et al. (1987) created TRASEE, a finite-element-based computer model that uses the Galerkin Weighted-residual technique to tackle the soil system's transient seepage problem. Although there can be significant water flow over the phreatic line, the findings suggest that the phreatic line is not a flow line.

Li and Desai (1983) established a finite element approach for stress, seepage, and stability analysis of embankments and earth dams in the saturated and unsaturated zones. Linear elastic, nonlinear elastic, and plastic-based principles were used to simulate the behaviour of the soil. For a variety of issues, the finite element model correlated well with analytical solutions and field measurements. The approach was shown to be suitable for non-linear stress, seepage, and stability analyses of dams and earth dams.

Malekpour et al. (2011) constructed physical models of earth dams that could be used to test for various drain thicknesses and lengths. Piezometers and pressure sensors were used to monitor pore pressure in both the steady and transient states. The effective length of drain estimated from the equations was shown to be beneficial in preventing the negative effects of excess pore water pressure.

Mauriya (2010) presented a review on geotechnical instrumentation in earth and rock-fill dams. Several instrumentation parameters such as seepage, pore pressure, internal deformation, surface settlements, and reservoir and tail water levels were reviewed. An emerging trend in instrumentations using distributed fibre optical technology was also discussed.

Foster (2020) reviewed the statistical analysis data of failures in earth dams due to piping and slope stability. Compilation of the dam incident was carried out on several

aspects of the dam, including dam zoning, filters, soil utilised in the core's construction, compaction, foundation cutoff and geology.

Miao et al. (2012) used 381 databases of field data to construct a generalized algorithm called Genetic Algorithm Levenberg-Marquardt (GA-LM) based on a neural network to anticipate the seepage of an earth dam in China. The estimated seepage using the GA-LM model was found to be in good agreement with field measurements, indicating that the model was capable of reliably forecasting earth dam seepage.

Misra et al. (1995) reviewed parameters affecting soil thermal conductivity. The thermal conductivity of gravel, sand, silt, clay, and peat using empirical and semi-empirical approaches was also reviewed. In a nearly dry state, a theoretical thermal conductivity model of granular soil material was established.

Ouzaid et al. (2020) used a finite element technique analysis to investigate the failure mechanism of seepage control systems. The elastic-plastic finite element method was used to anticipate the failure mechanism induced by groundwater flow and to assess the factor of safety values against the failure of the excavation base on a project plan in Germany that was subjected to seepage flow. The acquired data were used as a benchmark for assessing stability.

Pingyu et al. (2007) presented a temperature-based simulation to analyse seepage flow and monitor systems using distributed optical fibre sensing. The system was scattered with traditional hygro-thermographs and flowmeters. The results of tests using a field-installed fibre optic sensor cable and a seepage channel were also reported, as well as the arrangement of the sensing cable.

Radzicki and Bonelli (2010) used the Impulse Response Function Thermal Analysis model to identify a breach in earth hydraulic structures such as dams and embankments. Temperature measurements were carried out to minimize erosion, and the cost of the reparation work of the earth dam was minimized. The installation of fibre optic cable in the earth's downstream toe was recommended.

Refaiy et al. (2021) studied the influence of downstream drain geometry on seepage through homogeneous earth dams established on an impermeable foundation using experimental and computational models. The impact of the drain's shape on seepage characteristics is assessed using various height, length, and angle possibilities. It was

discovered that as the length of the drain is increased, the amount of seepage discharge rises.

Rerak (2017) reviewed a variety of sources to evaluate the soil's thermal conductivity. Experimental research was carried out, and an application range of various soil thermal conductivity was recommended, based on various soil states, texture, and water content.

Rezk and Senoon (2012) investigated the impact of an upstream blanket on seepage discharge through a vertical drain. Mathematically, the effect of both the length of the upstream blanket cover and the depth of the impervious layer on seepage discharge flowing through the vertical drain and head loss due to the blanket cover was investigated. The experimental result was compared to the estimated head loss using a computational model. To calculate seepage discharge via an earthen dam with an upstream blanket cover and head loss owing to the blanket; a mathematical approach was provided.

Roushangar et al. (2016) investigated seepage flow from an earth dam's body using Wavelet-mutual information-based Gaussian process regression models. A combination of piezometers and reservoir level models was discovered to offer reliable predicting results, and the piezometer installed in the foundation has better performance than installed in the dam’s body.

Sachpazis (2014) calculated seepage discharge via a homogeneous earth dam by constructing a trapezoidal cross-section of an earth dam with uniformly graded sand. It was discovered that locating the filter closer to the upstream side resulted in increased seepage losses and a longer filter length. The Casagrande correction was also found to be insufficient for determining the seepage losses and filter length necessary for a flatter upstream slope.

Salmasi and Jafari (2016) calculated seepage discharge via a homogeneous earth dam and compared the results to Casagrande and Schaffernak's equation by Seep/w software. The numerical results were found to be relatively greater higher, with a 30 per cent and 20 per cent difference compared with those obtained using Casagrande's and Schaffernak's, respectively.

Salmasi and Mansuri (2014) used a Seep/w model to compute discharge in an earth dam with a filter by changing the dam slope, horizontal drain length, and horizontal

conductivity ratio to vertical conductivity and comparing the results to Casagrande's equation.

Several researchers have researched the field of heat transfer in porous media, and the following are critical research carried out in this field.

Shrivastava et al. (2015) calculated seepage discharge by experimental model. They traced its phreatic line and compared it to the phreatic line obtained by solving Casagrande's equation analytically. Using a regression model, an equation was proposed, determining the phreatic line more accurately than Casagrande.

Sivakumar and Vasudevan (2008) developed an experimental model to assess seepage velocity and piping resistance of three distinct soil types mixed randomly with coir fibres at varying hydraulic heads, fibre percentages, and fibre lengths. Fibres have been shown to significantly lower soil seepage velocity while also enhancing the soil's piping resistance. For assessing seepage velocity and piping resistance while taking into account hydraulic gradient, density, and fibre length, regression equations based on experiments were created.

Athani et al. (2015) used Plaxis 3-dimensional software based on finite element analysis to calculate seepage discharge and slope stability in the earth dam. Surface water and groundwater interactions were also investigated. The angle of internal friction (Φ) and Young's modulus (E) were changed to study the influence on the earthen dam's stability. The safety factor was reduced when the angle of internal friction (Φ) and Young's modulus (E) were increased.

Sivakumar and Srivastava (2007) established an analytical solution for the design of the filters after examining numerous aspects such as pore size, permeability, and Factor of safety against soil boiling conditions. The results of this analytical solution demonstrated the influence of seepage velocity, the relative density of the filter material, and the filter density to base soil density ratio on the filter's efficiency.

Srivastava and Sivakumar Babu (2015) presented an analytical solution for obtaining the safety factor of base soil migration.

Tokoro et al. (2016) provided a thermal conductivity model for soil, as well as empirical formulae. The thermal probe method was used on three different soils to test thermal

conductivity under different moisture conditions. There was a non-linear connection between soil thermal conductivity and moisture content.

Xiao et al. (2017) proposed a numerical solution for free surface seepage flow in layered soil (MFS) using basic fundamental solutions. The domain method was used to quantify seepage in layered soil profiles, allowing the numerical model to account for flux conservation and the continuity of pressure potential at the interface between two conservative layers. It was discovered that the suggested MFS-based technique has better numerical stability for addressing seepage flow with a nonlinear free surface in layered heterogeneous soil, even when the hydraulic conductivity differences are considerable.

Yousefi et al. (2013) used seepage flow and thermal modelling to investigate leakage in an earth dam. Finite element analysis was used to discretize the convective diffusion equation and mass balance in saturated and unsaturated zones. The temperature change was shown to be more useful for leak detection than piezometric seepage levels.

Zadeh-Touri et al. (2015) evaluated seepage discharge in a laboratory flume and identified a phreatic line of a clay-based homogeneous earth dam model reinforced with recycled PET (Polyethylene Terephthalate). Using piezometers installed on the flume body, the water level in the earth dam body was monitored. With a control valve installed under the flume, the influence of reduced output discharge on dam stability was assessed and compared with PLAXIS, a finite element method-based programme. The PET was shown to lower output discharge, pore pressure, and waste material, all of which have positive environmental consequences.

Zhu et al. (2008) used an optical fibre sensor to construct a model for calculating seepage flow and settlement in an earth dam. In the earthen dam integrated optical fibre sensor, the developed model relates strains and temperature changes to the fibre Brillouin gain spectrum.

2.1 HEAT TRANSFER IN SOIL

"Thermal energy is transferred between objects by thermal conductivity, thermal convection, in which a fluid passes between temperature zones, or thermal radiation, in which energy is transmitted through electromagnetic radiation" (Kosky et al., 2012). Heat flux is caused by a temperature difference. It causes a heat flux to flow

from the hotter to the cooler medium; it necessitates a temperature difference as well as a medium through which heat may flow.

The thermal transfer coefficient of the soil used to construct the earth dam and its foundation also affects heat flux. Heat can flow through solid materials (conduction) and fluids (convection), and if a radiation source is present, then through electromagnetic waves, commonly known as radiation. The primary thermal loading of an earth dam is provided by the air temperature around the earth dam and the water in the reservoir upstream of the earth dam. Geothermal, a frozen process in colder places, variations in humidity around an earth dam, and wind effects are all potential sources of temperature variance within an earth dam.

2.1.1 Heat conduction

"It is defined as the amount of heat passing in unit time through a unit cross-sectional area of the soil under a unit temperature gradient". In an earth dam, viscosity and water density are temperature-dependent phenomena that impact heat conduction in the soil particles present in the body. The material property of soil contained in the earth dam body and foundation might cause heat conduction. The saturated/unsaturated zone in the earth dam affects heat conduction. Natural or free convection occurs below the phreatic line, whereas conduction predominates above the phreatic line. As there is little water movement above the phreatic line in the top zone of the dam, there is pure heat conduction and no heat advection; hence, gradual heat transfer from the dam surface into the dam occurs. Convection in the x-direction and conduction in the y-direction both occur in the central zone. No convection occurs in the lower zone near the foundation; conduction dominates this zone as water flow is deficient.

2.1.2 Convection in soil

When the temperature difference between the earth dam body and the upstream water is significant enough, convective heat transfer occurs. Natural convection is caused by convection currents, which are motions induced by density differences in a fluid owing to temperature differences. It will continue as long as there is a temperature variation between the water in an earth dam and the water upstream. Temperature serves as a natural tracer for locating seepage flow and water flux in embankment dams. Temperature readings are used in the earth dam to locate leakage zones and estimate

seepage velocity. When seepage water passes through the pores of an earth dam, it exchanges temperature with the surrounding soil medium (Cuong et al., 2017). The energy transported by seepage flow causes temperature variations in earth dams contributing to convection. A pressure drop can occur whenever there is a considerable heat transfer. Increased fluid speed enhances high heat transfer in the case of convection.

2.2 THERMAL PROPERTIES

2.2.1 Thermal conductivity

Thermal characteristics of soils were previously utilised to forecast water, heat, and solute transport in soils (Abu-Hamdeh 2003). Soil thermal conductivity, among other important thermal characteristics, plays an important role in temperature modelling in porous media. Moisture content, mineral composition, temperature, and texture each have significance. In low-density clayey soils, however, the critical moisture content is the same as the plastic limit. Coarse-textured, angular-grained soils have a higher thermal conductivity than fine-textured soils (Misra et al., 1995).

The thermal conductivity of soil at various temperatures and mineral compositions has been investigated by a number of authors. Thermal conductivity of 1.04 W/(m K) at the unfrozen state and 1.61 W/(m K) at the frozen state of -6 ºC were found for silty sand with a quartz content of 64%, water content of 15%, and a dry density of 1.77 g/cm^3 (Chuvilin and Bukhanov, 2019). At 20% water content, the thermal conductivity of sand obtained from the two locations was 1.9, 1.25. Saturated sand had a thermal conductivity of 3.12 W/(m K) (Buntebarth 2020). At 17ºC, the average water thermal conductivity value in W/(m. K) was 0.56 (Chuvilin and Bukhanov, 2019). Water possesses thermal conductivity of 0.594 W/(m. K), according to the reported research (Kosky et al., 2012).

2.2.2 Specific heat and Volumetric heat capacity

"The amount of heat required to change the temperature of a mass unit of a material by one degree is known as specific heat. In other terms, a substance's specific heat capacity is the heat capacity of a sample divided by the mass of the sample. It's utilised to figure out how much energy changes as the temperature changes." Soil heat capacity is influenced by a number of variables, the most important of which are water content and

soil density. For a given bulk density, specific heat is correlated with water content in sandy soil. When compared to other common substances, water has one of the greatest specific heat in the liquid state. A calorimeter was used to calculate the specific heat of soil by measuring its heat capacity and dividing its mass (Kosky et al., 2012). The Sum of volumetric heat capacities of each soil component multiplied by their fraction gives soil volumetric heat capacity. "It refers to a specific soil volume's stored internal energy capability when subjected to a temperature change." The temperature and heat transfer within an earth dam is greatly influenced by the study of coupled heat-water transport in soil.

Specific heat and volumetric heat capacity have been discussed in several publications, of which just a limited number are presented. Using a Calorimeter, dry sand has a specific heat of 932-958 J/ (kg. K) (Ižvolt and Dobeš, 2014). The specific heat of quartz sand is 830 J/kg. ºC, dry soil is 800 J/kg. ºC, and wet soil is 1480 J/kg. ºC (Engineering toolbox 2003, Specific heat of some common substances). Kodešová et al., 2013 reported that at a dry density of 1.34 g/cm^3, the specific heat of soil was found to be 0.73 (kJ/kg. K) and a volumetric heat capacity of 1.9 MJ/(m^3. K). The water had a specific heat of 4.18 kJ/(kg. K) and a volumetric heat capacity of 4.18 MJ/(kg. K) (m^3. K). Specific heat was 0.86 kJ/(kg. K), and volumetric heat capacity was 2.30 MJ/(kg. K) for clay with a dry density of 1.46 g/cm^3 (Kodešová et al., 2013). Water has a specific heat of 4190 J/kg (kg. K) (Ižvolt and Dobeš, 2014). At 30°C, the water's specific heat was measured as 4.1175 kJ/ (kg K) or 74.181 J/(mol k) (Engineering toolbox 2004, water-specific heat).

2.3 CONCLUSION

Several authors studied seepage in homogeneous earthen dams by changing several parameters like viscosity of fluid, filter length, location and thickness of horizontal filters, elastic modulus of the soil material, homogeneous earthen dam with coir fibre, Polyethylene terephthalate (PET) recycling effect on earthen dams, temperature effect, changing dimensions of the dam, longitudinal slope, etc. Several numerical modelling were carried out using various software such as ANSYS, SEEP/W, GEO STUDIO, PLAXIS-3D, etc. Various Analytical solutions also have been developed.

2.4 GAPS IN LITERATURE REVIEW

On the following topics, significantly less or no work has been done

1. Earth dam with coir fibre.
2. Effect of different materials used for horizontal filters.
3. Seepage analysis of non-homogeneous dam.
4. Effect of Hydraulic conductivity ratio on the non-homogeneous dam.
5. Effect of Polyethylene terephthalate (PET) recycling admixtures in non-homogeneous dams.
6. Viscosity's effect of fluid, on the seepage line, in an earthen dam with filter.
7. Temperature measurement along seepage line.
8. Elastic modulus of the soil material.
9. Seepage effect on earthen dam, due to different compositions of soil.
10. Effect of fly ash of different grades in the dam's core.

However, these parameters have been chosen as objectives to study:

1. **Properties of the soil used for the shell and core of the earthen dam.**
2. **Effect of viscosity of fluid flowing.**
3. **Effect of dam's geometry on seepage.**
4. **The filter of the dam.**
5. **The location of the phreatic line.**

CHAPTER 3

MATERIALS AND THEIR TESTING

3.1 SOIL PROCUREMENT AND ITS TESTING

The soil was obtained from Delhi Technological University, Delhi, India (28.7501° N, 77.1177° E) at a depth of at least two metres below ground level using a digital weight balance of 10 kg used with a sensitivity of 10 g. Soil clods were broken down using a wooden mallet, and then the soil was taken for air drying in a non-rusting tray and spread on a polyethene sheet for air drying (IS 2720-1983, part 1). Parts 1-, 5, 7, 13, 15, and 17 of the Indian standard codes -IS 2720 were utilised to evaluate the geotechnical qualities of the soil used to construct the dam in the hydraulic flume in the laboratory. The dam model was developed using the test findings of geotechnical properties such as natural moisture content, sieve analysis, index properties, permeability, and shear strength.

To determine the crystalline minerals in the soil that was used to build the shell and core of the earth dam models in the hydraulics laboratory, X-ray diffraction (XRD) test was performed using Bragg-Brentano in a Bruker D8 advance machine. An X-ray beam was directed at the soil sample, and the scattered intensity was measured as a function of the outgoing direction. "d is the separation between planes, and Ɵ is the angle of incidence that the incident X-ray beam makes with the plane of atoms (h, k, l)," according to Bragg's equation. For each number of X-rays seen, the detector recorded the angle (2Ɵ).

3.1.1 Moisture content

The water content of soils is calculated as a percentage of oven-dry weight using this method. Oven drying of soil was done in a thermostatically controlled oven, which has the interior of non-corroding material and was maintained at about 105-110º C for 24 hours. 204 g of this oven-dried soil sample was taken with a digital weighing balance of accuracy of 1g (IS 2720-1973, part 2).

3.1.2 Specific gravity

A 1kg sample passing through a 4.75mm sieve was taken and placed on a tray using a digital weighing scale with a 1g accuracy. This sample was then immersed in distilled

water at 27º C. After 24 hours of immersion in distilled water, the soil sample was gently stirred with a rod to eliminate any trapped air bubbles inside the soil. Decantation via filter paper was used to remove the water from the sample. The soil particles that remained on the filter paper were reintroduced into the soil sample. The soil was then taken for oven-drying at 110º C for 24 hours.

The specific gravity is determined by placing an oven-dried sample in a pycnometer filled with distilled water. By turning the pycnometer on its side and covering the cone's apex hole with a finger, any trapped air could be released. To eliminate froth from the surface and to keep the water in the hole flat, the pycnometer was filled to the top. The outer surface of the pycnometer was dried and weighed. The soil sample inside the pycnometer was then emptied into the tray with care, assuring that all the soil aggregates were transferred. After that, the pycnometer was cleaned and refilled with distilled water before being weighed once again. Water was carefully drained from the sample, making sure that no soil particles were washed away with it. This soil sample was dried in an oven at 110º C for 24 hours, stirring many times to achieve adequate drying. The sample was then weighed after cooling and storing in an airtight container. An average of three determinations of specific gravity was taken (IS 2720-1980, part 3).

3.1.3 Grain size analysis- Sieve and Hydrometer

Oven-dried soil sample at 110º C for 24 hours, weighing 1kg, was taken with digital weight balance with an accuracy of 1g for sieve analysis. The soil fraction that was kept on the 4.75mm IS sieve was weighed, and the fraction that passed through 4.75 mm was collected separately for examination. 4.75 mm, 2.36 mm, 1.18 mm, 0.600 mm, 0.425 mm,0.300 mm, 0.150 mm, and 0.075 mm sieve sizes were utilised in the test. From top to bottom, the sieves were arranged in descending order of size, with the pan at the bottom, i.e., coarser to finer from top to bottom. A mechanical sieve shaker was used to agitate the soil sample to cause irregular motion for about 20 minutes. The fraction of soil and weight retained on each sieve were recorded separately. The total mass of soil fraction held on each sieve, as well as the percentage of soil fraction kept on each sieve, were computed, as well as the gradation based on the total soil sample obtained for analysis (IS 2720-1985, part 4).

"A hydrometer is a device that measures the specific gravity (or density) of a suspension, allowing the proportion of particles with a certain equivalent particle diameter to be computed. The particle size distribution of soil particles less than 75 microns was quantitatively determined using a hydrometer test." In a clean, dry beaker, 50g of oven-dry soil sample was added and mixed with 150ml of Hydrogen peroxide. After that, the sample was left to sit for 24 hours. The mixture was then gradually heated in a conical flask and left to boil until the final volume was decreased to 50ml, stirring occasionally. One litre of distilled water was used to dissolve 33g of sodium hexametaphosphate and 7g of sodium carbonate. The hydrometer was slowly placed in the cylinder containing the mixture, and the time was recorded using a stopwatch. Hydrometer readings were recorded after a period of 0.5, 1, 2, 4, 8, 15, 30 minutes and 1, 2, 4, 8, 24 hours. The temperature of the suspension was taken once during the first 15 minutes and then every 15 minutes after that. The hydrometer analysis findings were plotted on a semi-logarithmic chart, with particle size on the log scale versus a percentage finer than the comparable size on the ordinary scale (IS 2720-1985, part 4).

3.1.4 Consistency limit

3.1.4.1 Liquid Limit

The liquid limit was determined using the Casagrande instrument. A soil sample of 270 g was obtained and oven-dried at 110º C before passing through a 0.425 mm sieve. On a flat glass plate, this soil sample was thoroughly mixed with distilled water to make a homogenous paste. Using a spatula, a piece of the soil sample paste was deposited to a depth of 1cm in a Casagrande's apparatus cup. A spatula was used to remove any excess soil. A forceful stroke of the grooving tool along the diameter was made along the middle line to make a clean groove that separated the soil. By revolving the crank at a rate of two revolutions per second, the cup was fitted and dropped until the two halves of the soil cake placed at the start came into touch with each other. A percentage of the soil sample was obtained to evaluate the water content of the soil, and the number of drops necessary to close the groove was recorded. This test was performed by adding a little amount of water to the soil sample and then repeating the entire procedure. On a semi-log graph, the measured value of water content in relation to the number of blows was shown. On 25 blows, the water content measurement was recorded, indicating the soil's liquid limit (IS 2720-1985, part 5).

3.1.4.2 Plastic limit

A 60g air-dried soil sample passed through a 0.425 mm sieve was being used to determine the plastic limit. Distilled water was mixed to the soil sample on a flat glass plate until it reached a stage when the soil became sufficiently plastic to be easily moulded into any shape with fingers. After mixing, around 8g of this soil sample was shaped into a ball. Then it was rolled between the fingers and glass plate, with such pressure that the thread of uniform diameter along the length was made. The rolling rate was around 85 strokes/min; while counting a stroke as one sweeping motion of the hand, i.e. forward and backwards from the starting position, the rolling rate was roughly 85 strokes/min. Rolling was maintained until a soil sample thread with a diameter of 3 mm was achieved. After that, the soil was kneaded into a homogenous mass and rolled once again. This process continued until the thread crumbled under the pressure required for rolling, and the soil could no longer be rolled into thread. Finally, the moisture content of crumbled soil was tested after it was collected in an airtight container. The plastic limit of the soil is determined by the moisture content measured. Three soil results from three sections of soil passed through a 0.425 mm sieve were averaged (IS 2720-1985, part 5).

3.1.4.3 Shrinkage limit

A 30g oven-dried soil sample was placed in the evaporating dish and well mixed with distilled water, which was adequate to entirely cover the voids in the soil sample and make the soil pasty enough to be easily moulded into a shrinkage dish. There should be no trapped air bubbles. The clean shrinkage dish's weight and volume were measured. Filling the shrinkage dish with mercury provided the volume of the wet soil pat. By placing the plain glass plate firmly over the top of the shrinkage dish, any extra mercury was eliminated. The volume was calculated by dividing the weight by the unit weight of mercury. The volume of the wet soil pat was recorded as this volume. To prevent the soil from adhering to the shrinkage dish, a small coating of Vaseline (petroleum jelly) was applied. In the centre of the shrinkage dish, around one-third of the volume of the shrinkage dish was filled with soil paste. The shrinkage dish was placed on a firm surface with many layers of blotting paper as a cushion, and tapping was allowed on the shrinkage dish so that soil paste flowed to the edges of the shrinkage dish. This process was continued till the soil get completely filled. The surplus soil was removed

from outside the shrinkage dish, and the shrinkage dish with soil was weighed. The soil pat was left to air dry till it turned from dark to light in colour. Then the oven-drying of soil pat was carried out at 105 degrees Celsius. Soil pat was cooled after oven-drying and weighed immediately, and the weight of the shrinkage dish and dried soil was recorded. By removing the dried soil pat from the shrinkage dish and immersing it in a measuring cup filled with mercury, the volume of the pat was obtained. When submerging the soil pad in mercury, precautions were taken to ensure that no air was trapped beneath it. The weight of displaced mercury was recorded to an accuracy of 0.1g, and for the determination of volume, the weight of mercury displaced is divided by the unit weight of mercury. An average of two shrinkage limits calculated was considered (IS 2720-1972, part 6).

3.1.5 Light compaction test

The Light compaction method was used to determine the connection between the water content and the dry density of the soil. A 5 kg air-dried soil sample was weighed using a digital scale with a 1 g accuracy and passed through a 4.75 mm sieve. This soil was fused with distilled water before being used. The light compaction mould was weighed, and then the extension collar was attached to the mould before it was laid on a solid concrete floor to start the compaction of soil in three layers. Twenty-five rammer blows weighing 2.6 kg were dropped from a height of 310 mm above the soil for each layer of soil. Blows were applied evenly across the surface of each layer before another layer of soil was placed on top of it. While compacting, it was made sure that the rammer fell freely upon each soil layer. Then the extension collar placed on the mould was removed, and extra soil was trimmed off.

The compacted soil was transferred from the mould to the mixing tray. The soil sample's water content was determined. First, with a wooden mallet and by hand, the leftover soil from the mould was broken into pieces. It was passed through a 4.75 mm filter once more before being combined with the original sample. For the next iteration, water was increased, and the whole process was repeated until five iterations were completed. Dry density was calculated by subtracting the measured value of masses of the mould with the mould containing soil dividing them by the volume of the mould. The dry density obtained from a set of measurements was plotted versus the moisture content. A smooth curve was formed by freely connecting the points drawn on the graph. The maximum

point on the moisture content/dry density curve was recorded in g/ml, which was the closest to 0.01 value. This value gives us the maximum dry density, and the moisture content percentage that corresponds to it is optimum (IS 2720-1980, part 7).

3.1.6 Direct shear test

In a direct shear test fitted with a digital data acquisition system, a 1kg oven-dried at 110 ºC soil sample passing through a 4.75 mm sieve is obtained. In the shear box, the soil sample was compacted at its optimal moisture content. The load frame was fitted with the shear box with the specimen, a plain grid plate over the base plate at the bottom of the specimen, and a plain grid plate at the top of the specimen. The strain rate in mm/min was kept constant, and pressure in kg/cm^2 was varied for three tests; vertical and horizontal deformation was recorded from the data acquisition system. The shear normal-stress displacement curve plot was drawn, which offered a cohesive intercept and angle of shearing resistance (IS 2720-1986, part 13).

3.1.7 Triaxial test

The Tri-axial test was used to measure the shear strength characteristics of soil utilised in the construction of earth dam models. The experiment was conducted in a laboratory with a constant temperature. The triaxial test were conducted with unconsolidated undrained (UU) condition. All valves in the triaxial cell were initially closed, and the pedestal at the cell's base was covered in water. The test needed two filter paper discs, the first of which was placed on porous stone and over which the prepared soil sample was placed. The soil sample was then covered with a second filter paper disc. The soil specimen was mounted in a rubber membrane on the pedestal of the triaxial cell and fastened using O-rings. The membrane of the loading cap was sealed with a rubber O-ring, preventing cell fluid from entering the voids of the soil specimen. The loading platform of the triaxial testing machine was used to mount the triaxial cell. The top of the specimen was brought into contact with the loading ram. The axial deformation dial gauges and the proving ring were both fixed in position.

The soil specimen failed at the maximum deviator stress; thus, the axial load was removed, and the cell pressure was brought to zero. The air-release valve was opened, and the cell fluid was totally drained from the triaxial cell. The specimen assembly was dismantled, the soil sample was removed, and the final water content was determined.

The mode of soil specimen failure was recorded. At varying cell pressures, the test was performed on identical soil materials. In the triaxial compression test, the direction of primary stresses is known. The major principle stress is vertical, while the minor principal stress is horizontal, equivalent to cell pressure. The dial gauge of the lateral pressure assembly apparatus directly indicates the magnitude of cell pressure. Shear strength characteristics such as friction angle and cohesion were calculated using the triaxial test results by plotting a Mohr circle for the state of stress at failure in terms of effective stresses for each of the three samples. In MS Excel, the best common tangent to the three circles was drawn. The angle the tangent makes with the horizontal is the angle of shearing resistance in terms of effective stresses, and the intercept the tangent makes on the y-axis is the cohesion intercept in terms of effective stresses as cohesion (IS 2720-1986, part 12).

3.1.8 Consolidation

A consolidation test or Oedometer test was carried out in the consolidometer apparatus to determine the rate and degree of soil compaction of soil utilised in the earth dam's core. The empty consolidation ring was weighed with a digital weighing machine with an accuracy of 1g. The Soil (used in the core) sample was then placed in the consolidation ring, and the top and bottom of the ring were trimmed of excess soil material. A trimmed soil sample was used to determine the moisture content of the soil. The soil sample's height was determined by measuring the thickness of the ring. A digital weighing machine with a 1g precision was used to weigh the soil sample. The initial pressure load applied on the soil specimen was 0.1 kgf/cm^2, loading rate was doubled for every succeeding stage. Reading on dial gauge was measure at time sequence of 0, 0.25, 1, 2.25, 4, 6.25, 9, 12.25, 16, 20.25, 25, 36, 60, 120 and 1440 min. For each load increase, the dial gauge reading was plotted vs the square root of time by connecting the points to form a smooth curve. The coefficient of consolidation (C_v) and coefficient of volume change (m_v) were calculated using the formula given in 6.1.1.5 and 6.2.1.8, respectively (IS 2720-1986, part 15).

3.1.9 Permeability

A falling head test was used to determine the soil's permeability (shell). A 2.5kg of oven-dried soil was used, which was passed through a 4.75mm sieve after being dried at 110^o C for 24 hours. To achieve the optimum moisture content, the soil was

moistened with distilled water. The permeameter mould was weighed before the soil sample was placed in it. The interior of the mould was greased before it was fastened between the compaction base plate and extension collar and then set on a solid horizontal basis. Compaction was achieved in the mould at optimal moisture content by dropping a 2.6 kg rammer from a height of 310 mm above the soil and striking it 25 times. Blows were applied evenly across the surface of each layer before another layer of soil was placed on top of it. It was made sure that the rammer fell freely onto each soil layer during compacting, similar to how the light compaction test was done. The base was detached, and the collar attached to the mould was removed. The weight of the compressed soil specimen in the mould was then determined. A drainage base and cap with porous discs were used to assemble the mould with a soil specimen. Before placing the porous disc into the mould assembly, it was saturated. For ensuring proper saturation, the outlet valve was kept open until de-aired water started to flow from it. The top inlet of the falling head test device was connected to the strand pipe, and the outlet valve was initially closed. After that, the bottom outlet was opened, and the time required for the water level to drop from the initial head to the final head was measured. The standpipe was replenished with water, and the test was repeated three times until the results were almost identical. The length and diameter of the specimen were measured and noted; hence, the standpipe area was calculated. Also, the temperature of the water was measured using a mercury thermometer. Permeability at 27 ^{o}C was calculated, which gives us soil permeability in cm/s (IS 2720-1986, part 17).

The permeability of soil used in the core of the earth dam was calculated by multiplying by the coefficient of consolidation (C_v), coefficient of volume change (m_v), and density of water (Υ_w).

CHAPTER 4

METHODOLOGY

4.1 SCALING OF DAM

The physical model was downsized so that experiments could be carried out in the lab. Because the size of the hydraulic flume is restricted, the model must be scaled. The experimental model has a scale factor of 1/100. The length, width, height, and outflow discharge of the dam were all scaled using this factor (Wood D.M., 2004). The experimental model was scaled down; the numerical modelling was kept at the exact dimensions in seep/w, slope/w and temp/w of Geostudio 2020. The numerical model were kept at original (large) scale so as to relate it with the real life scenario. The scaling effect on length, width, height and other dimensions was linear for steady state seepage flow study. This effect is nonlinear in case of dynamic modelling i.e. dam breach study as the acceleration due to gravity on the soil particle in breach section will affect the scaling factor non-linearly. Hence study of earth dam breach requires centrifugal modelling, which is not required in the present study. (Wood D.M., 2004).

4.2 DAM GEOMETRY

Various Indian standard codes for construction have also been considered while constructing the earth dam models, such as IS 8826-1978, IS-8237-1985, IS- 10635-1993. To investigate the seepage effect, 24 models (M) were built, with the upstream slope, downstream slope, top width, and length of the dam varied according to Indian standard (IS) codes. As per IS 8826-1978 recommendations, no dam should have a crest width of less than 6 m. To avoid seepage capillary syphoning, IS 10635-1993 specifies a normal freeboard of at least one metre above the maximum water level. In models 9 and 10, impervious clay cores of different dimensions were built to investigate the seepage impact of the core's material composition and width. Table 4.1 presents the various dimensions of earth dam models, as well as their dimensions and upstream head. Tables 4.2, 4.3, 4.4, and 4.5 depict earth dam models with various longitudinal slopes, clay core, fluid viscosity, and downstream filter length, respectively.

Table 4.1: Earth dam models' dimensions and upstream head of homogeneous section

Model No.	Upstream water head (m)	Upstream slope (degree)	Downstream slope (degree)	Bottom width of the dam (m)	Height of dam (m)
M1	13.5	38	45	52	20
M2	13.5	38	59	52	20
M3	13.5	50	34	52	20
M4	13.5	50	34	56	20
M5	13.5	50	34	56	15
M11	13.0	38	45	52	20
M18	13.5	45	45	52	20
M19	13.5	50	45	52	20

Table 4.2: Earth dam models' dimensions with different longitudinal slope

Model No.	Upstream slope (degree)	Downstream slope (degree)	Bottom width of the dam (m)	Height of dam (m)	Longitudinal slope %
M1	38	45	52	20	0.00
M6	38	45	52	20	6.07
M7	38	45	52	20	2.28
M8	38	45	52	20	4.00

Table 4.3: Earth dam models' dimensions with different clay core

Model No.	Upstream slope (degree)	Downstream slope (degree)	Bottom width of the dam (m)	Height of dam (m)	Bottom with of core (m)	Top width of core (m)
M1	38	45	52	20	0	0.0
M9	38	45	52	20	18	2.4
M10	38	45	52	20	18	1.9

Table 4.4: Earth dam models' dimensions with different viscosity of the fluid

Model No.	Upstream slope (degree)	Downstream slope (degree)	Bottom width of the dam (m)	Height of dam (m)	Dynamic Viscosity of fluid (Pa.s)	Temperature during measurement (ºCelsius)
M1	38	45	52	20	8.900×10^{-4}	25
M12	38	45	52	20	9.078×10^{-4}	25
M20	38	45	52	20	9.345×10^{-4}	25
M21	38	45	52	20	9.790×10^{-4}	25

Table 4.5: Earth dam models' with different filters length

Model No.	Upstream slope (degree)	Downstream slope (degree)	Bottom width of the dam (m)	Height of dam (m)	Length of the filter from the downstream end (m)	% length ratio of filter to the total length (m)	Thickness of filter from the downstream end (m)
M1	38	45	52	20	0.0	00.00	0.0
M13	38	45	52	20	15.5	29.80	3.0
M14	38	45	52	20	23.0	44.23	3.0
M15	38	45	52	20	13.0	25.00	3.0
M16	38	45	52	20	07.8	15.00	3.0
M17	38	45	52	20	13.0	25.00	1.5

4.3 COMPACTION

A proper compacted earth dam has increased stiffness and strength, which in turn lowers the amount of settlements taking place and keeps the dam from sliding failure. Compaction of required magnitude helps in obtaining required imperviousness in the core zone. For achieving proper compaction, a Proctor penetrometer was used to construct 24 models of the earth dam. A needle with a surface area of 6 cm^2 was coupled to the Proctor penetrometer. The surface area of the needle was selected in such a manner that the reading obtained on the scale of the stem of the penetrometer was between 10 to 40. Using a Proctor penetrometer, the soil was laid in 5 layers of 4cm each at optimal moisture content with 90-95 per cent variation while maintaining the penetration rate of each layer at 1.3cm/s. An average of five readings of penetration force were taken at each layer to ensure minimal error. The average penetration force was multiplied by the needle area to obtain penetration resistance. The moisture-penetration resistance and moisture-density curve relationship were compared to the penetration resistance. Hence, compaction was controlled in the earth dam to achieve uniform compaction throughout the earth dam, using the Proctor penetrometer (ASTM D1558-10).

4.4 SLOPE STABILITY

In all 24 models, slope stability for both the upstream and downstream face of the earth dam was investigated using Indian standard code: IS 7894-1975 and Slope/w in Geostudio software. The Morgenstern-Price approach, was used to examine the slope stability of an earth dam in Slope/w 2020 software. The stability was checked by computing for full reservoir condition and automatic search procedure for critical slip surface. The Seep/w study in Geostudio software was used to determine the pore-water conditions. The soil input parameters for slope/w were derived from several geotechnical lab experiments for C, Φ, and unit weight. For both upstream and downstream slopes of earth dam models, the factor of safety was estimated.

4.5 PHREATIC LINE

It's the line within an earth dam section under which positive hydrostatic pressures exist. The pressure on the phreatic line itself is equivalent to atmospheric pressure. A saturated soil mass is separated from an unsaturated soil mass by this line. This line

denotes the top streamline and so aids in the construction of the flow net (Dvinoff 1987). The effective weight of the soil is reduced when water flows through the earth's dam body below the phreatic line. The shear strength of the soil is reduced due to pore pressure created below the phreatic line. Hence it is a necessity for determining the location of the phreatic line.

In the earth dam models built in a hydraulic flume, the fluorescent dye was used to trace the phreatic line. Commercial dyes have intense fluorescence properties, making them suitable for water tracer studies such as locating the phreatic line. “Fluorescent materials emit radiation (fluoresce) in the form of light upon receiving radiation from an external source. In the process, some energy is wasted while the remainder is absorbed. The higher the percentage of absorbed energy that is released, the more intensely fluorescent the materials will be” (Martin et al., 1999). The phreatic line was traced on transparent polymer sheets and drawn on A3 sized graph paper using fluorescent dye in upstream water. Pavlovsky's equation was also used to compare the earth dam's phreatic line of homogeneous models with the phreatic line generated using the seep/w programme.

4.6 FILTERS

Firstly, granular filters restrict seepage pressure forces from allowing the earth's base soil to migrate or from being washed away. Secondly, it allows water to flow freely, preventing excessive pore-water pressure from forming. The size of the voids in the filter media should be small enough to meet the first criteria while also satisfying the second. These are the two requirements for Terzaghi’s design criteria while designing the filter in earth dam models. In this study, a horizontal drainage filter was designed and included in the dam section as a seepage control device. As shown in Table 4.5, Model 13-17 was built with a downstream filter of varying lengths. The phreatic line was kept well within the dam due to these horizontal filters.

4.7 EXPERIMENTAL SETUP

For experimental work, a known-sized earthen dam was scaled down; 24 earth dam models were built in a hydraulic flume with dimensions of 300cm in length, 30.5 cm in width, and 40 cm in height. The moisture content of the soil was kept at an optimum moisture content to ensure adequate compaction of the layers. The size of the flume

was significant enough against the fluctuation impact of discharge measurement, causing the discrepancy. The seepage study in earth dam models were performed under steady state conditions. During the construction of the earth dam, a Proctor penetrometer was used to control compaction in the layers. The effect of scaling was taken into account because it has an impact on the final results. The phreatic line was traced with fluorescent dye. A homogeneous, as well as earth dam with a central clay core, was constructed. To obtain a discharge for corresponding 2-D earth dam models, seepage discharge was estimated by measuring volumetric discharge in a hydraulic flume and diving by width. The seepage of a homogenous earth dam was compared to that of a clay-cored earth dam. The longitudinal slope of a hydraulic flume was changed to investigate the effect on seepage discharge. The viscosity of the fluid was changed by adding sugar, and the effect on seepage discharge was measured using a rotational rheometer, a viscosity measurement instrument in the physics lab. A rotational rheometer works by confining the liquid between a plate and cone by the effect of a shearing action. The rotational rheometer measures torque, angular displacement and angular velocity. The shear stress is calculated from the reading of applied torque action by multiplying it by the stress constant. The viscosity of fluid was hence measured by dividing the shear stress by the shear rate (IS 1448-2018); (Wang et al., 2019).

For the purpose of studying the effect of a longitudinal filter on seepage, its length and thickness were changed. The impact of soil properties employed in the construction of the shell and core of an earth dam was investigated. Model M1 was built with silty sand in the core and shell. At the same time, M22 was built with clay in both core and shell. At the same time, M9 was built with silty sand in the shell and clay in the core. Soil properties were changed by adding 15% clay and 30% clay in silty sand in Model M23 and M24, respectively.

The quantity of discharge obtained from experimental and numerical models was compared in this study. The quantity of seepage discharge for homogeneous models was also calculated using the Dupuit formula, Casagrande, Pavlovsky and Schaffernak, to compare it with the respective experimental models. Figure 4.1 shows homogeneous earth dam model M1 in a hydraulic flume.

Figure 4.1: M1- Homogeneous earth dam

The effect of temperature variation on seepage in porous media like earth dams was examined. Temperature variation inside earth dam models was studied using experimental models using fifteen different models of an earth dam. In earth dam models built in a hydraulic flume, the temperature was monitored using a digital thermometer at various locations. The temperature of the air around the earth dam was measured to be 30°C. The heat flux across the earth dam in each model due to convective water flow was calculated by measuring the temperature variation inside the dam. The longitudinal slope of a hydraulic flume was changed to evaluate the effect on water and heat flux. In the present study, the temperature variation was studied by the following fifteen models, namely, M1, M2, M3, M4, M5, M6, M7, M8, M9, M10, M13, M14, M15, M18, and M19. The heat flux in the models was estimated using temperature observations, whereas the water flux was computed using seepage discharge calculations. The earth dam model with central impervious clay core is shown in figure 4.2, whereas the earth dam model with downstream filter is shown in figure 4.3.

Figure 4.2: M8- Earth dam with central impervious clay core

Figure 4.3: M13- Earth dam with downstream filter

4.8 NUMERICAL MODELLING

Geostudio 2020 software is a mainstream finite element software that can simulate and investigate seepage using Seep/w and slope stability using Slope/w. Seepage discharge, pore water pressure, water pressure head, and the phreatic line of two-dimensional models were found in seep/w and critical slip surface, strength, and safety factor, respectively, on slope/w. It can also simulate and evaluate water and heat fluxes using Seep/w and Temp/w. After carefully analyzing multiple trial calculations by varying the mesh size, a finite element mesh of size 0.1m was chosen in seep/w, and 1.25 m

was chosen in Temp/w. Mesh should be chosen as such until it delivers good results and still has a low impact on calculation time. The mesh quality was found to be adequate for the analysis.

For studying the variation of temperature and comparative study of water flux and heat flux in the earth dam models, fifteen models were studied in Temp/w, namely, M1, M2, M3, M4, M5, M6, M7, M8, M9, M10, M13, M14, M15, M18, and M19. The temperature variation in earth dam models was also modelled using Temp/w, a finite element based programme. The finite element mesh in the model 1 (M1) model is shown in Figure 4.4. Figure 4.4 depicts a finite element mesh in model 1 (M1), showing elevation in metres on the y-axis while showing the distance in metres on the x-axis. Figure 4.5 depicts a flowchart illustrating the Seep/w numerical modelling procedure and input requirements (Geostudio).

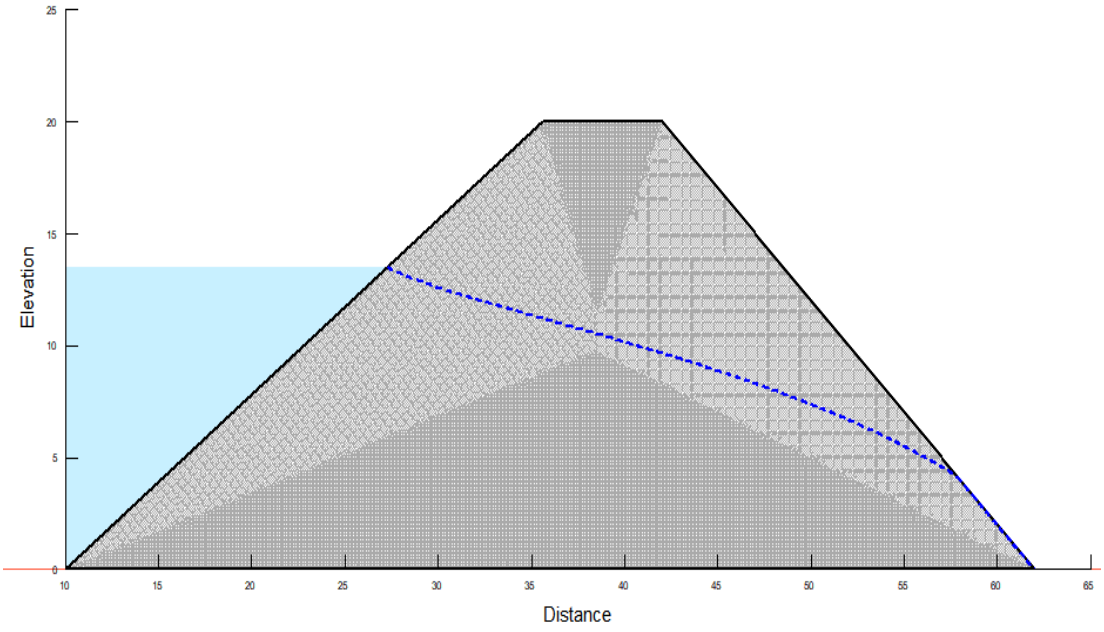

Figure 4.4: Finite element mesh of M1

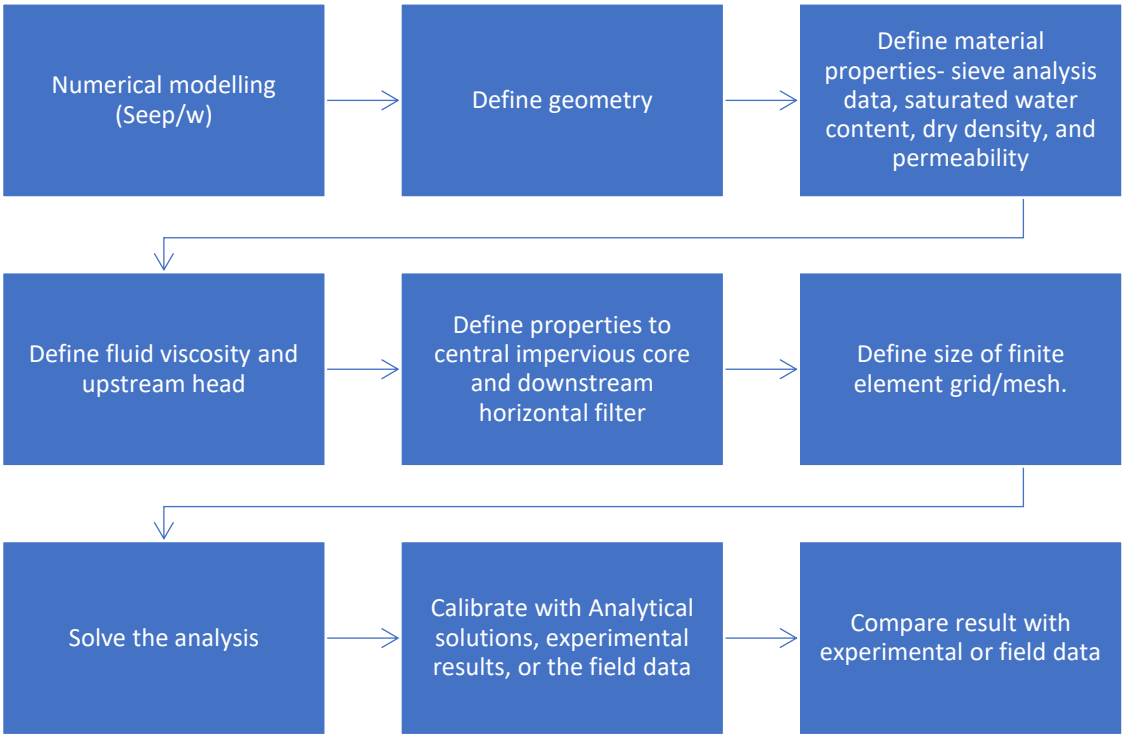

Figure 4.5: Input requirements and the numerical modelling process of Seep/w (Geostudio)

CHAPTER 5

RESULTS AND DISCUSSION

5.1 RESULT OF SEEPAGE MODELLING USING EXPERIMENTAL AND NUMERICAL MODELS

Twenty-four models of earth dams were built to study the seepage behaviour under different fluid and geometrical variations. Modelling of the earth dam was done experimentally in a hydraulic flume and using a finite element software, Seep/w. The earth dam's upstream and downstream slopes were tested for safety against sliding failure using Geostudio 2020's slope/w programme.

The soil's geotechnical properties were tested, and the findings are presented in Table 5.1. These findings were fed into Slope/w and Seep/w in Geostudio 2020 software.

Table 5.1: Geotechnical properties of soil in core and shell

S.No.	Name of the test		Core	Shell
1	Natural moisture content		11.8%	1.49%
2	Specific Gravity		2.66	2.57
3	Grain size distribution	D_{60}	0.016	1.614
		D_{30}	0.007	0.363
		D_{10}	0.002	0.094
		C_u	07.08	17.19
		C_c	01.33	0.87
		% finer than 4.75 mm	100%	83.62%
		% finer than 0.075 mm	98.19%	13.20%
		% finer than 0.002 mm	08.66%	01.41%
		Soil classification	Clay (CL)	Silty Sand (SM)

4	Atterberg's limit	Liquid limit	33.40%	26.24%
		Plastic limit	24.96%	12.69%
		Shrinkage limit	08.68%	-
5	Light compaction test	Dry unit weight of the soil	21.70 kN/m^3	18.05 kN/m^3
		Optimum moisture content	17.22%	13.10%
6	Direct shear test	Cohesion (c)	-	19 kPa
		Friction angle (Φ)	-	33º
	Triaxial test (UU test)	Cohesion (c)	26kPa	-
		Friction angle (Φ)	17.22 º	-
7	Permeability of soil	By consolidation test	$5x10^{-8}$ m/s	-
		By falling head test	-	$6.785x\ 10^{-6}$ m/s
8	Consolidation test	Coefficient of volume change (m_v) of soil.	$3.00\ x\ 10^{-5}$ m^2/kg	-
		Coefficient of consolidation (C_v) of soil (Core).	$1.69\ x10^{-7}$ m^2/s	-

Using light compaction of the soil, the light compaction method was used to determine the relationship between the water content and the dry density of the soil. Table 5.2 shows result of light compaction for DTU soil used in the construction of shell in earth dam models. The graph for the light compaction test of DTU soil is shown in Figure 5.1, with the y-axis representing dry density and the x-axis representing water content. Table 5.3 show result of light compaction for clay used in the construction of core in earth dam models. The graph for the light compaction test of clayey soil is shown in Figure 5.2, with the y-axis representing dry density and the x-axis representing water content.

Table 5.2: Light compaction for DTU soil used in the construction of shell in earth dam models

Water content (%)	Dry density (kN/m^3)
08.33	15.10
10.50	16.40
13.10	18.05
18.51	15.80

Table 5.3: Light compaction for clay used in the construction of core in earth dam models

Water content (%)	Dry density (kN/m^3)
10.26	13.02
13.97	14.27
18.44	15.40
23.36	16.23
30.93	14.62

Determination of particle size distribution was done using two experiments 1) sieve analysis and 2) hydrometer for particles finer than 0.075mm. Table 5.4a shows the particle size distribution of DTU soil used in the earth dam model using sieve analysis, and table 5.4c shows the particle size distribution of DTU soil used in the earth dam model using hydrometer test. While using the values given in this table, a graph was plotted to present the particle size analysis for the DTU soil used in the model of the earth dam, as shown in figure 5.3. Similarly, Table 5.5a shows the particle size distribution of clayey soil used in the earth dam model using sieve analysis and table 5.4c shows the particle size distribution of DTU soil used in the earth dam model using hydrometer test. While using the values given in this table, a graph was plotted to present the particle size analysis for the clayey soil used in the model of the earth dam, as shown in figure 5.4. Data of hydrometer test of DTU soil is presented in table 5.4b, while that of clayey soil is present in table 5.5b.

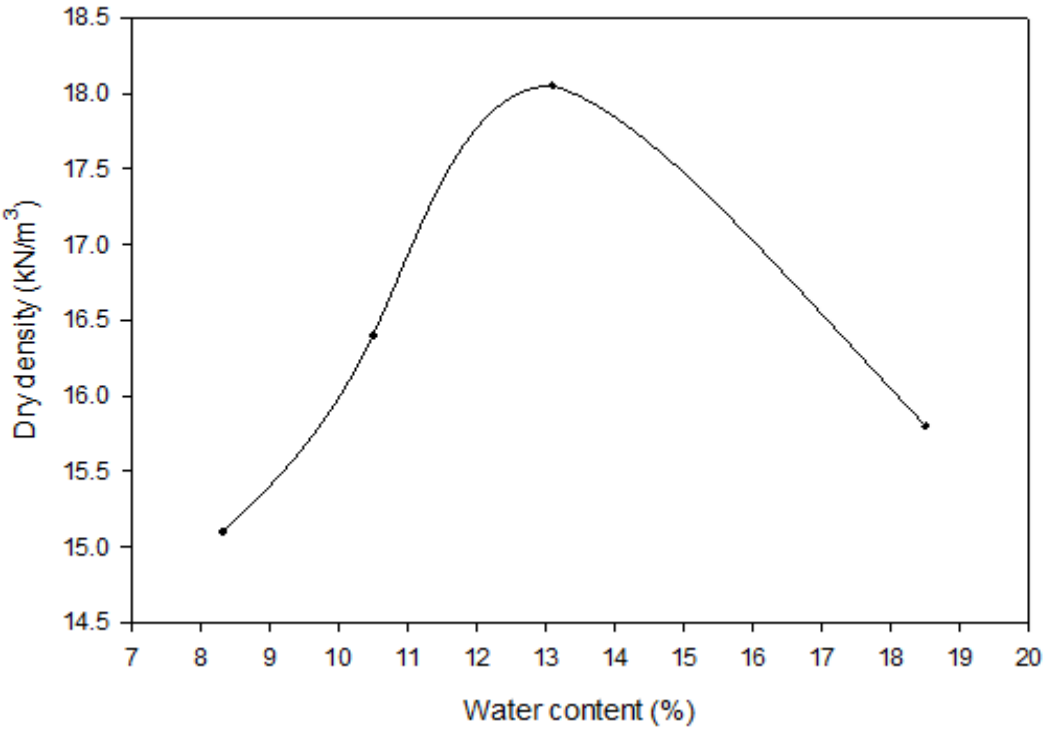

Figure 5.1: Variation of dry density with water content for DTU soil

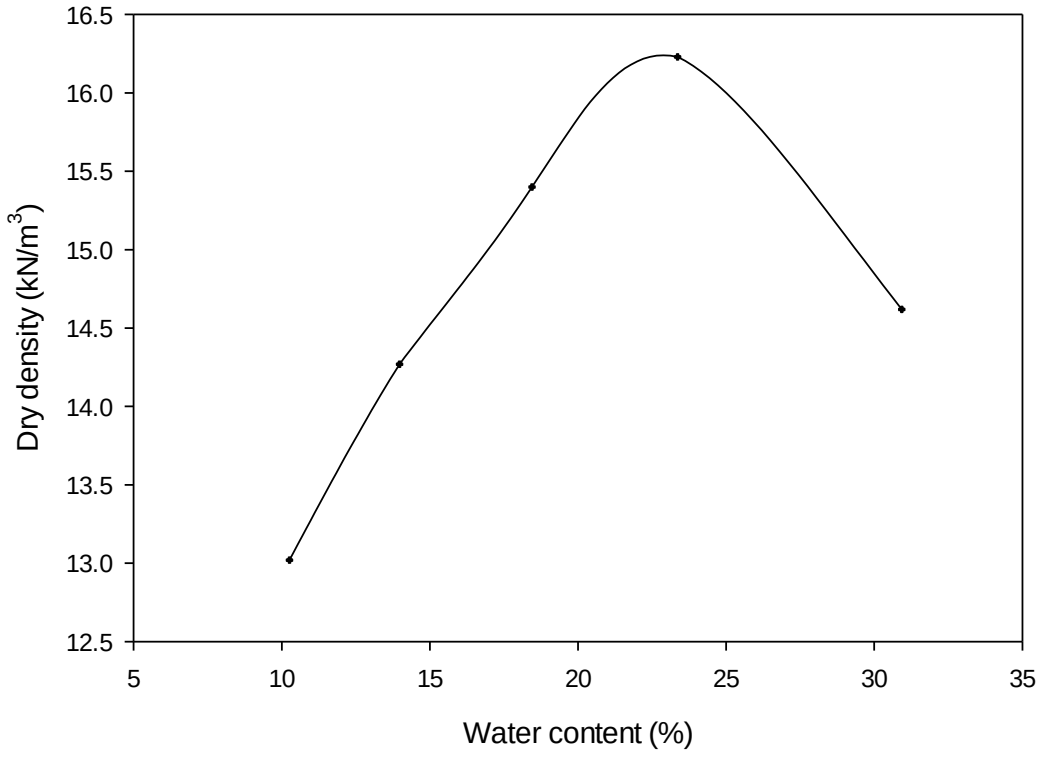

Figure 5.2: Variation of dry density with water content for clayey soil

Table 5.4a: Particle size distribution of DTU soil used in earth dam model using sieve analysis

Grain size (mm)	% finer than
4.7500	83.82
2.3600	71.58
1.1800	59.11
0.6000	43.73
0.4250	38.47
0.3000	32.52
0.1500	21.11
0.0750	13.20

Table 5.4b: Percent finer of DTU soil on total weight in hydrometer test.

Time (s)	R_h Hydrometer reading)	$R_h' = R_h + C_m$	He (Effective depth) (cm)	$\sqrt{\frac{He}{t}}$	K	D (Particle size) (mm)	$R = R_h' + C_t - C_d$	% finer (N')	% finer on total weight (N)
1	26.00	26.25	12.57	3.546	0.01362	0.048312	25.75	82.90	10.943
2	22.50	22.75	13.90	2.636	0.01362	0.035923	22.25	71.63	09.455
5	19.75	20.00	14.95	1.729	0.01362	0.023558	19.50	62.78	08.287
10	17.25	17.50	15.90	1.260	0.01362	0.017179	17.00	54.73	07.224
15	15.00	15.25	16.75	1.056	0.01362	0.014399	14.75	47.48	06.268
30	12.50	12.75	17.70	0.768	0.01362	0.010466	12.25	39.43	05.205
60	10.50	10.75	18.46	0.554	0.01362	0.007558	10.25	33.00	04.356
120	08.50	08.75	19.22	0.400	0.01362	0.005453	08.25	26.56	03.506
240	05.25	05.50	20.46	0.291	0.01362	0.003978	05.00	16.09	02.124
1440	03.00	03.25	21.31	0.121	0.01362	0.001658	02.75	08.85	01.168

Table 5.4b and table 5.5b were calculated using the below formula: -

$$D = K \times \sqrt{\frac{He}{t}}$$

Where, $K = \sqrt{\frac{30\,\mu}{980(G-G1)}}$

D = diameter of the particle in suspension, in mm.

μ = coefficient of viscosity of water at the temperature of the suspension, at the time of taking the

hydrometer reading, in poises;

G = specific gravity of the soil fraction used in the sedimentation analysis;

G1 = specific gravity of water;

He = effective depth corresponding to R_h in cm

t = time elapsed between the beginning of sedimentation and recording the hydrometer reading in minutes.

Table 5.4c: Particle size distribution of DTU soil used in earth dam model using hydrometer test

Grain size (mm)	% finer than
0.0461	10.94
0.0331	09.45
0.0229	08.28
0.0170	07.22
0.0149	06.26
0.0110	05.20
0.0079	04.35
0.0056	03.50
0.0040	02.12
0.0016	01.16

Table 5.5a: Particle size distribution of clayey soil used in the construction of core in earth dam model using sieve analysis

Grain size (mm)	% finer than
4.7500	100.00
2.3600	99.97
1.1800	99.84
0.6000	99.68
0.4250	99.54
0.3000	99.47
0.1500	98.81
0.0750	98.19

Table 5.5b: Percent finer of clayey on total weight in hydrometer test.

Time (s)	R_h (Hydrometer reading)	$R_h' = R_h + C_m$	He (Effective depth) (cm)	$\sqrt{\frac{He}{t}}$	K	D (Particle size) (mm)	$R = R_h' + C_t - C_d$	% finer (N')	% finer on total weight (N)
1	30.0	30.25	11.055	3.3249	0.0128	0.04259	29.75	95.78	94.04
2	28.0	28.25	11.815	2.4305	0.0128	0.03113	27.75	89.34	87.72
5	26.0	26.25	12.575	1.5858	0.0128	0.02031	25.75	82.90	81.40
10	20.0	20.25	14.855	1.2188	0.0128	0.01561	19.75	63.58	62.43
15	17.0	17.25	15.995	1.0326	0.0128	0.01322	16.75	53.92	52.95
30	14.5	14.75	16.945	0.7515	0.0128	0.00962	14.25	45.87	45.04
60	13.0	13.25	17.515	0.5402	0.0128	0.00692	12.75	41.04	40.30
120	09.0	09.25	19.035	0.3982	0.0128	0.00510	08.75	28.17	27.66
240	05.0	05.25	20.555	0.2926	0.0128	0.00374	04.75	15.29	15.01
1440	02.5	02.75	21.505	0.1222	0.0128	0.00156	02.25	07.24	07.11

Table 5.5c: Particle size distribution of clayey soil used in earth dam model using hydrometer test

Grain size (mm)	% finer than	Grain size (mm)	% finer than
0.0425	94.04	0.0096	45.04
0.0311	87.72	0.0069	40.30
0.0203	81.40	0.0051	27.66
0.0156	62.43	0.0037	15.01
0.0132	52.95	0.0015	07.11

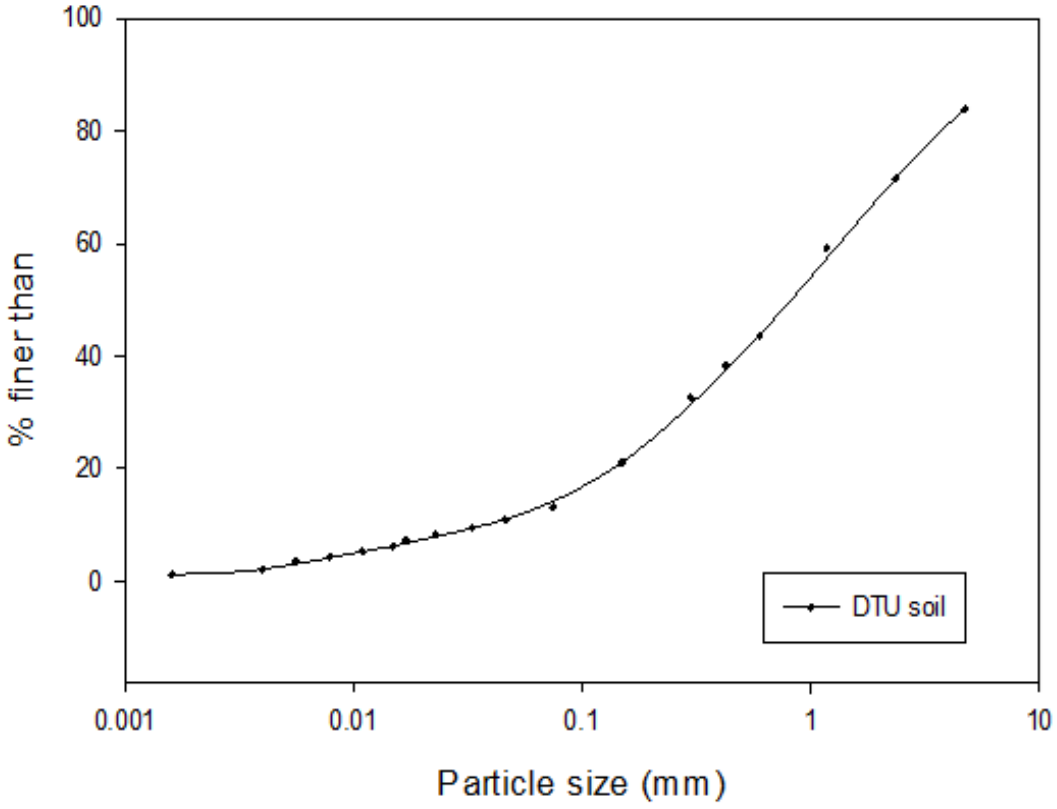

Figure 5.3: Particle size gradation analysis of DTU soil

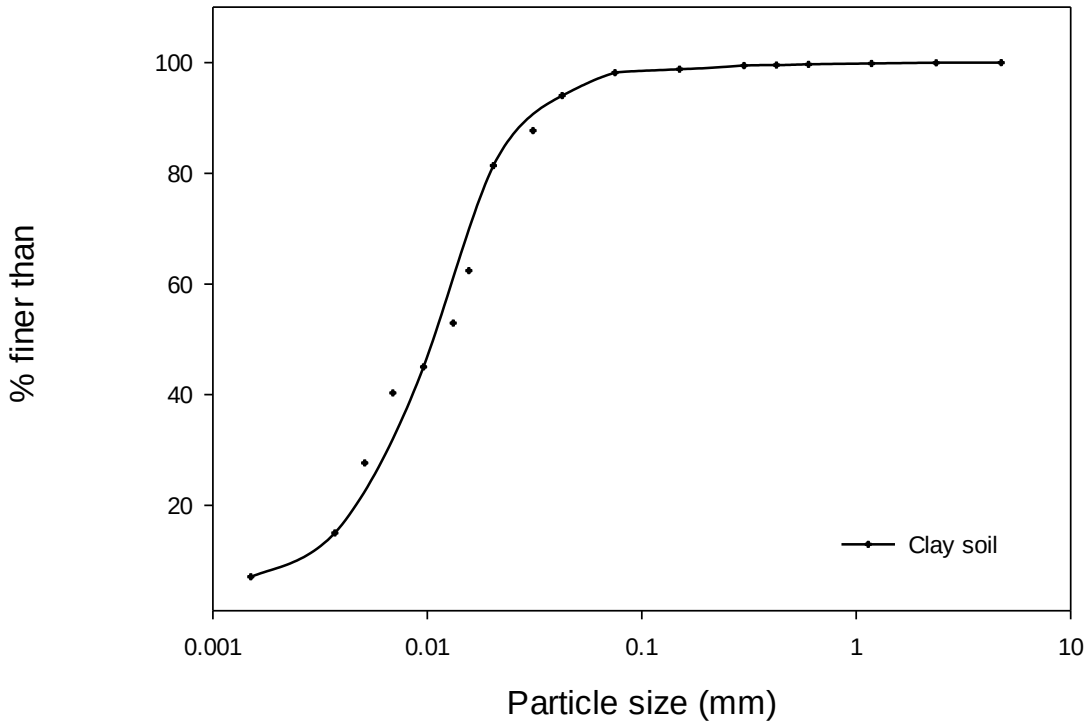

Figure 5.4: Particle size gradation analysis of clayey soil

The results of the consolidation test on clayey soil was carried out to determine the coefficient of compressibility (a_v), the coefficient of volume change (m_v) and coefficient of consolidation (C_v). Table 5.6 shows the variation of consolidation pressure with respect to the void ratio for the determination of a_v and m_v. While table 5.7 shows the coefficient of consolidation at different consolidation pressure. A plot was drawn against deformation in dial gauge readings vs the square root of time, and different values of C_v were evaluated using a graph at different values of consolidation as shown in figure 5.5a to figure 5.5g.

Table 5.6: Variation of consolidation pressure with the void ratio for determination of coefficient of compressibility and coefficient of volume change.

Applied effective pressure	P_1 (kPa)	100
	P_2 (kPa)	200
Void ratio	e_1	0.56
	e_2	0.22
Coefficient of compressibility	a_v (1/kPa)	0.0034
Coefficient of volume change	m_v (1/kPa)	0.00306

Table 5.7: Determination of Coefficient of consolidation at different consolidation pressure

Consolidation pressure	25 kPa	50 kPa	100 kPa	200 kPa	400 kPa	800 kPa	1600 kPa
t_{90} (min)	7.0	7.1	7.5	7.2	7.2	7.3	8.0
H_{dr} (cm)	0.9945	0.9835	0.9695	0.942	0.921	0.887	0.845
Coefficient of consolidation (C_v) cm^2/min	0.1198	0.1155	0.1062	0.1046	0.1000	0.0914	0.7577
Average C_v	0.10193 cm^2/min						

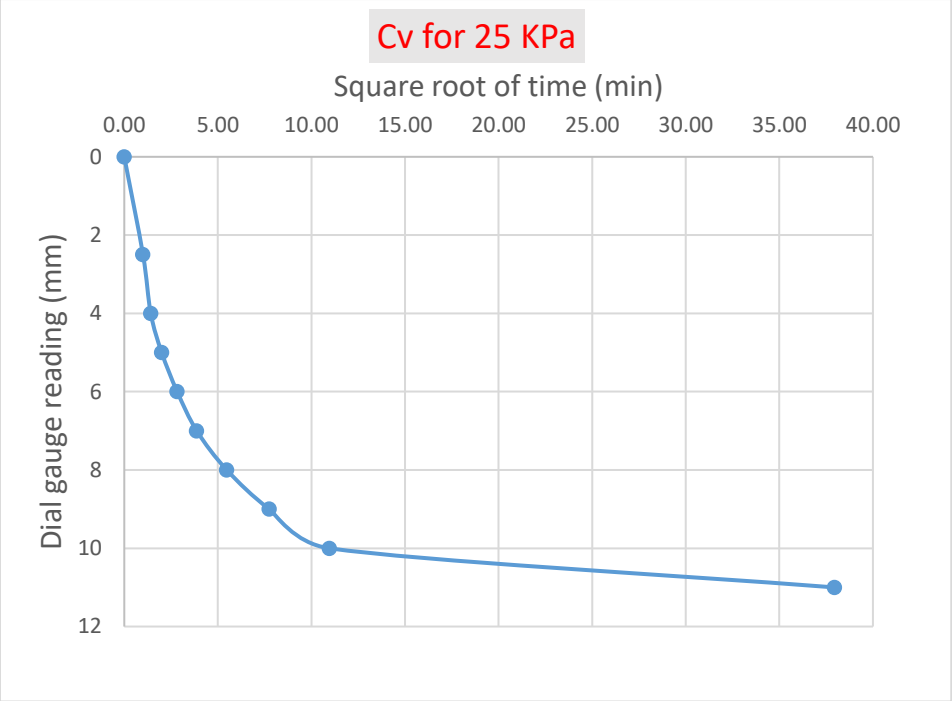

Figure 5.5a: Square root of time fitting curve at 25kPa

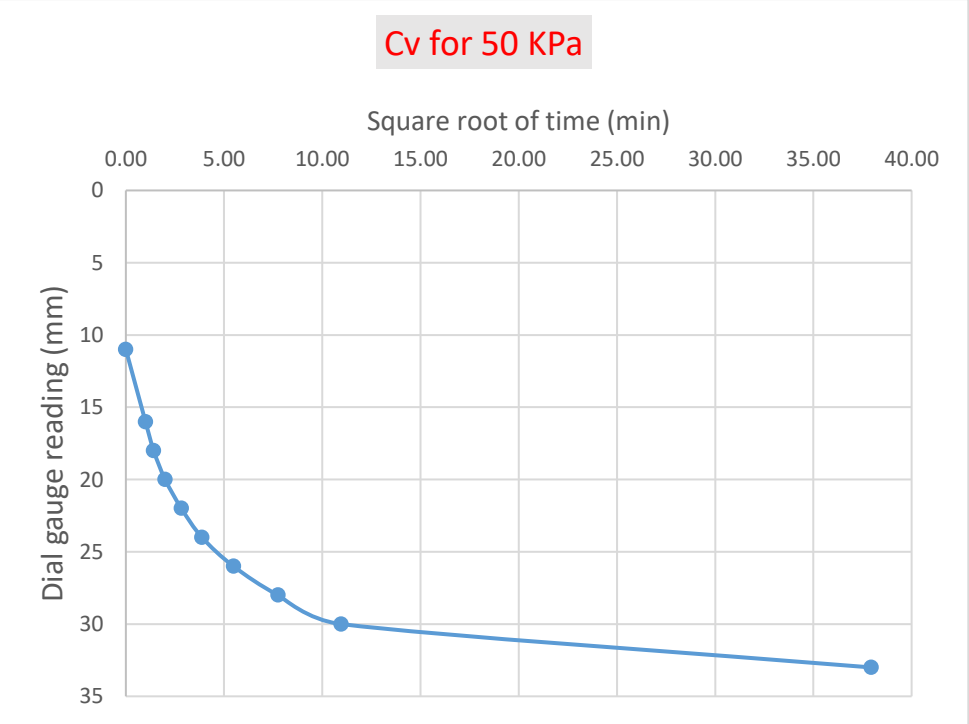

Figure 5.5b: Square root of time fitting curve at 50kPa

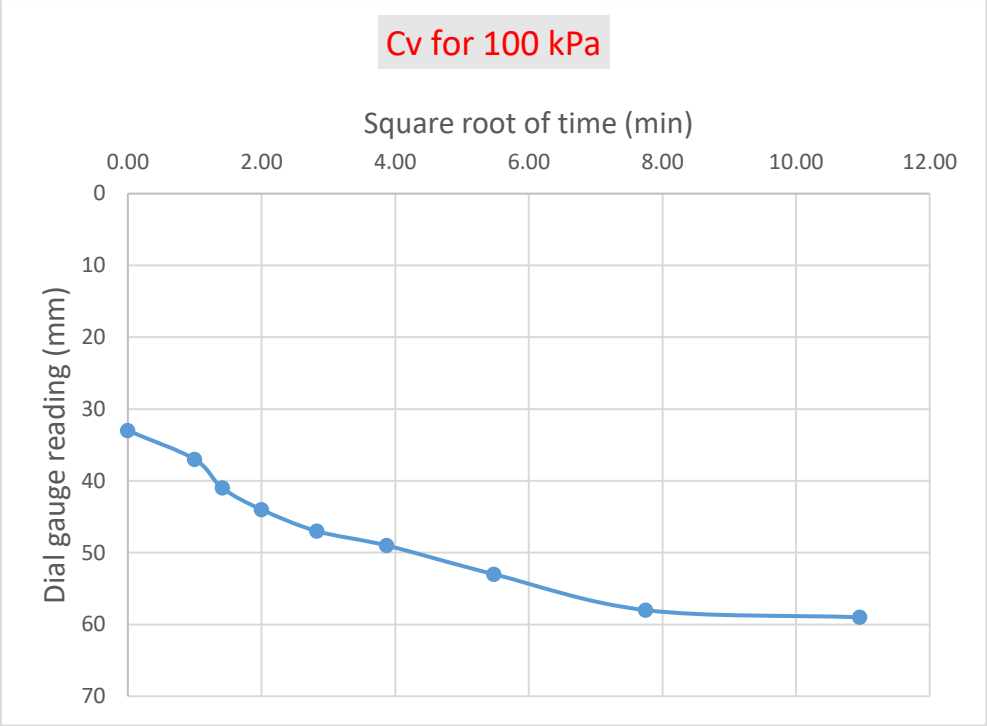

Figure 5.5c: Square root of time fitting curve at 100kPa

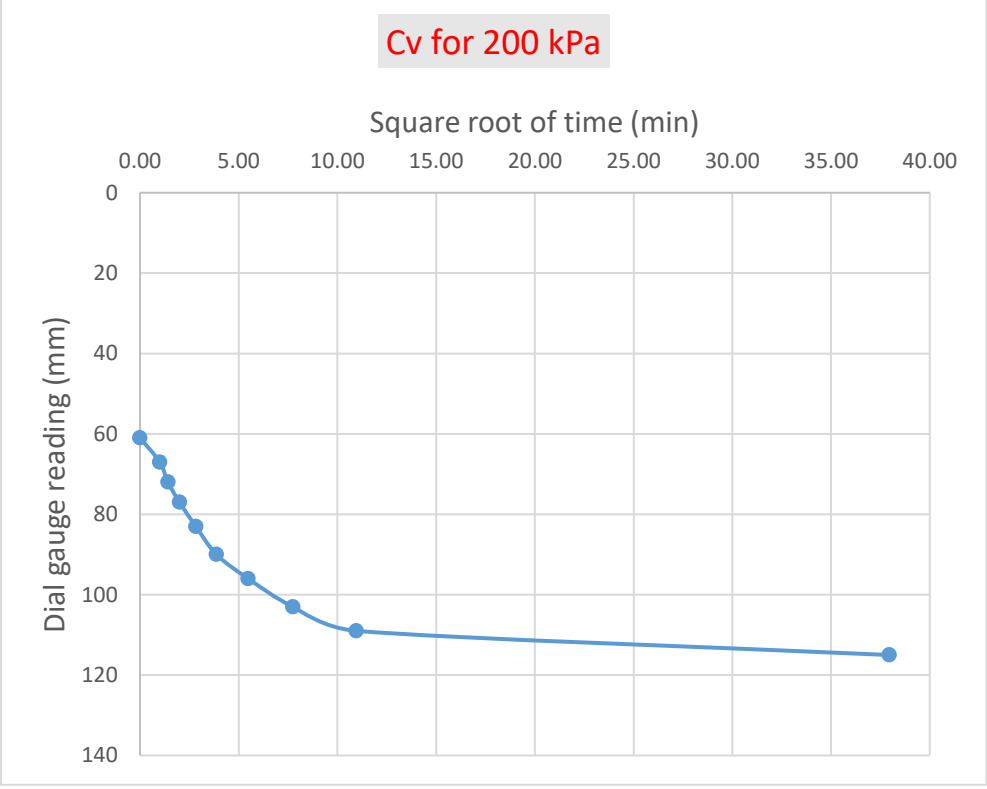

Figure 5.5d: Square root of time fitting curve at 200kPa

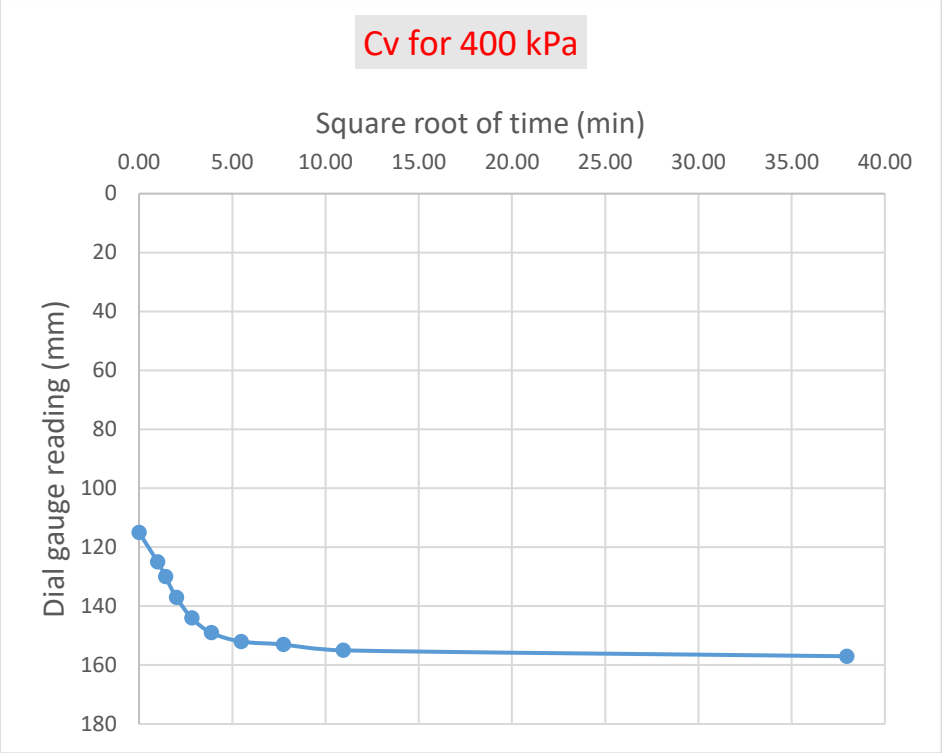

Figure 5.5e: Square root of time fitting curve at 400kPa

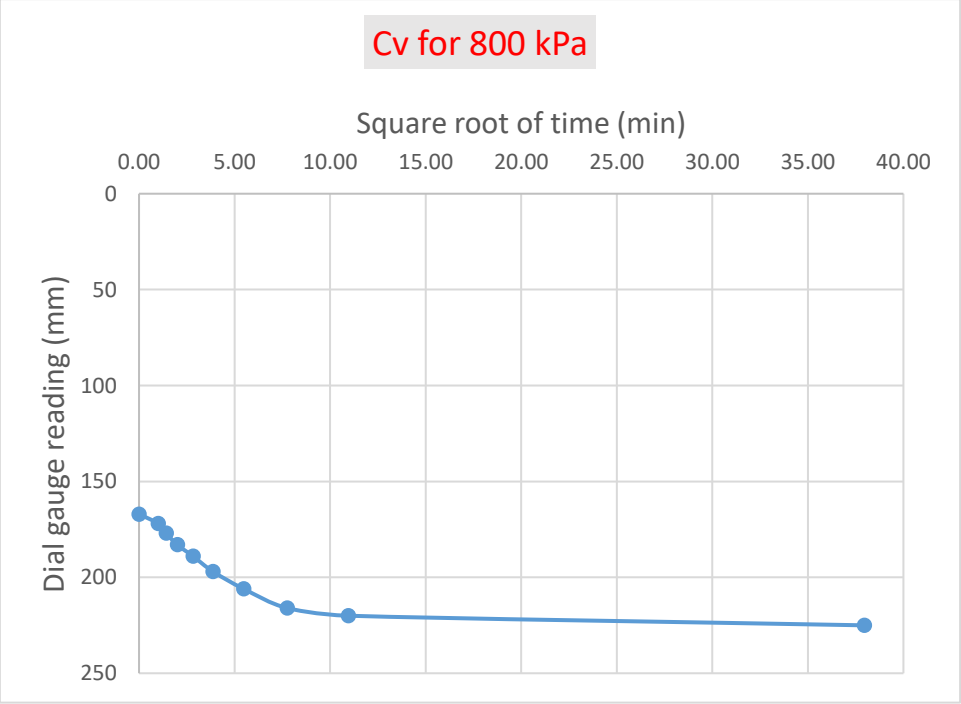

Figure 5.5f: Square root of time fitting curve at 800kPa

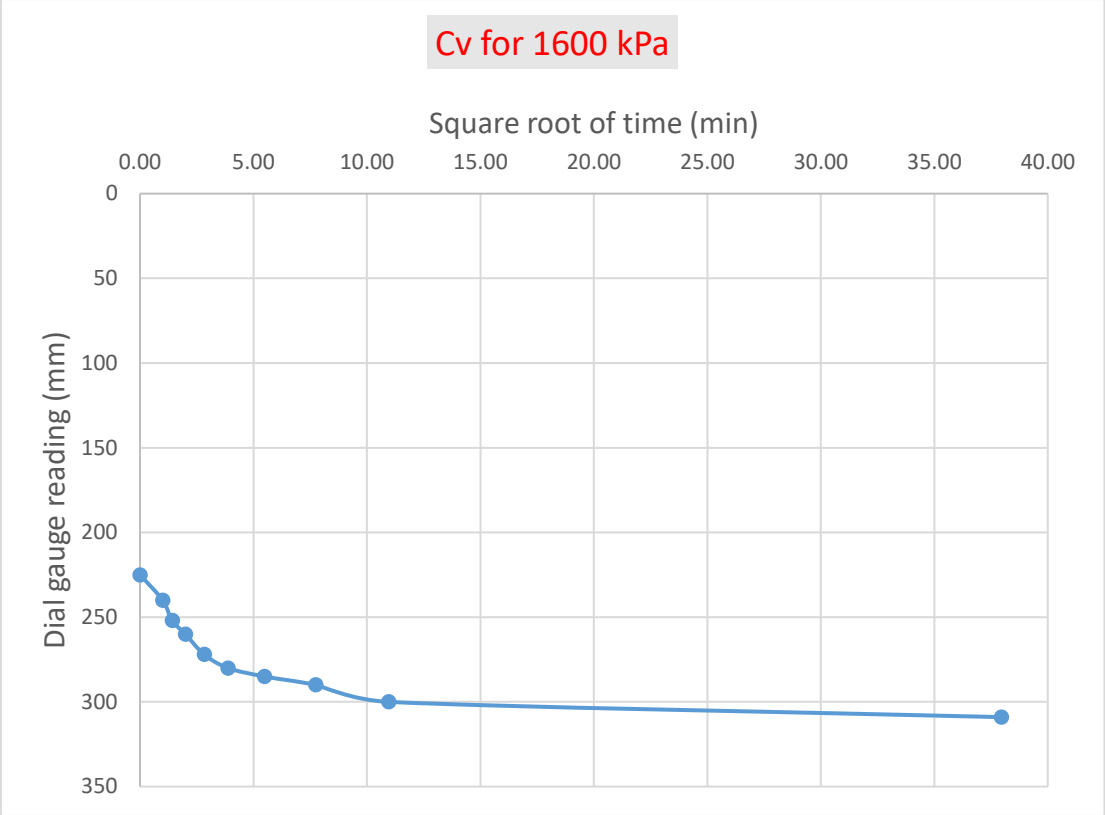

Figure 5.5g: Square root of time fitting curve at 1600kPa

To determine the shear strength parameters direct shear test was conducted on DTU soil. The drainage conditions were undrained unconsolidated condition. Cohesion and internal angle of friction were obtained. The result of normal stresses and shear stresses are given in table 5.8. A graph was plotted against it as shown in figure 5.6. While for clayey soil, cohesion and internal angle of friction were determined using a tri-axial test, and the results are shown in figure 5.7.

Table 5.8: Direct shear analysis of soil used in the shell (DTU soil)

Normal stress (kg/cm^2)	Shear stress (kg/cm^2)
0.5	0.494
1	0.893
1.5	1.145

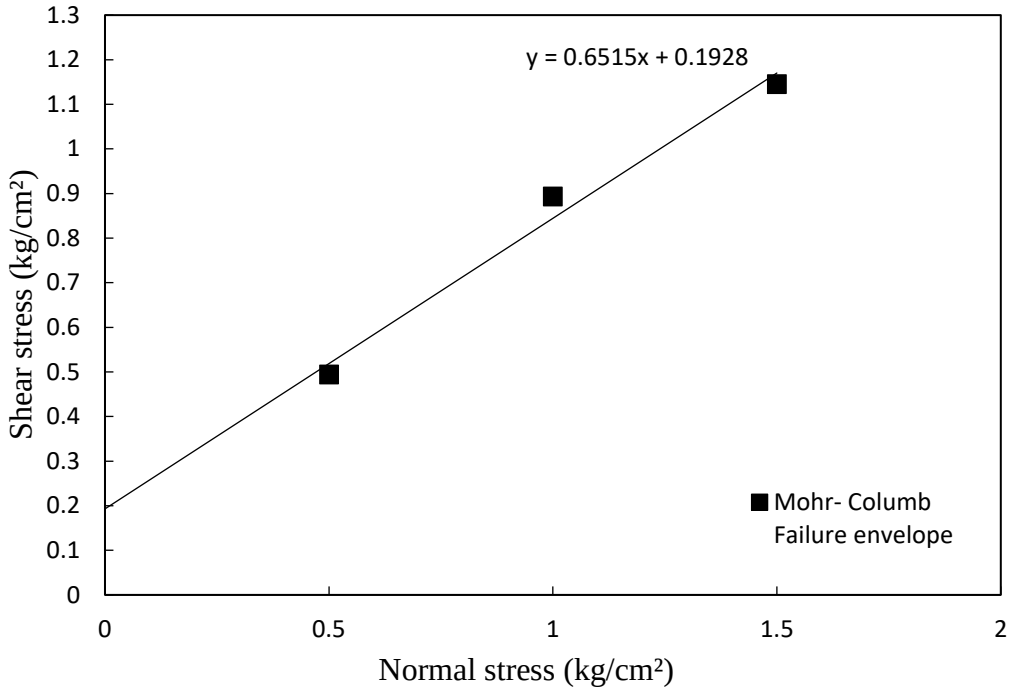

Figure 5.6: Direct shear test of DTU soil

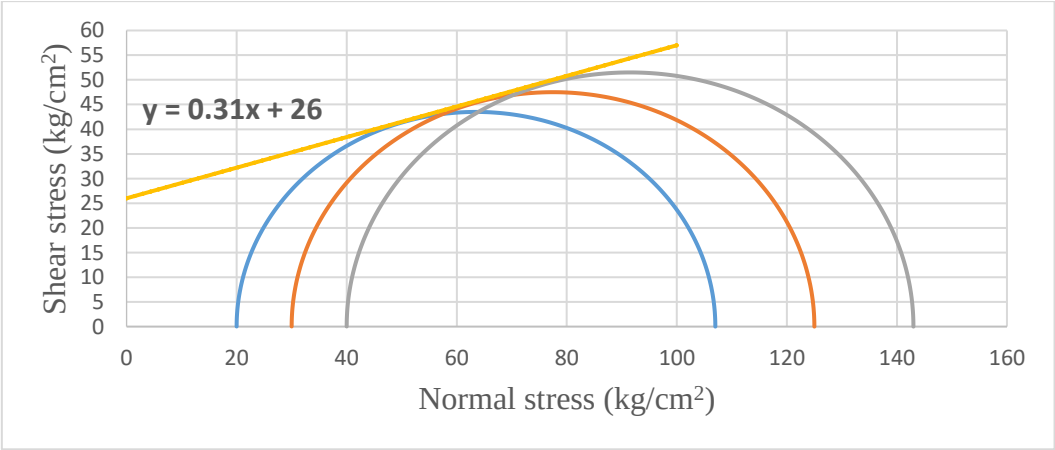

Figure 5.7: Triaxial test of clayey soil

The viscosity of water and viscosity of water with sugar at different concentration was used to determine the effect of viscosity on the seepage flow rate of earth dam models, and using rotational rheometer shear strain vs shear rate curve was achieved as shown in figure 5.8, while figure 5.9 shows the relation of dynamic viscosity of water with temperature, and figure 5.10 shows dynamic viscosity of water with sugar solution in different earth dam models.

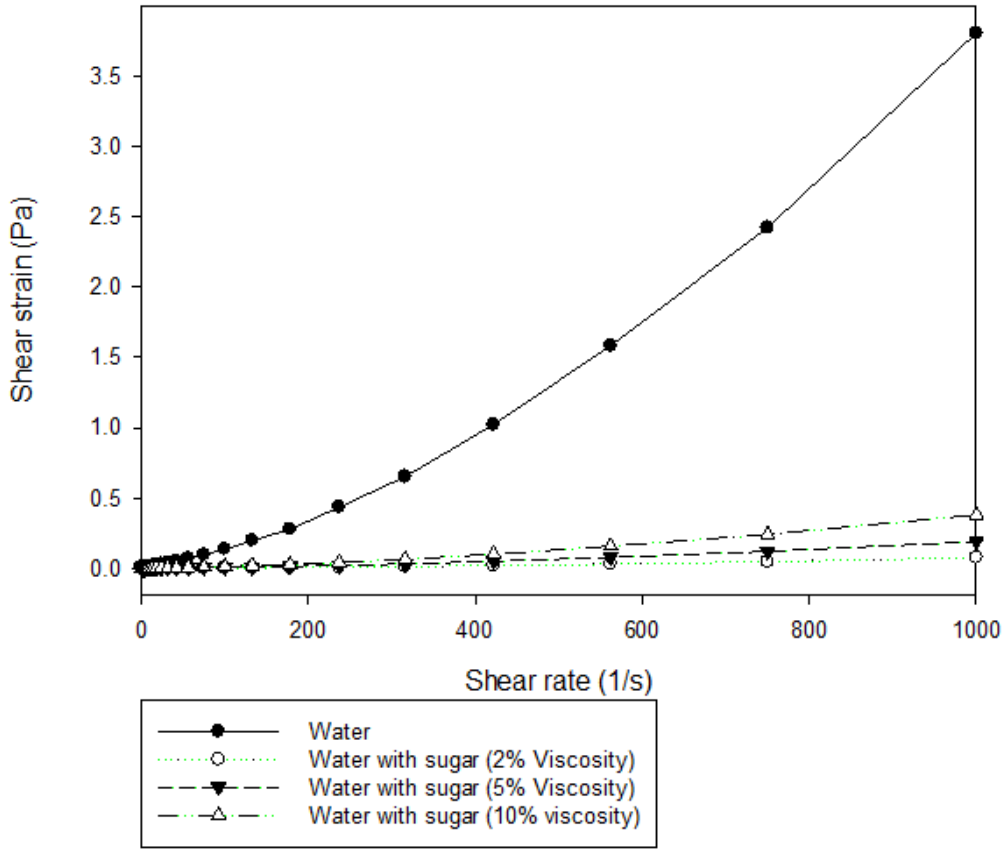

Figure 5.8: Relation of shear strain vs shear rate of water and sugar solution using a rotational rheometer

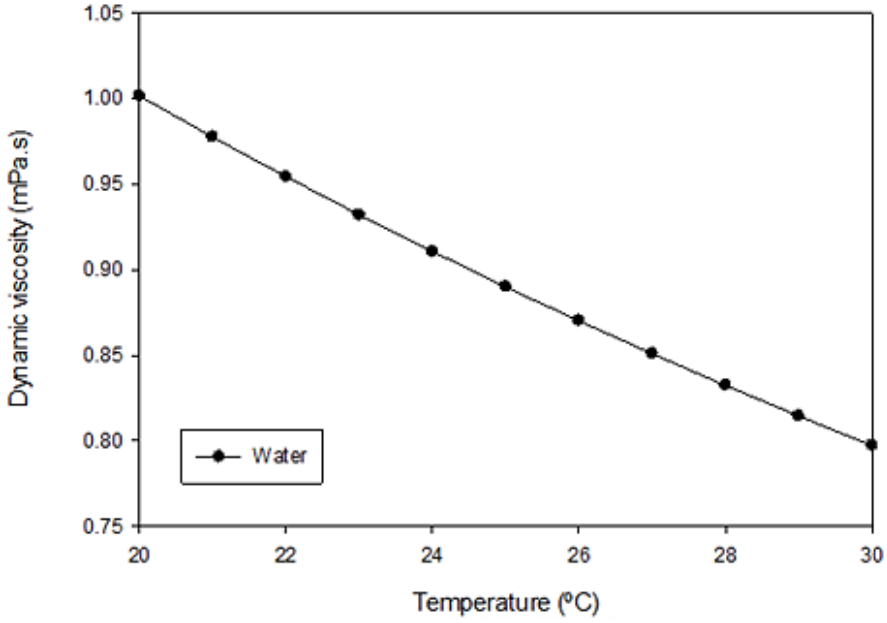

Figure 5.9: Relation of dynamic viscosity of water with temperature

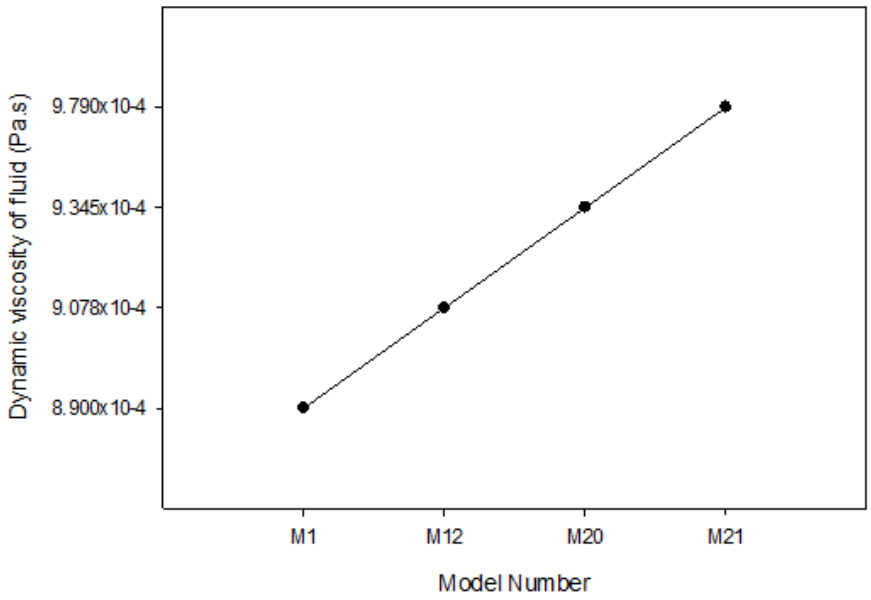

Figure 5.10: Dynamic viscosity of sugar water solution in different earth dam models

Elevation (in cm) of h_1 and h_2 in the phreatic line obtained using Pavlovsky's solutions, experimental models, and numerical models are shown in figure 5.11 and are also mentioned in table 5.9. Figure 5.11 shows elevation in metres on the y-axis while showing the distance in metres from the upstream section of the earth dam on the x-axis.

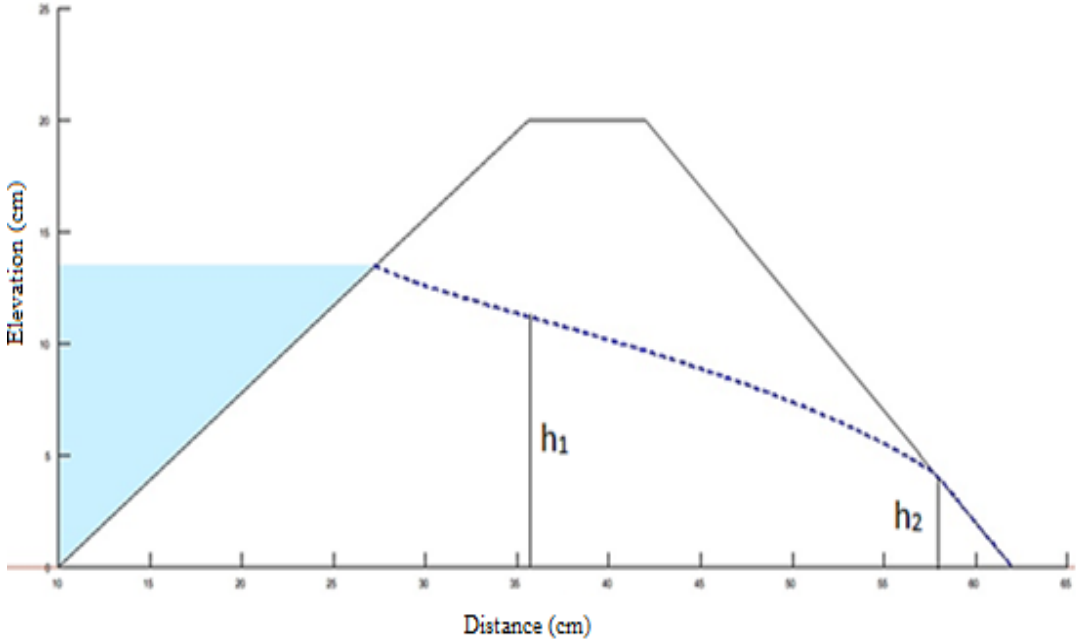

Figure 5.11: h_1 and h_2 of earth dam model-M1.

Table 5.9: Coordinates of h_1 and h_2 of the phreatic line using Pavlovsky solutions

Model No.	Pavlovsky's solutions (cm)		Physical model (cm)		Numerical model (m)	
	h_1	h_2	h_1	h_2	h_1	h_2
M1	11.23	4.027	10.60	3.60	11.23	4.02
M2	11.24	3.129	10.66	2.27	11.24	3.12
M3	12.15	4.748	12.22	4.20	12.15	4.74
M4	12.29	4.193	12.10	4.15	12.29	4.19
M5	13.14	4.260	13.00	4.25	13.14	4.26
M6	11.60	4.000	11.92	4.45	11.60	4.00
M7	11.60	4.380	11.90	4.52	11.60	4.38
M8	11.19	4.400	11.30	4.55	11.19	4.40
M9	12.13	0.000	12.61	1.63	12.13	0.00
M10	12.18	0.000	12.75	1.55	12.18	0.00
M11	11.10	3.800	10.66	3.30	10.70	3.68
M12	11.20	4.028	10.60	3.60	11.20	4.02
M13	10.90	1.500	08.60	0.50	10.90	1.50
M14	10.76	1.568	08.42	0.40	10.76	1.56
M15	10.95	1.425	08.84	0.50	10.95	1.42
M16	11.07	1.388	08.80	0.50	11.07	1.38
M17	11.06	1.122	08.82	0.60	11.06	1.12
M18	11.86	3.677	09.29	3.10	11.86	3.67
M19	12.20	3.517	10.80	3.00	12.20	3.51
M20	11.26	3.970	10.50	2.80	11.26	3.97
M21	11.22	3.968	10.60	2.85	11.22	3.96
M22	10.43	3.460	10.39	3.12	10.43	3.46
M23	10.25	3.340	10.10	3.26	10.25	3.34
M24	10.24	3.330	10.08	3.21	10.24	3.33

Note: Physical model was scaled down to 1:100. i.e. 1cm in the physical model represents 1m in the numerical model.

The soils used in the construction of the earth dams' model were examined in X-Ray Diffraction (XRD) machine. Figure 5.12 shows the intensity vs diffraction angle (2Ɵ)

results for soil used in the building of homogeneous earth dam models and in the shell of the earth dam in non-homogeneous earth dam models. While figure 5.13 shows the XRD results for soil material used in the core of non-homogeneous earth dam models. As the diffraction angle (2Θ) was at 26.715 with an intensity of 100 per cent and the empirical formula was O_2Si, silicon oxide (SiO_2) was the predominant chemical compound in the soil (Shell). The values for h, k, and l were (0,1,1), while the distance between planes (d) was 3.33420 Aº. Quartz, with the chemical formula SiO_2 and the empirical formula O_2Si, was the predominant chemical constituent found in the soil (core). The hexagonal crystal system of the lattice had an angle (2Θ) of 26.64 at 100 per cent intensity. The lattice's h, k, and l values were (0,1,1), and the spacing between planes (d) was 3.34353 Aº.

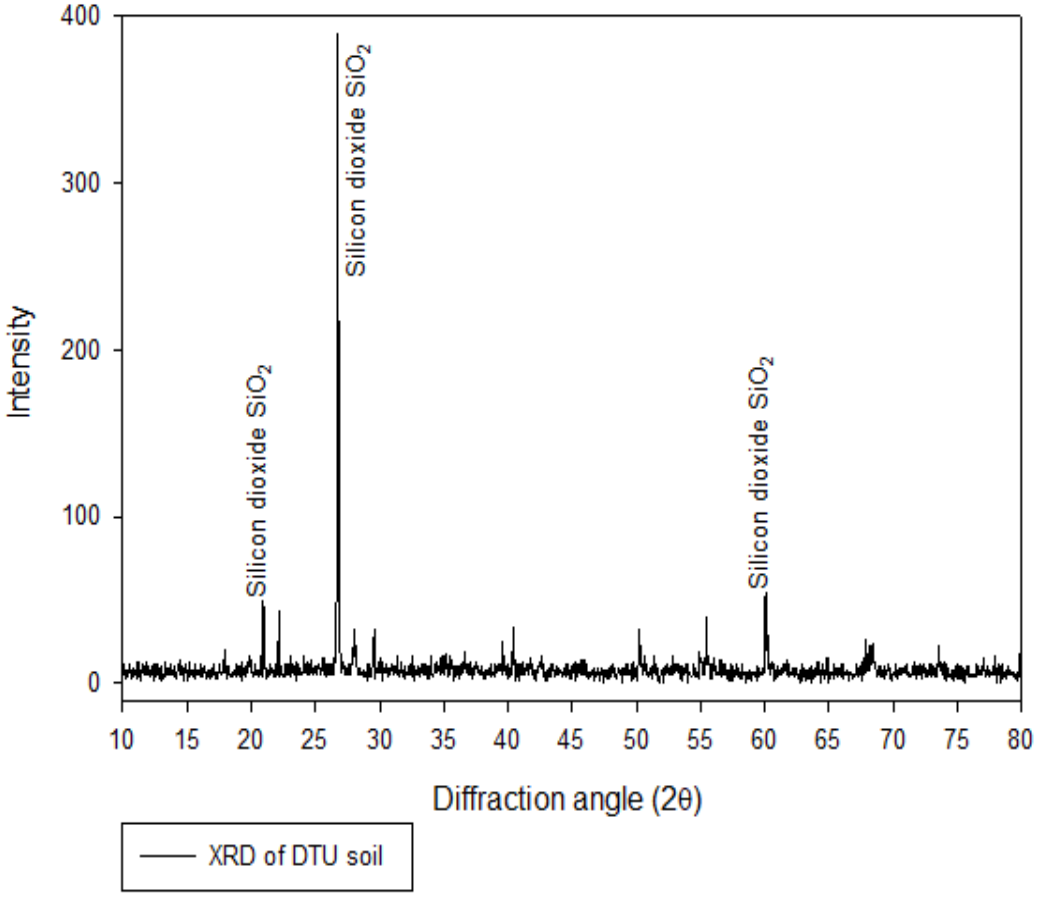

Figure 5.12: XRD of Soil used in the shell of earth dam models

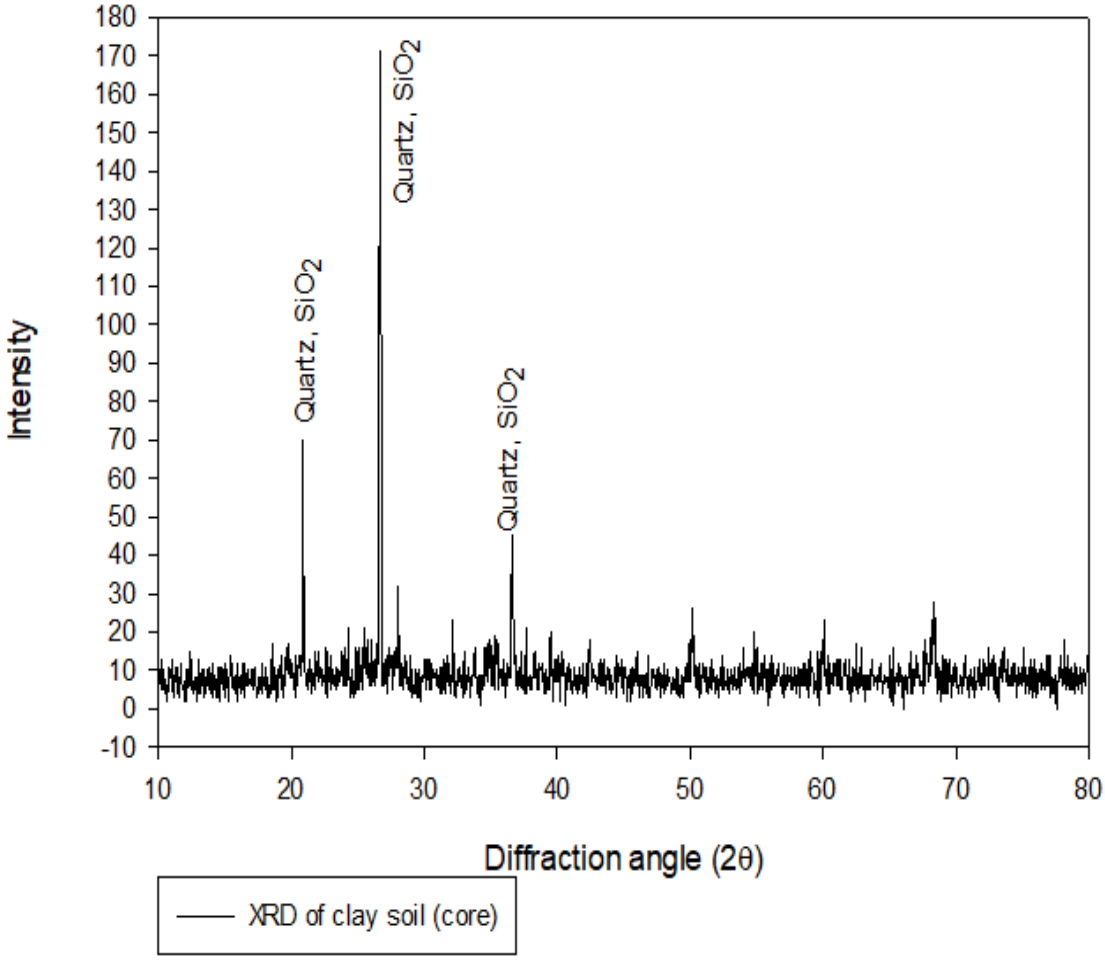

Figure 5.13: XRD of Clayey soil used in the core of the earth dam models

5.1.1 Contours of Seep/w modelling

5.1.1.1 Pore-water pressure

Figures 5.14 to 5.37 show the contours of pore-water pressure in kPa for models M1 to M24, where the elevation of the dam was shown in metres on the y-axis while the distance from upstream heel in metres on the x-axis. The variation in pore-water pressure as a function of location is shown. The pressure is negative above the phreatic line (shown with a dotted line) and positive below. These figures represents the water pressure value in kPa, which shows the pressure on soil particle due to water in different zones of the earth dam. These pressure contours are important as they play a crucial role in maintaining stability of an earth dam.

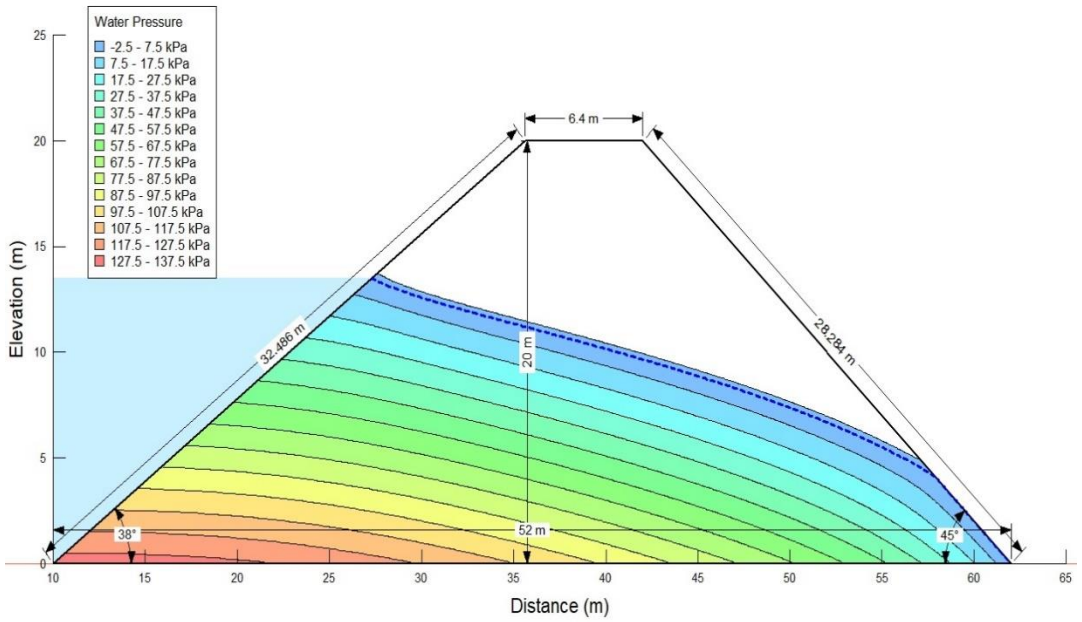

Figure 5.14: Pore water pressure in M1

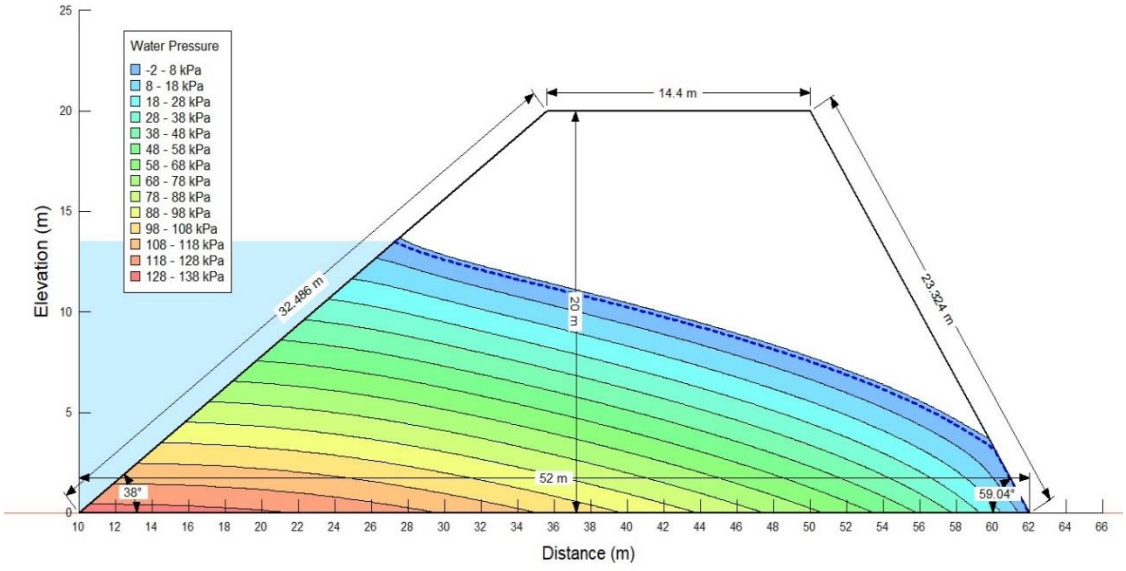

Figure 5.15: Pore water pressure in M2

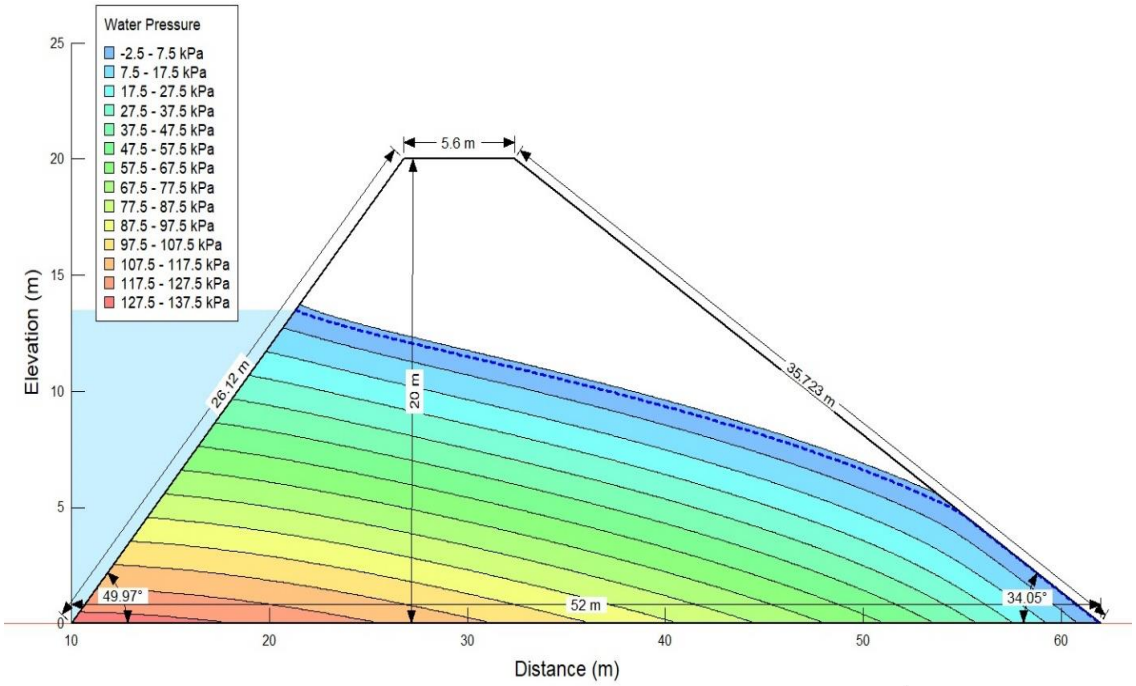

Figure 5.16: Pore water pressure in M3

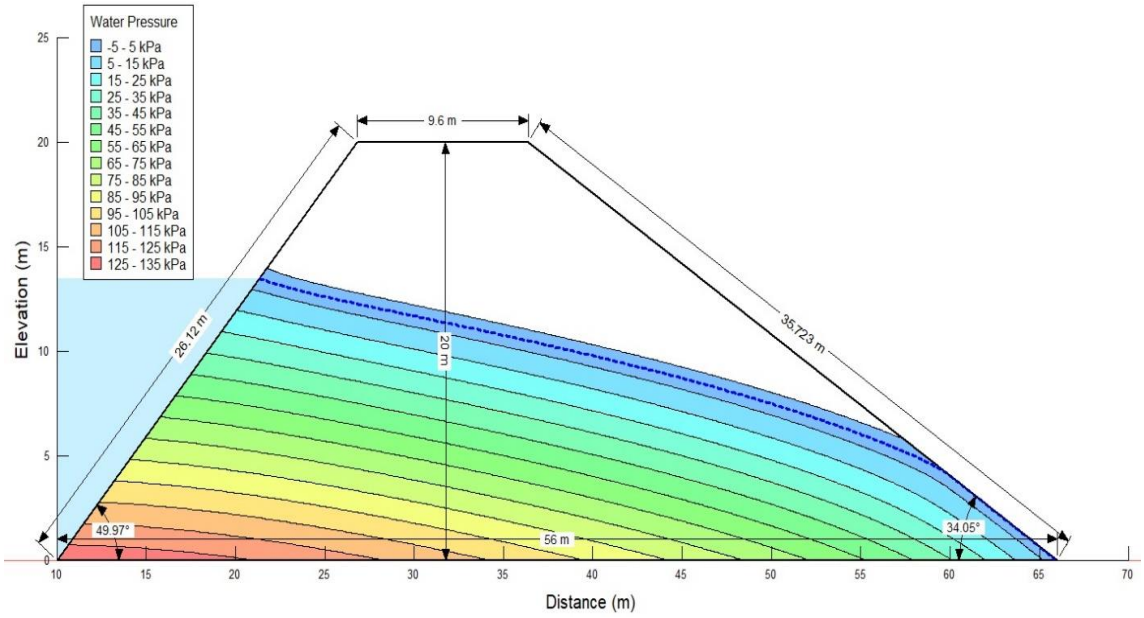

Figure 5.17: Pore water pressure in M4

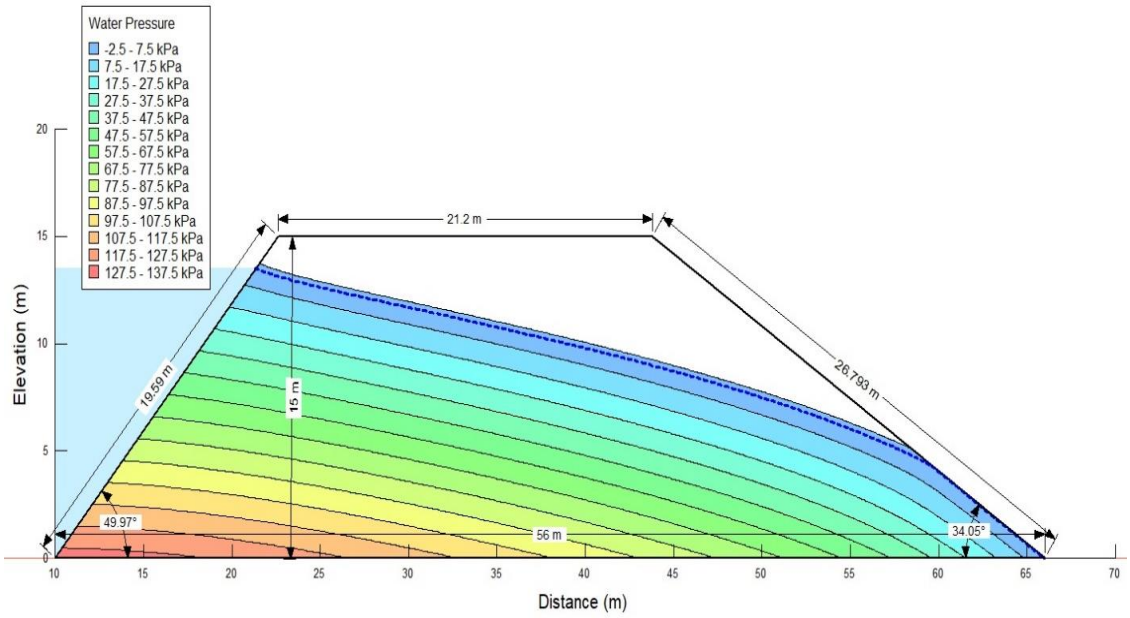

Figure 5.18: Pore water pressure in M5

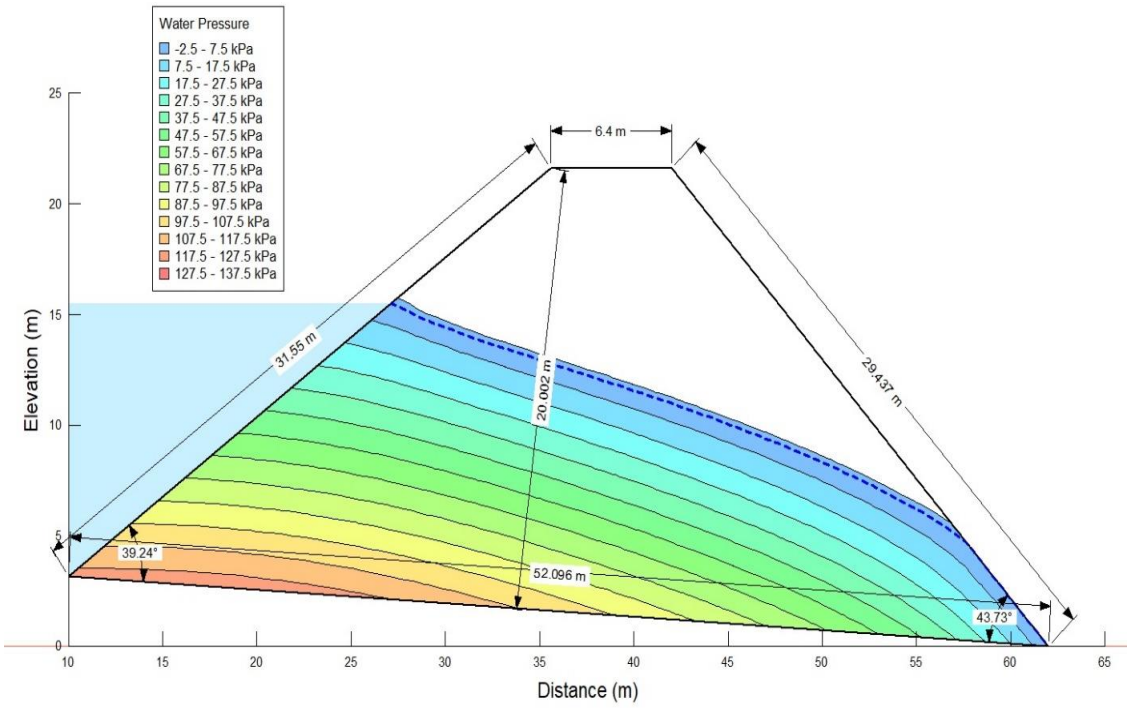

Figure 5.19: Pore water pressure in M6

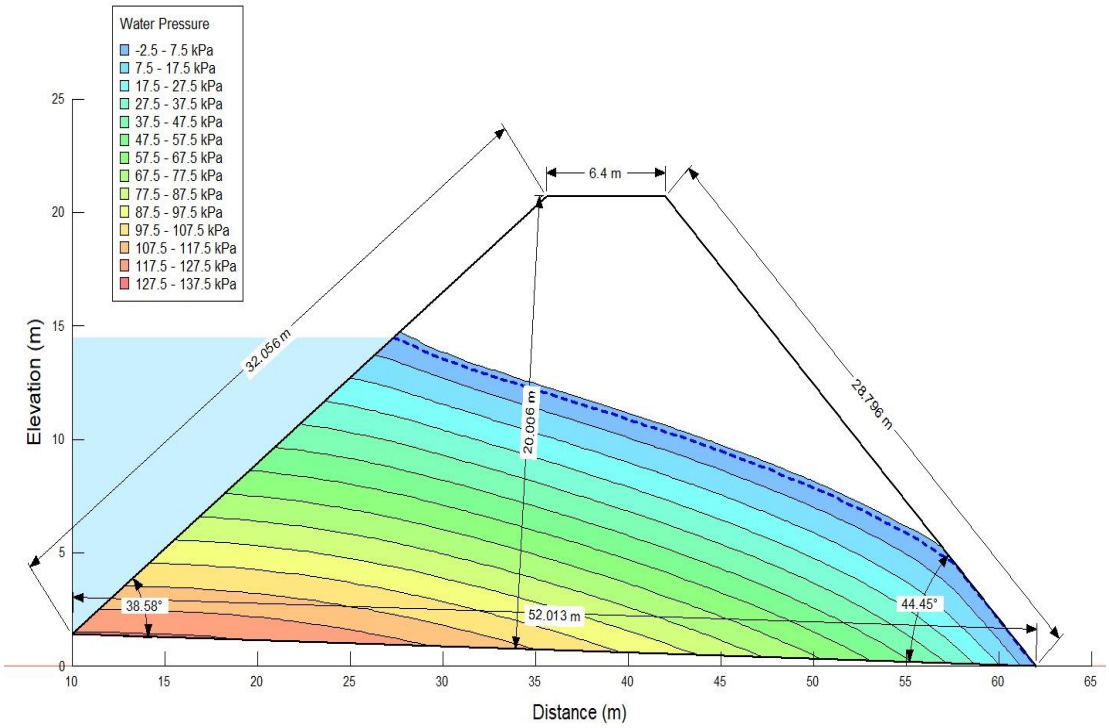

Figure 5.20: Pore water pressure in M7

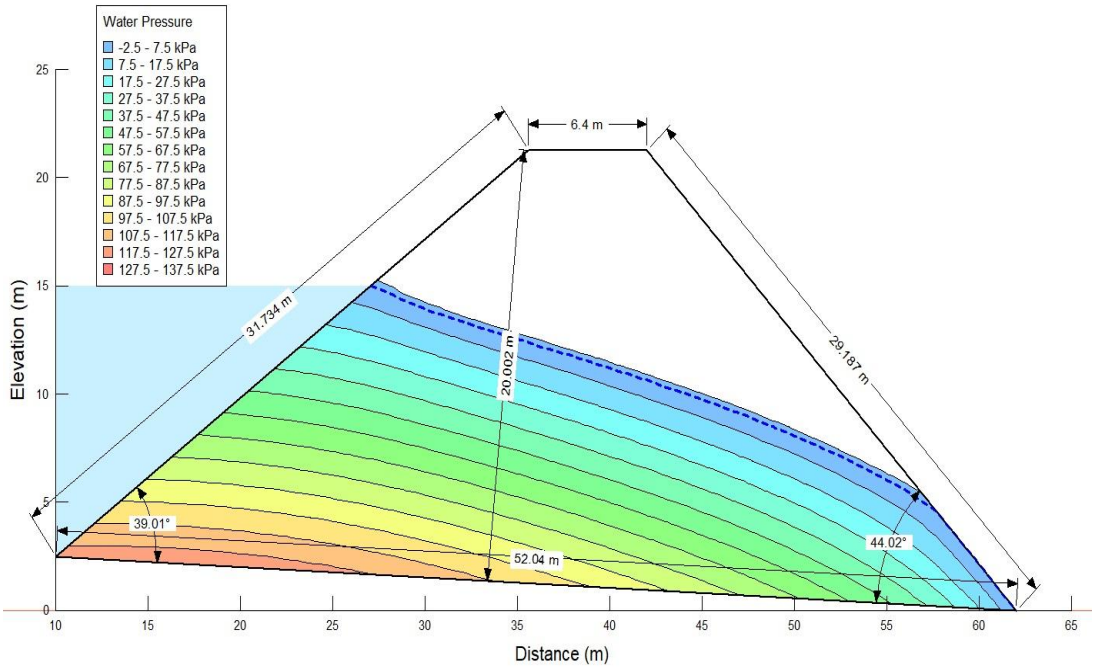

Figure 5.21: Pore water pressure in M8

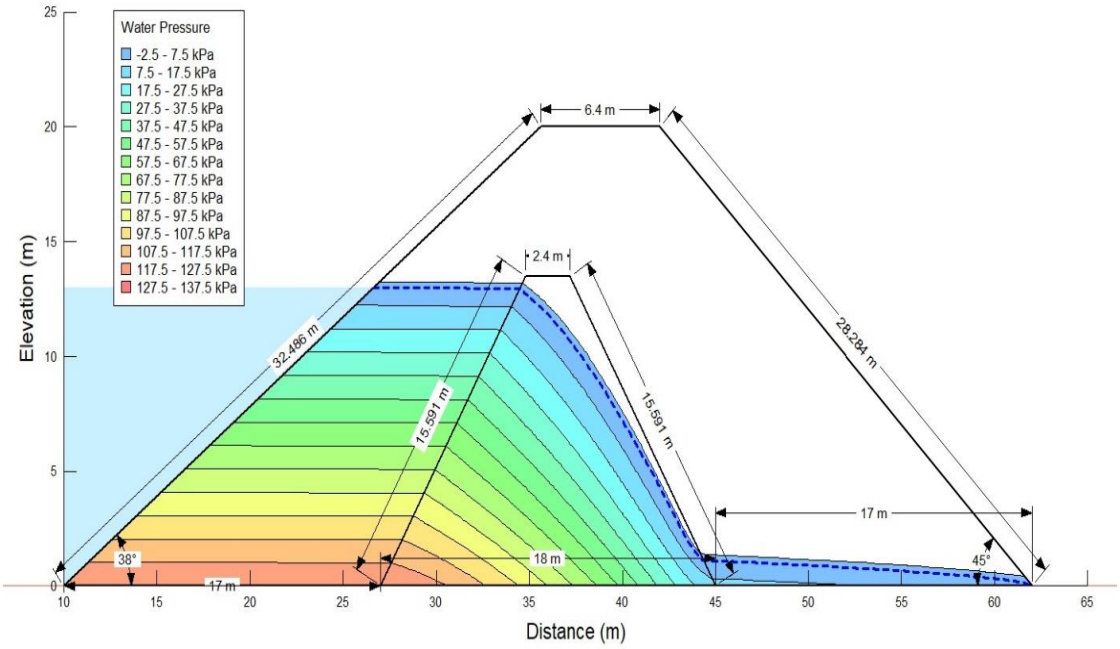

Figure 5.22: Pore water pressure in M9

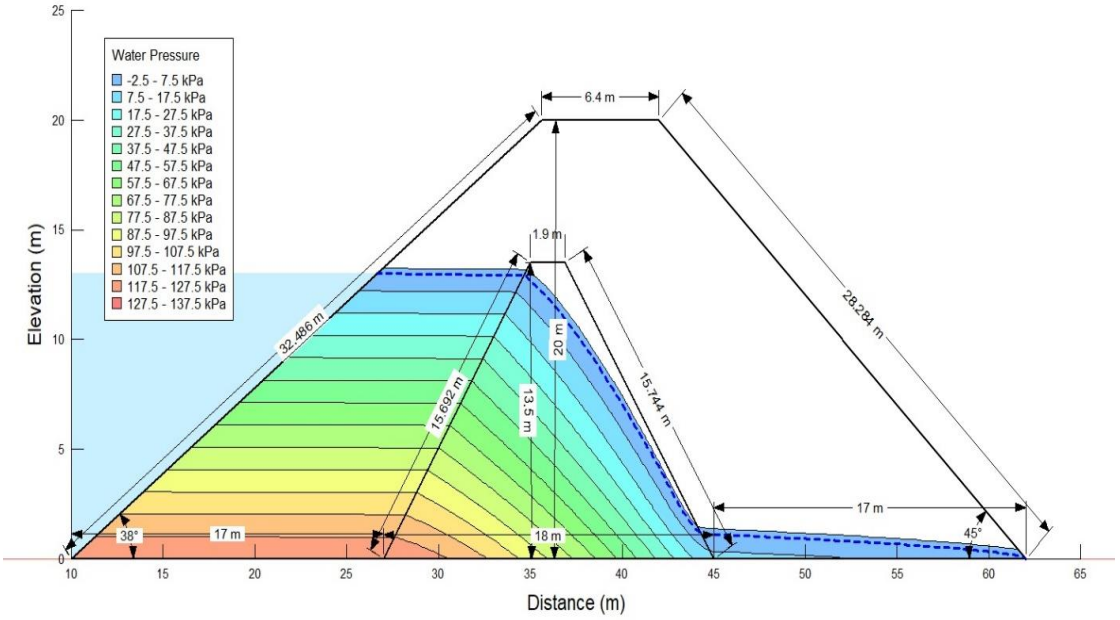

Figure 5.23: Pore water pressure in M10

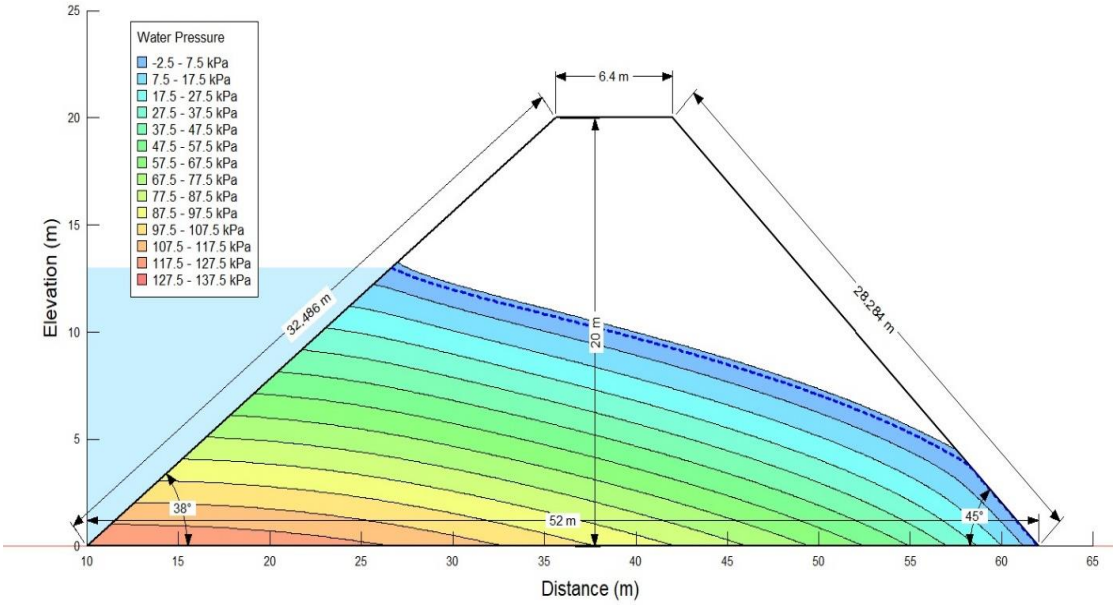

Figure 5.24: Pore water pressure in M11

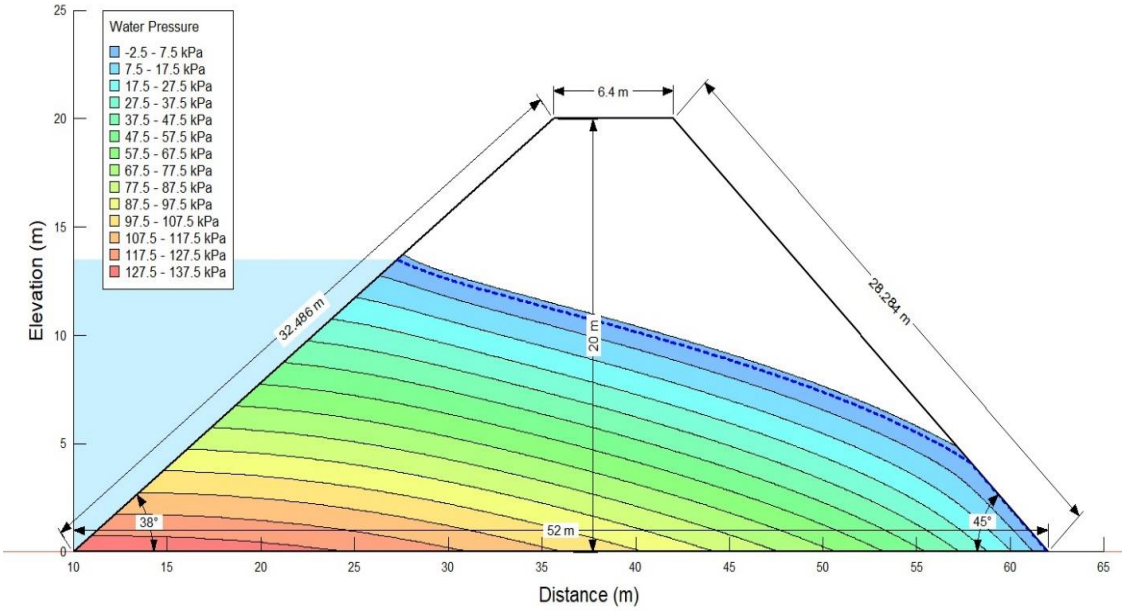

Figure 5.25: Pore water pressure in M12

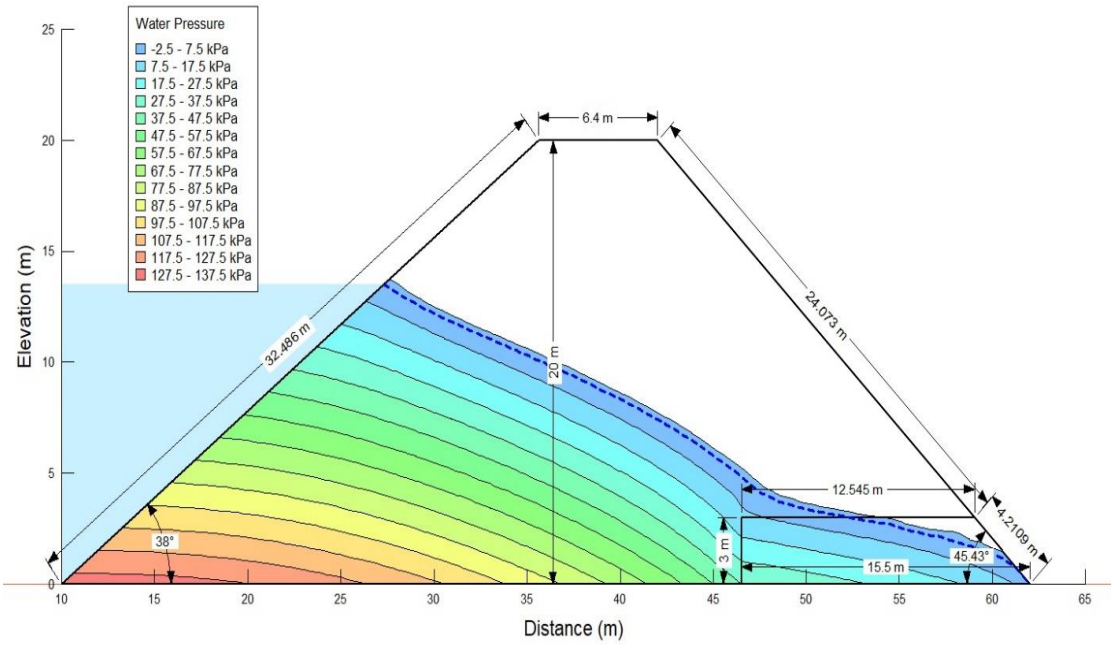

Figure 5.26: Pore water pressure in M13

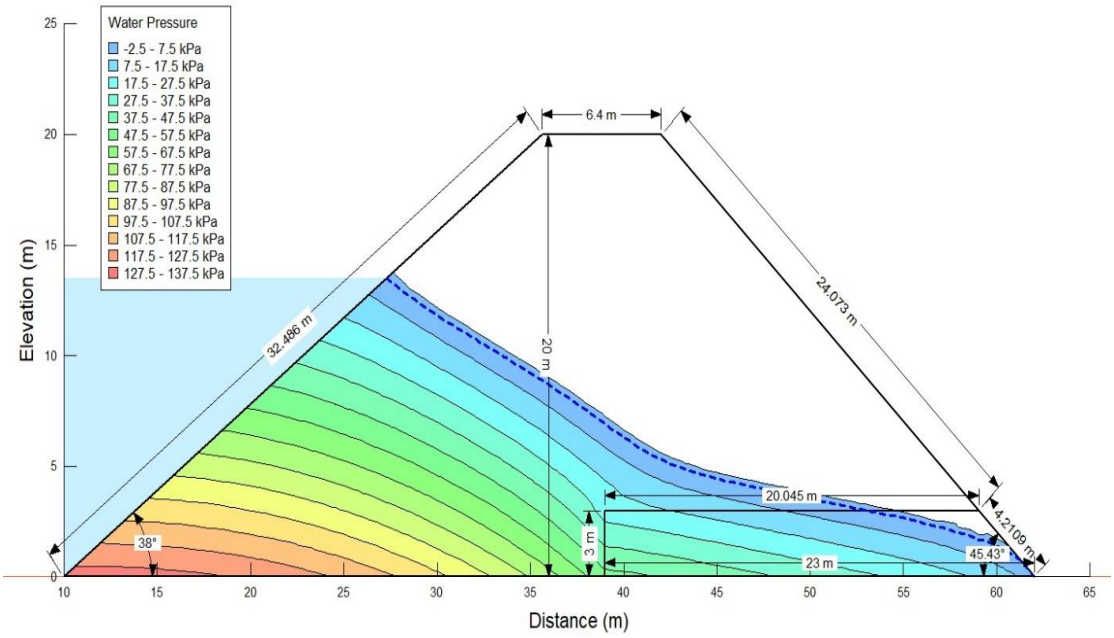

Figure 5.27: Pore water pressure in M14

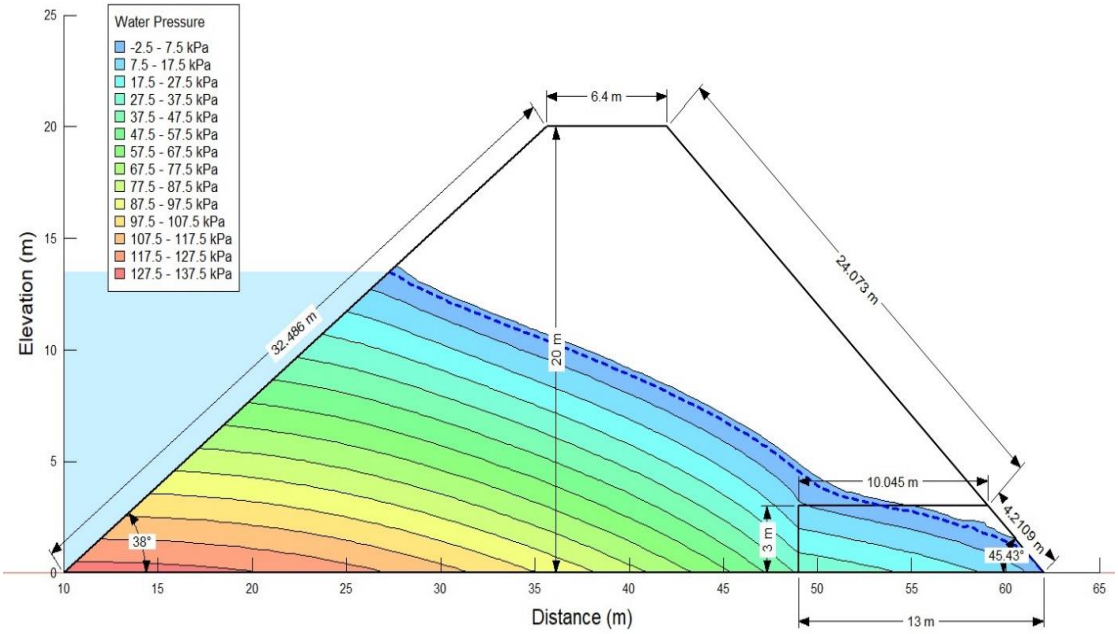

Figure 5.28: Pore water pressure in M15

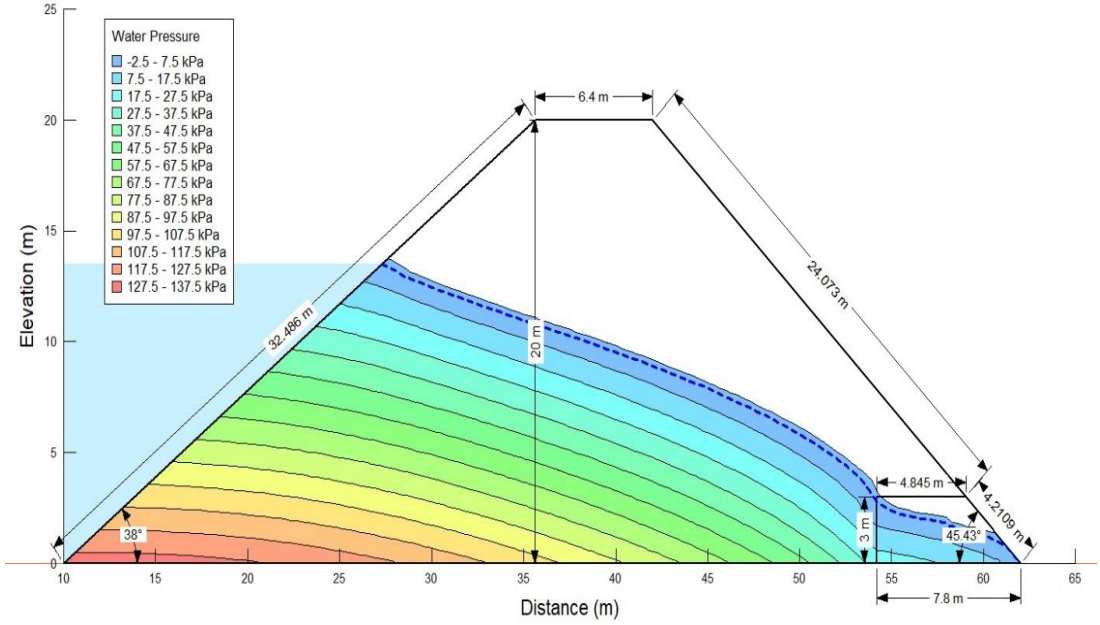

Figure 5.29: Pore water pressure in M16

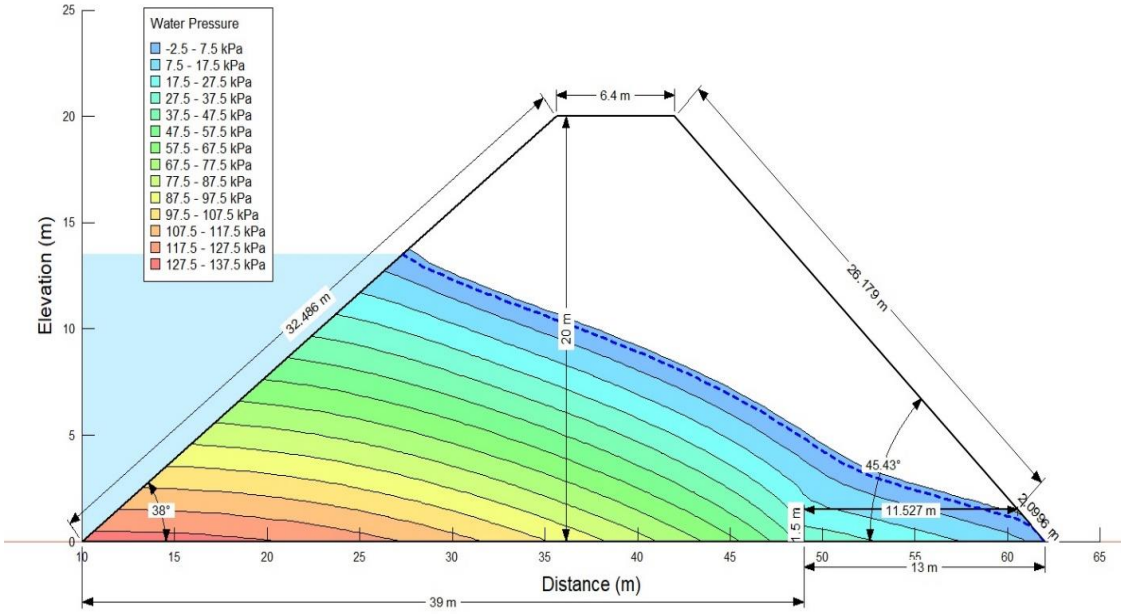

Figure 5.30: Pore water pressure in M17

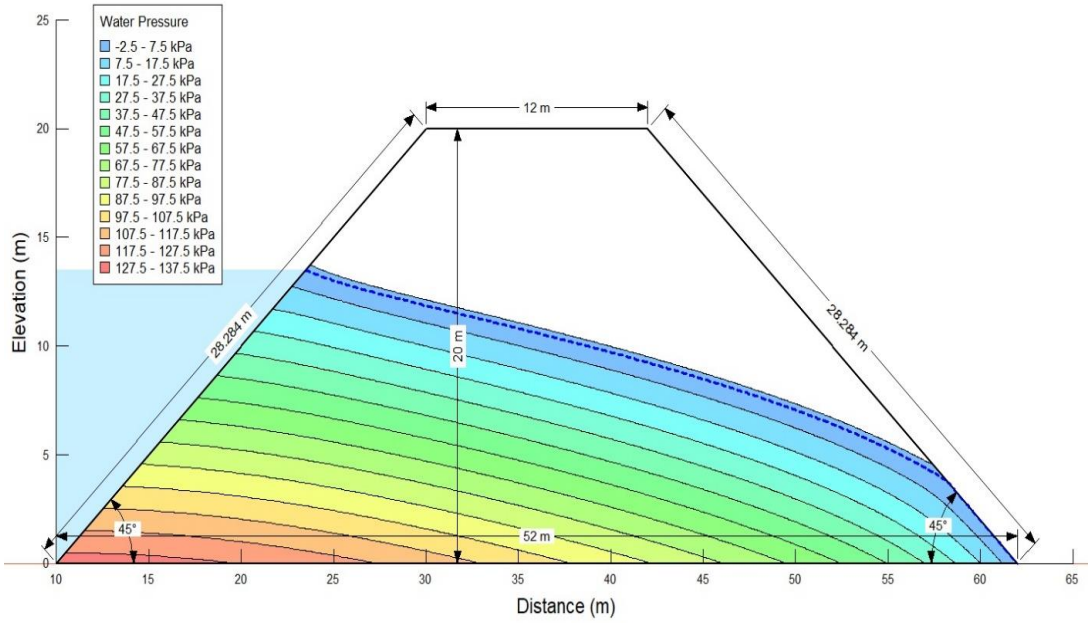

Figure 5.31: Pore water pressure in M18

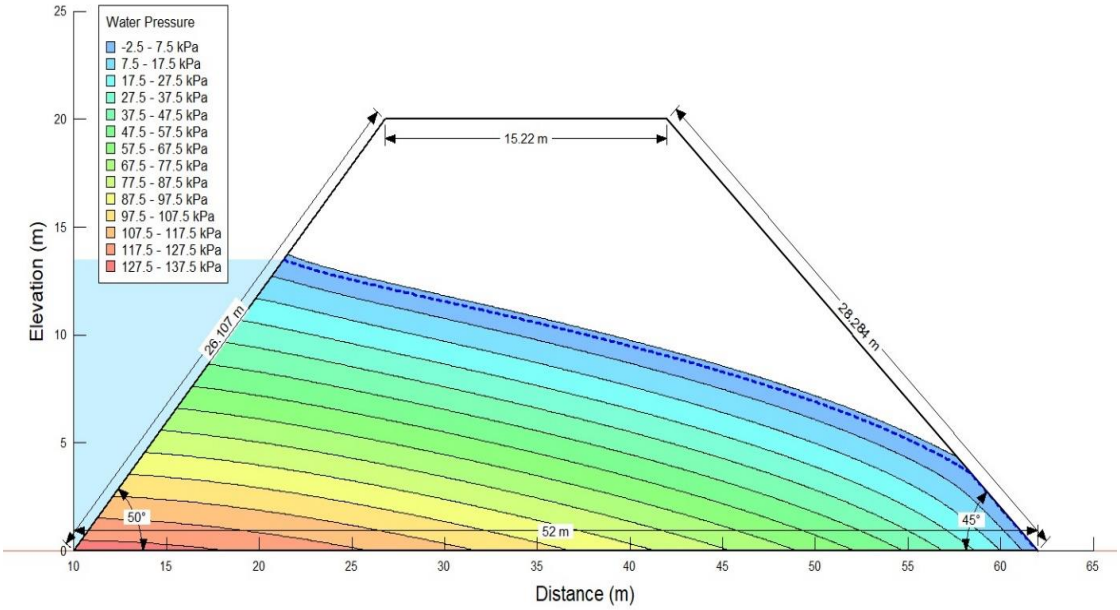

Figure 5.32: Pore water pressure in M19

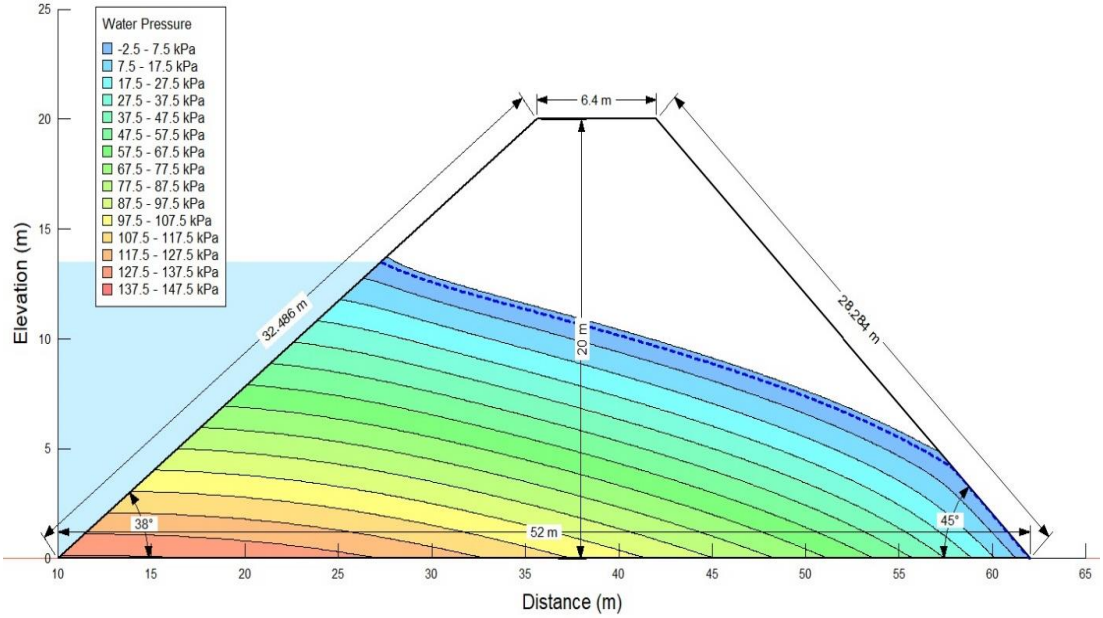

Figure 5.33: Pore water pressure in M20

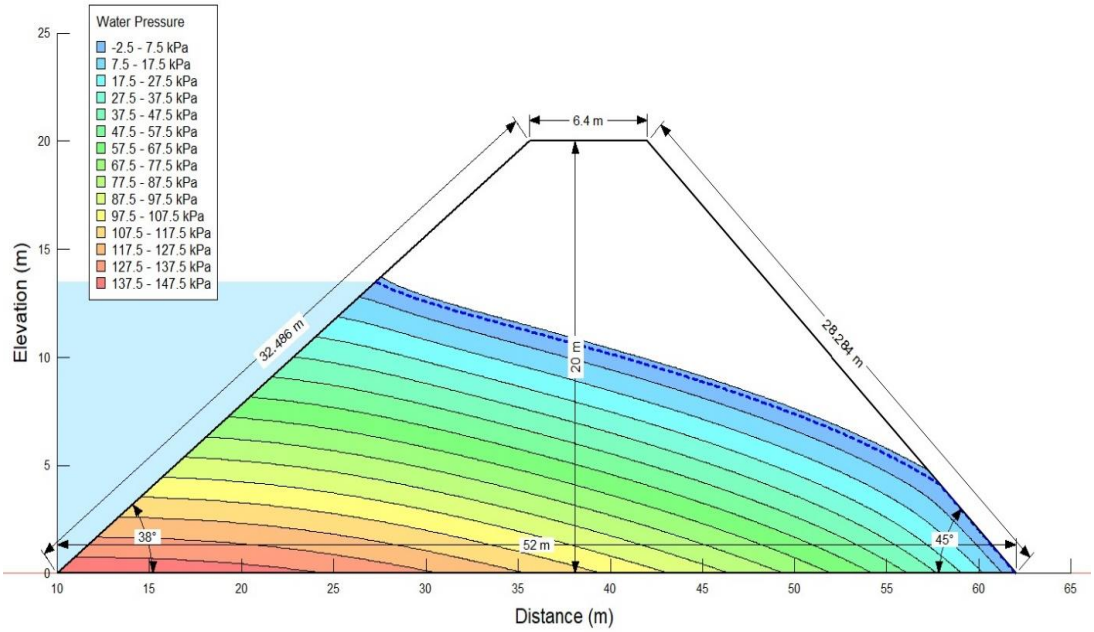

Figure 5.34: Pore water pressure in M21

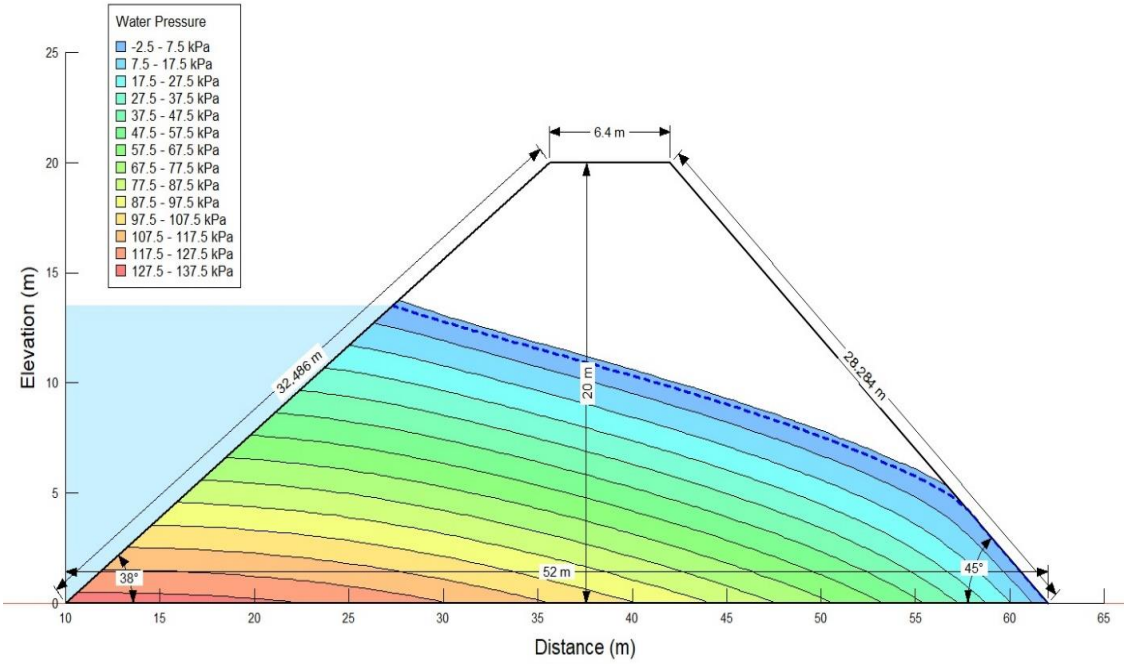

Figure 5.35: Pore water pressure in M22

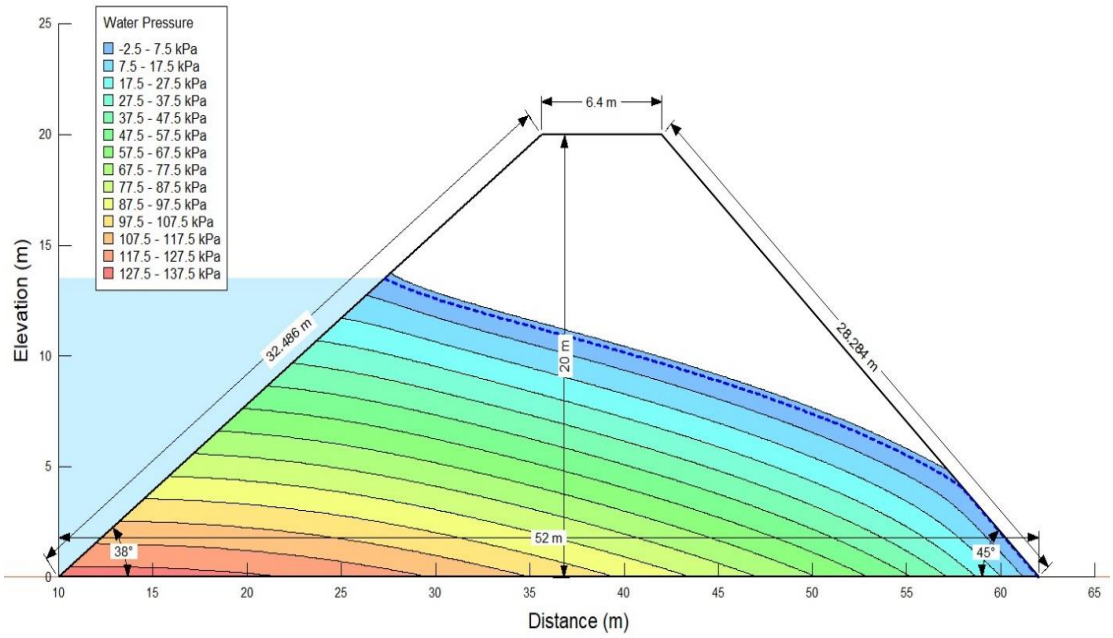

Figure 5.36: Pore water pressure in M23

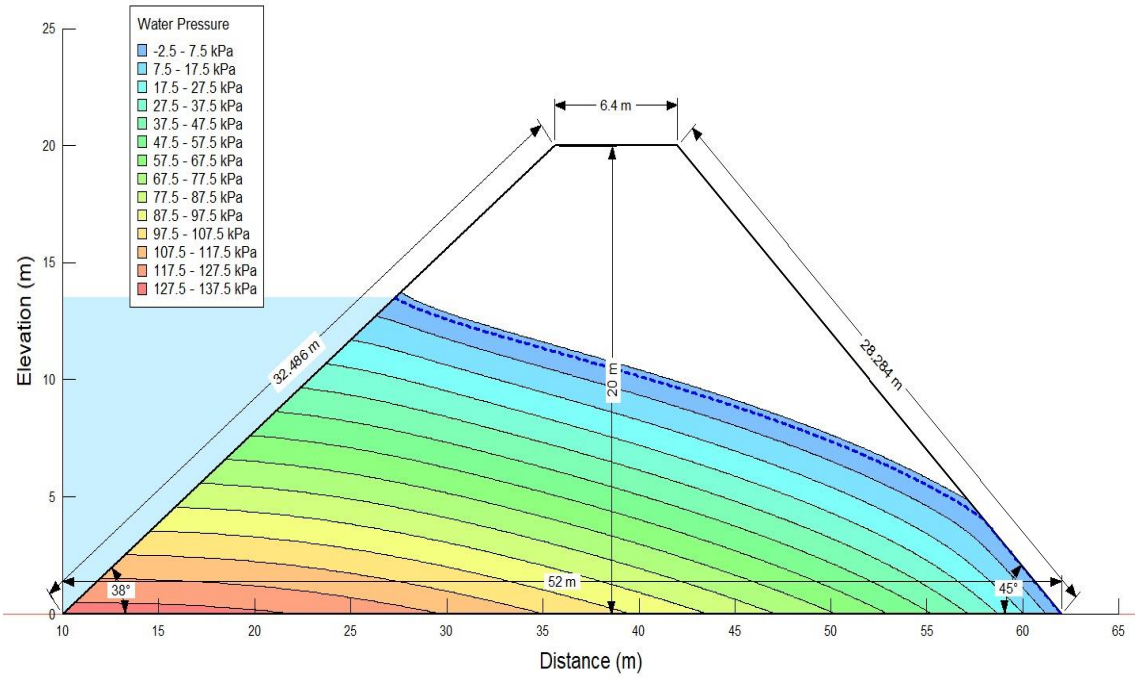

Figure 5.37: Pore water pressure in M24

5.1.1.2 Pressure head

Figures 5.38 to 5.61 show the contours of the water pressure head in metre for models M1 to M24, where the elevation of the dam was shown in metres on the y-axis while the distance from upstream heel in metres on the x-axis. The pressure variation in terms of location is depicted. The pressure is negative above the phreatic line (shown with a dotted line) and positive below. These figures represents the water pressure head (P/ρg) value in kPa, which represents the pressure head on soil particle due to water in different zones of the earth dam. These pressure head contours are important as they play a cruicual role in maintaining stability of an earth dam.

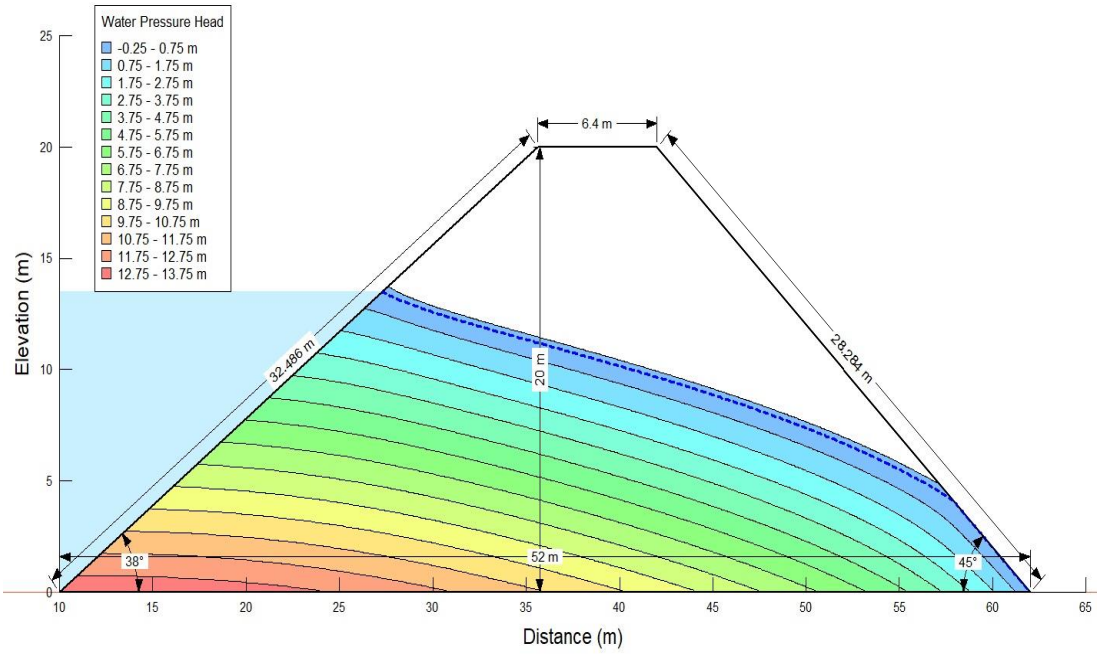

Figure 5.38: Water pressure head in M1

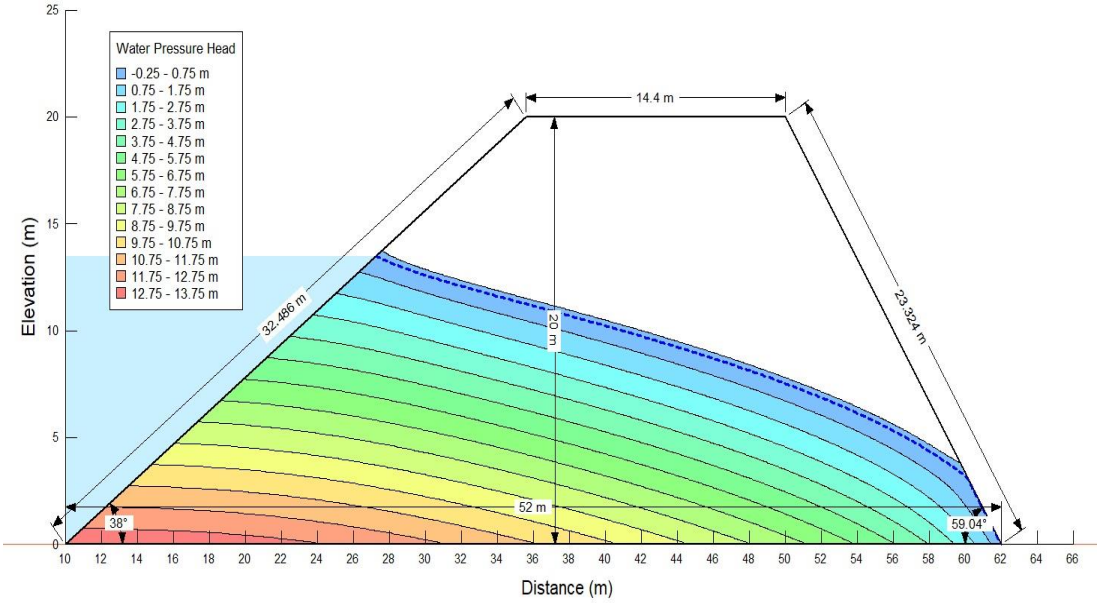

Figure 5.39: Water pressure head in M2

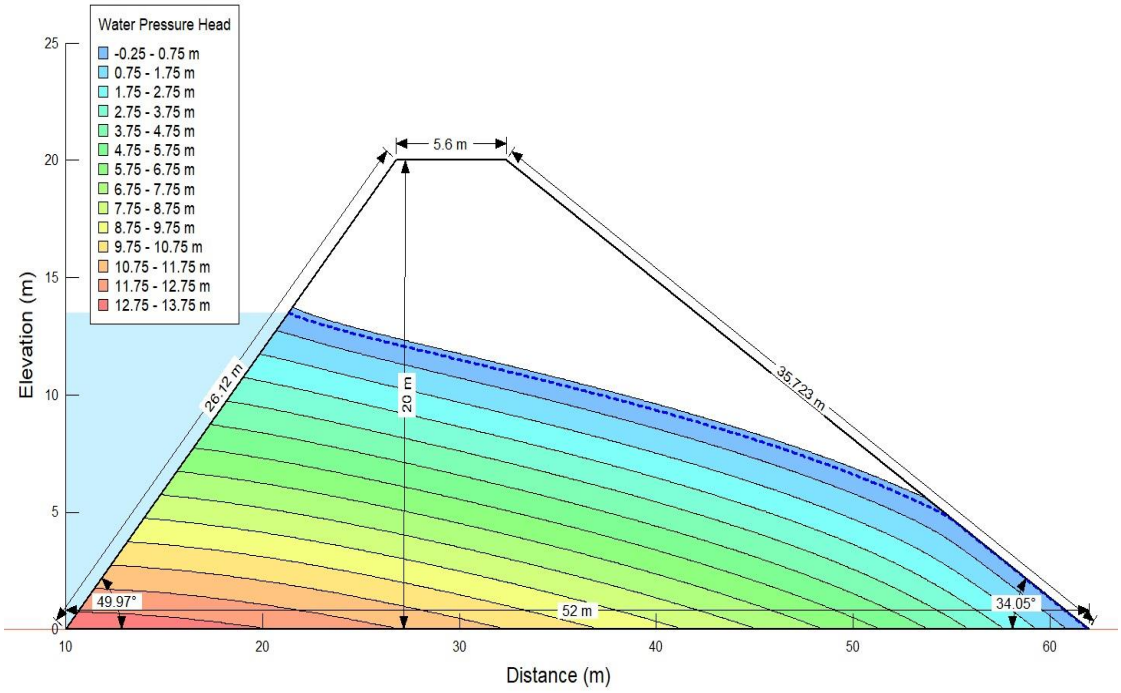

Figure 5.40: Water pressure head in M3

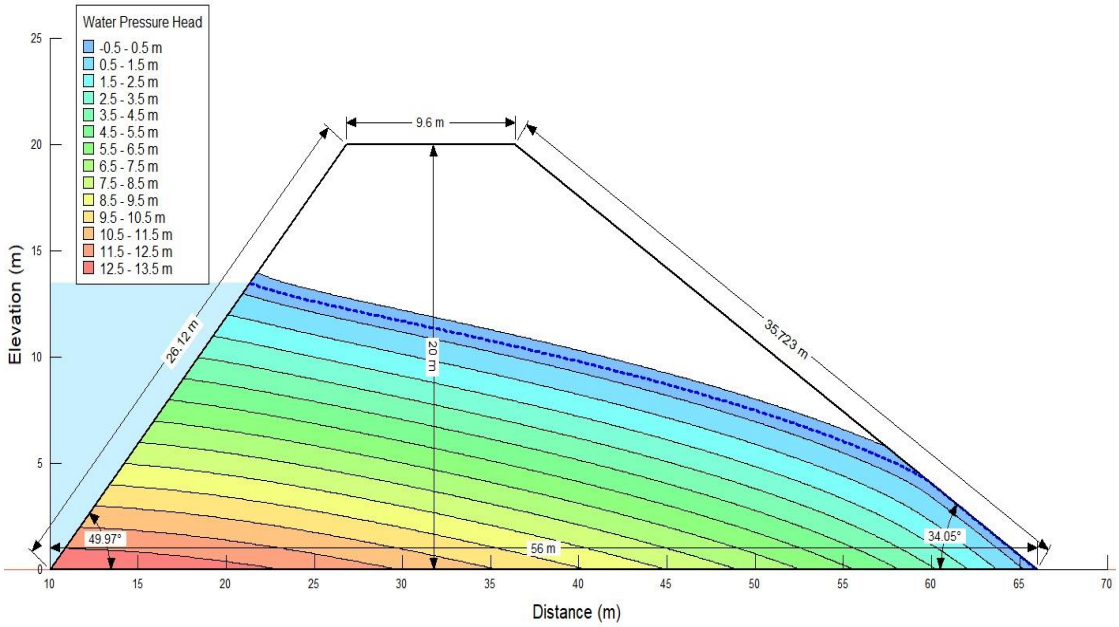

Figure 5.41: Water pressure head in M4

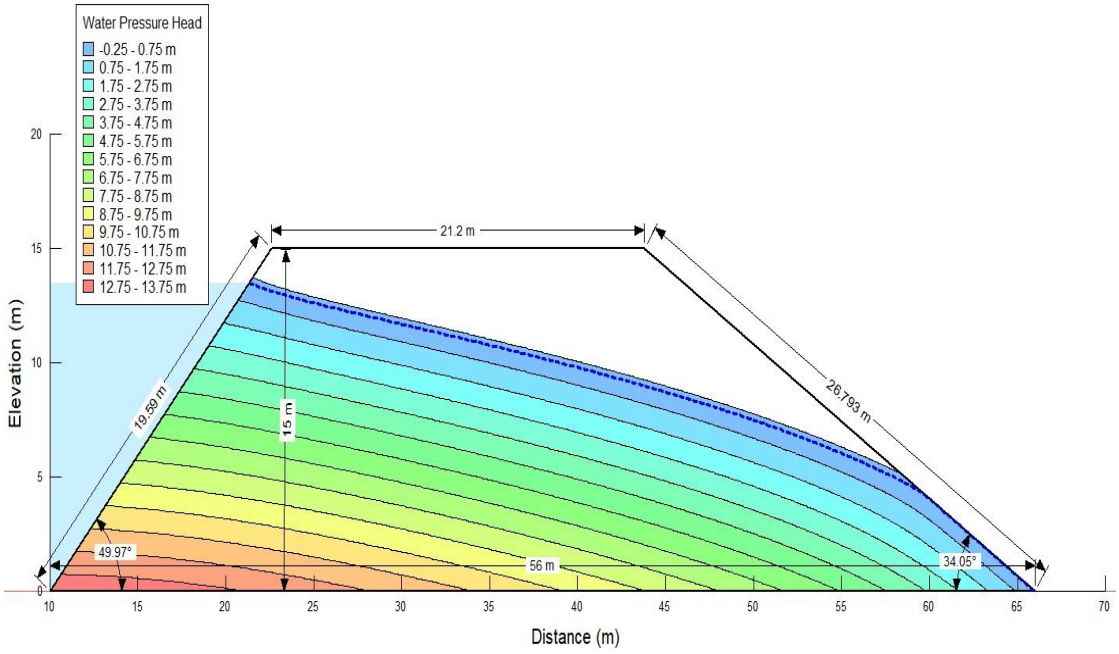

Figure 5.42: Water pressure head in M5

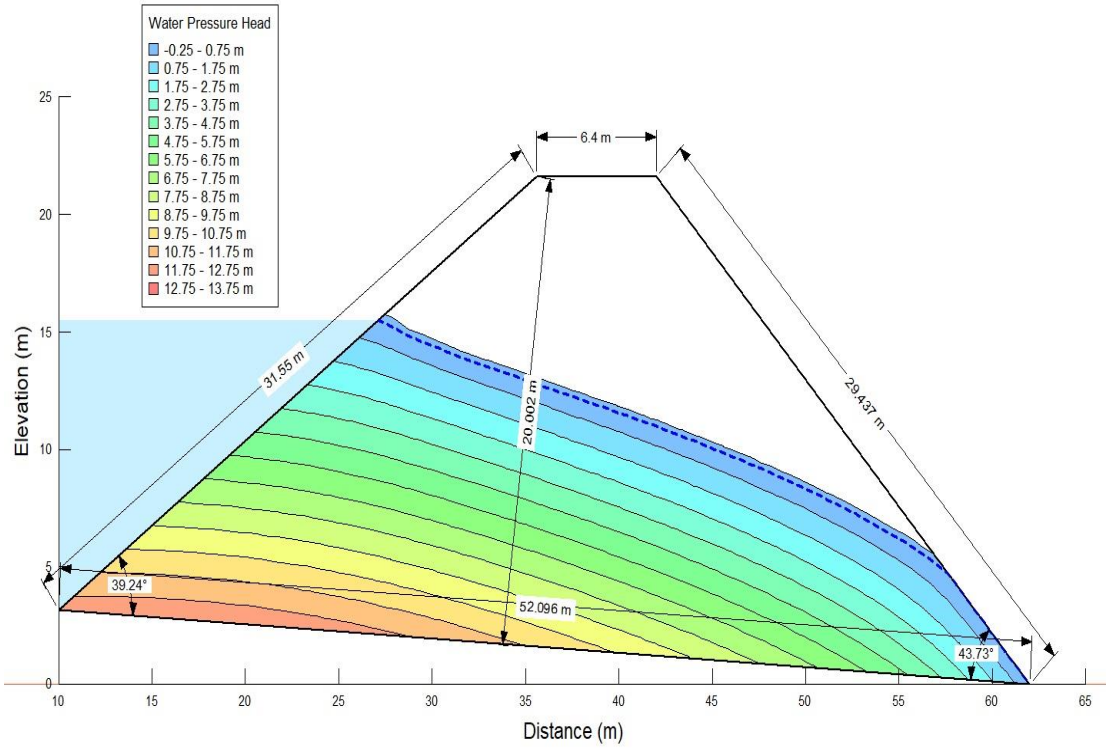

Figure 5.43: Water pressure head in M6

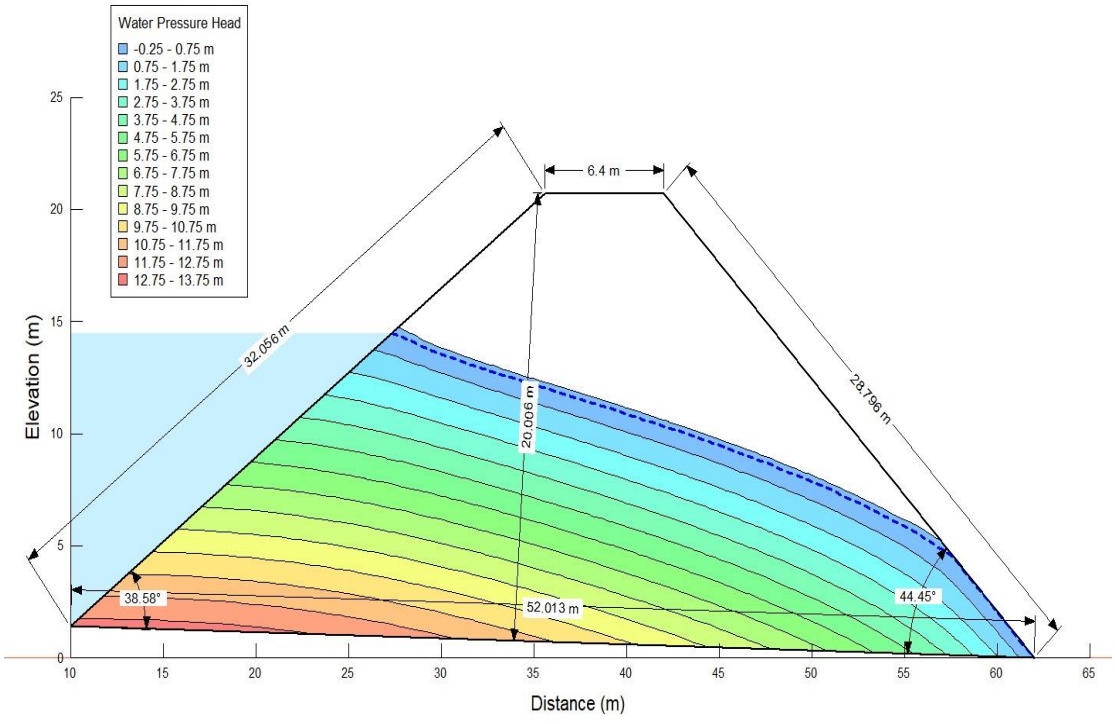

Figure 5.44: Water pressure head in M7

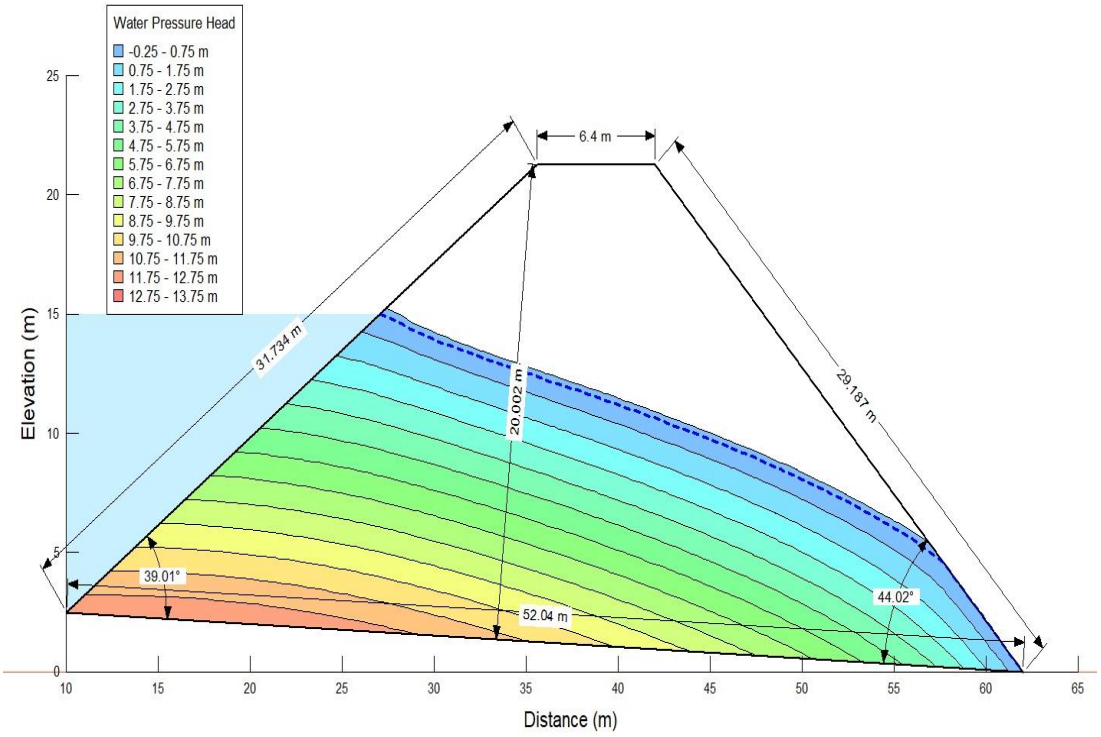

Figure 5.45: Water pressure head in M8

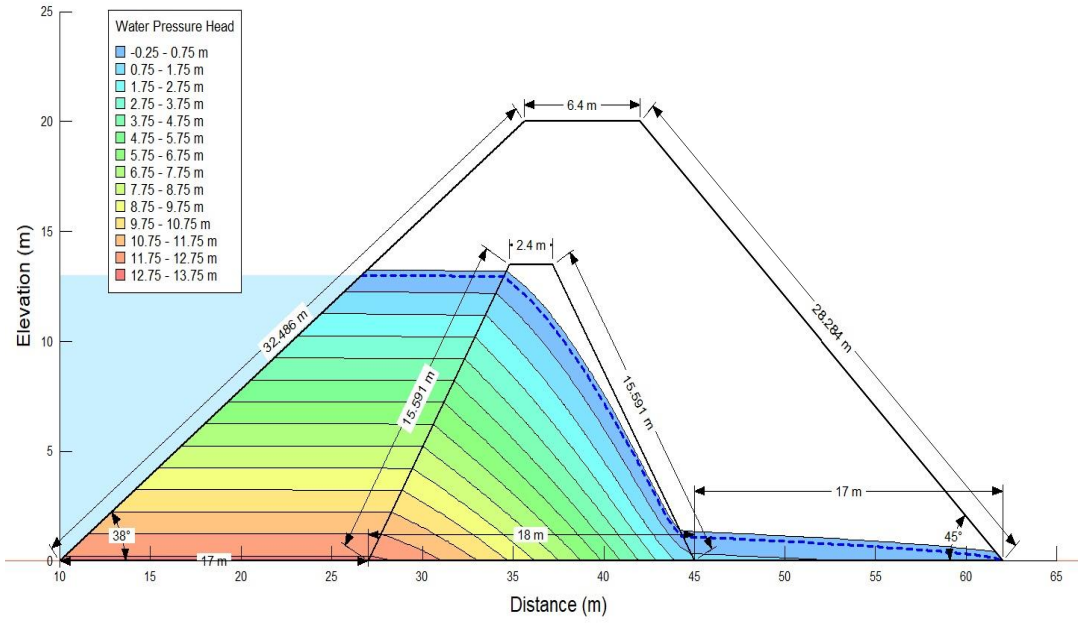

Figure 5.46: Water pressure head in M9

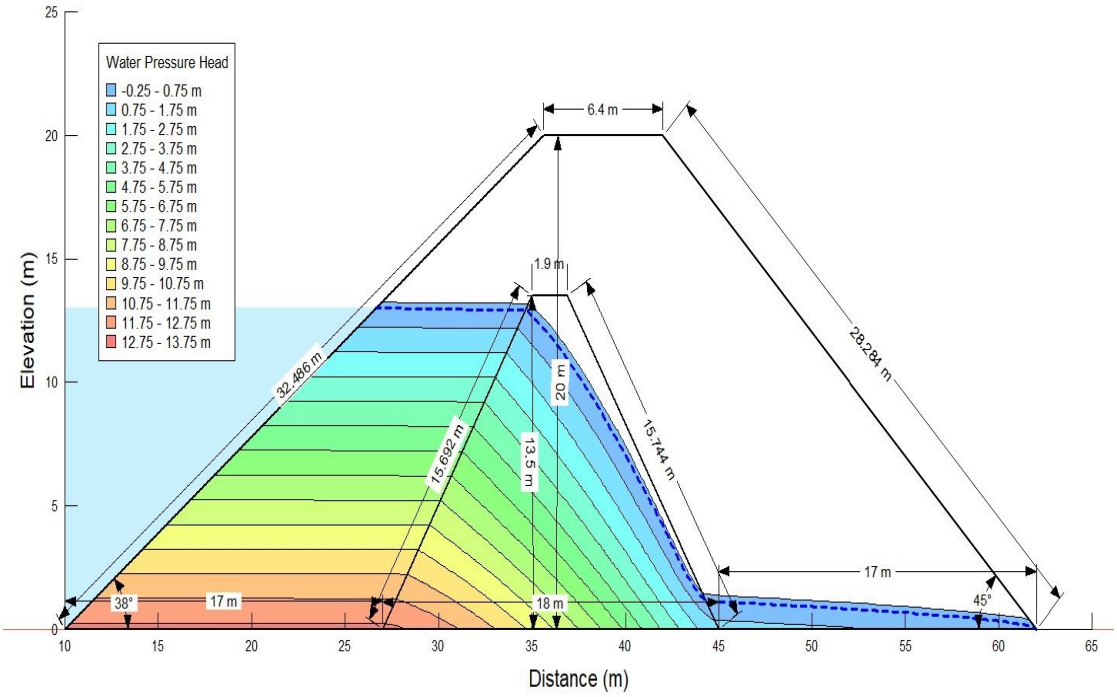

Figure 5.47: Water pressure head in M10

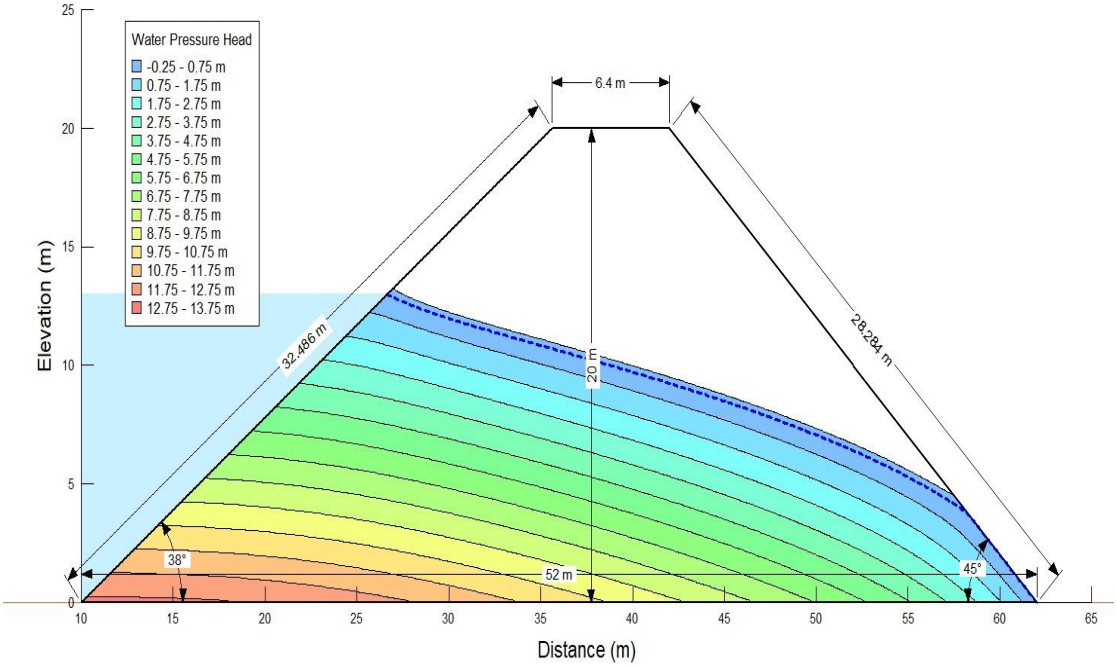

Figure 5.48: Water pressure head in M11

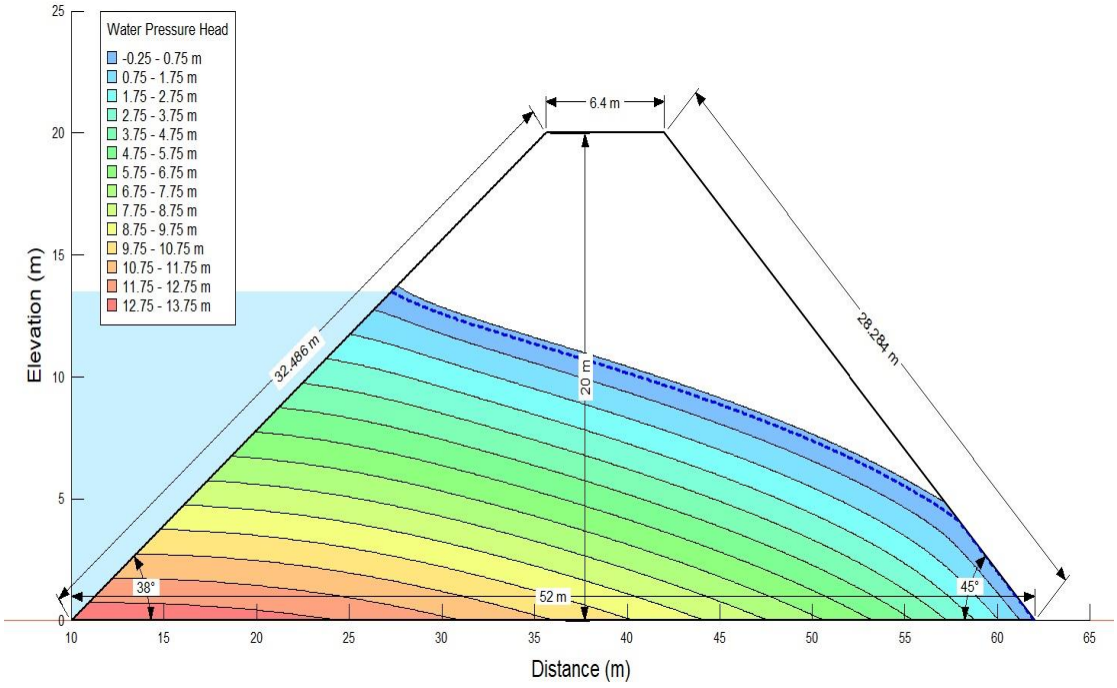

Figure 5.49: Water pressure head in M12

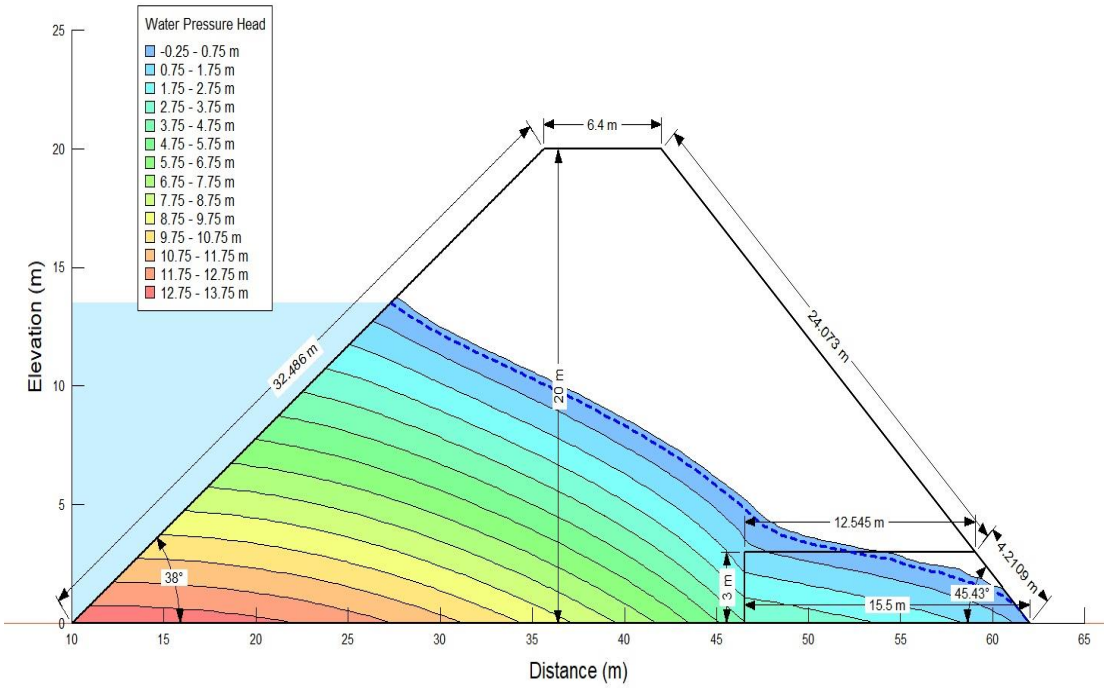

Figure 5.50: Water pressure head in M13

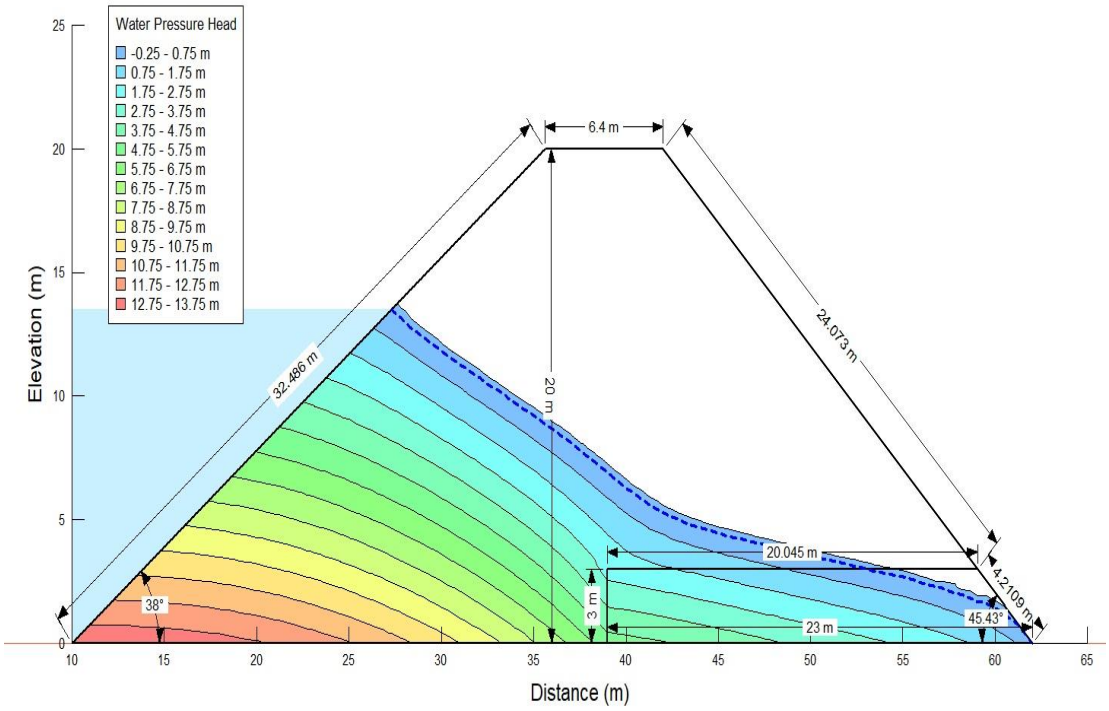

Figure 5.51: Water pressure head in M14

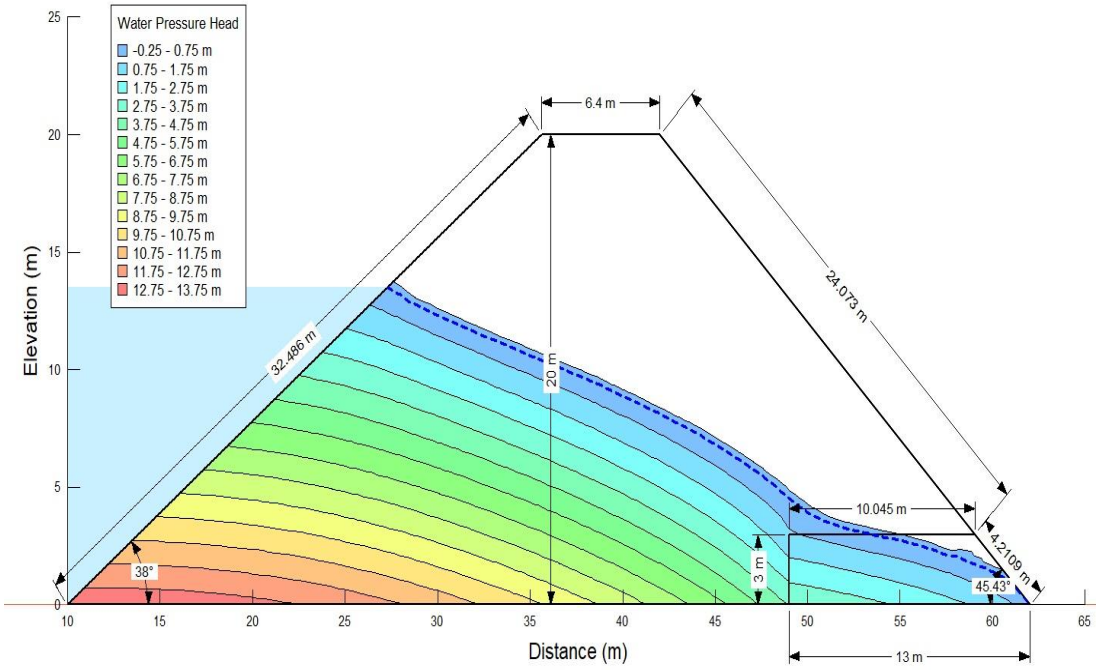

Figure 5.52: Water pressure head in M15

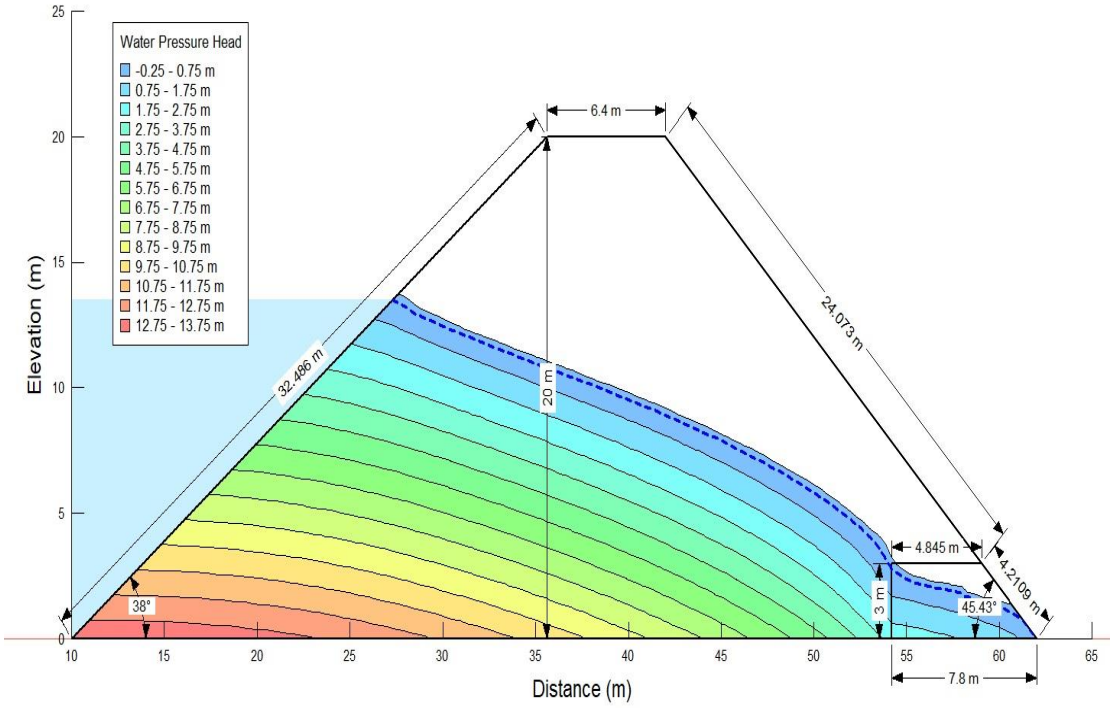

Figure 5.53: Water pressure head in M16

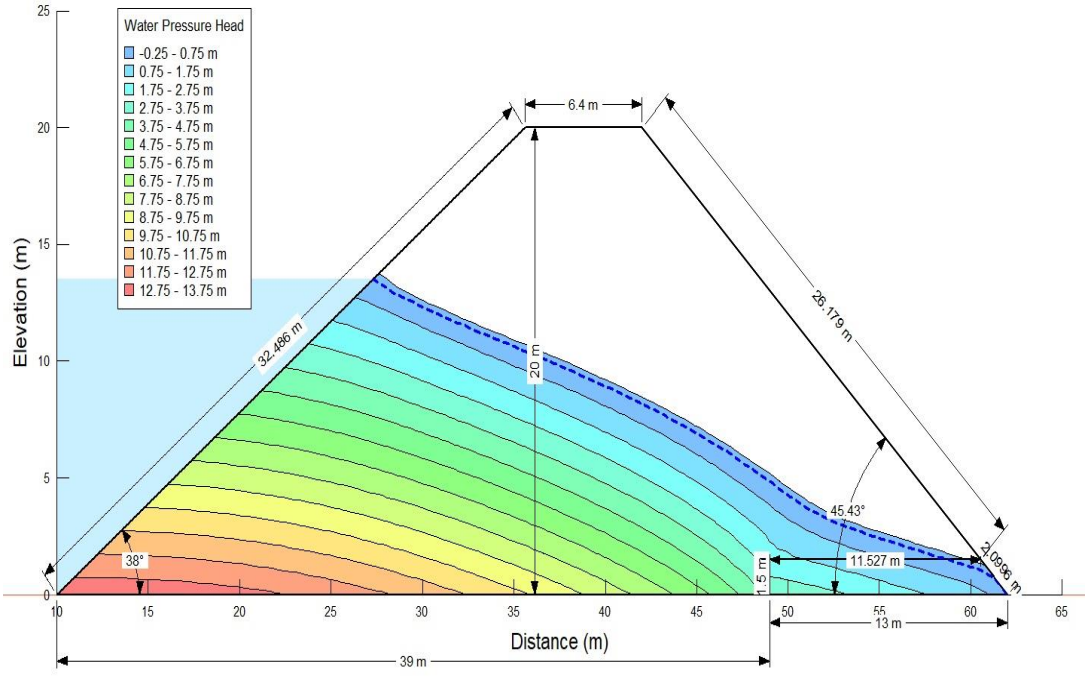

Figure 5.54: Water pressure head in M17

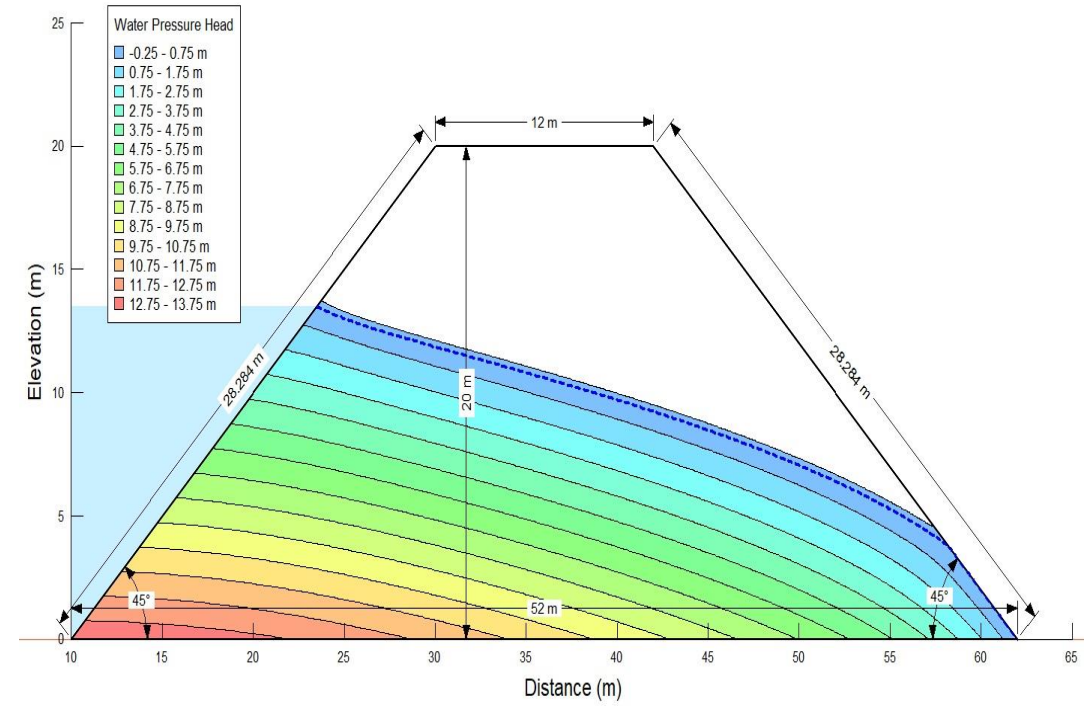

Figure 5.55: Water pressure head in M18

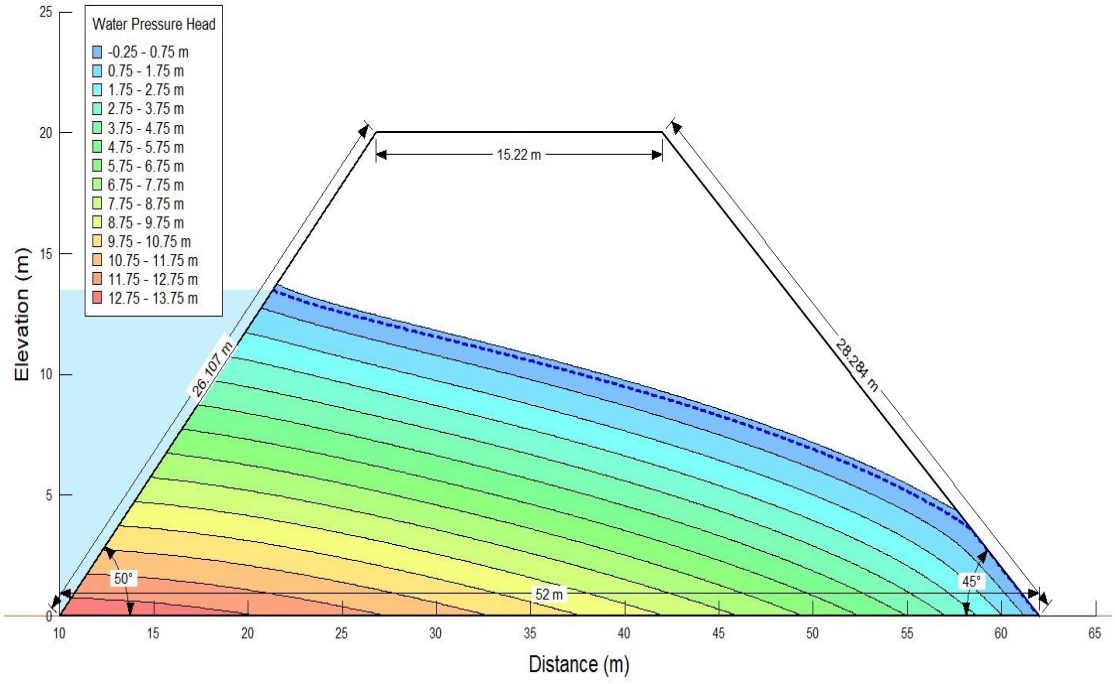

Figure 5.56: Water pressure head in M19

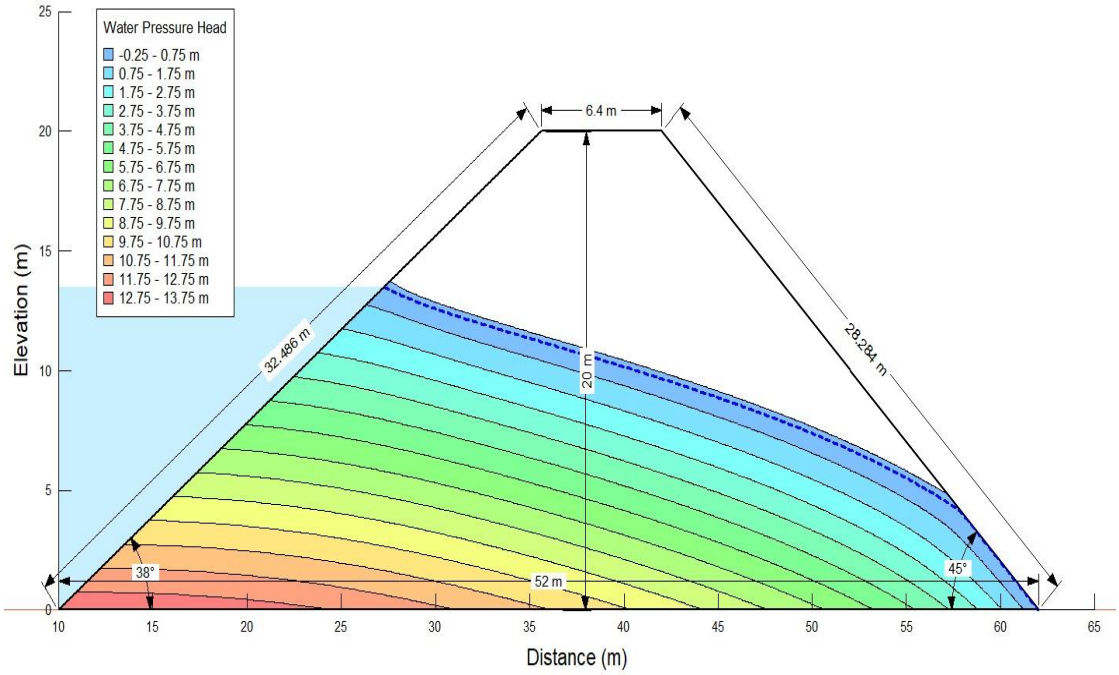

Figure 5.57: Water pressure head in M20

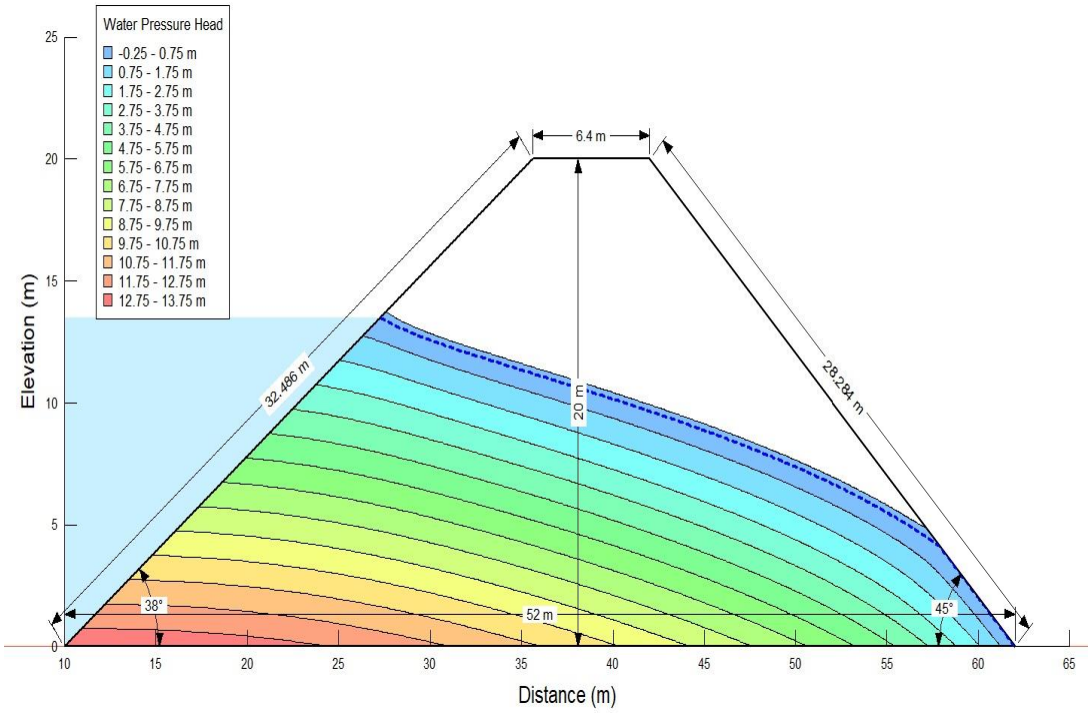

Figure 5.58: Water pressure head in M21

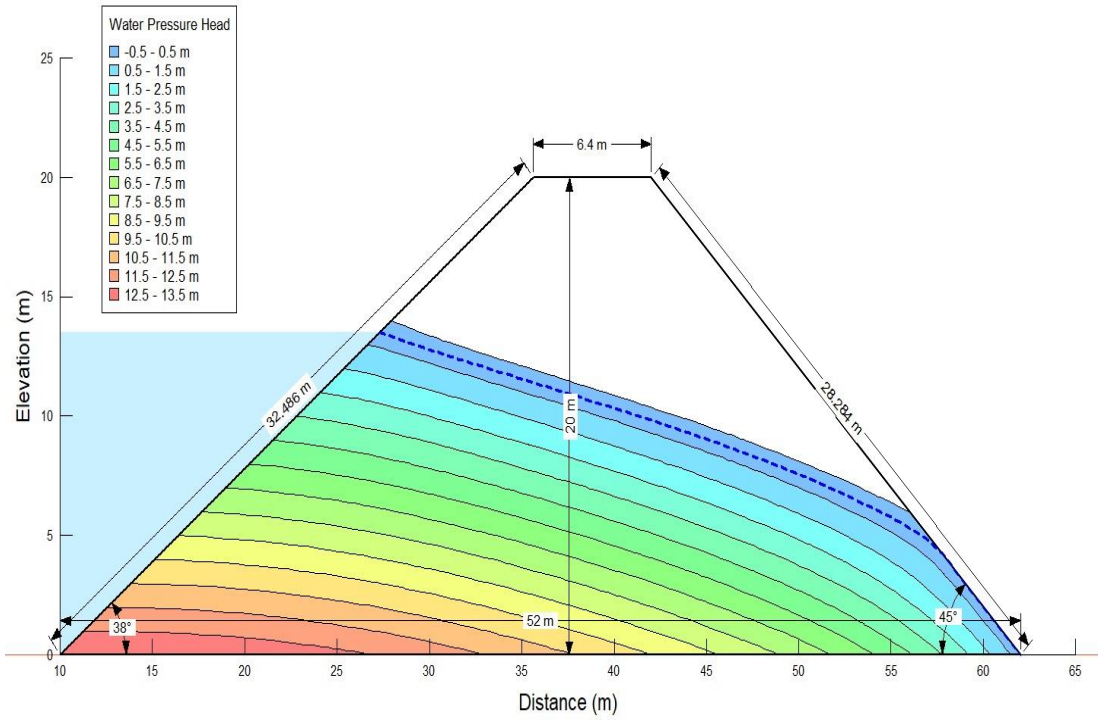

Figure 5.59: Water pressure head in M22

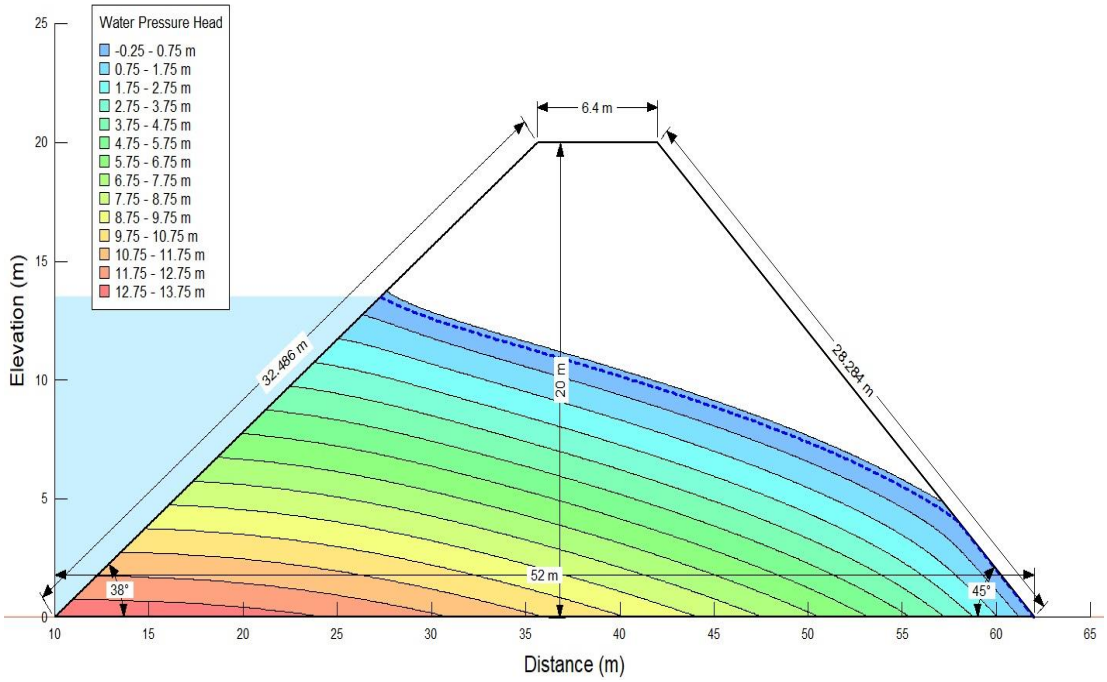

Figure 5.60: Water pressure head in M23

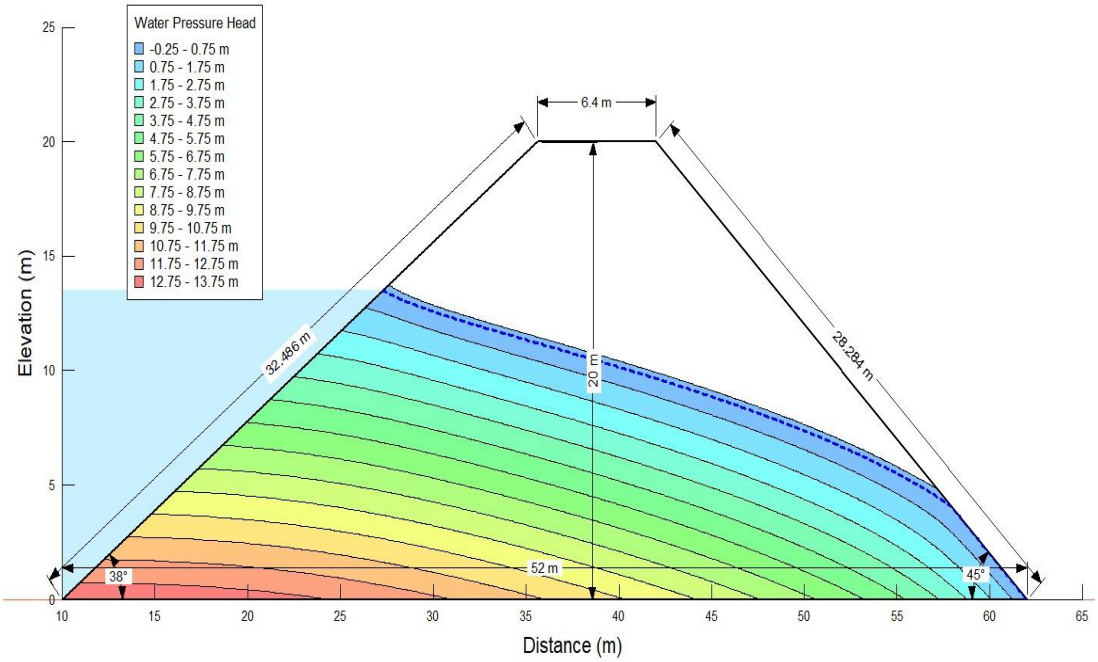

Figure 5.61: Water pressure head in M24

5.1.1.3 Water total head

The contours of the total water head in metre are shown in figure 5.62 to figure 5.85 for models M1 to M24, where the elevation of the earth dam model was shown in metres on the y-axis while the distance from upstream heel in metres on the x-axis. The variation of the total head of water in terms of the location is depicted. The pressure is negative above the phreatic line (shown with a dotted line) and positive below. These water total head contours or equipotential lines are important as direction of seepage is always perpendicular to the equipotential lines, so these contours of water total head helps in visualising the direction of seepage flow in an earth dam.

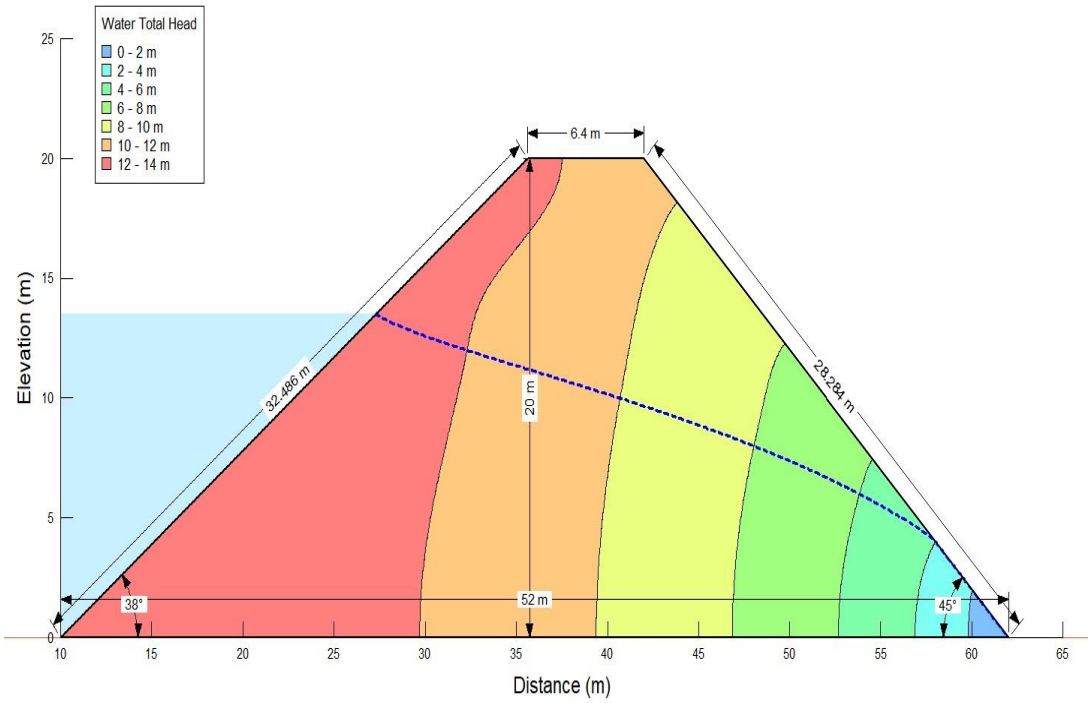

Figure 5.62: Water total head in M1

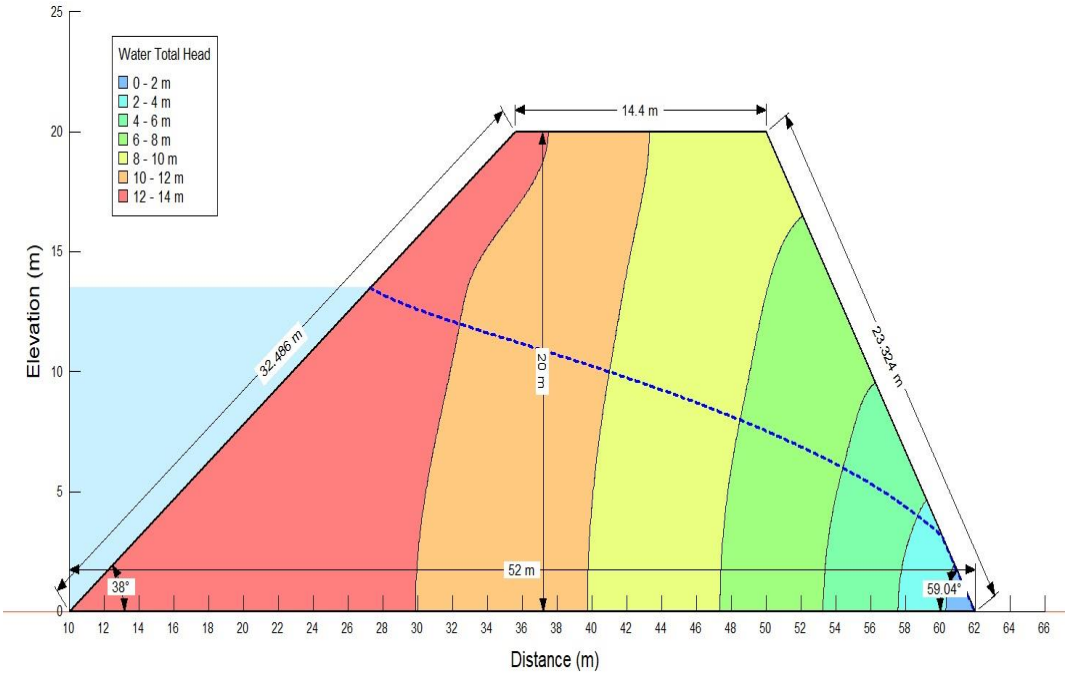

Figure 5.63: Water total head in M2

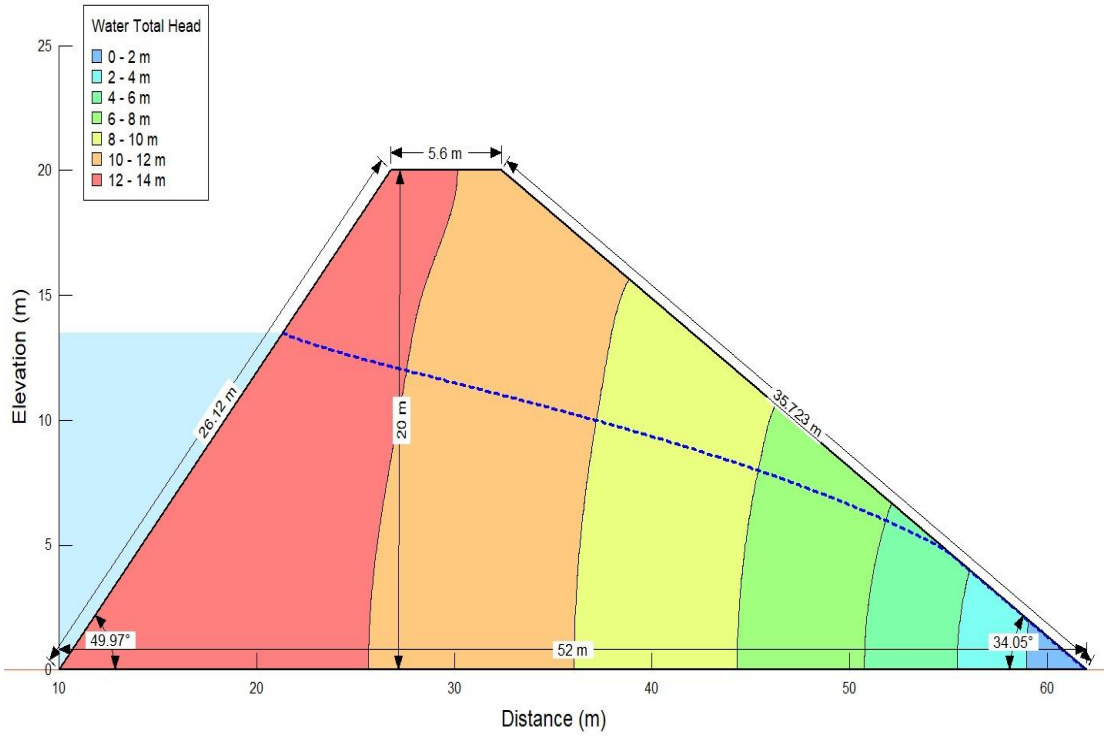

Figure 5.64: Water total head in M3

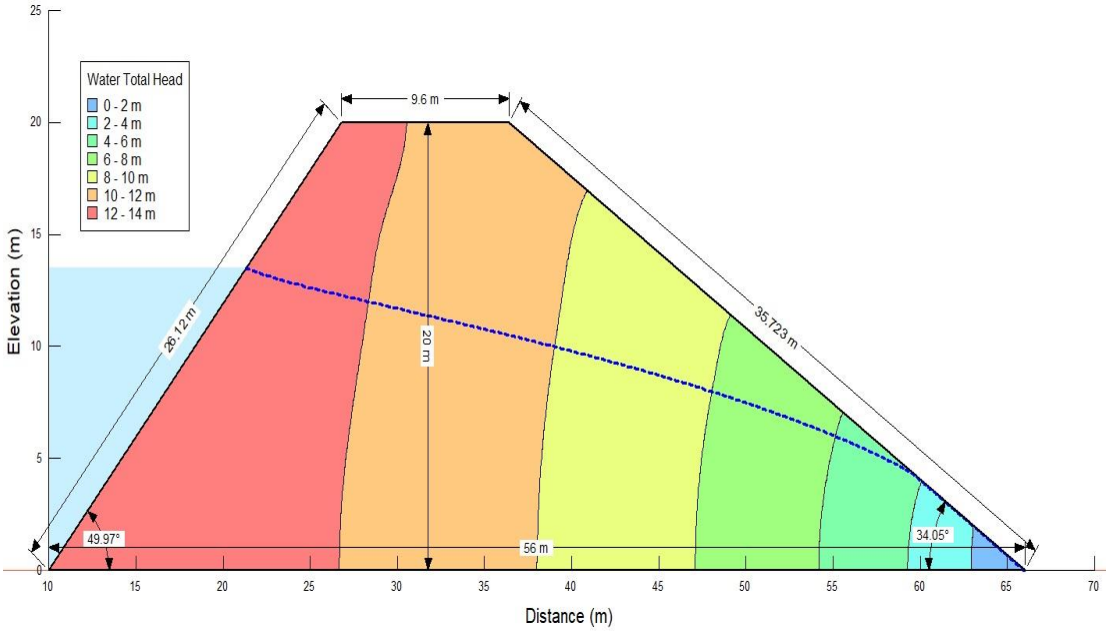

Figure 5.65: Water total head in M4

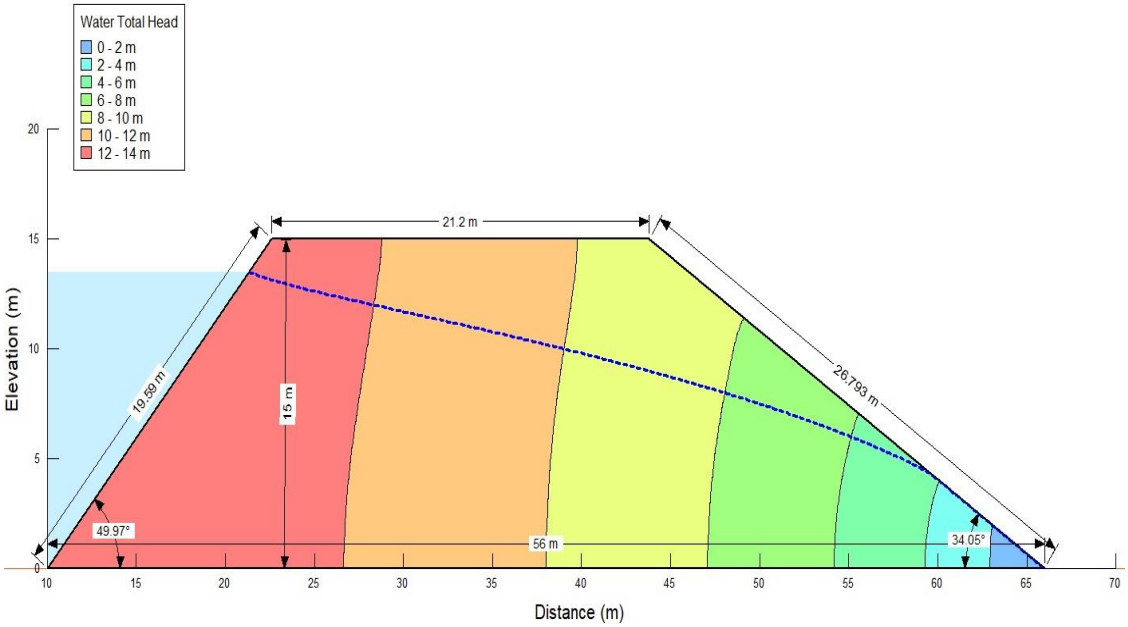

Figure 5.66: Water total head in M5

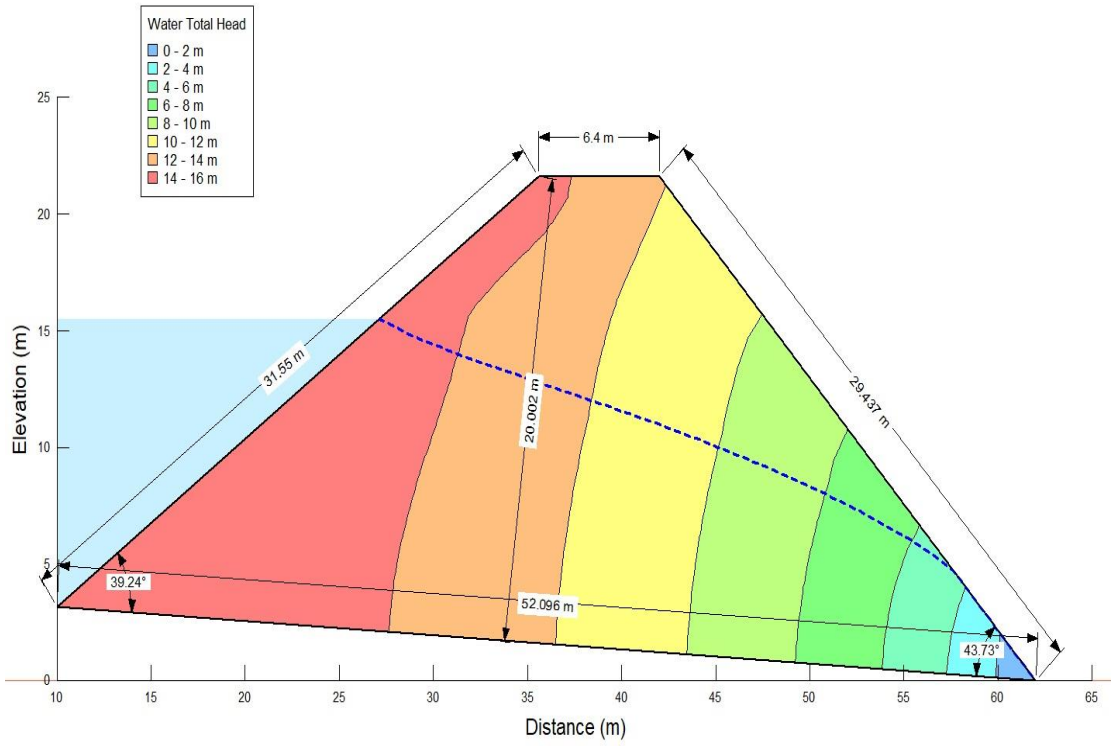

Figure 5.67: Water total head in M6

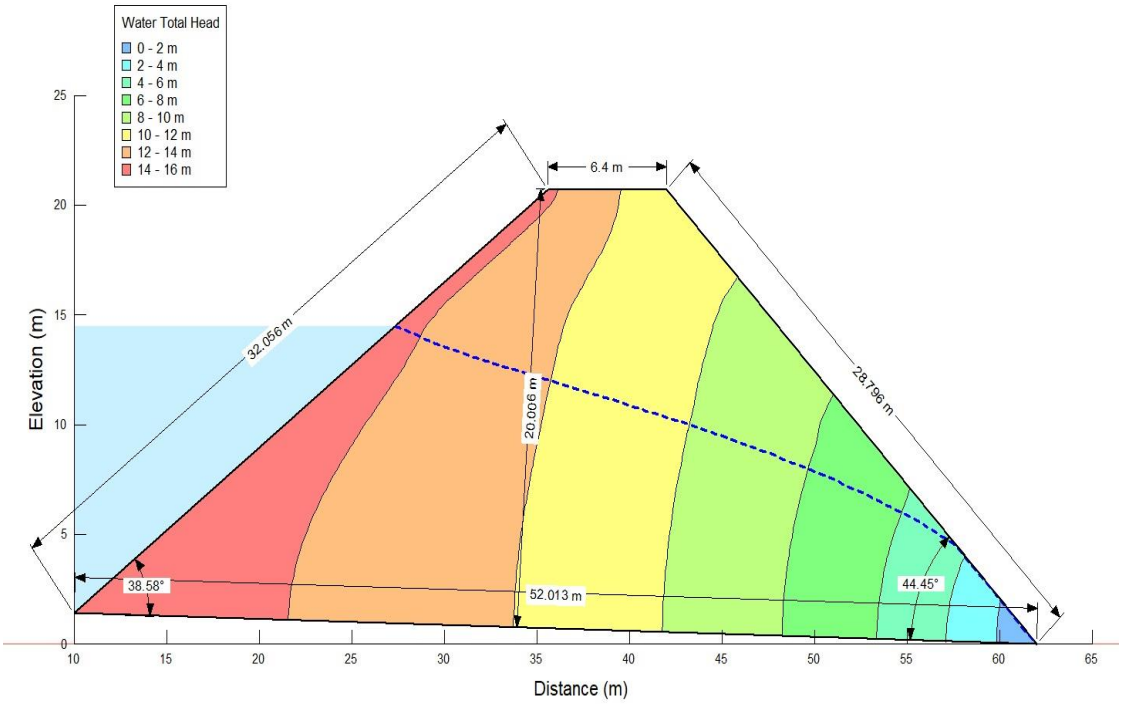

Figure 5.68: Water total head in M7

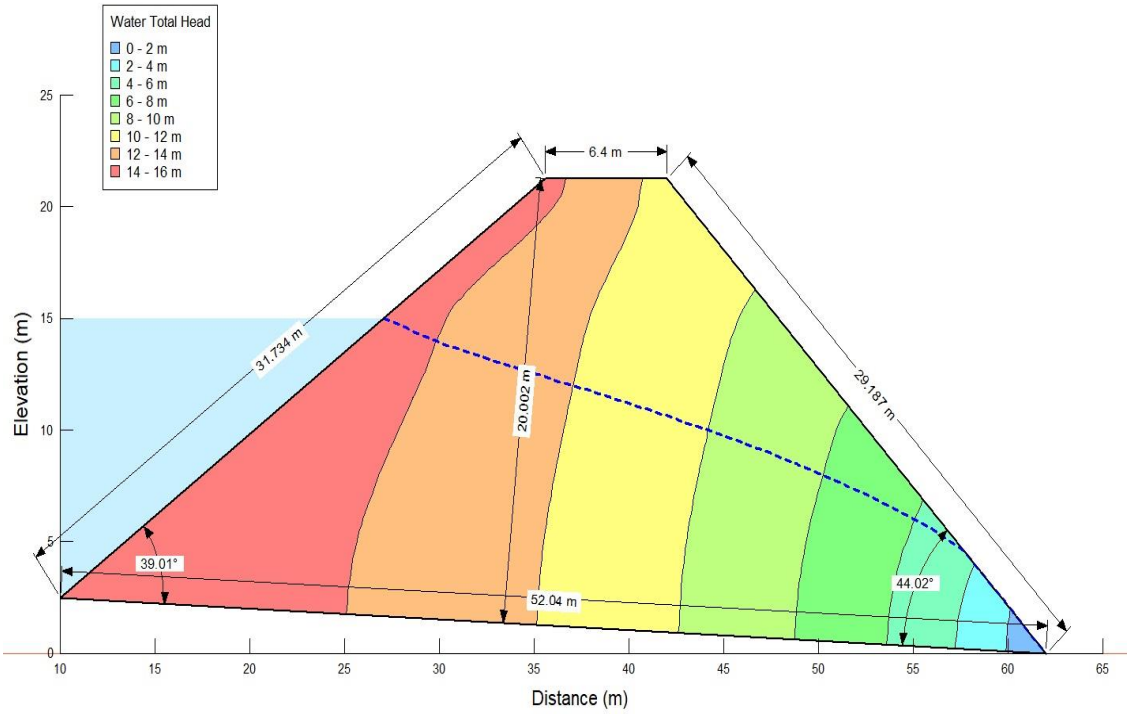

Figure 5.69: Water total head in M8

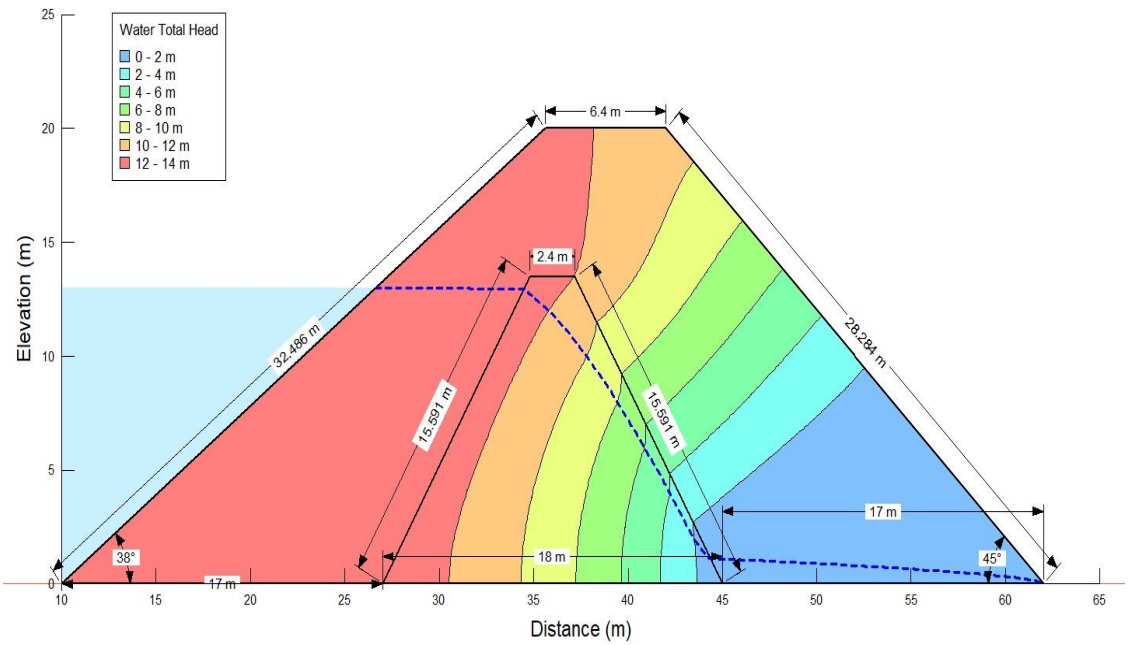

Figure 5.70: Water total head in M9

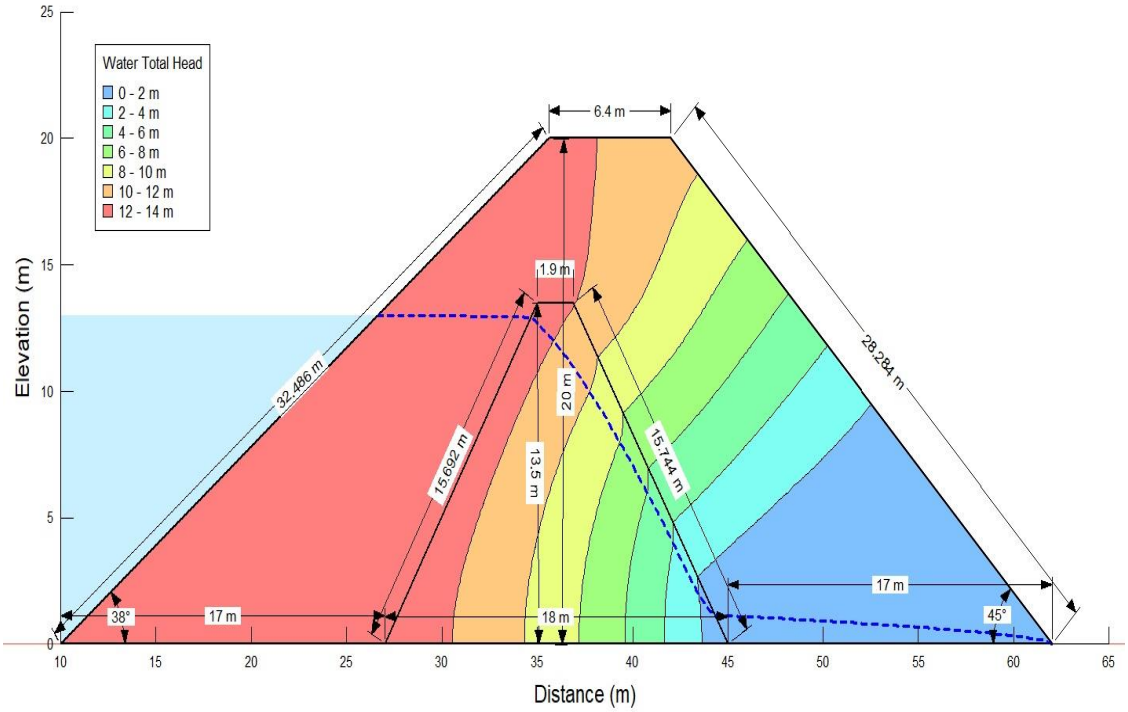

Figure 5.71: Water total head in M10

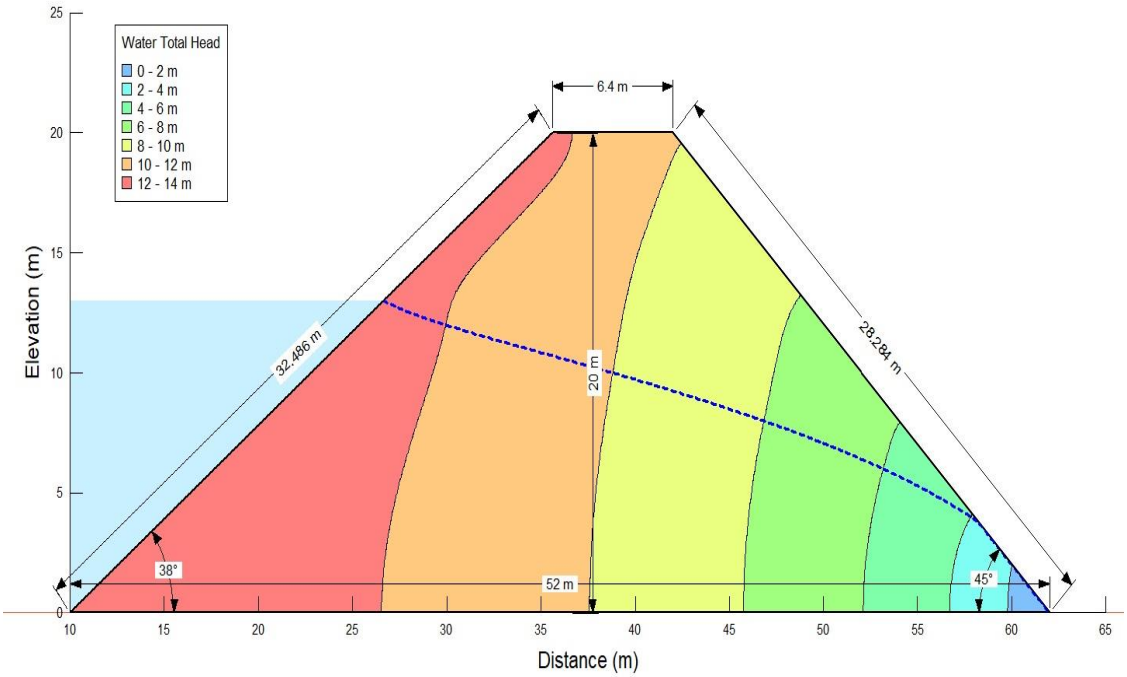

Figure 5.72: Water total head in M11

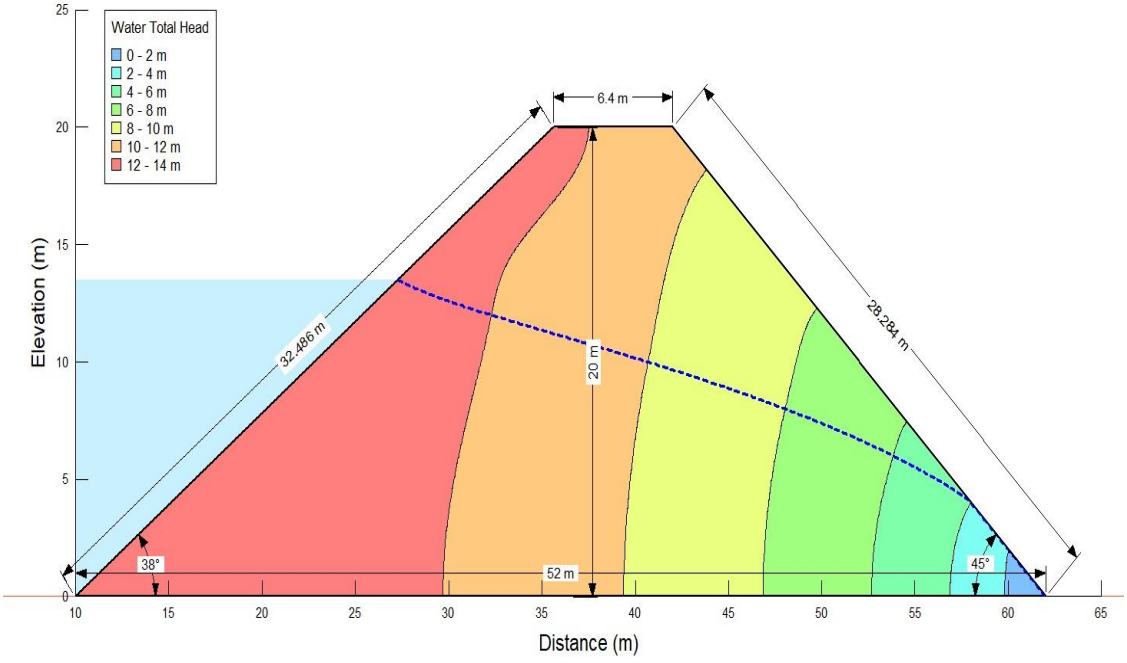

Figure 5.73: Water total head in M12

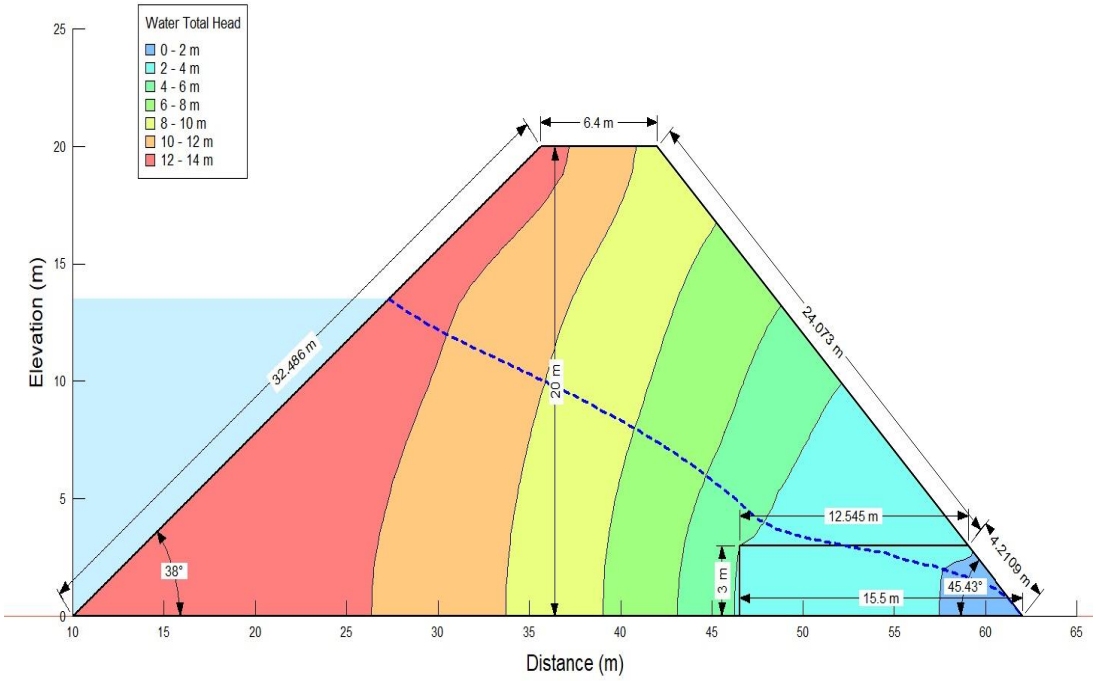

Figure 5.74: Water total head in M13

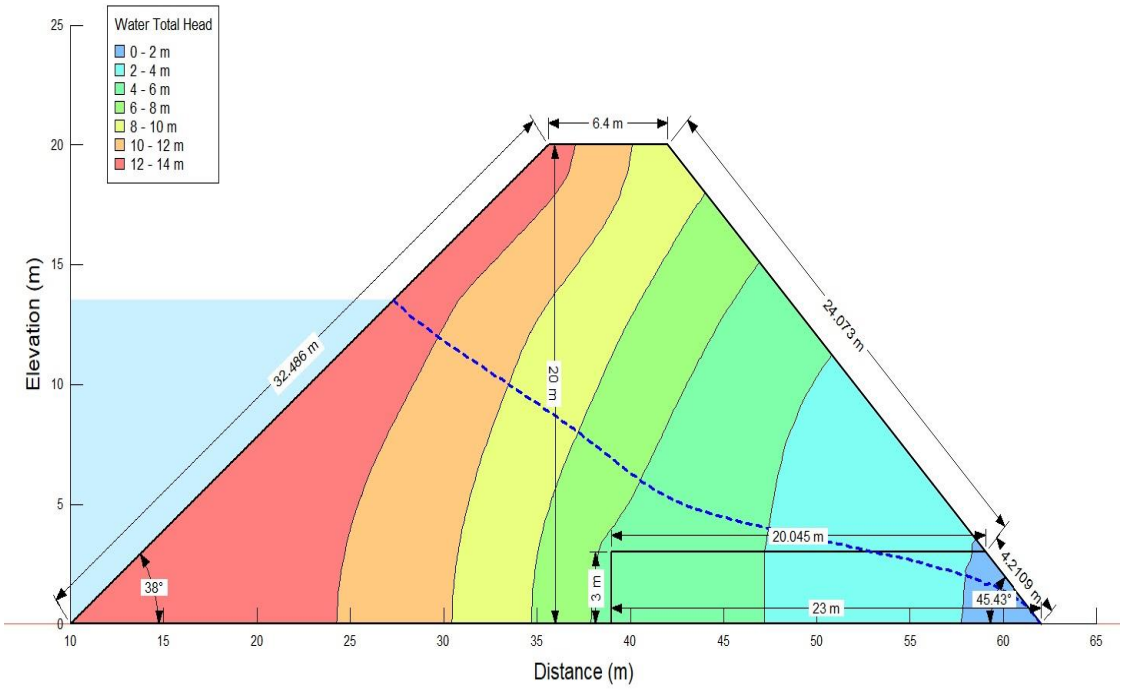

Figure 5.75: Water total head in M14

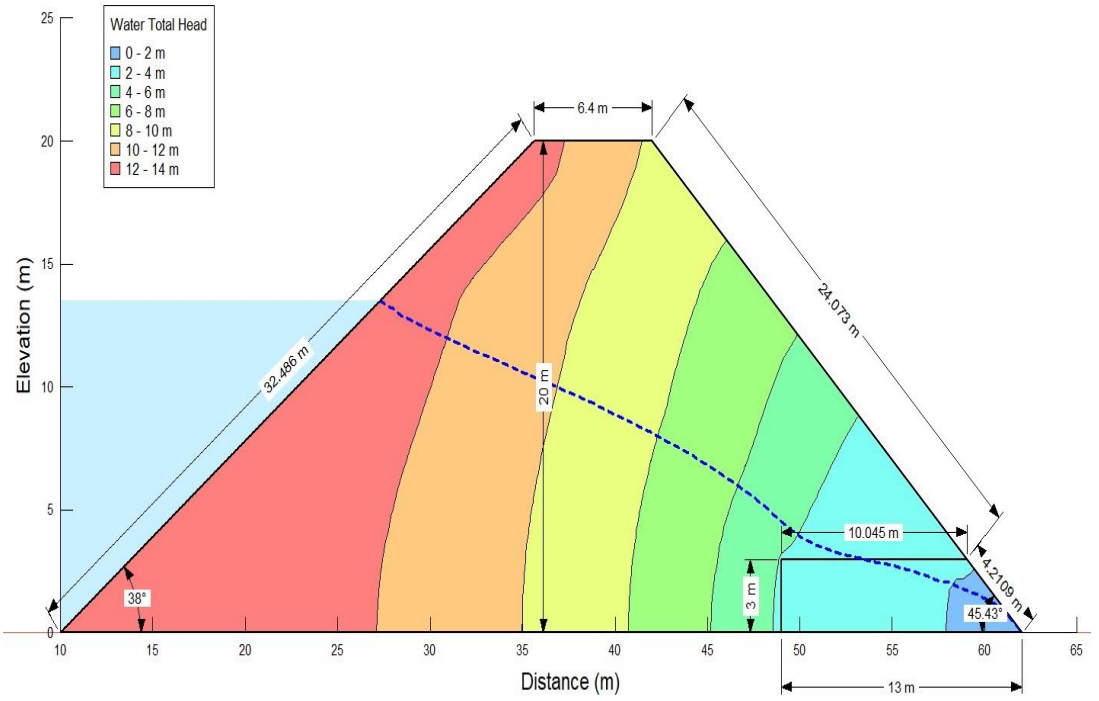

Figure 5.76: Water total head in M15

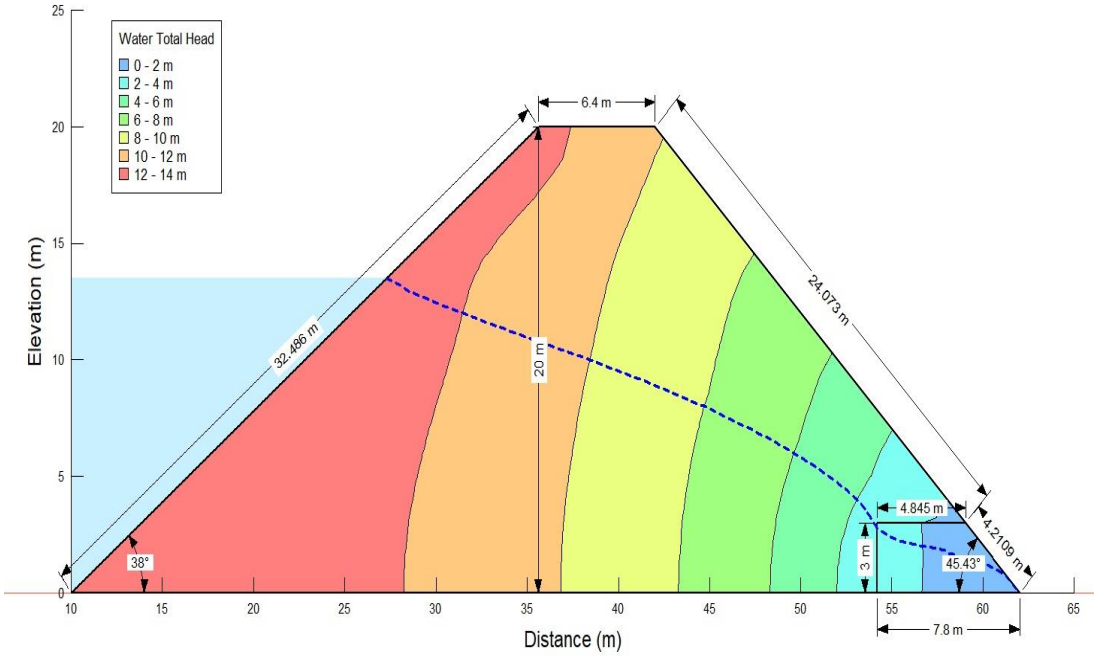

Figure 5.77: Water total head in M16

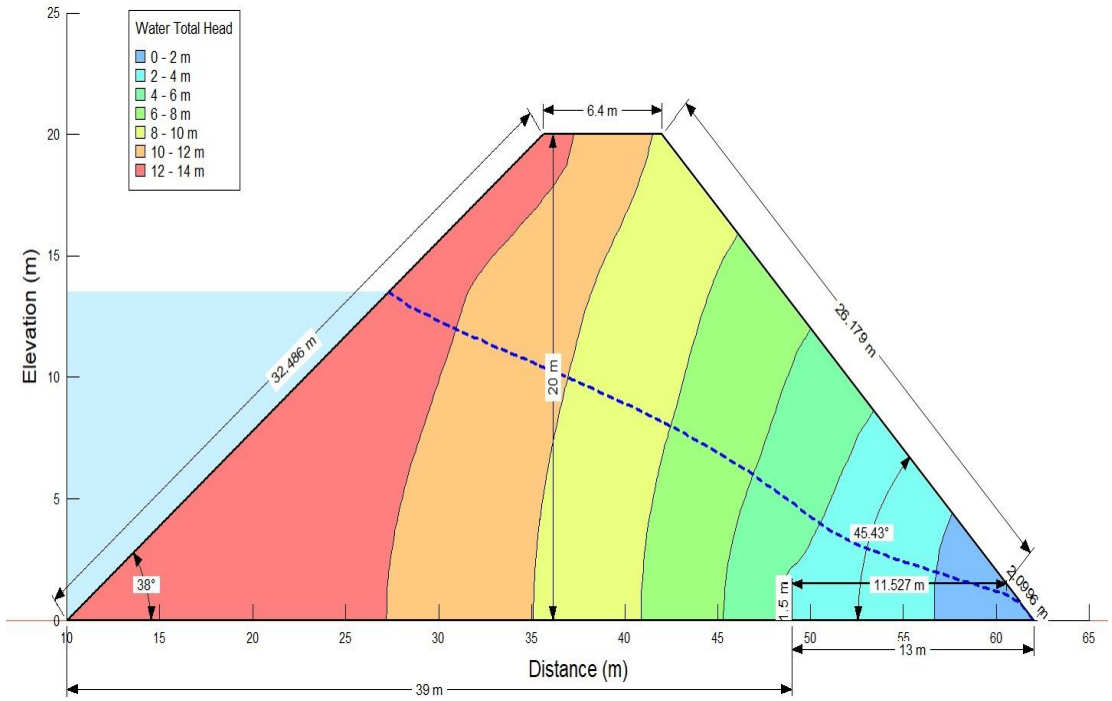

Figure 5.78: Water total head in M17

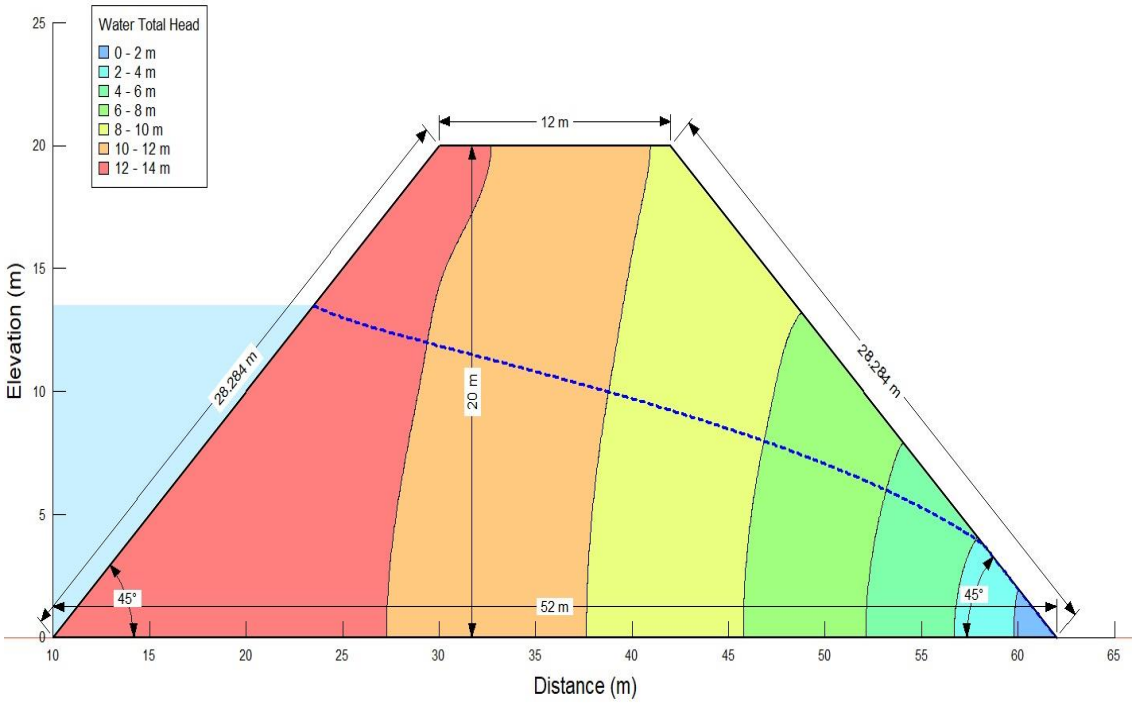

Figure 5.79: Water total head in M18

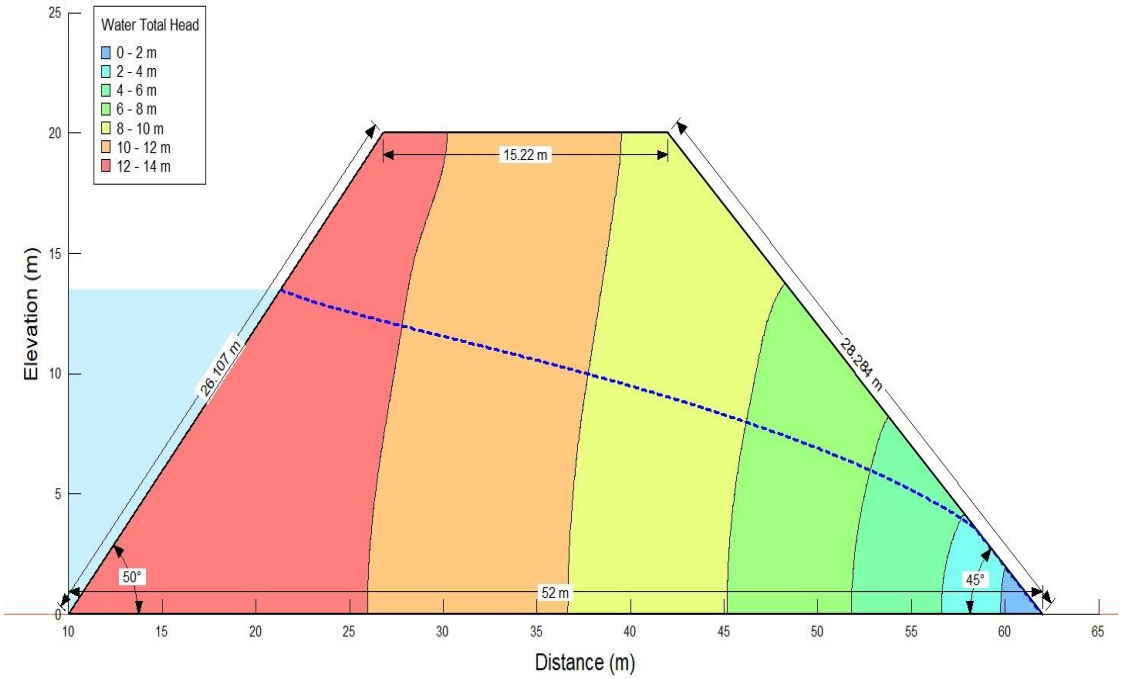

Figure 5.80: Water total head in M19

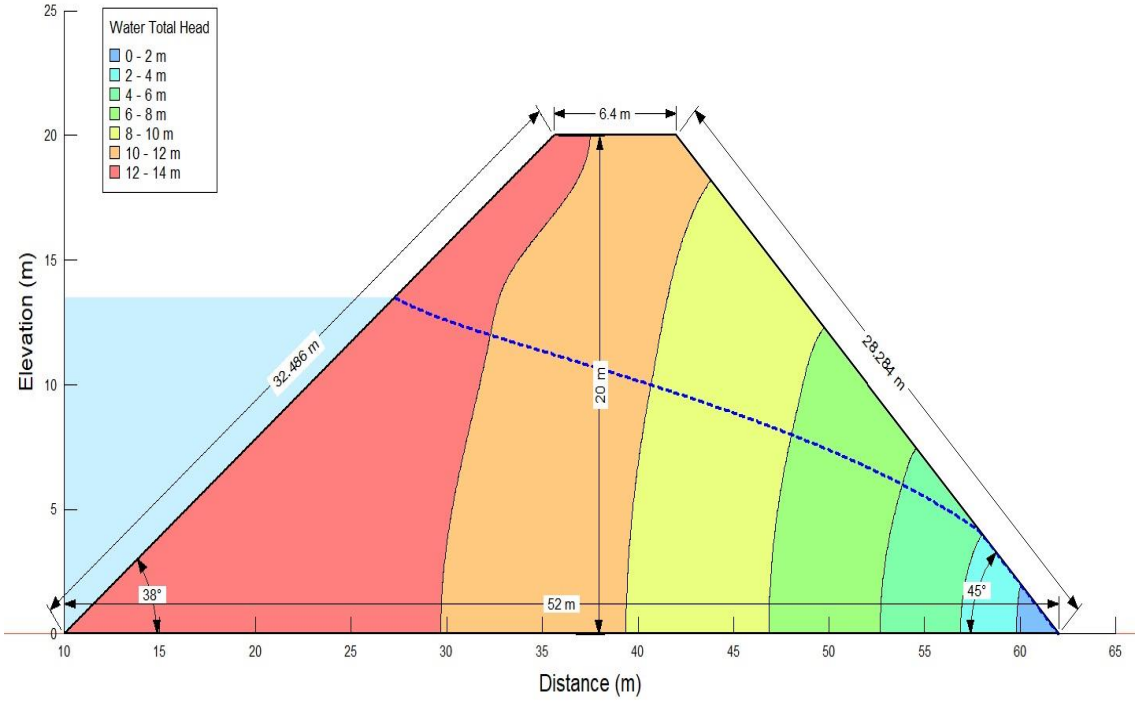

Figure 5.81: Water total head in M20

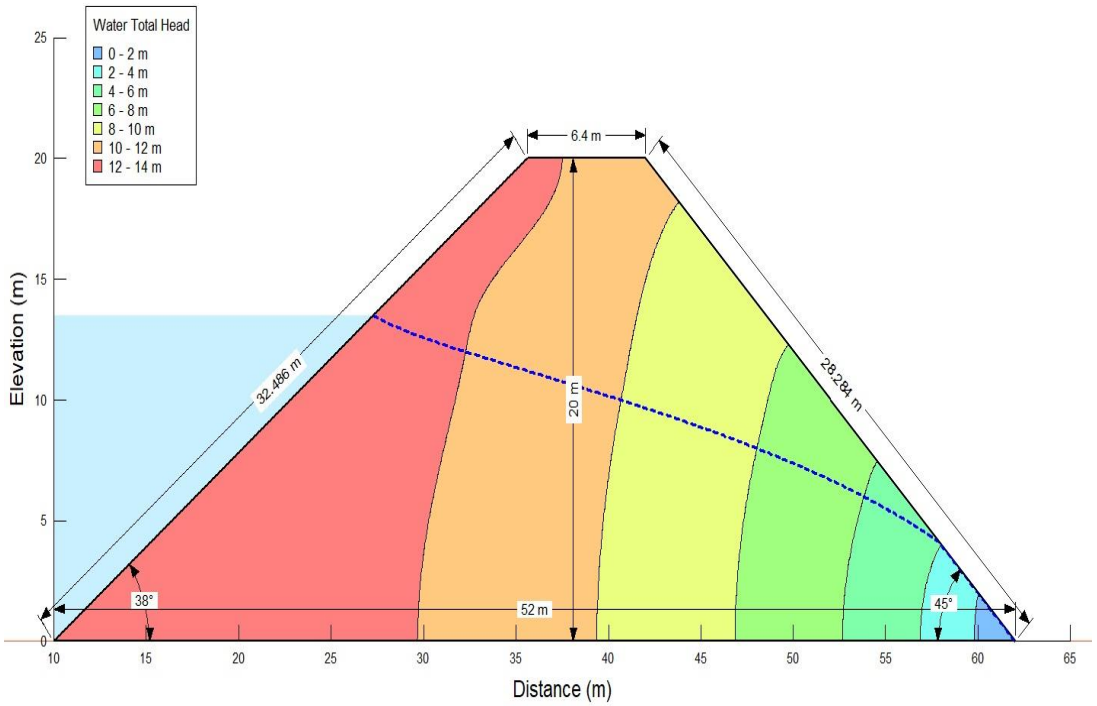

Figure 5.82: Water total head in M21

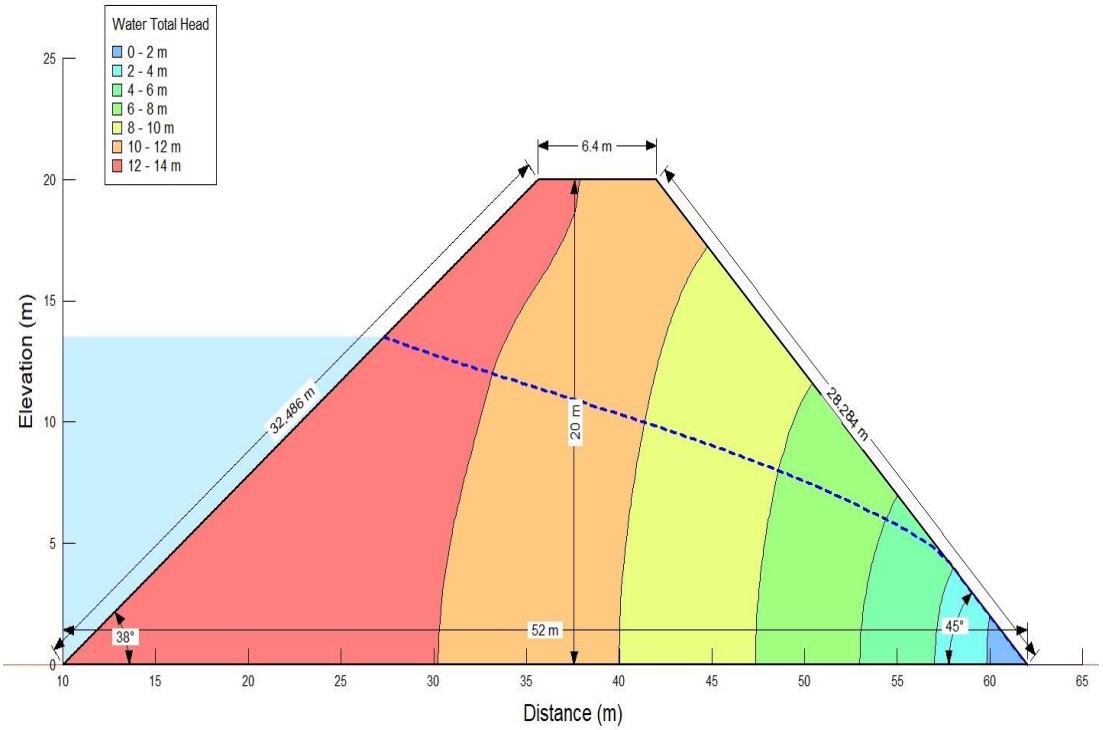

Figure 5.83: Water total head in M22

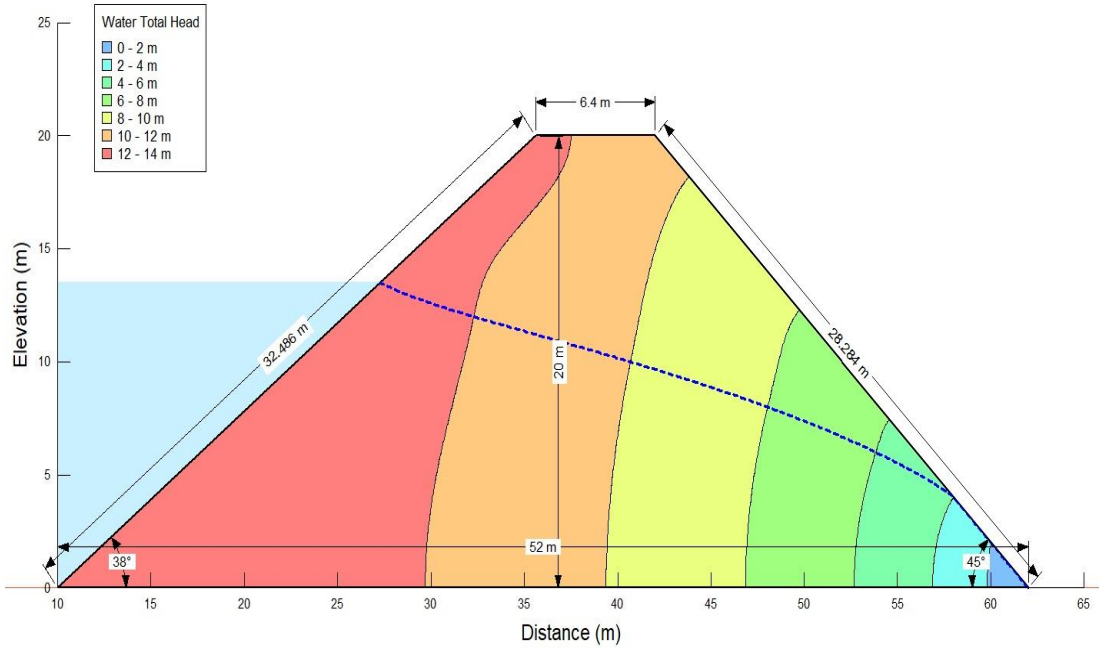

Figure 5.84: Water total head in M23

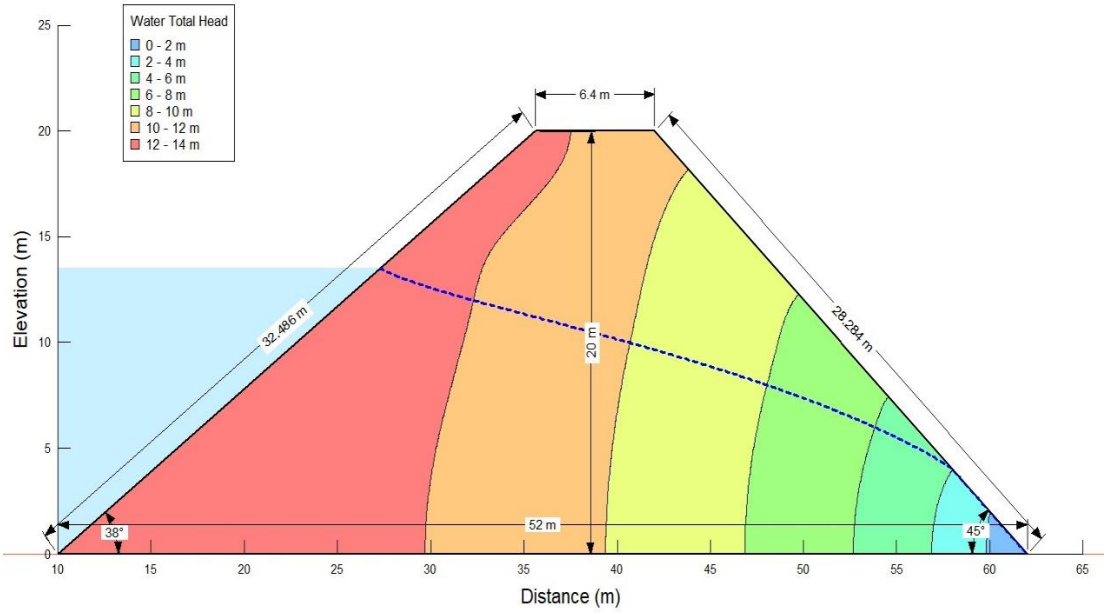

Figure 5.85: Water total head in M24

5.1.2 Slope stability

The results of Slope/w indicate that slopes were found to be stable under seepage since the factor of safety (FOS) for each slope was greater than one. As per recommendation of the Indian standard code (IS 7894-1975), the factor of safety was well within the permissible limit. All the cases were studied under steady state seepage as no sudden

drawdown condition occurred in any of the cases. Table 5.10 shows the safety factor upstream and downstream for each of the 24 models. The factor of safety in all models at 13 m upstream head was found to be above one, which indicated a stable slope.

Table 5.10: Factor of safety (FOS) of upstream face and downstream face of earth dam models

Model NO.	FOS (Upstream face)	FOS (Downstream face)
M1	1.895	1.169
M2	1.849	1.010
M3	1.568	1.383
M4	1.503	1.407
M5	2.105	1.489
M6	2.014	1.066
M7	1.929	1.114
M8	1.970	1.088
M9	1.708	1.369
M10	1.694	1.369
M11	1.853	1.164
M12	1.881	1.159
M13	1.890	1.245
M14	1.911	1.239
M15	1.887	1.246
M16	1.881	1.237
M17	1.881	1.215
M18	1.596	1.181
M19	1.505	1.179
M20	1.894	1.146
M21	1.915	1.135
M22	1.884	1.158
M23	1.895	1.169
M24	1.895	1.169

5.1.2.1 Contours of Factor of safety for upstream and downstream face

The contours of the factor of safety (FOS) for different slices are shown in Figures 5.86a and 5.86b to figure 5.109a and 5.109b, for upstream and downstream faces, respectively of models- M1 TO M24, respectively. The elevation of the earth was shown in metres on the y-axis, while the distance from the upstream heel was in metres on the x-axis. These FOS contours represents the stability of the slopes as higher the value of FOS better the stability. White coloured slice is the critical slice where failure might occur; the red colour slice has a low value of the factor of safety, while blue coloured slice has the highest factor of safety. FOS is very useful for checking the slope stability in real life scenario before constructing any earth dam. Without this study failure of slopes can take place which can cause economical and human loss. Hence, before constructing the earth dam models in the hydraulic laboratory, models were tested in the Slope/w software.

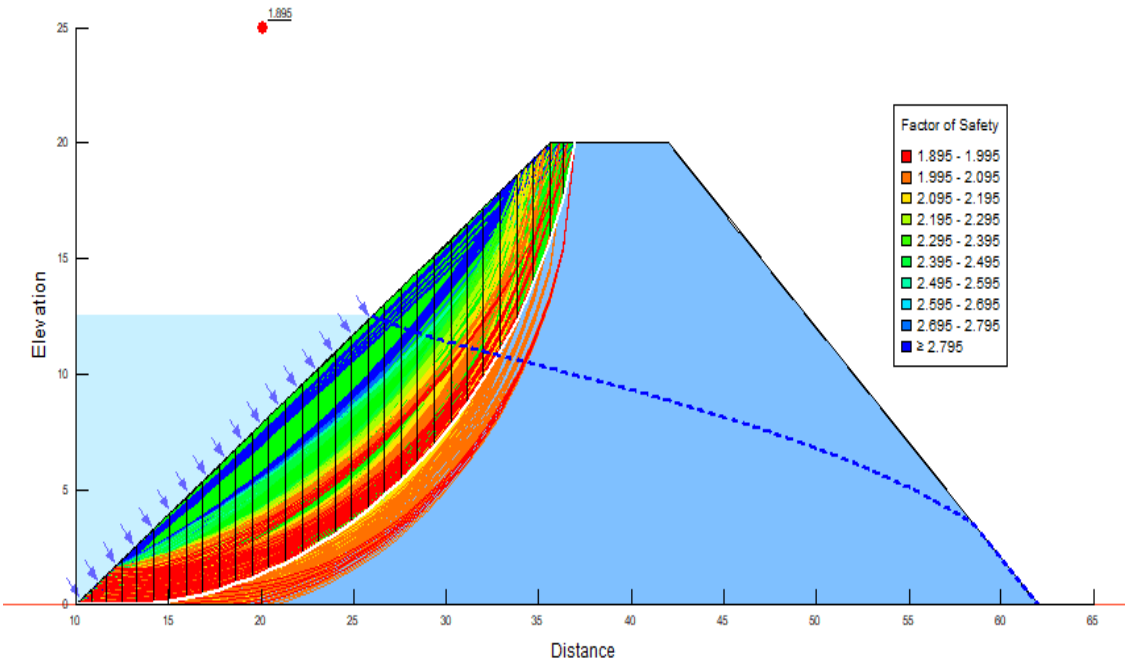

Figure 5.86a: FOS against sliding in upstream face of M1

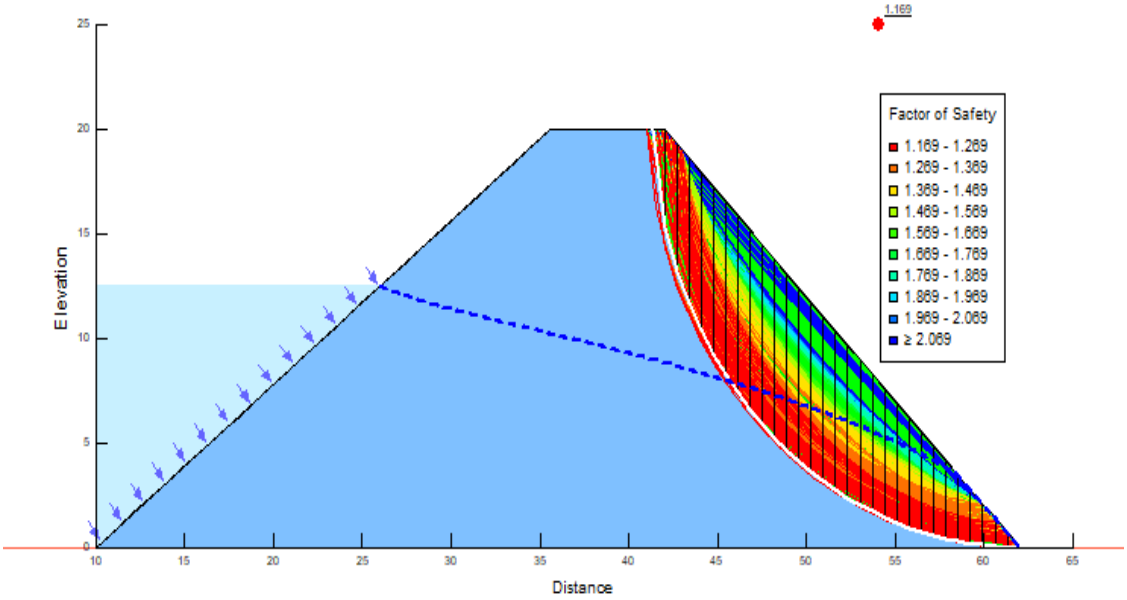

Figure 5.86b: FOS against sliding in downstream face of M1

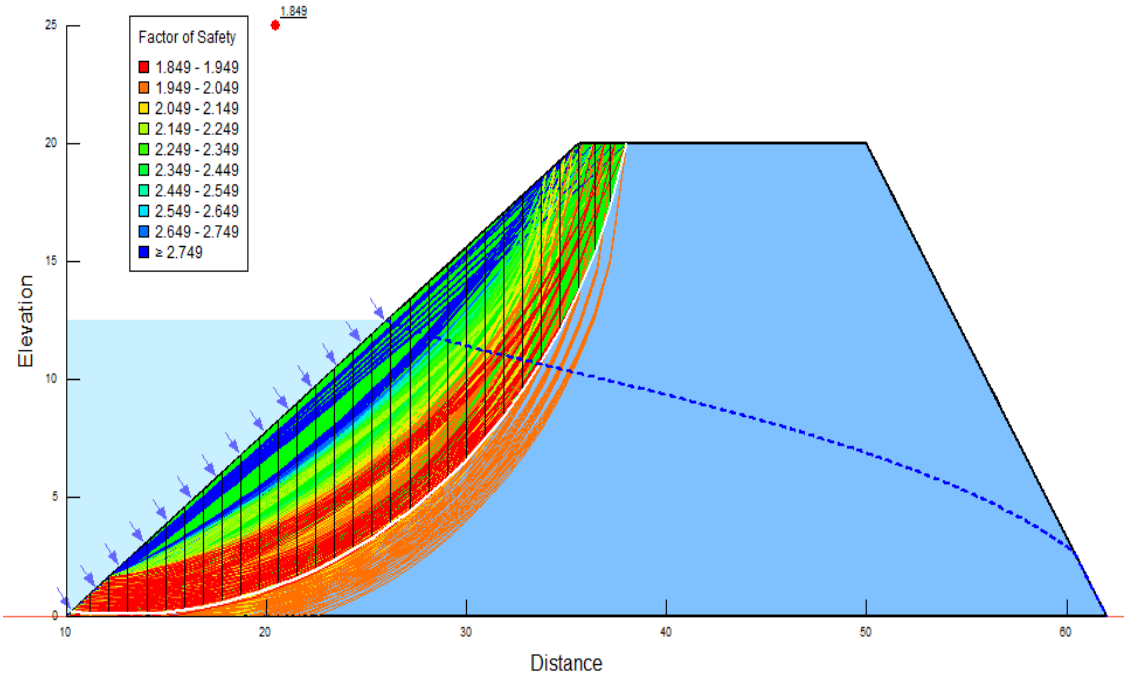

Figure 5.87a: FOS against sliding in upstream face of M2

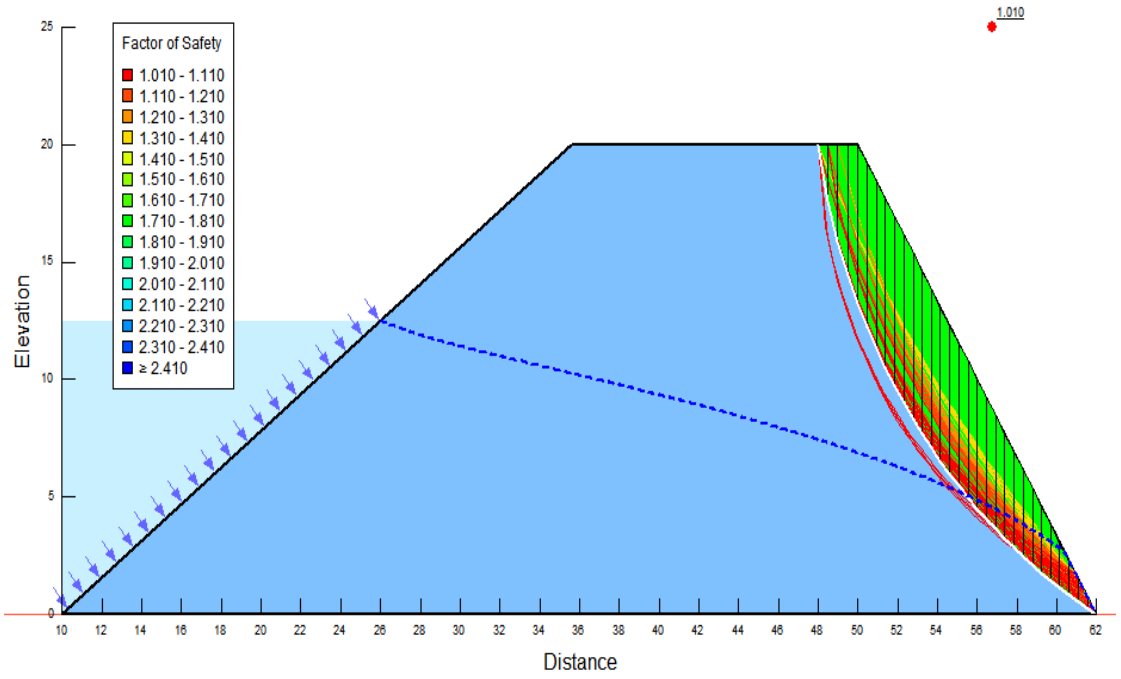

Figure 5.87b: FOS against sliding in downstream face of M2

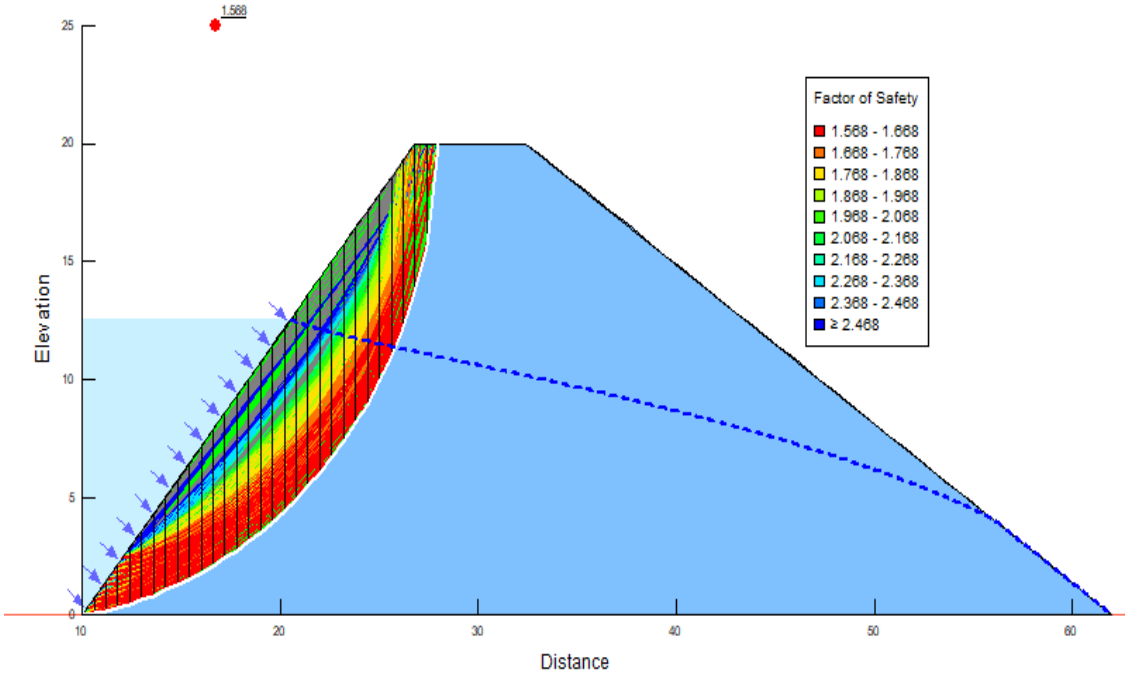

Figure 5.88a: FOS against sliding in upstream face of M3

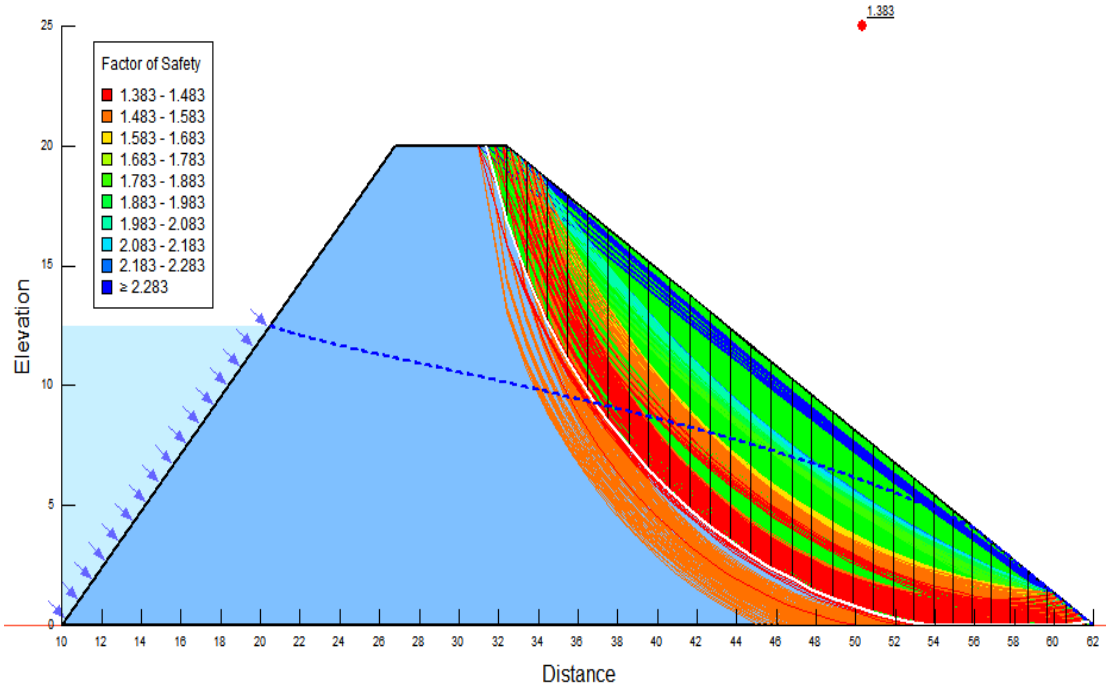

Figure 5.88b: FOS against sliding in downstream face of M3

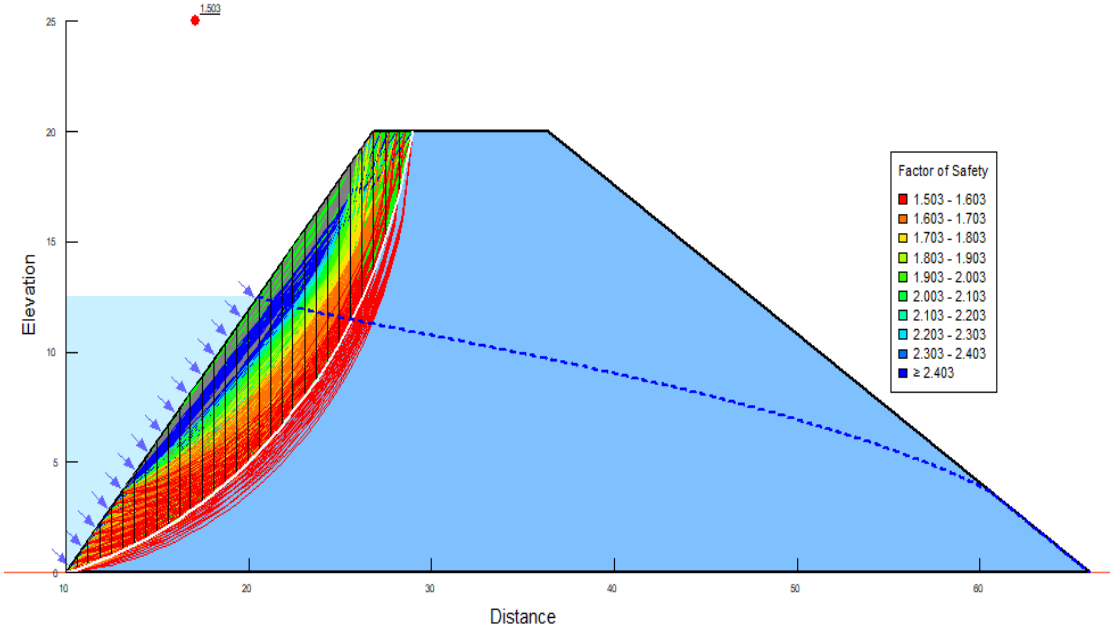

Figure 5.89a: FOS against sliding in upstream face of M4

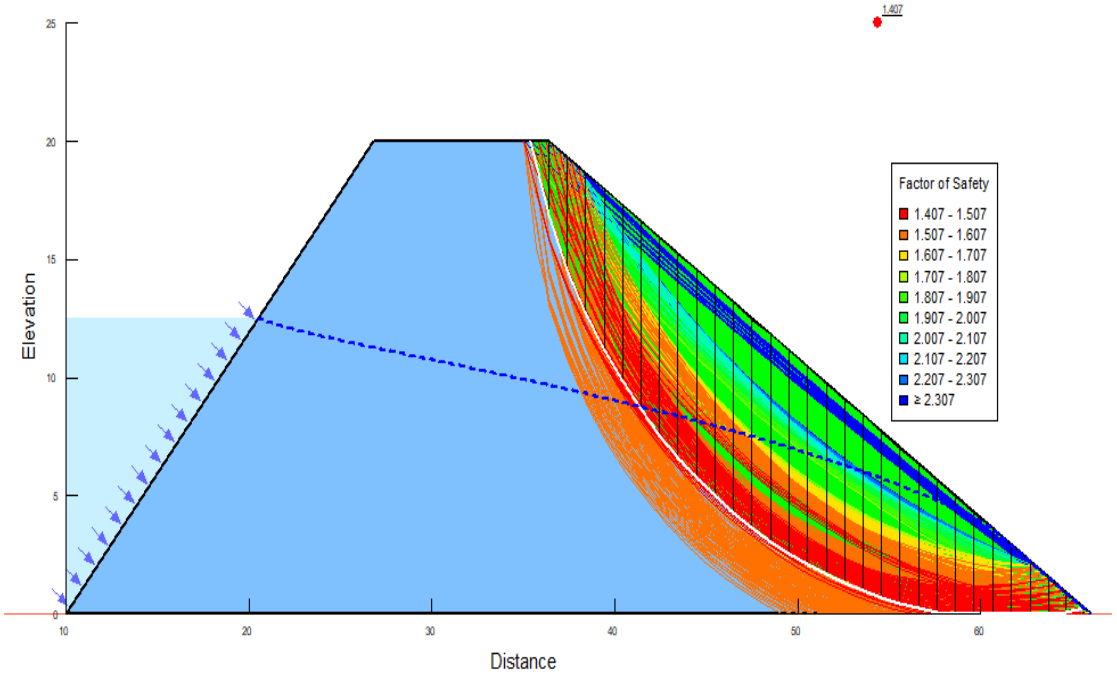

Figure 5.89b: FOS against sliding in downstream face of M4

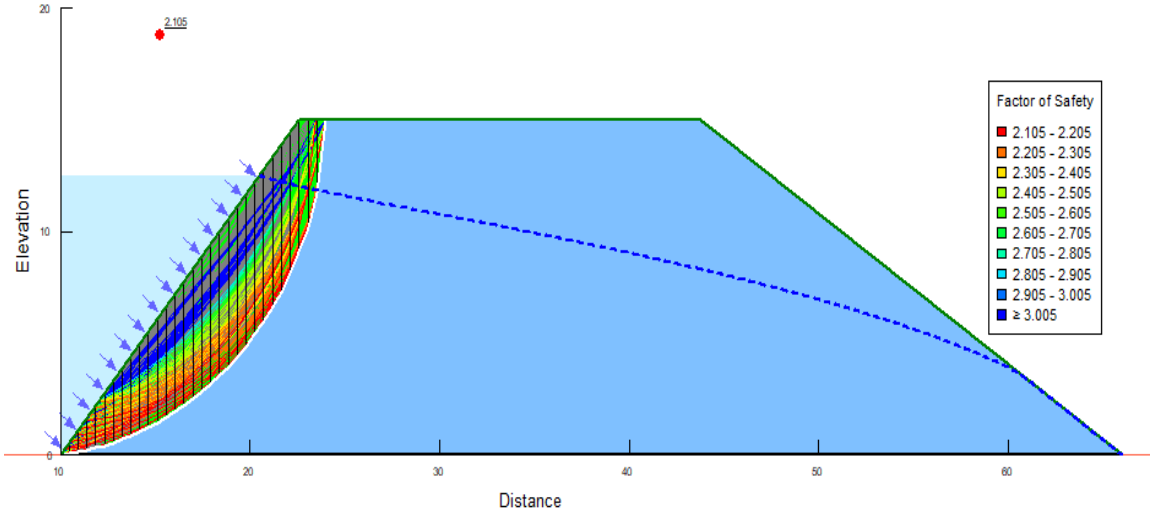

Figure 5.90a: FOS against sliding in upstream face of M5

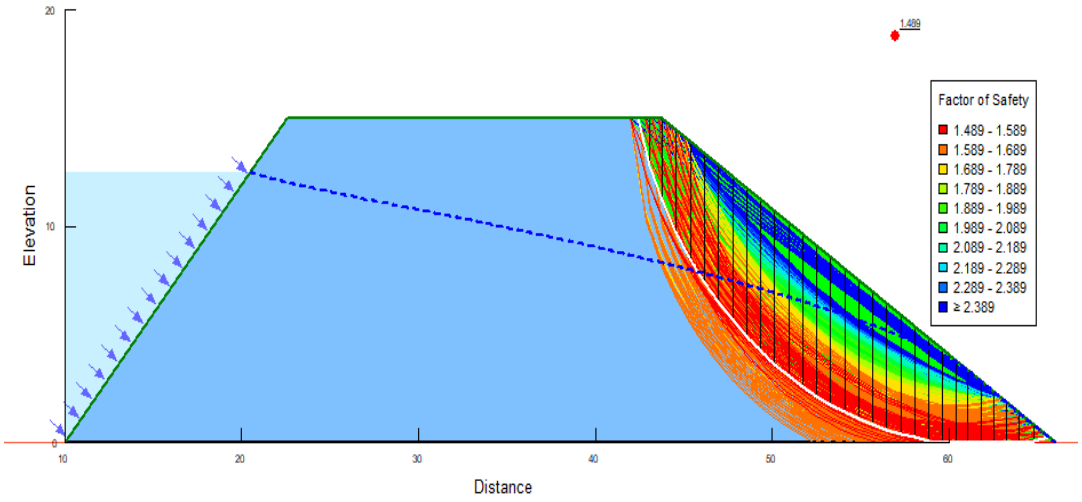

Figure 5.90b: FOS against sliding in downstream face of M5

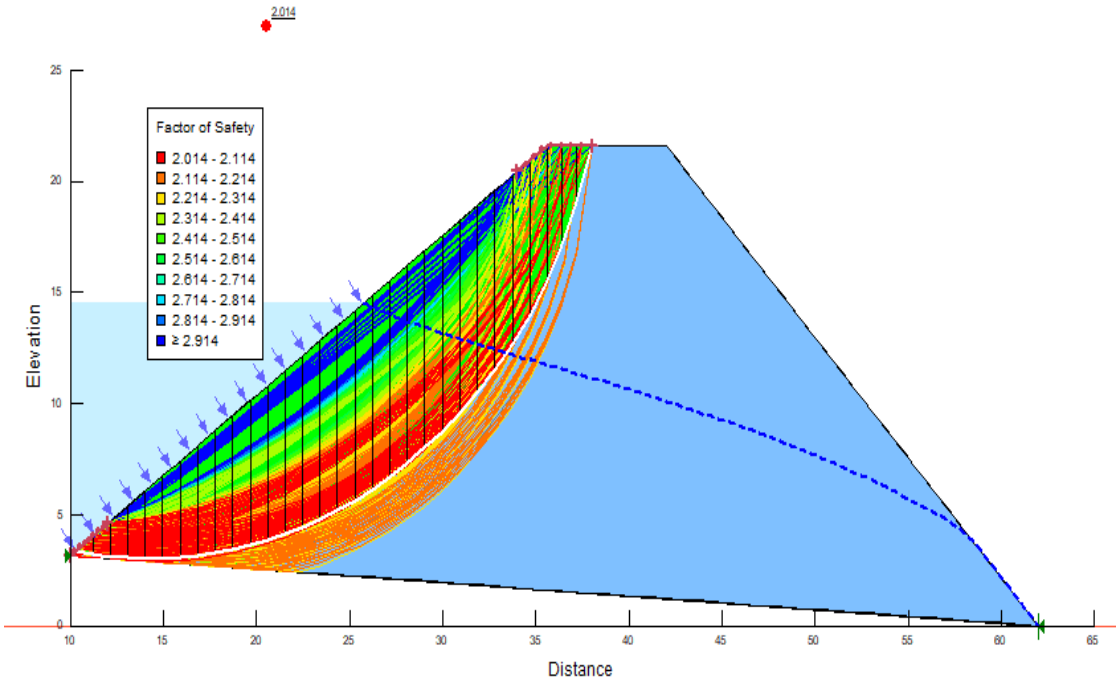

Figure 5.91a: FOS against sliding in upstream face of M6

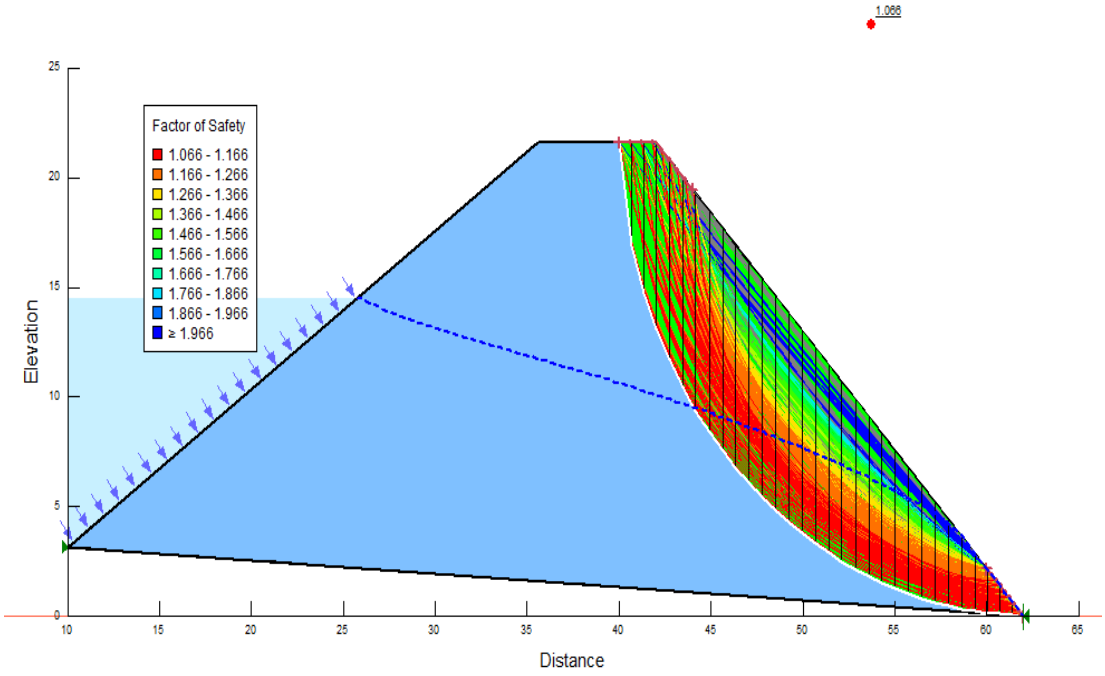

Figure 5.91b: FOS against sliding in downstream face of M6

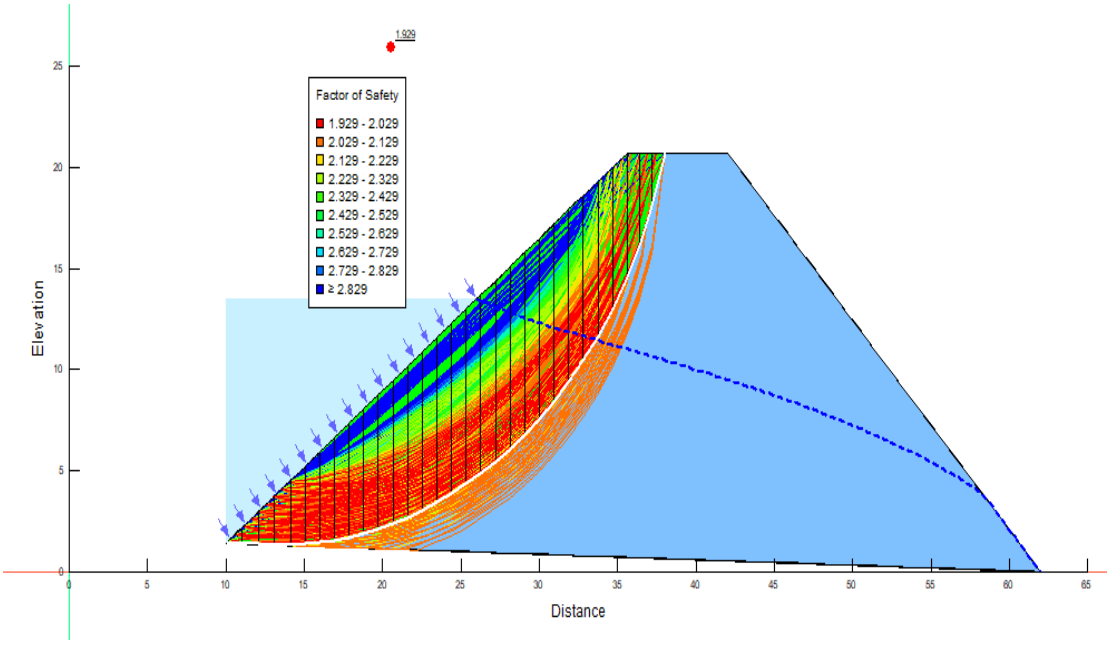

Figure 5.92a: FOS against sliding in upstream face of M7

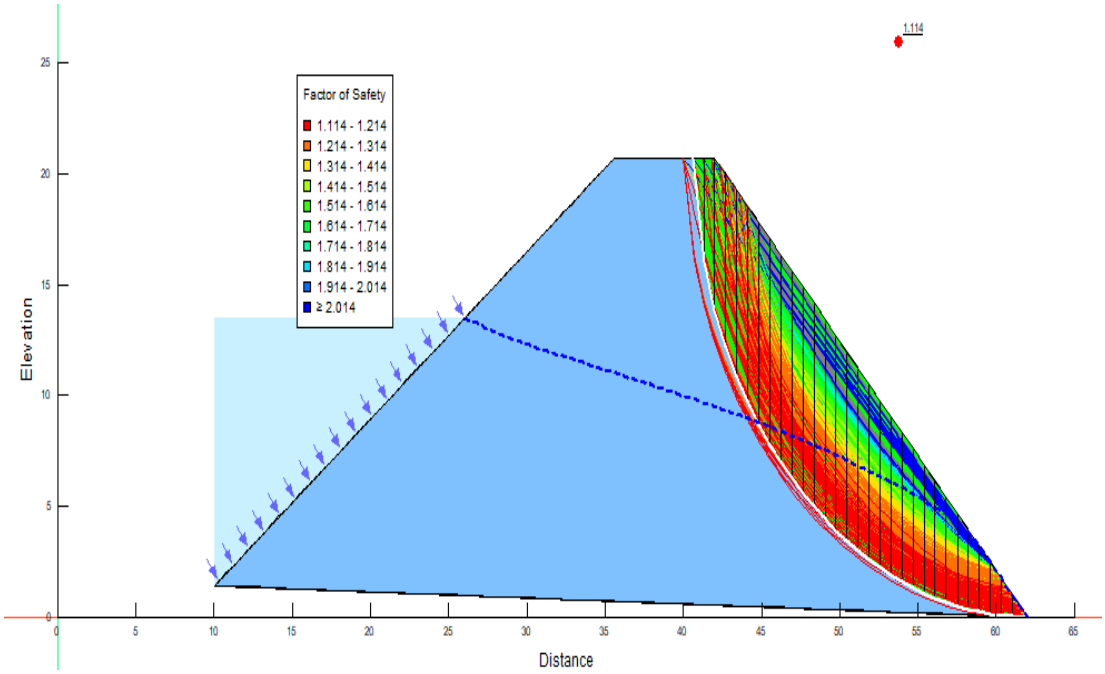

Figure 5.92b: FOS against sliding in downstream face of M7

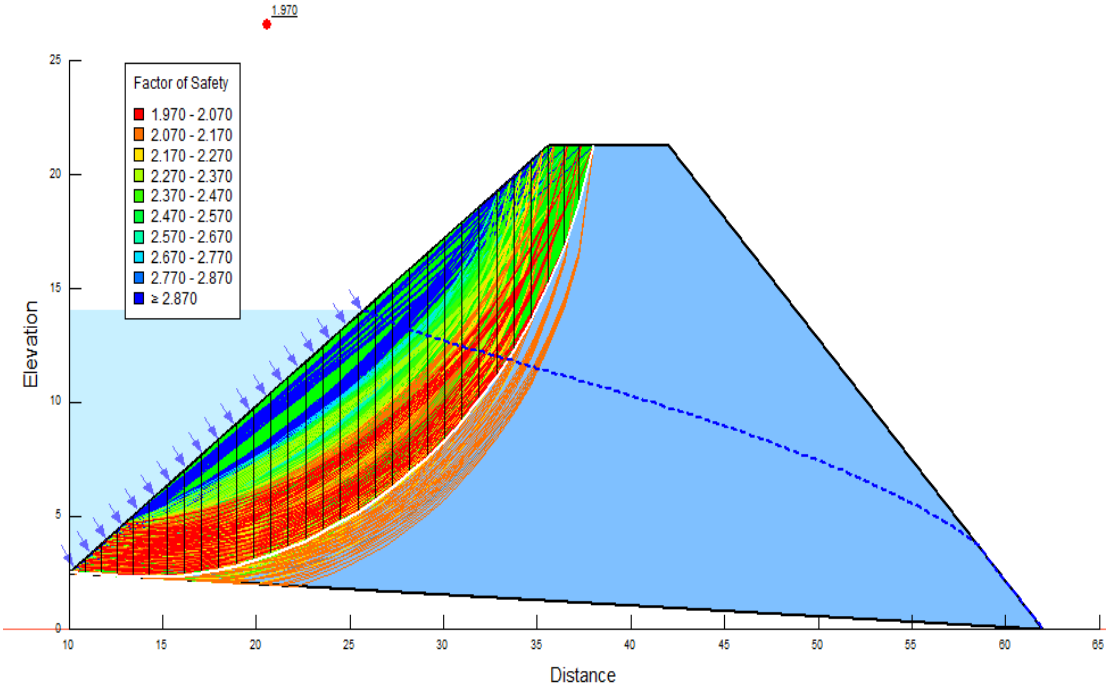

Figure 5.93a: FOS against sliding in upstream face of M8

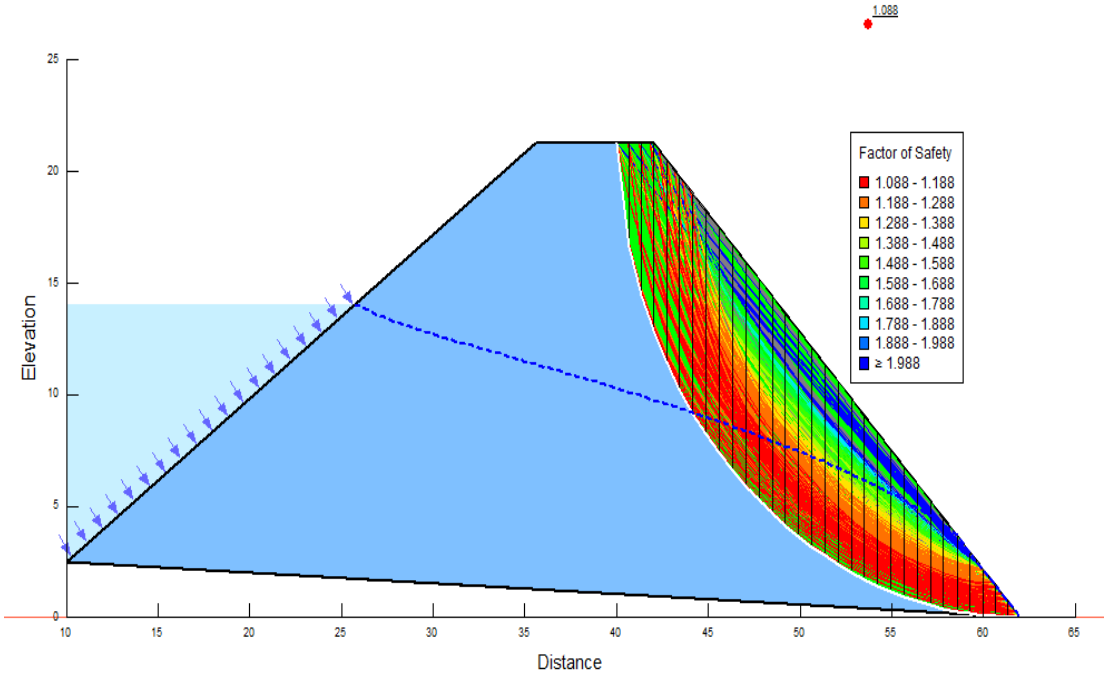

Figure 5.93b: FOS against sliding in downstream face of M8

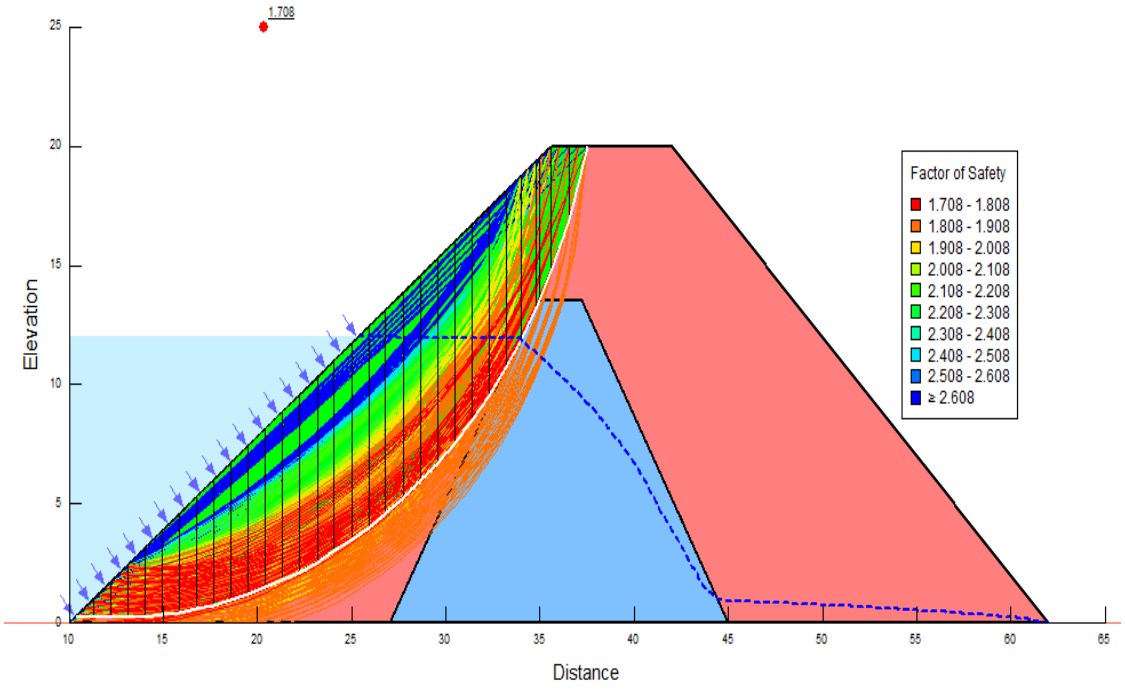

Figure 5.94a: FOS against sliding in upstream face of M9

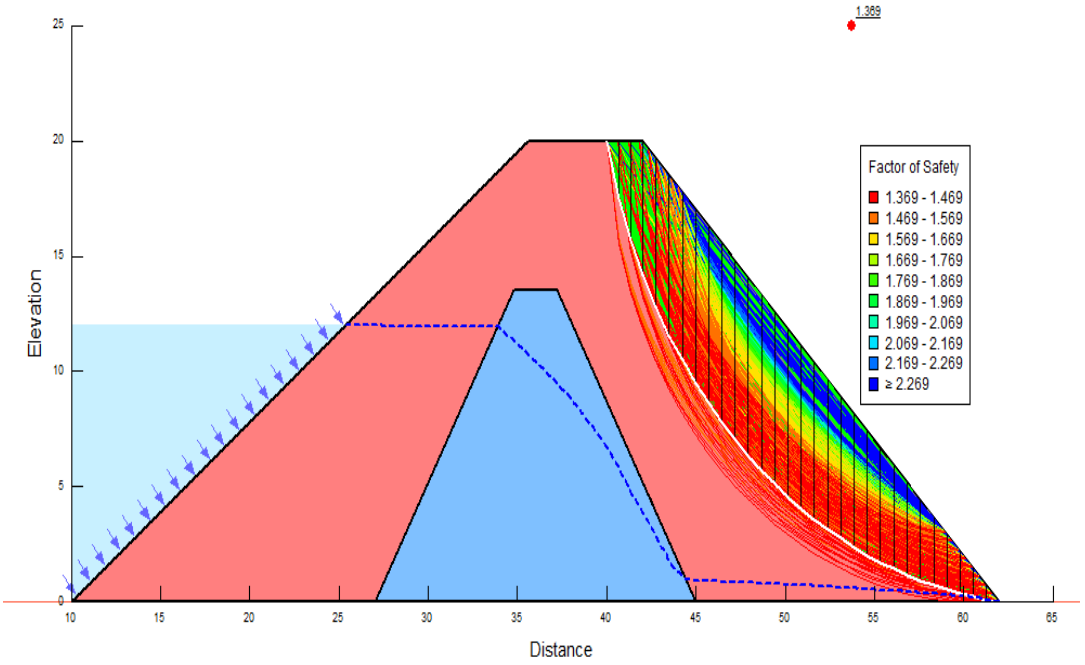

Figure 5.94b: FOS against sliding in downstream face of M9

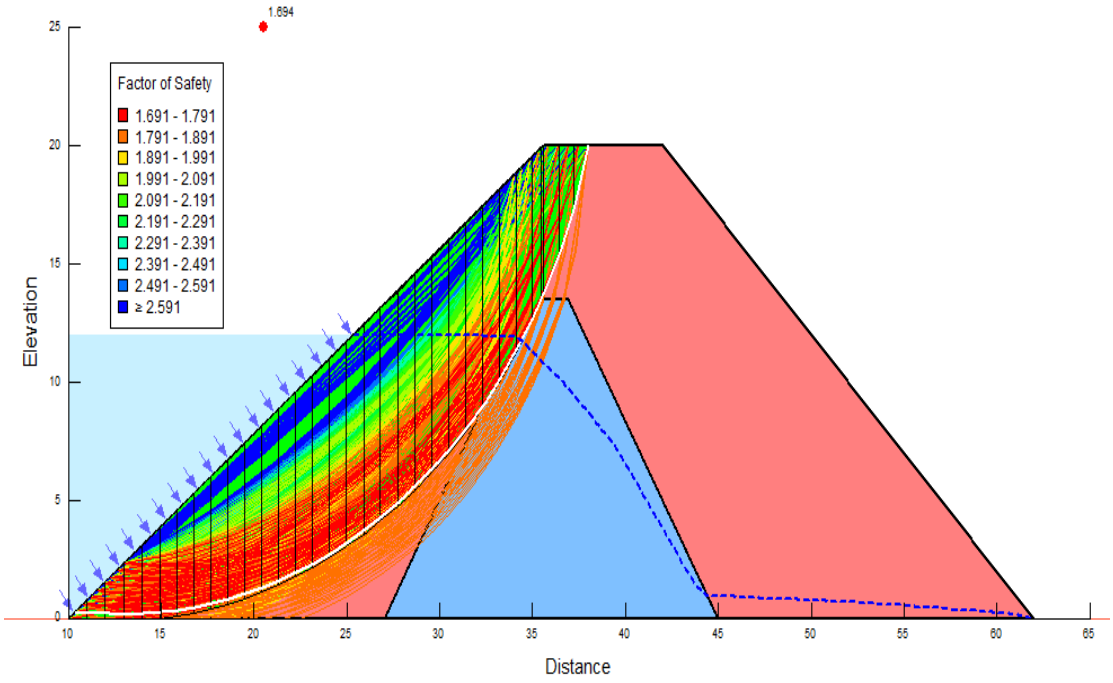

Figure 5.95a: FOS against sliding in upstream face of M10

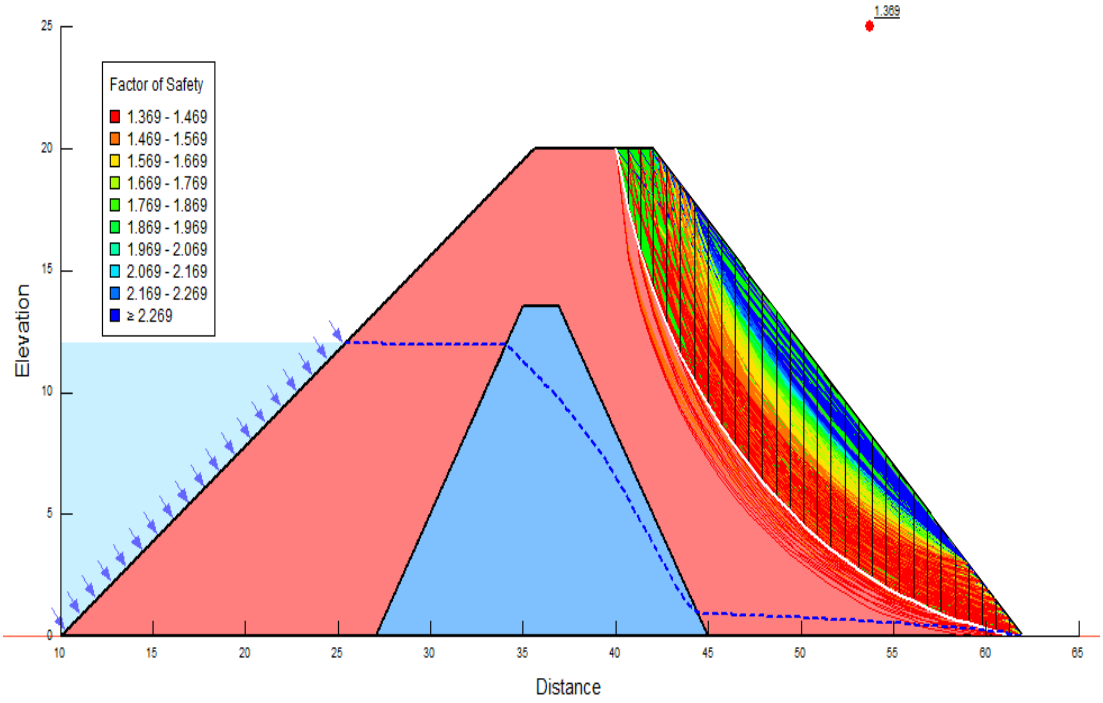

Figure 5.95b: FOS against sliding in downstream face of M10

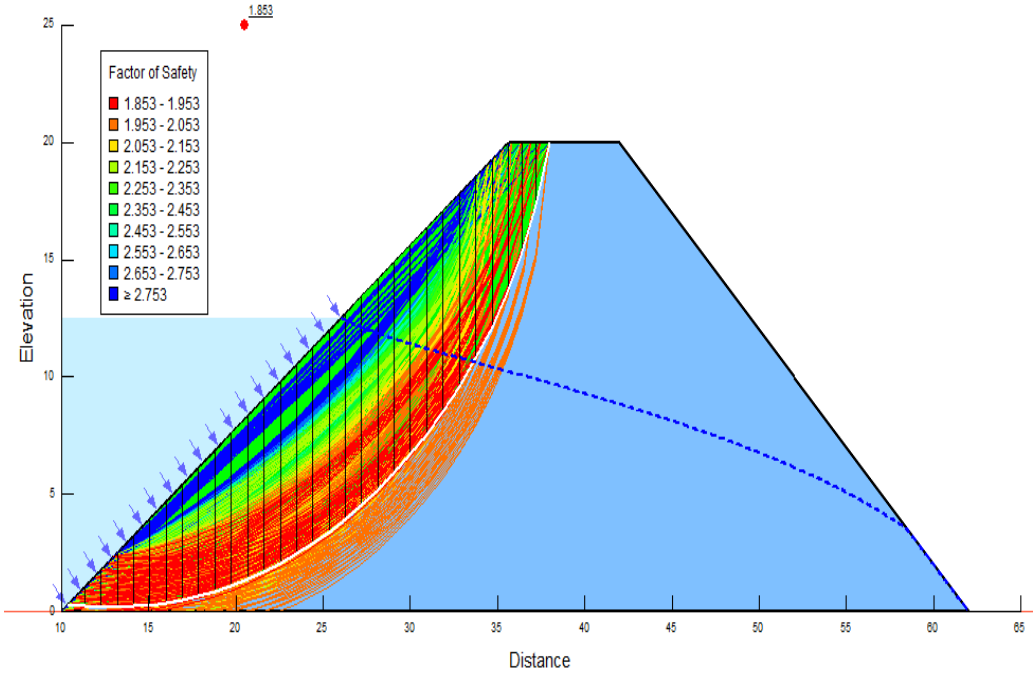

Figure 5.96a: FOS against sliding in upstream face of M11

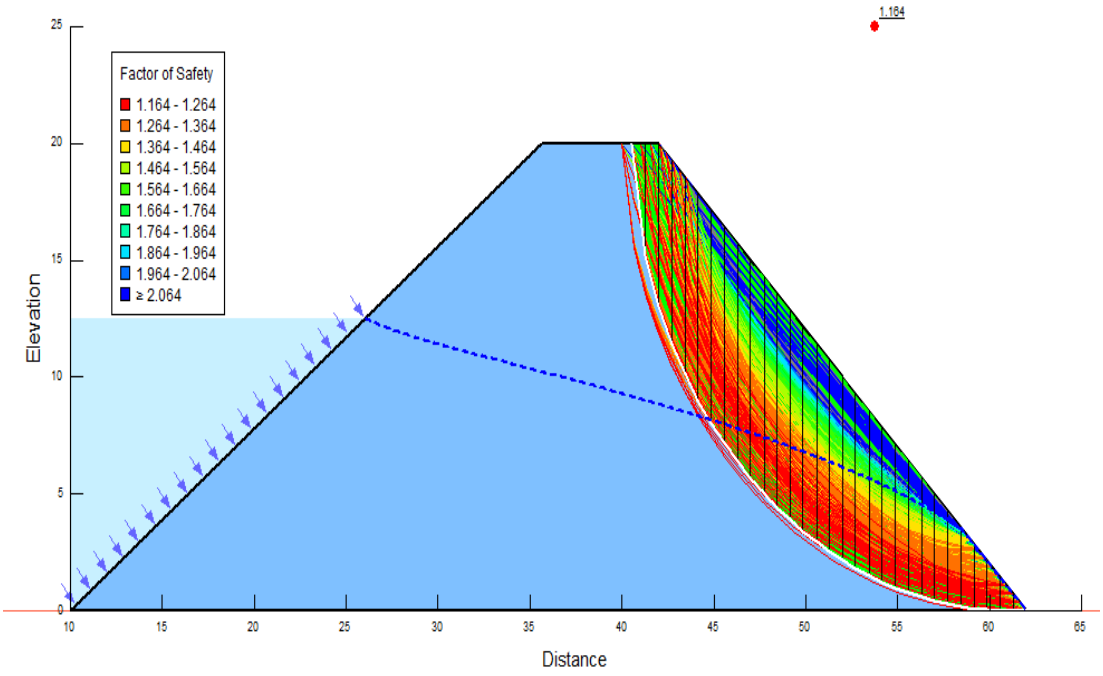

Figure 5.96b: FOS against sliding in downstream face of M11

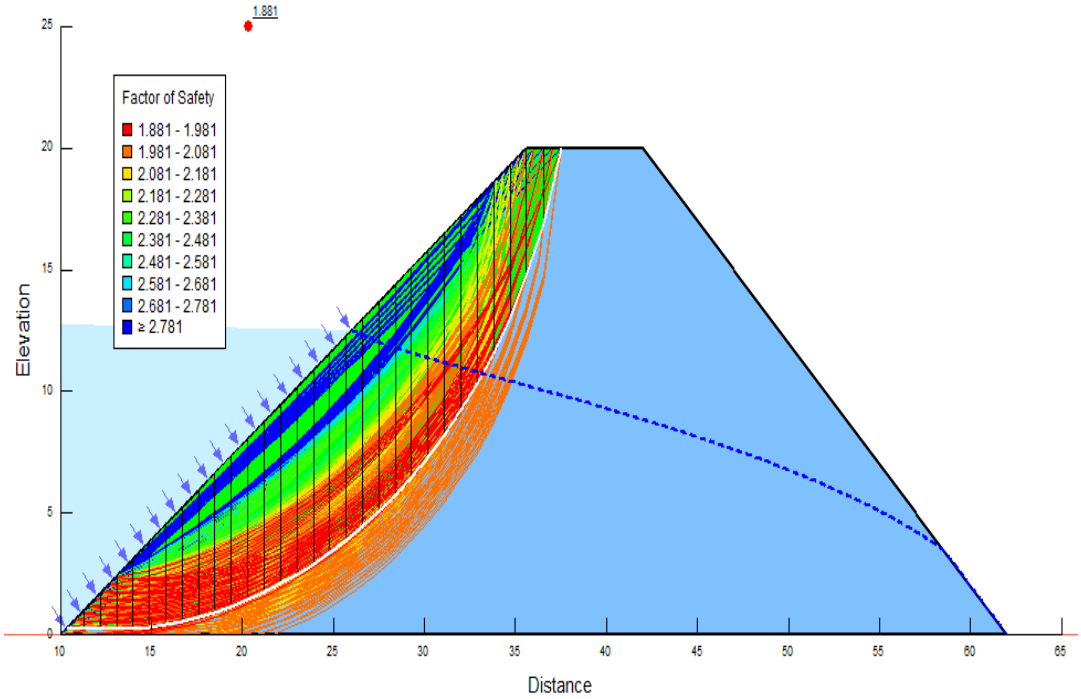

Figure 5.97a: FOS against sliding in upstream face of M12

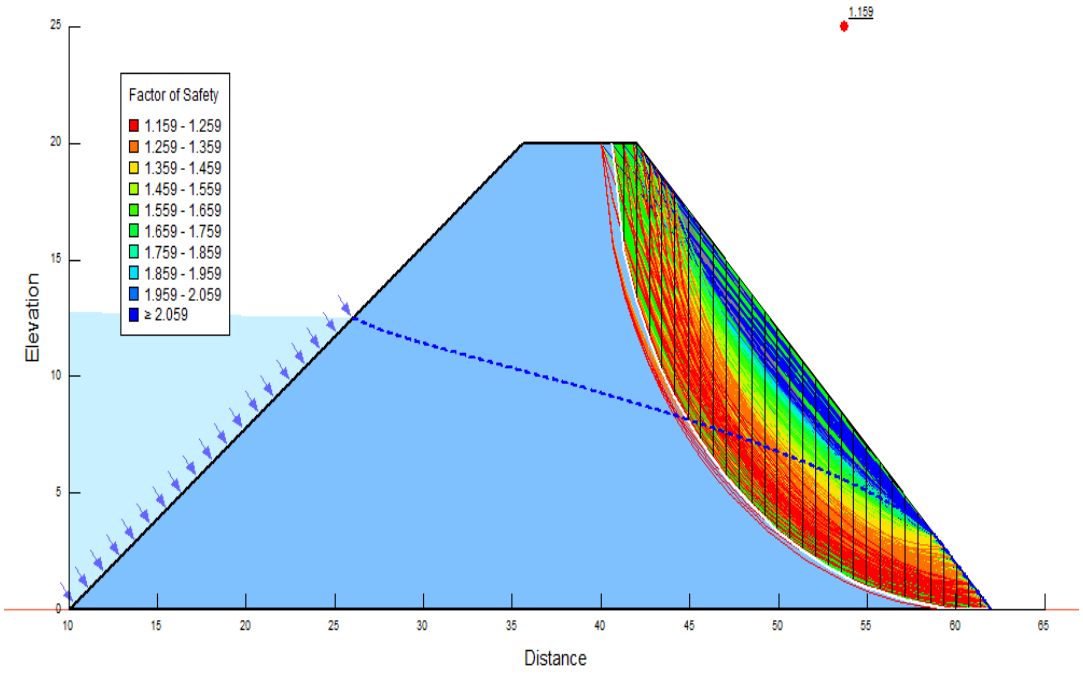

Figure 5.97b: FOS against sliding in downstream face of M12

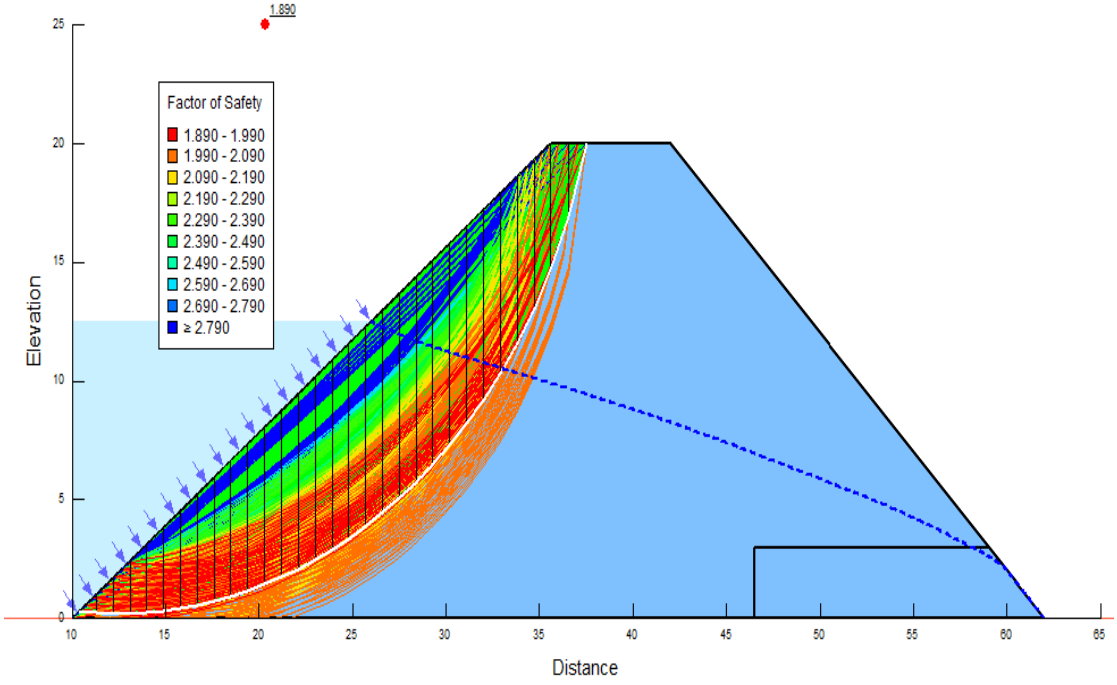

Figure 5.98a: FOS against sliding in upstream face of M13

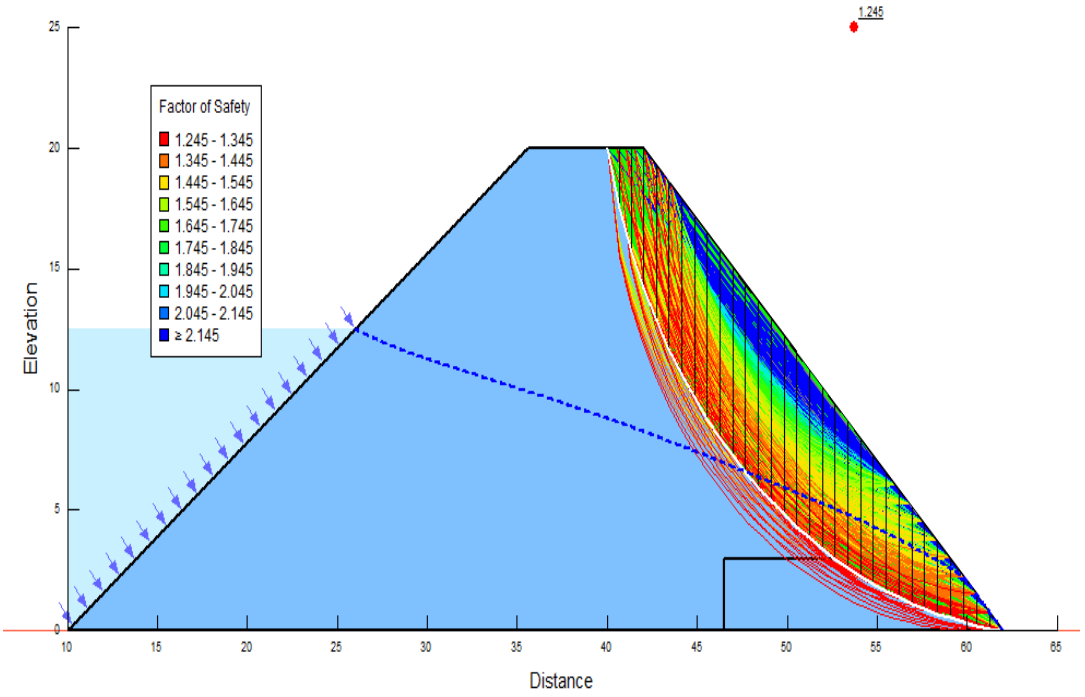

Figure 5.98b: FOS against sliding in downstream face of M13

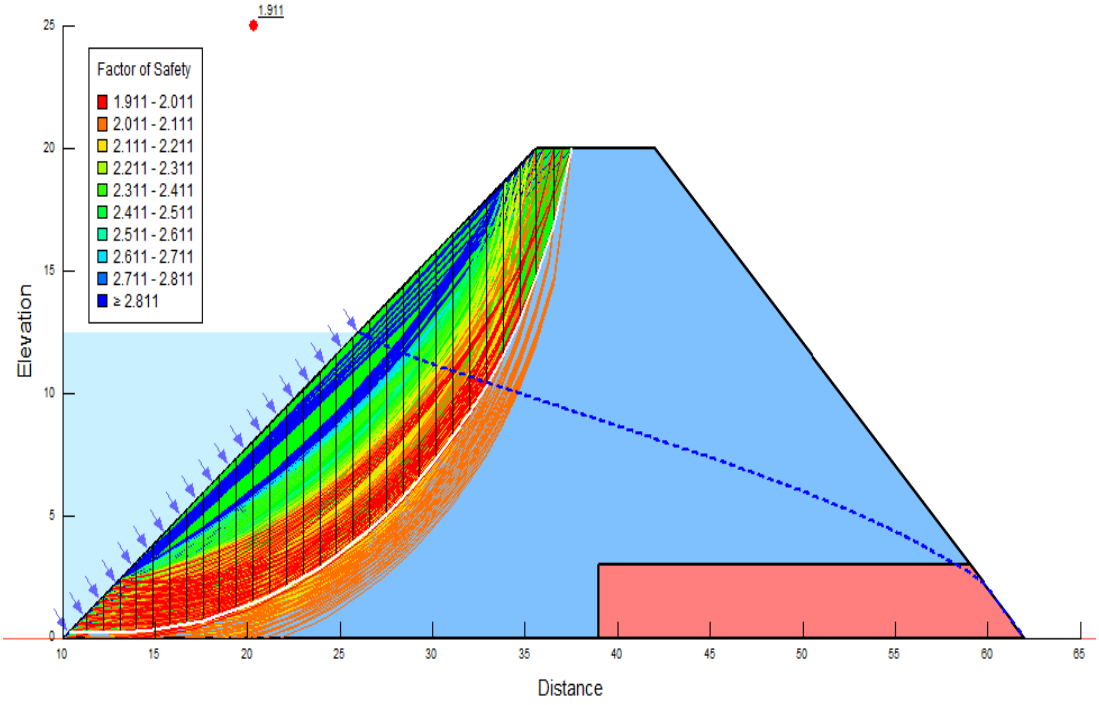

Figure 5.99a: FOS against sliding in upstream face of M14

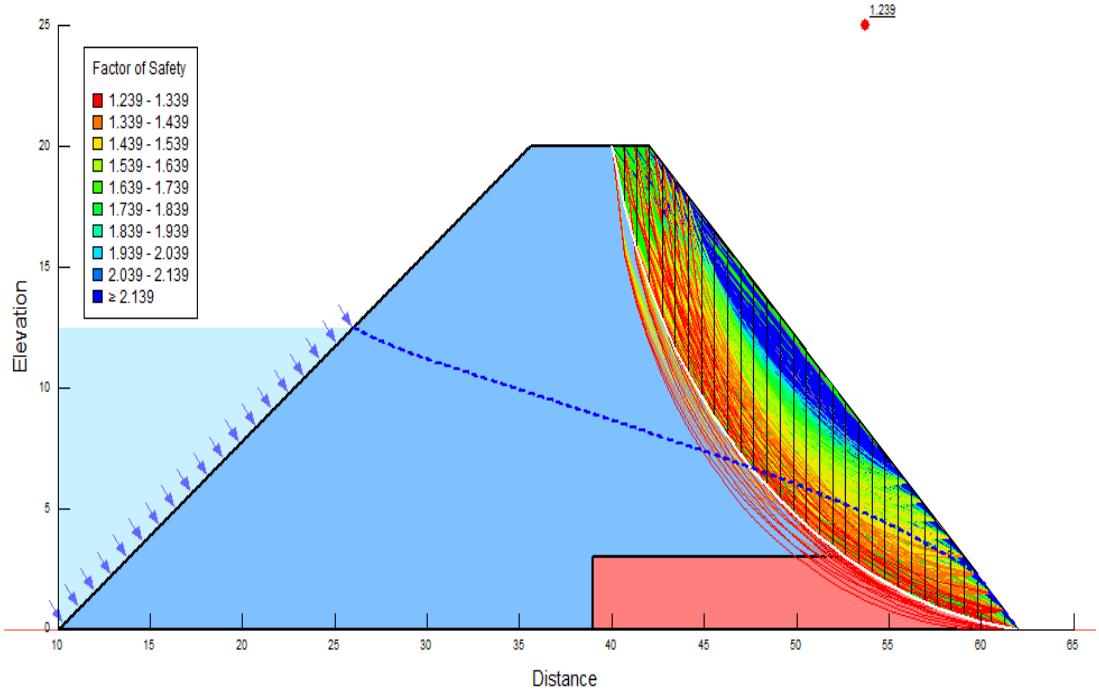

Figure 5.99b: FOS against sliding in downstream face of M14

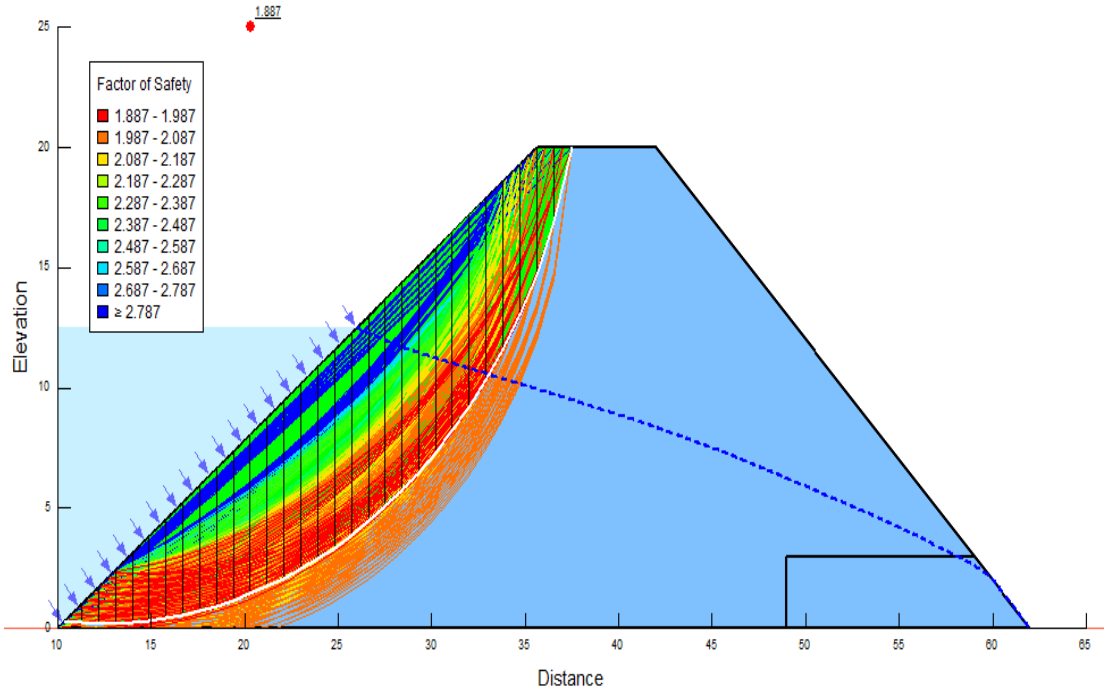

Figure 5.100a: FOS against sliding in upstream face of M15

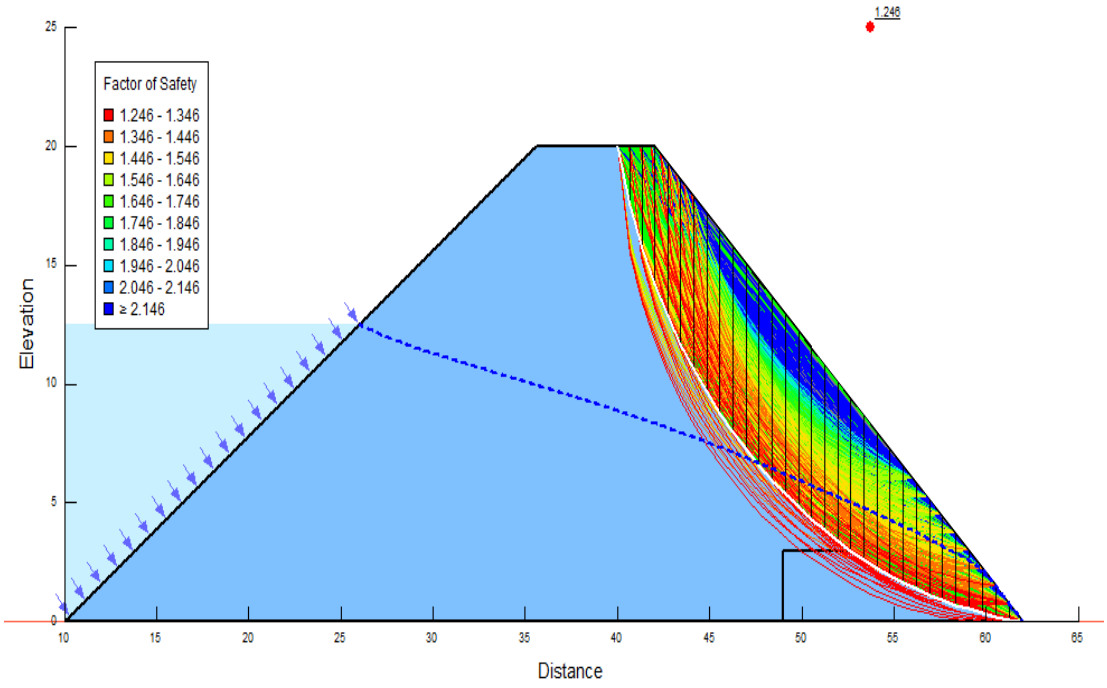

Figure 5.100b: FOS against sliding in downstream face of M15

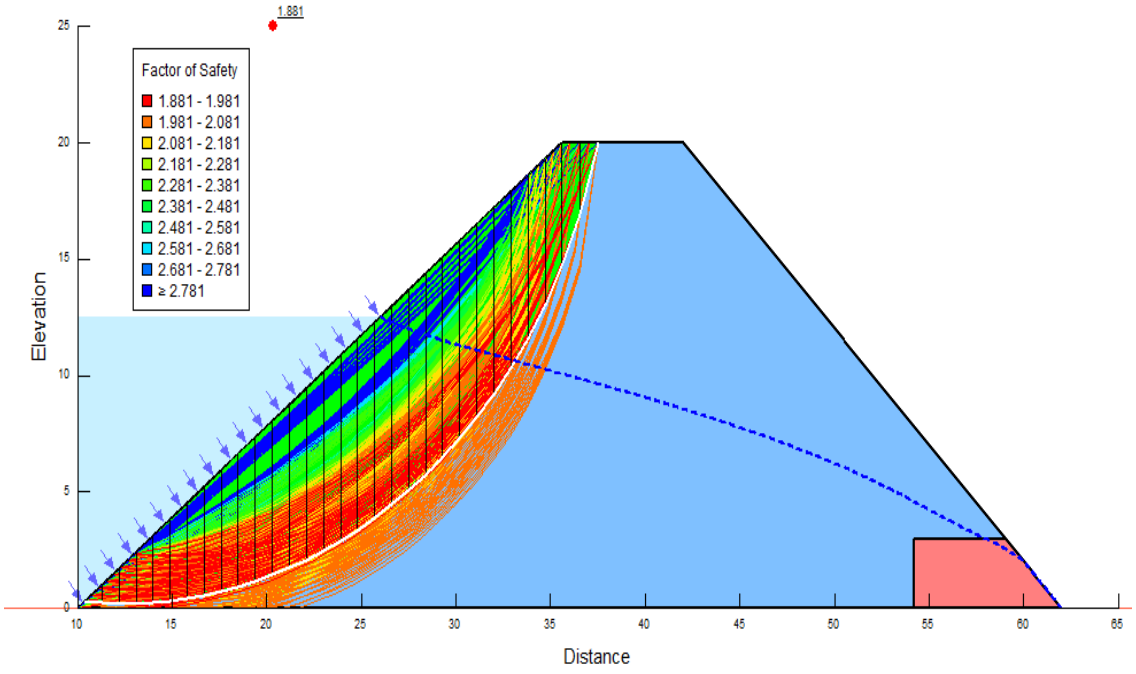

Figure 5.101a: FOS against sliding in upstream face of M16

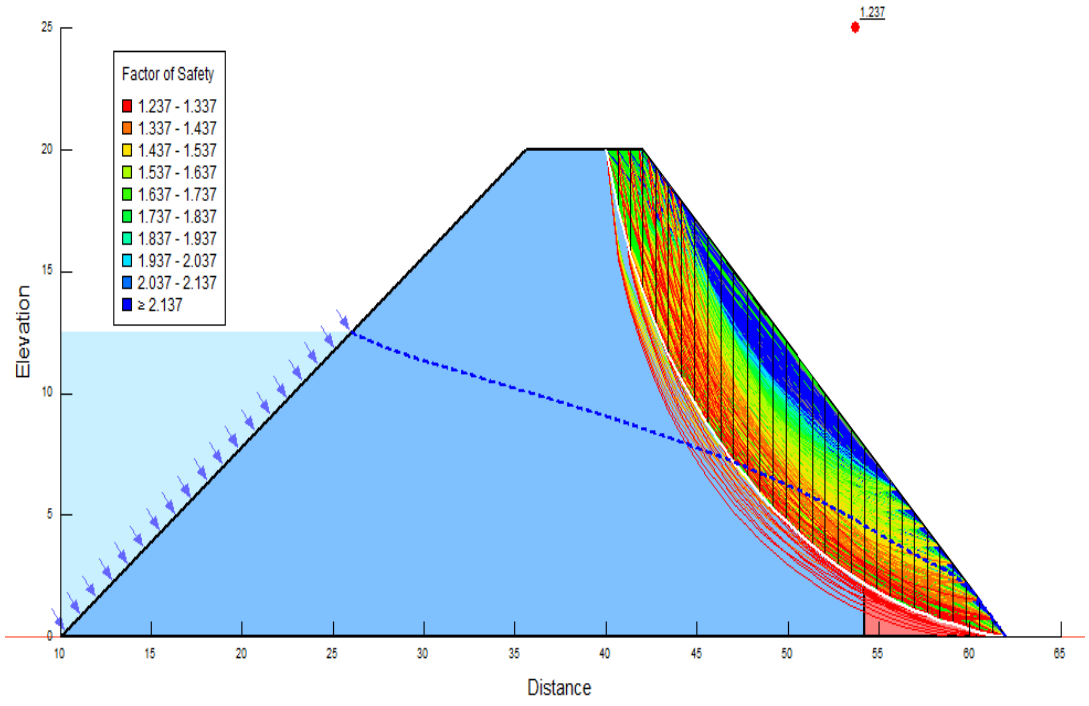

Figure 5.101b: FOS against sliding in downstream face of M16

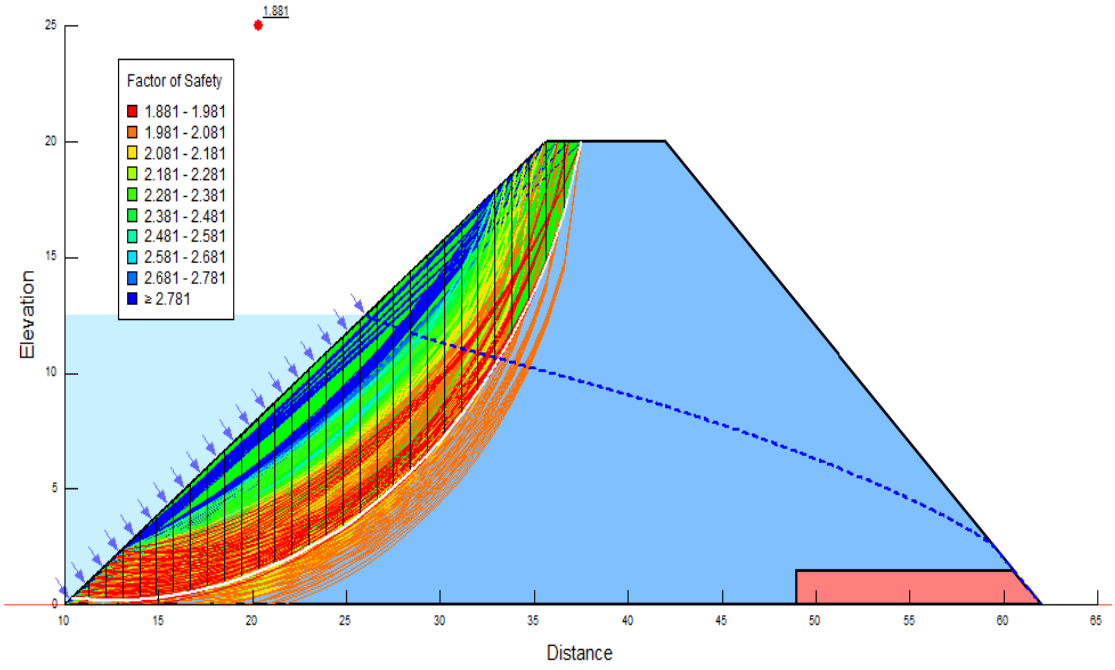

Figure 5.102a: FOS against sliding in upstream face of M17

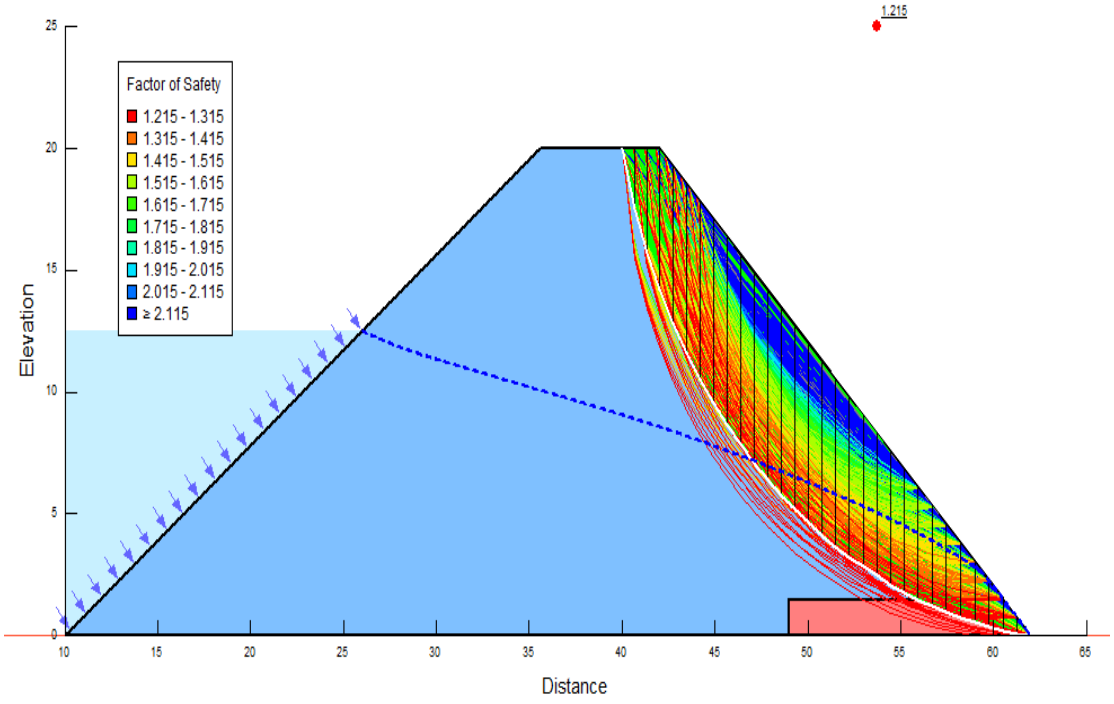

Figure 5.102b: FOS against sliding in downstream face of M17

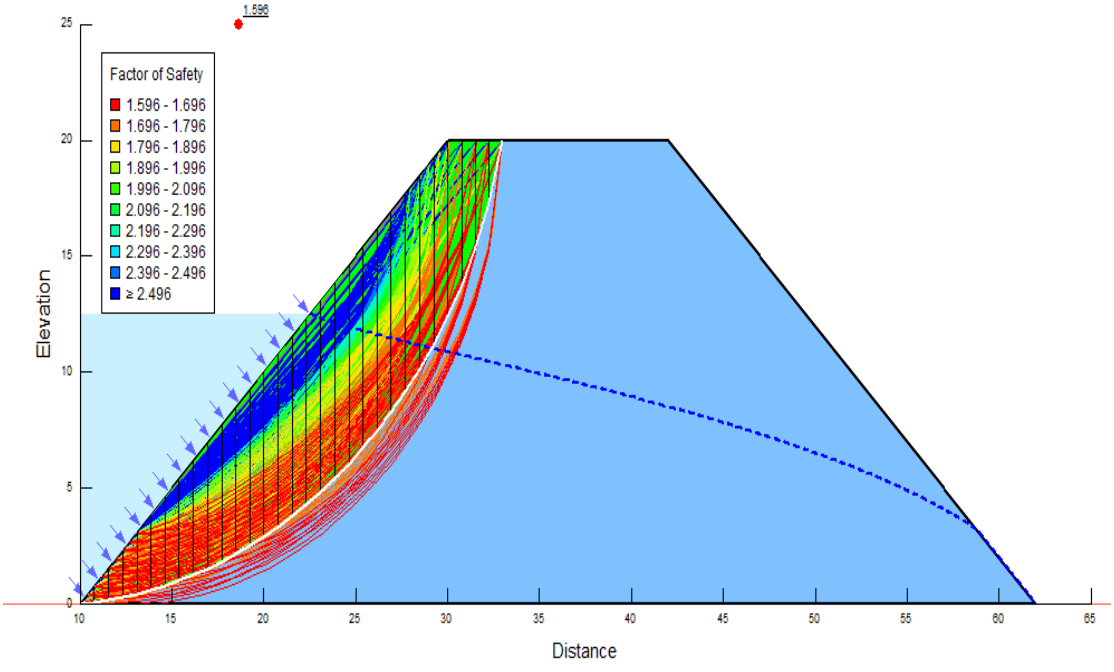

Figure 5.103a: FOS against sliding in upstream face of M18

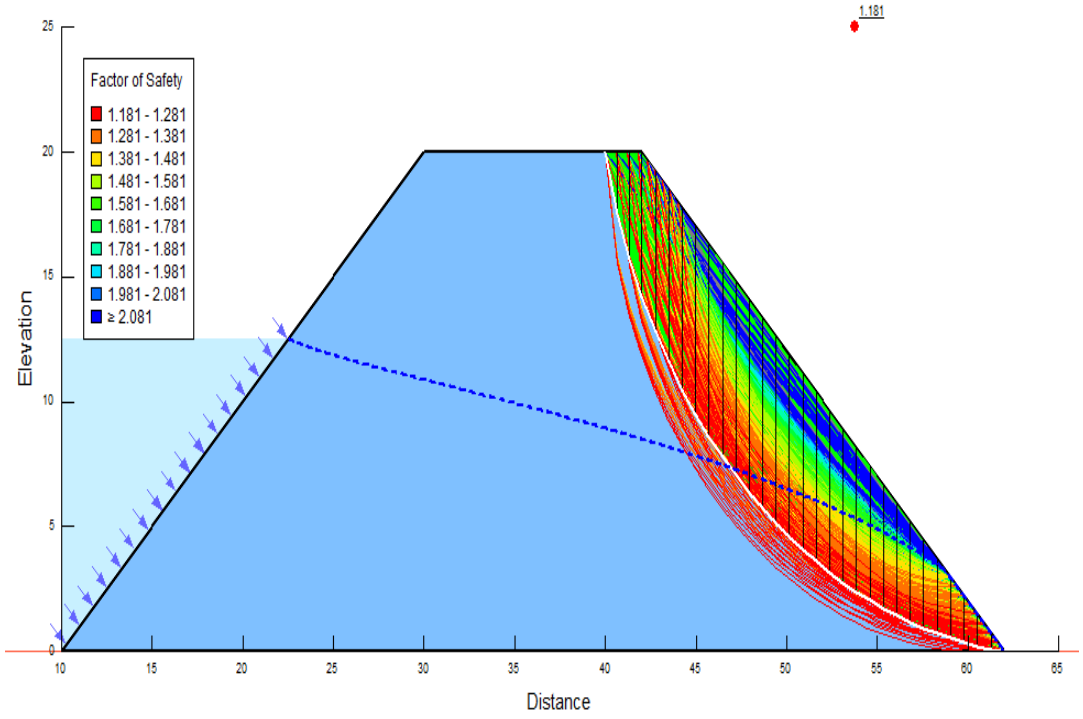

Figure 5.103b: FOS against sliding in downstream face of M18

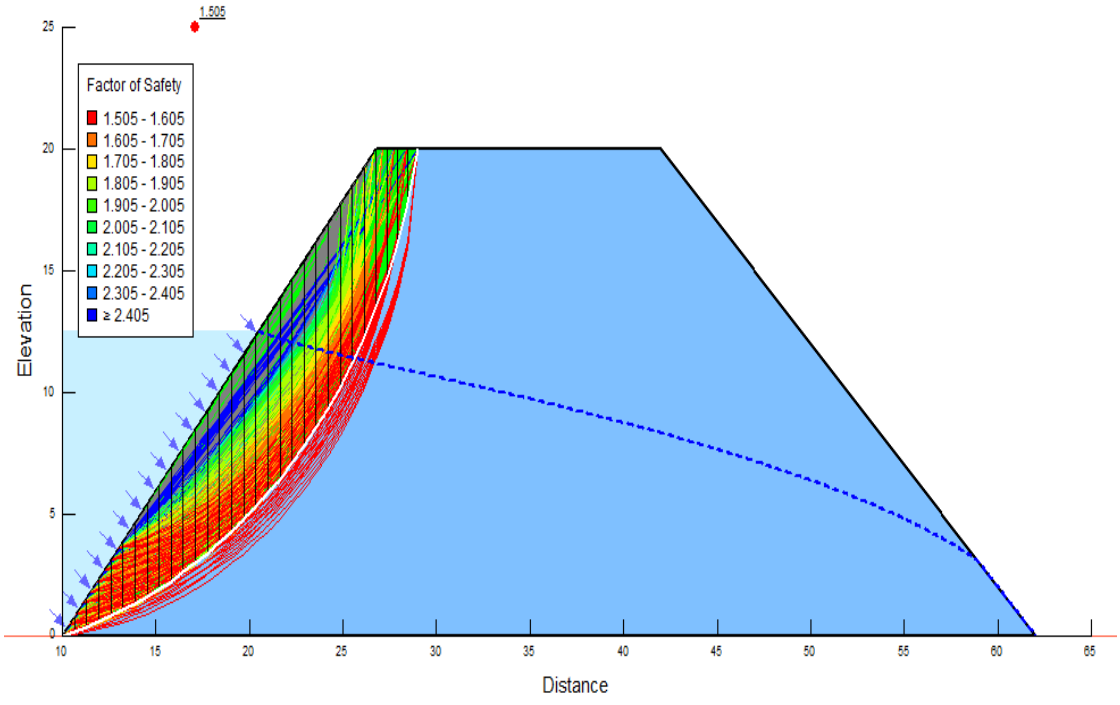

Figure 5.104a: FOS against sliding in upstream face of M19

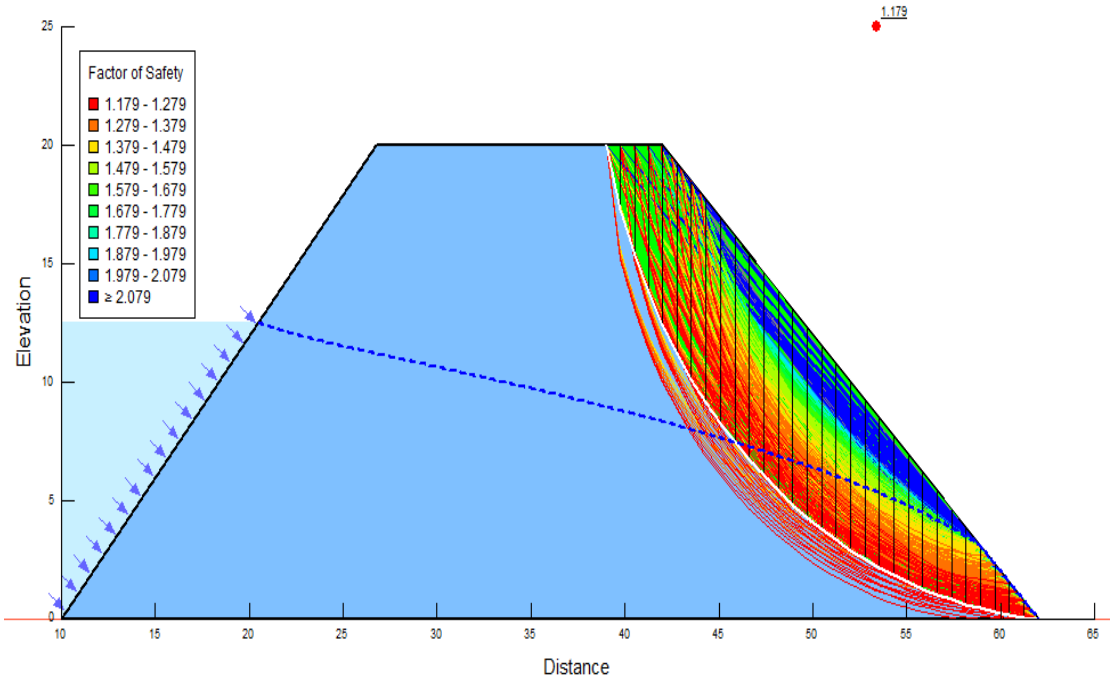

Figure 5.104b: FOS against sliding in downstream face of M19

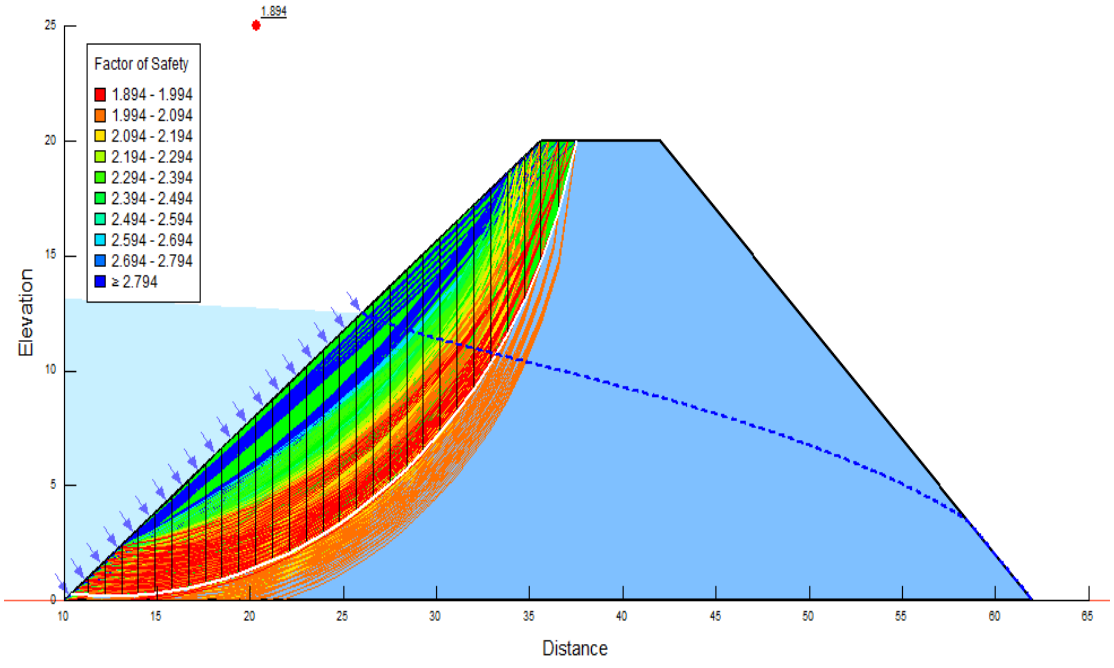

Figure 5.105a: FOS against sliding in upstream face of M20

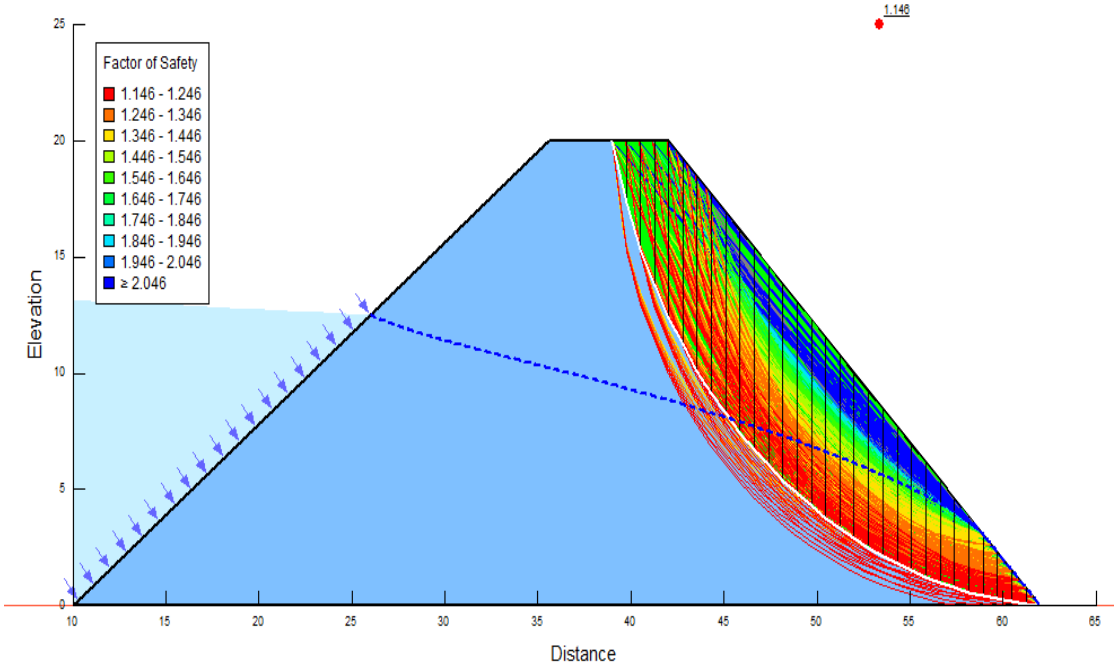

Figure 5.105b: FOS against sliding in downstream face of M20

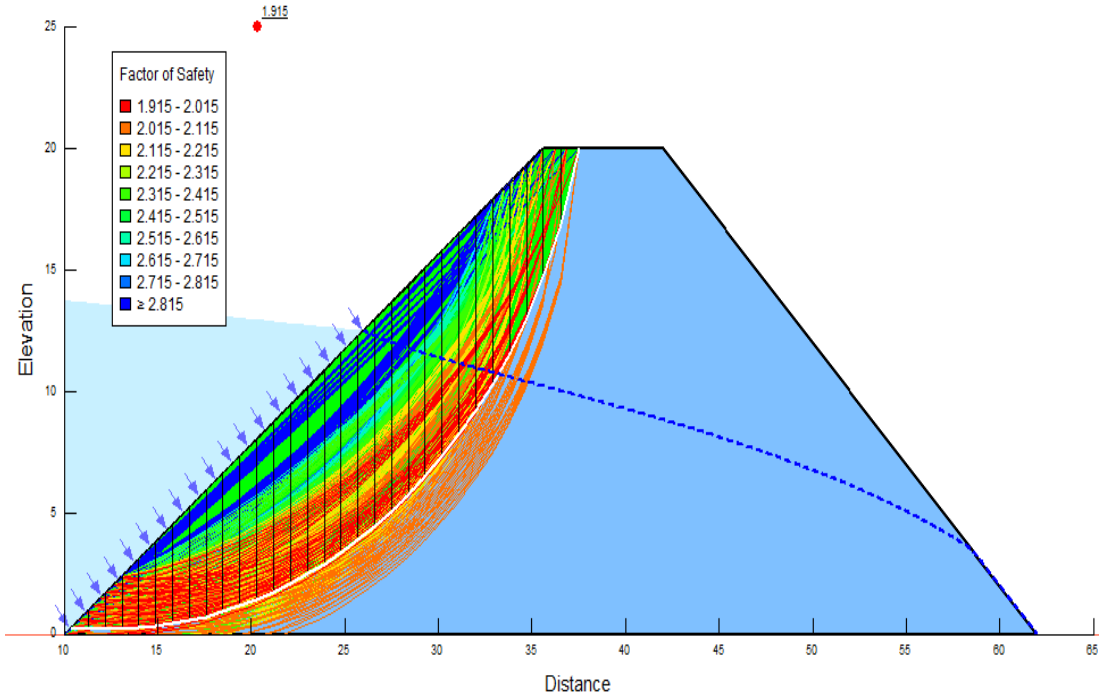

Figure 5.106a: FOS against sliding in upstream face of M21

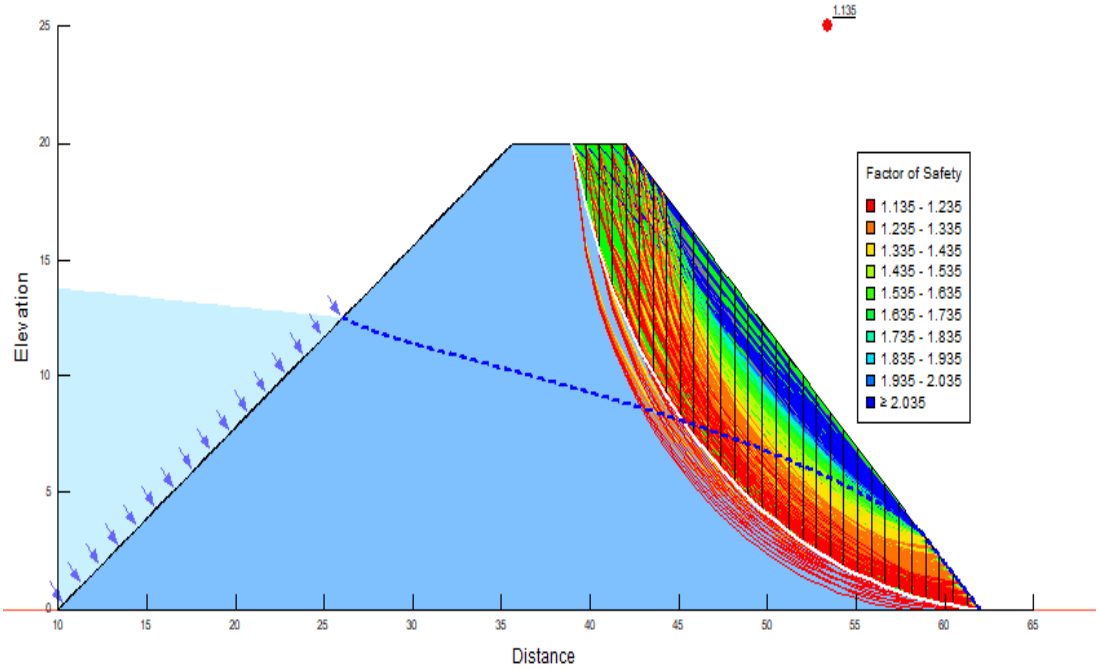

Figure 5.106b: FOS against sliding in downstream face of M21

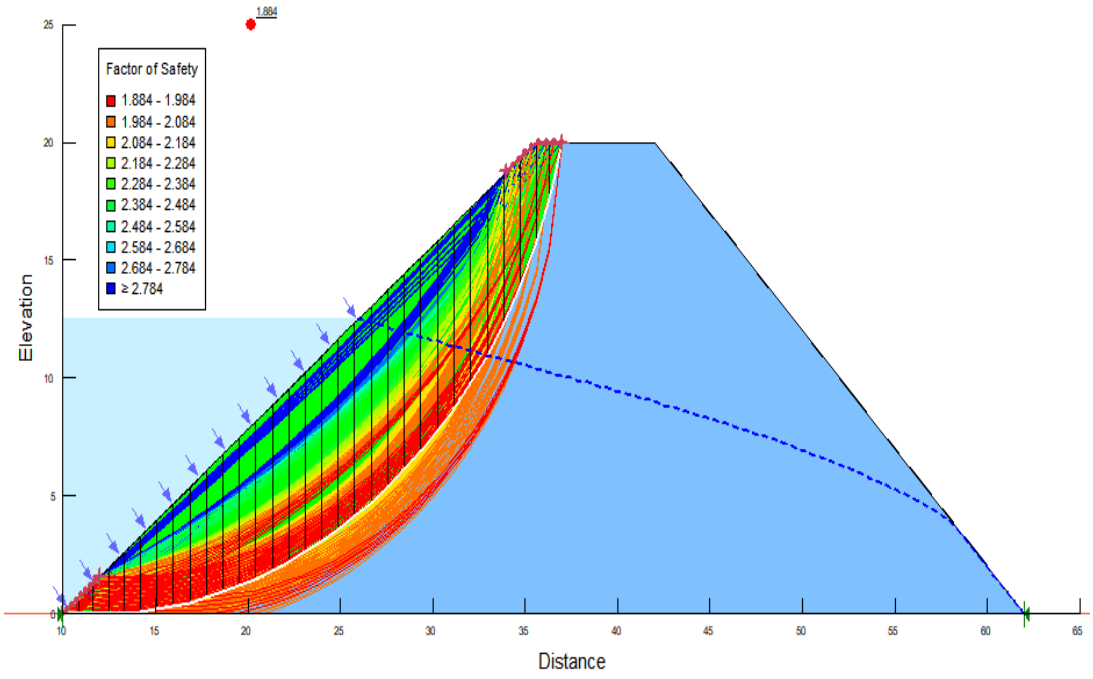

Figure 5.107a: FOS against sliding in upstream face of M22

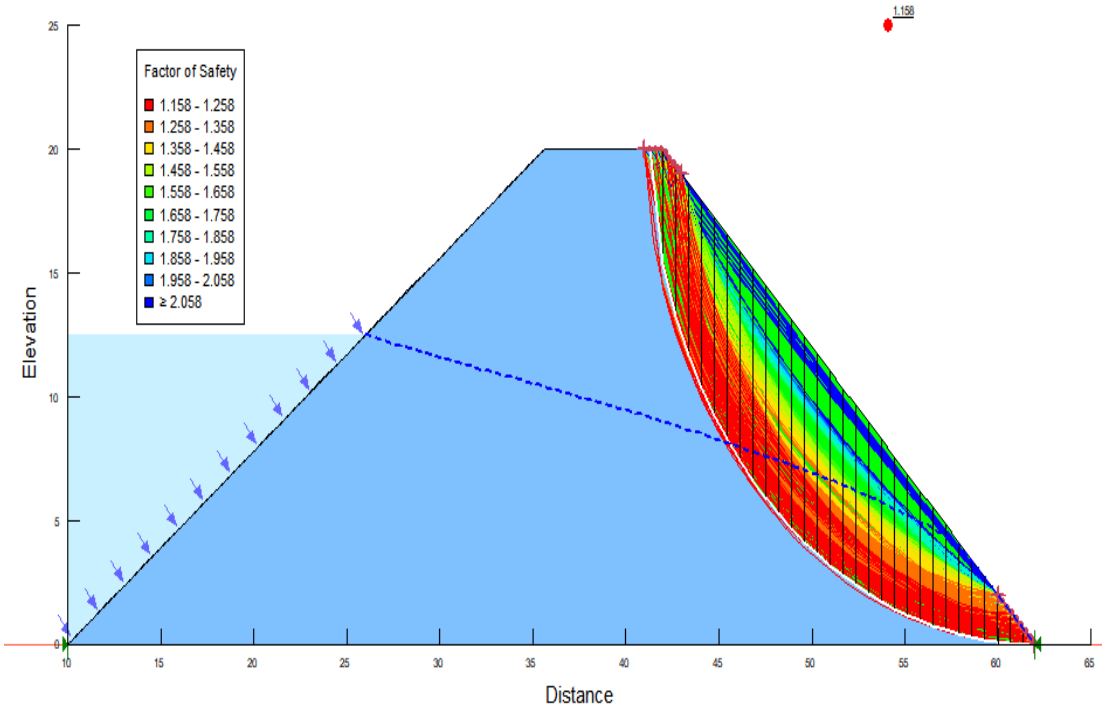

Figure 5.107b: FOS against sliding in downstream face of M22

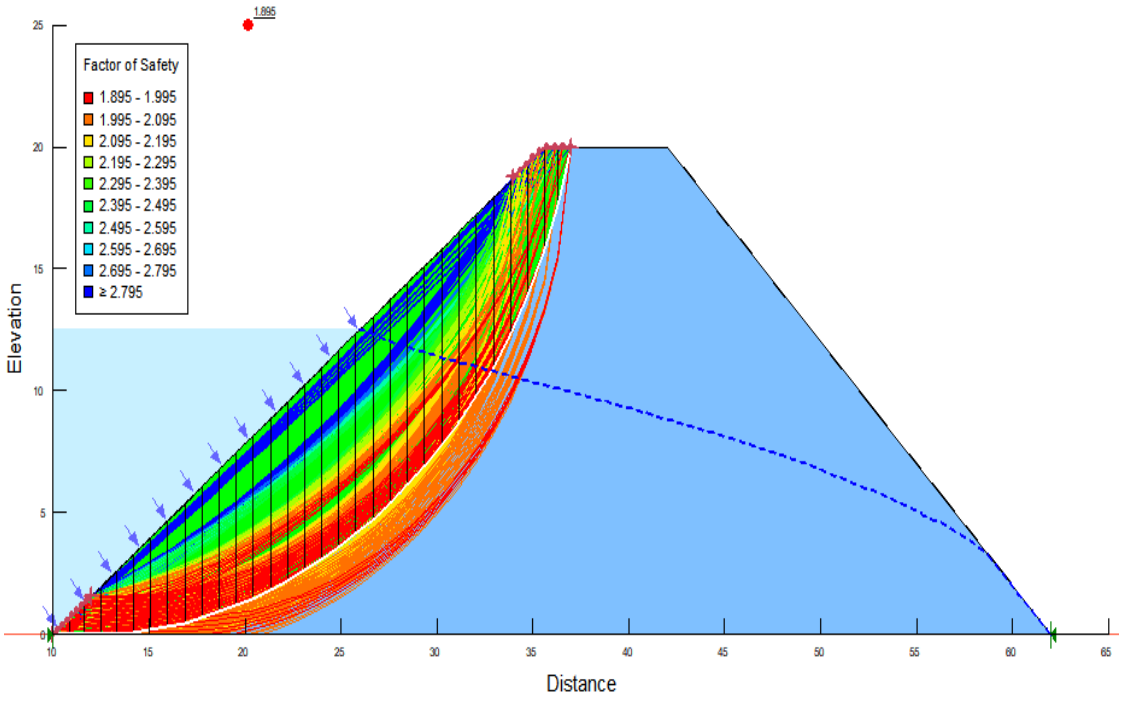

Figure 5.108a: FOS against sliding in upstream face of M23

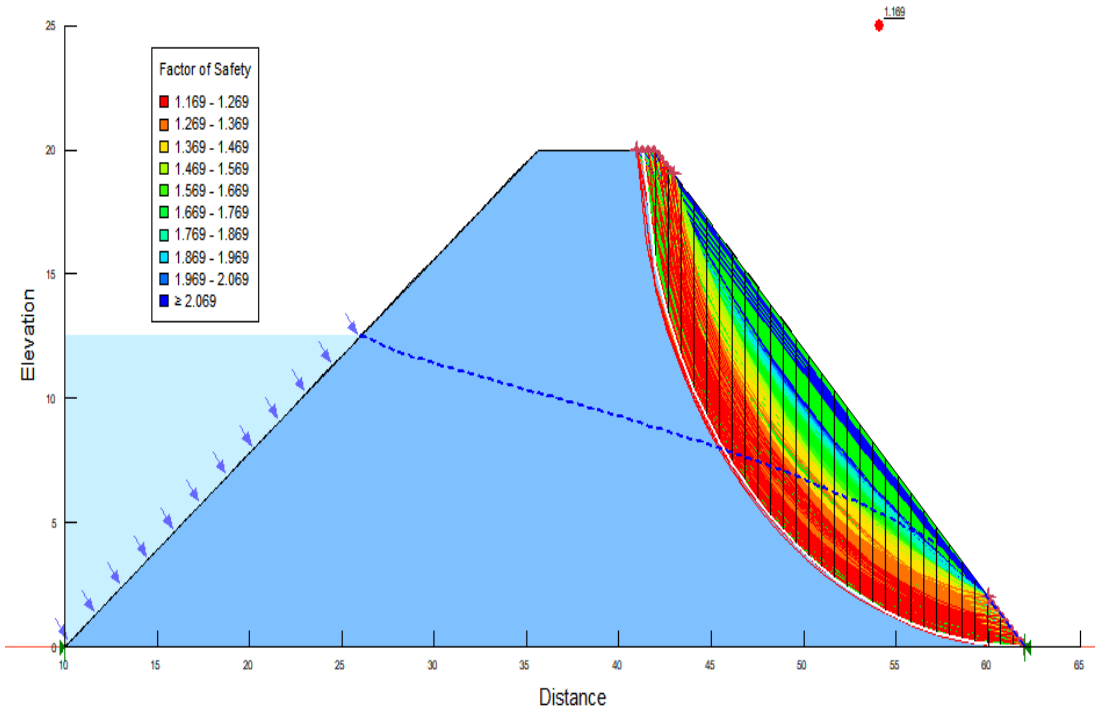

Figure 5.108b: FOS against sliding in downstream face of M23

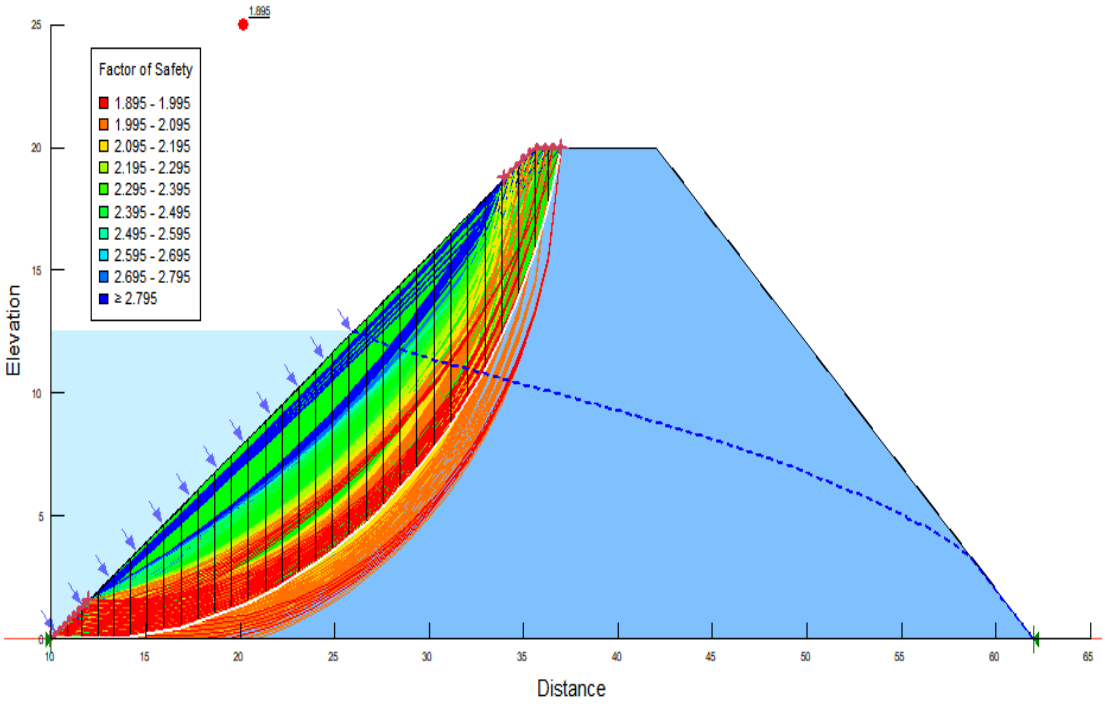

Figure 5.109a: FOS against sliding in upstream face of M24

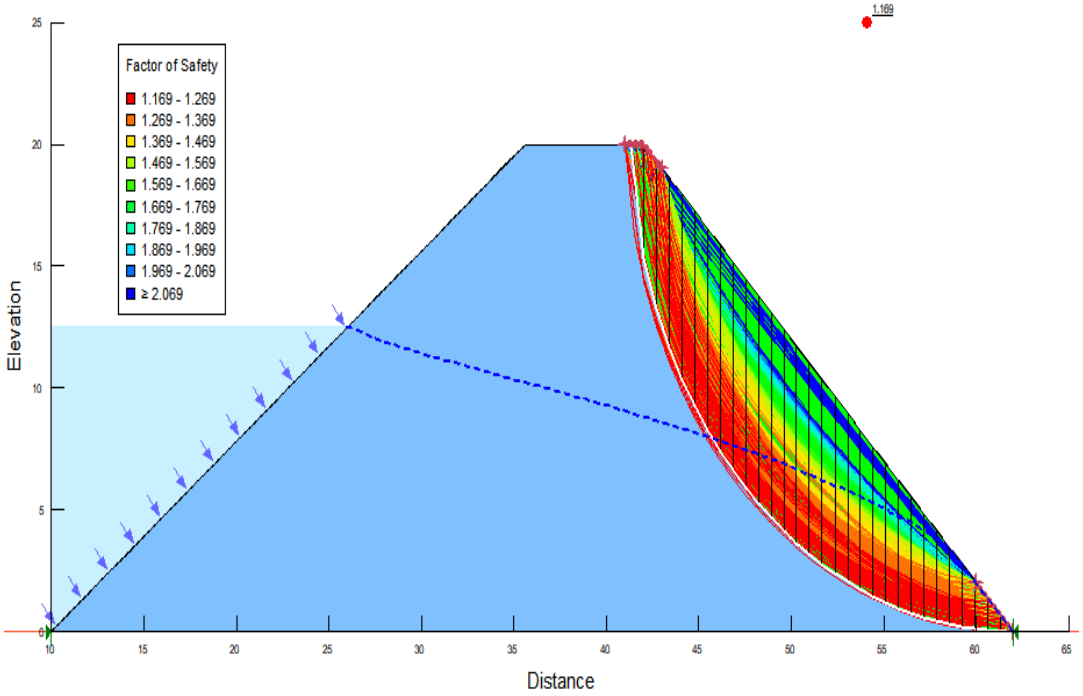

Figure 5.109b: FOS against sliding in downstream face of M24

5.1.3 Seepage discharge

Experimental and numerical models were compared. The results of the experimental model were in good agreement with those of the numerical model. For experimental and numerical homogeneous models, the determination coefficient for a polynomial trendline (R^2) was 0.92 and 0.87, respectively. The value of the coefficient of determination (R^2) can be considered good above 0.75 for scholarly research and above 0.6 as an acceptable solution; the value of R^2 equal to 1 represents a perfect determination (Vogt and Johnson; 2015) (Sarstedt and Mooi; 2014). Table 5.11 shows the seepage discharge comparison between experimental and numerical models. The percentage error in respect of seepage discharge in the experimental model is also presented in Table 5.11. Percentage error shows a value of less than 10% except in models M2, M7 and M10. It was a little higher than 10per cent and within 12 per cent. Figure 5.110 depicts a graph comparing seepage discharge from several experimental and numerical models.

Table 5.11: Comparison of seepage discharge by experimental and numerical modelling

Model No.	Seepage discharge from physical model (m^3/s)	Seepage discharge from numerical model (m^3/s)	% Error
M1	0.1639×10^{-6}	0.173822×10^{-6}	06.05
M2	0.2995×10^{-6}	0.330324×10^{-6}	10.29
M3	0.1402×10^{-6}	0.128399×10^{-6}	08.41
M4	0.1265×10^{-6}	0.128396×10^{-6}	01.49
M5	0.1248×10^{-6}	0.128277 x 10-6	02.78
M6	0.1908×10^{-6}	0.202950×10^{-6}	06.36
M7	0.1768×10^{-6}	0.196742×10^{-6}	11.27
M8	0.1822×10^{-6}	0.198662×10^{-6}	09.03
M9	0.0901×10^{-6}	0.094837×10^{-6}	05.25
M10	0.0978×10^{-6}	0.108371×10^{-6}	10.80
M11	0.1524×10^{-6}	0.160240×10^{-6}	05.14
M12	0.1630×10^{-6}	0.173822×10^{-6}	06.63
M13	0.3326×10^{-6}	0.343686×10^{-6}	03.33
M14	0.3853×10^{-6}	0.393922×10^{-6}	02.23
M15	0.2911×10^{-6}	0.303594×10^{-6}	04.29
M16	0.2609×10^{-6}	0.278359×10^{-6}	06.69
M17	0.2796×10^{-6}	0.283218×10^{-6}	01.29
M18	0.1624×10^{-6}	0.173674×10^{-6}	06.94
M19	0.1609×10^{-6}	0.171922×10^{-6}	06.85
M20	0.1596×10^{-6}	0.173821×10^{-6}	08.91
M21	0.1584×10^{-6}	0.173819×10^{-6}	09.73
M22	0.0013×10^{-6}	0.001377×10^{-6}	05.92
M23	0.0820×10^{-6}	0.084675×10^{-6}	03.26
M24	0.0717×10^{-6}	0.073179×10^{-6}	02.06

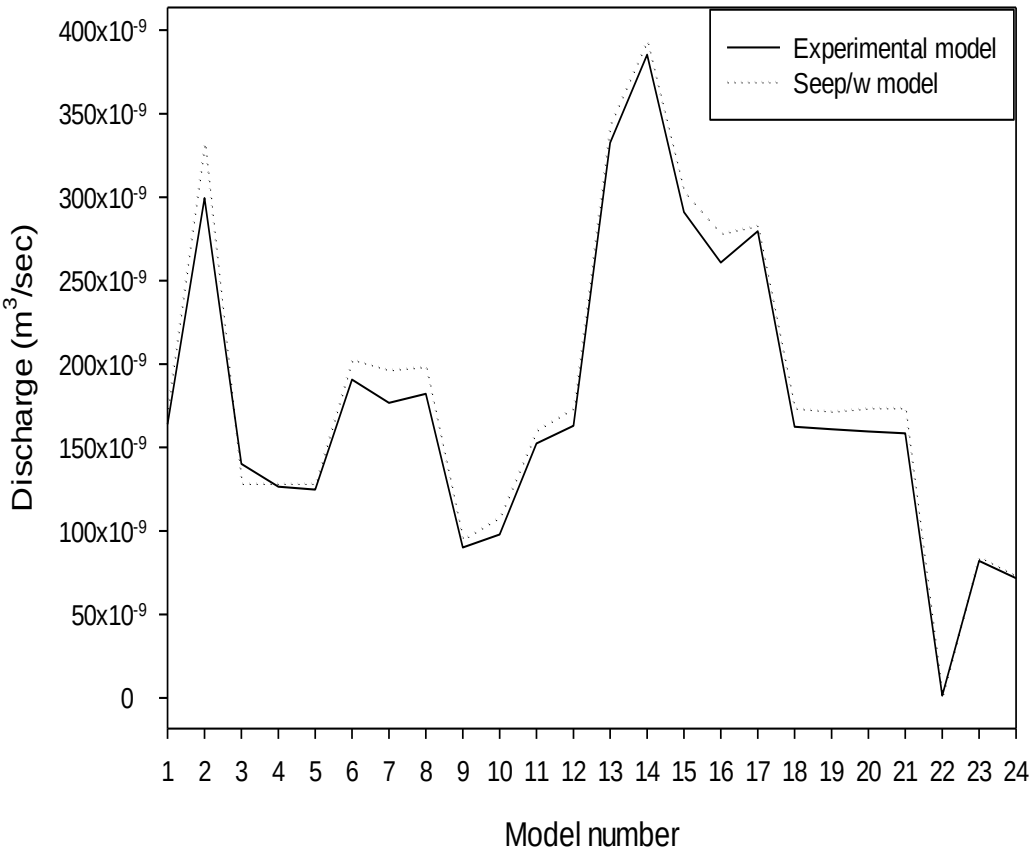

Figure 5.110: Graph showing discharge comparison between Experimental results and results obtained using Seep/w for different models

The seepage discharge obtained through experimental and numerical modelling was compared to the seepage discharge derived from Dupuit's, Casagrande's, Schaffernak's, and Pavlovsky's analytical solutions in a homogeneous earth dam model M1-M5, M11, M18, and M19. Figure 5.111 shows a graphical comparison of seepage discharge, recorded in table 5.12.

Table 5.12: Comparison of seepage discharge (m^3/s) of experimental and numerical models of a homogeneous earth dam with seepage discharge obtained using analytical solutions given by Dupuit, Casagrande, Pavlovsky, and Schaffernak.

Model No.	Experimental results of the physical model	Numerical results of the FEM model using Seep/w		Analytical results using Dupuit's solution		Analytical results using Casagrande's solution		Analytical results using Schaffernak's solution		Analytical results using Pavlovsky's solution	
		Value	% error	Value	% error	Value	% error	Value	% error	Value	% error
M1	0.1639 x 10^{-6}	0.1738 x 10^{-6}	06.05	0.1781 x 10^{-6}	08.71	0.1555 x 10^{-6}	15.55	0.1597 x 10^{-6}	02.55	0.1289 x 10^{-6}	21.34
M2	0.2995 x 10^{-6}	0.3303 x 10^{-6}	10.29	0.1781 x 10^{-6}	40.50	0.1726 x 10^{-6}	42.34	0.1566 x 10^{-6}	47.70	0.1303 x 10^{-6}	56.46
M3	0.1402 x 10^{-6}	0.1283 x 10^{-6}	08.41	0.1519 x 10^{-6}	08.35	0.1453 x 10^{-6}	03.69	0.1483 x 10^{-6}	05.78	0.1647 x 10^{-6}	17.51
M4	0.1265 x 10^{-6}	0.1283 x 10^{-6}	01.49	0.1383 x 10^{-6}	09.34	0.1320 x 10^{-6}	13.20	0.1346 x 10^{-6}	06.46	0.1281 x 10^{-6}	01.29
M5	0.1248 x 10^{-6}	0.1282 x 10^{-6}	02.78	0.1383 x 10^{-6}	10.83	0.1286 x 10^{-6}	03.09	0.1312 x 10^{-6}	05.13	0.1304 x 10^{-6}	04.51
M11	0.1524 x 10^{-6}	0.1602 x 10^{-6}	05.14	0.1621 x 10^{-6}	06.39	0.1422 x 10^{-6}	06.63	0.1018 x 10^{-6}	33.19	0.1221 x 10^{-6}	19.86
M18	0.1624 x 10^{-6}	0.1736 x 10^{-6}	06.94	0.1605 x 10^{-6}	01.11	0.1454 x 10^{-6}	10.41	0.1491 x 10^{-6}	08.15	0.1329 x 10^{-6}	18.11
M19	0.1609 x 10^{-6}	0.17192 x 10^{-6}	06.85	0.1519 x 10^{-6}	05.58	0.1403 x 10^{-6}	12.74	0.1436 x 10^{-6}	10.70	0.1323 x 10^{-6}	17.77

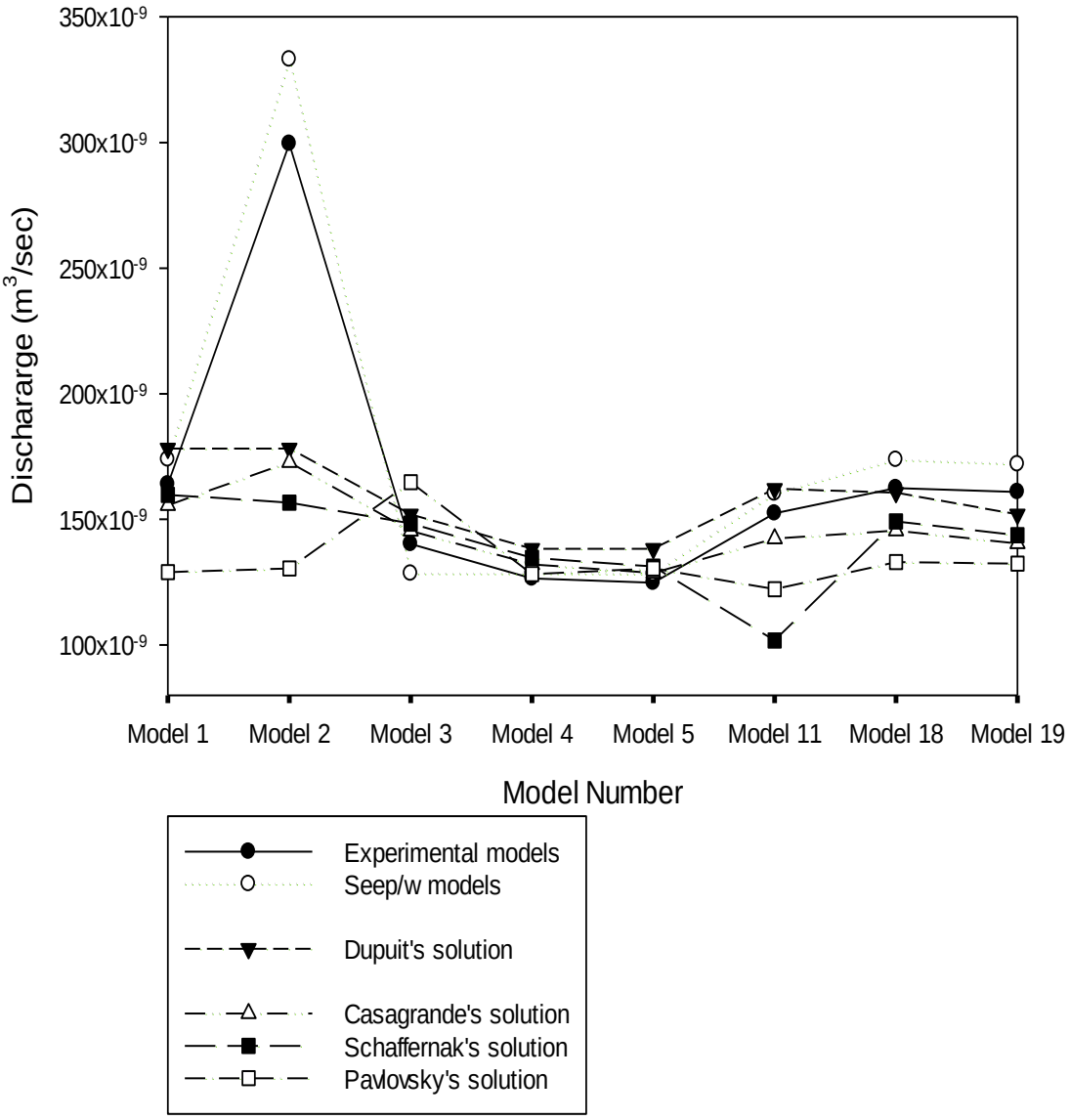

Figure 5.111: Graph showing discharge comparison between Experimental results and the results obtained using Seep/w, Casagrande's, Dupuit's, Pavlovsky's, and Schaffernak's solution for homogeneous earth dam models.

The percentage error in seepage discharge in physical models was calculated with respect to the numerical model, Casagrande's, Dupuit's, Pavlovsky's, and Schaffernak's solution and shown in figure 5.112. It was seen that second to the discharge obtained using numerical models, Schaffernak's solution yielded the closest result in general when compared with seepage discharge in homogeneous earth dam models using physical and numerical models except in M2, M11 and M19 models.

Casagrande's solution had an acceptable solution only for M3, M5 and M11 models. While Dupuit's model didn't yield a good result except in M18 and M19. Pavlovsky's solutions were not in the acceptable range except for models M4 and M5. Hence Pavlovsky's solution, Casagrande's, and Dupuit's solution were not in the acceptable range. Hence numerical models had the closest results to the physical models.

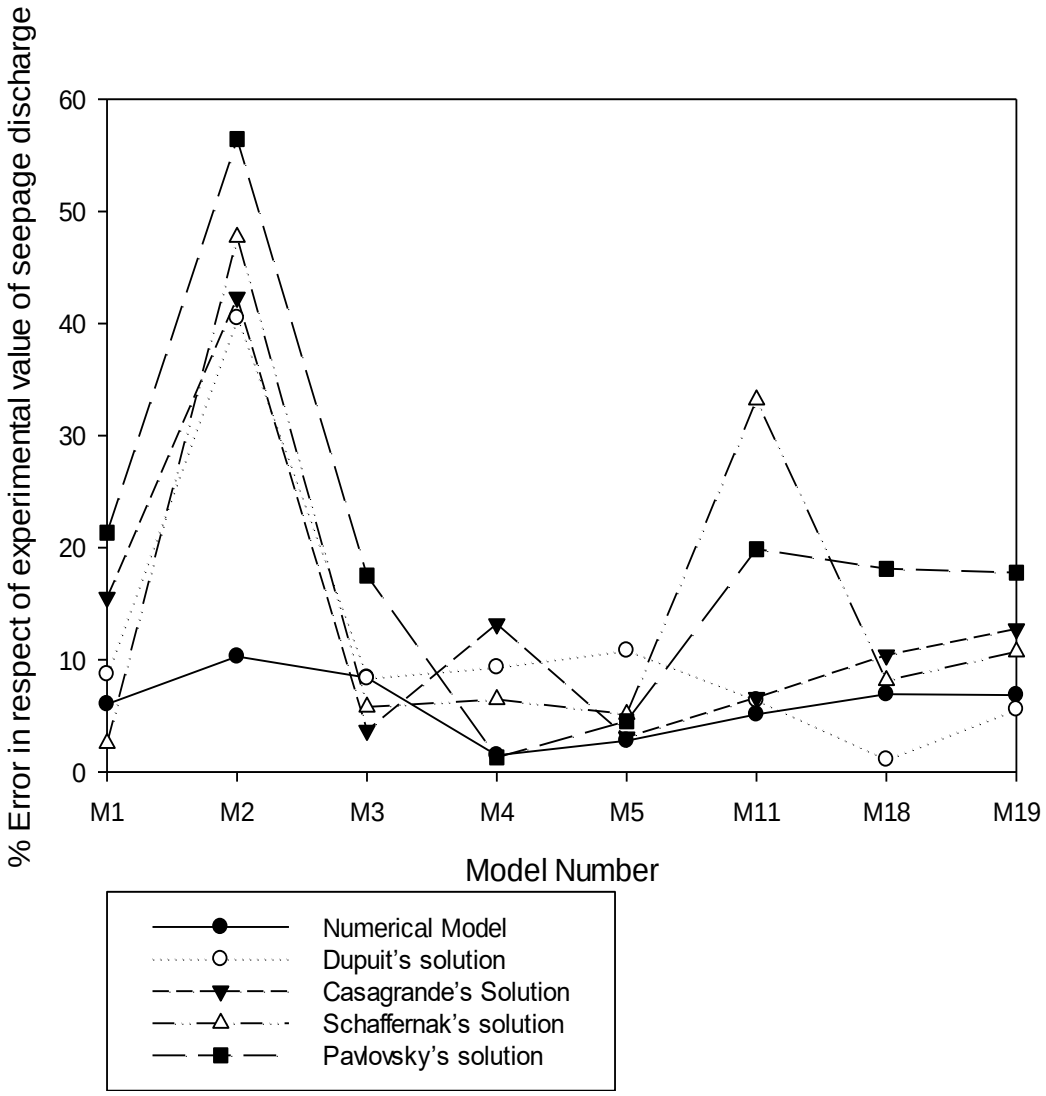

Figure 5.112: Percentage error in respect of the experimental value of seepage discharge with Numerical model, Casagrande's, Dupuit's, Pavlovsky's, and Schaffernak's solution for homogeneous earth dam models.

The seepage discharge increased by 67.815 per cent when the downstream slope of an earth dam was raised by 31.11 per cent, from 45 degrees (in M1) to 59 degrees (in M2). The seepage discharge increased by 14.765 per cent when the downstream slope was raised from 34 degrees (in M3) to 45 degrees (in M19). It was observed that when the

downstream slope increases, the discharge increases; this impact is more sensitive at higher slopes, i.e., beyond 45 degrees. It demonstrates a direct relationship between seepage discharge and the dam's downstream slope.

The seepage discharge value reduces slightly as the upstream slope of an earth dam is increased. The seepage discharge drops by 0.915 per cent when the upstream slope is increased from 38 degrees (in M1) to 45 degrees (in M18). The seepage discharge drops by 0.92 per cent when the upstream slope is increased from 45 degrees (in M18) to 50 degrees (in M19). At the same time, seepage discharge reduced by 1.83 per cent when the slope increased from 38 degrees (in M1) to 50 degrees (in M19). There is an inverse relationship between seepage discharge and the dam's upstream slope. Similar results were seen by Abdul Alim et al. (2017), Chahar (2004), Fu and Jin (2009), and Jiang et al. (2010).

The seepage discharge is lowered by 9.77 per cent when the dam length is increased from 52m (in M3) to 56m (in M4). It shows an inverse relation between seepage discharge and the length of the dam. Similar results were found by Kamanbedast and Delvari (2012) and Jiang et al. (2010).

The seepage discharge increased by 1.36 per cent when the height of the earth dam was increased by 33.33 per cent keeping the same upstream head or freeboard, i.e., 15 m (in M5) to 20 m (in M4). However, the amount of discharge increased slightly as the percentage of height increased. Seepage discharge increases by 7.5 per cent when the upstream head of water is increased from 13 m (in M11) to 13.5 m (in M1). Similar results were seen by Abdul Alim et al. (2017), ho (2012), and Kamanbedast and Delvari (2012).

Seepage discharge increased by 7.87 per cent when the longitudinal slope was raised by 2.28 per cent (in M1 to M7), and by 11.16 per cent when the longitudinal slope was increased by 4 per cent (in M1 and M8). At the same time, discharge increased by 16.41 percent as the slope increased by 6.07 per cent (from M1 to M6). Similar results were seen by Al-Mansori et al. (2020) and Salmasi and Mansuri (2014).

In M9, seepage discharge was reduced by 45 per cent when comparing seepage discharge obtained in a homogenous dam versus seepage discharge obtained in an earth dam with a clay core of upstream and downstream angles of 60 degrees and bottom

width of 18 m. In M10, seepage discharge was decreased to 40.33 per cent with a clay core's bottom width of 18 m and a top width of 1.9 m. Simultaneously, it was found that when the top width of the clay core is reduced by 20.83 per cent in model M9 compared to M10, the discharge through the earth dam's body increases by 8.55 per cent. Seepage discharge increases when the top width of the clay core reduces. Similar results were seen by Aniskin et al. (2016), Fakhari and Ghanbari (2013), and Farzampour et al. (2014).

When the viscosity of water was reduced by 2 per cent in M12 compared to normal viscosity in M1, seepage discharge was reduced to 0.55 per cent, and when viscosity was further reduced to 5percent in M20, discharge was reduced to 2.62 per cent, and when viscosity was further reduced to 10 per cent in M21, discharge was reduced to 3.36 per cent. The discharge is getting reduced with an increase in viscosity because the permeability of soil reduces. Similar results were found in Starov and Zhdanov (2001) and Rinehart et al. (2021).

The discharge increased by 59.18 per cent when the downstream filter of length 7.8m in M16 was introduced from the downstream end, compared to the discharge of homogeneous dam M1. While discharge increased by 77.61 per cent, 102.93 per cent, and 135.08 per cent, respectively, with filters with lengths of 13 m (in M15), 15.5 m (in M13), and 23 m (in M14). The discharge increased by 4.11 per cent when the filter thickness was raised from 1.5 m (in M17) to 3 m (in M15), which is an inconsiderable increase. Similar results were seen by Indraratna et al. (2008), Sivakumar Babu and Srivastava (2007), Malekpour et al. (2011), and Refaiy et al. (2021).

On changing the material properties by adding clay in the homogeneous silty sand by 15 per cent of its weight in the M23 model, the seepage discharge reduced by 51.28 per cent compared with the M1 model. While increasing the clay content to 30 per cent in M24, seepage discharge was reduced by 57.90 per cent. It was observed that seepage reduced with the addition of clay content in the soil of the earth dam. While replacing the silty sand of the earth dam with clay in M22, seepage drastically reduces by 98.11 per cent. While changing the properties of the dam's core while comparing silty sand in M1 and clay core in M9, seepage discharge in M9 was reduced by 45 per cent. Similar results were seen by Salmasi and Mansuri (2014) and Salmasi and Jafari (2016).

5.2 RESULT OF TEMPERATURE AND FLUX MODELLING

The effect of temperature variation in porous media such as earth dams on seepage was studied by constructing fifteen models of earth dams in a hydraulic flume. Temperature variation inside earth dam models was studied using experimental models and Temp/w; a finite element based software was also used to model the temperature variation in earth dam models. Heat flux and water flux were obtained using Temp/w and also using experimental models.

5.2.1 Contours of heat flux

The heat flux contours are shown in figures 5.113 to figure 5.127 for models- M1 to M10, M13, M14, M15, M18, and M19, respectively. The elevation of the dam was shown in metres on the y-axis while the distance from the upstream heel in metres on the x-axis. The heat flux variation for the location is depicted. The phreatic line of the earth dam model, which is represented as a dotted line in its corresponding figure and maintains the flow of heat below it, as shown.

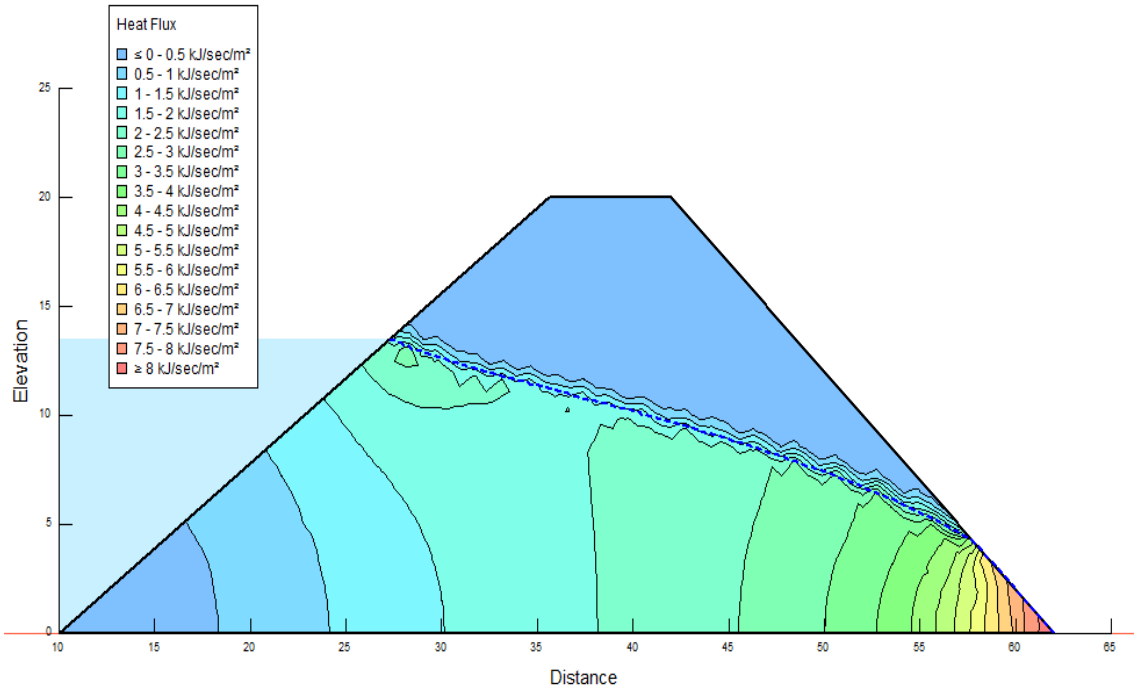

Figure 5.113: Heat flux in M1

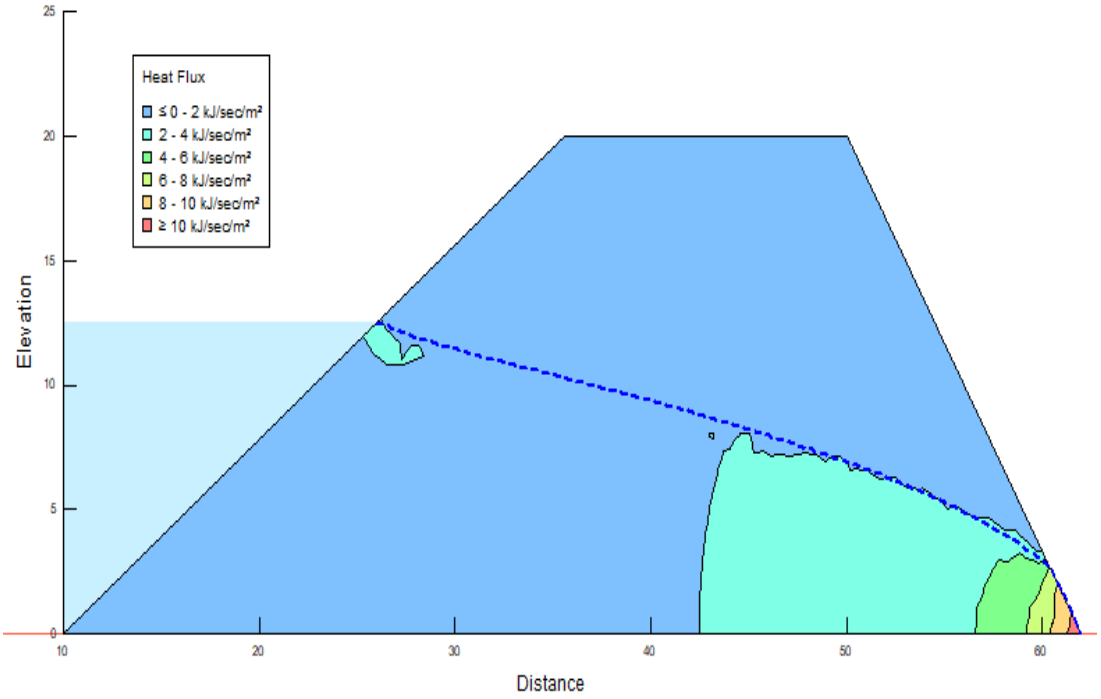

Figure 5.114: Heat flux in M2

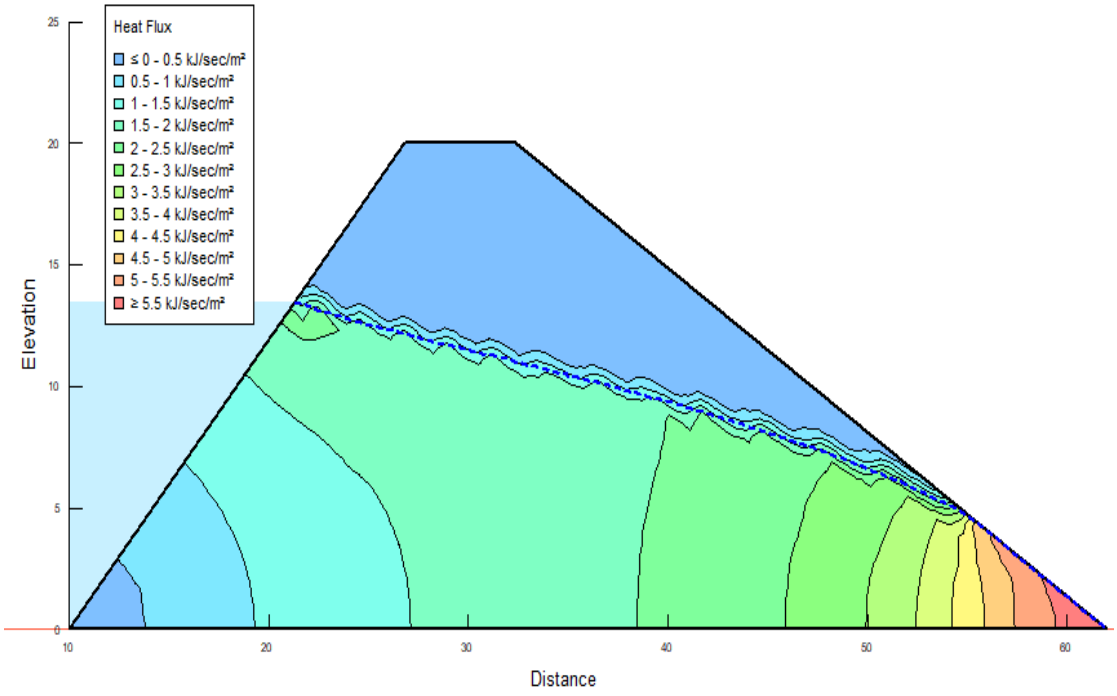

Figure 5.115: Heat flux in M3

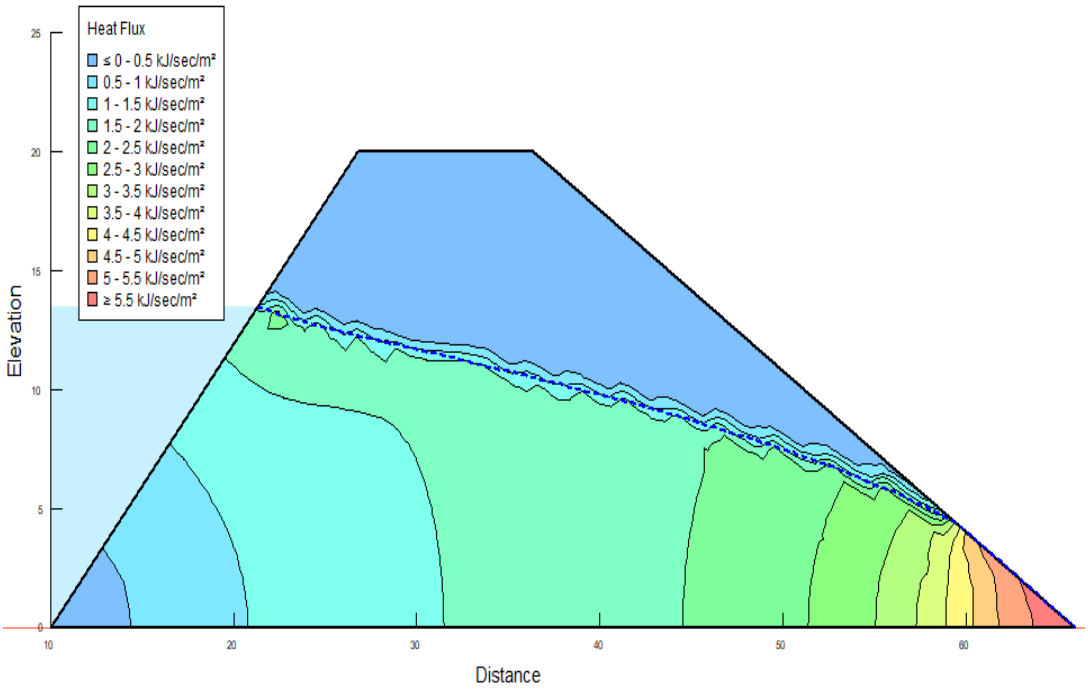

Figure 5.116: Heat flux in M4

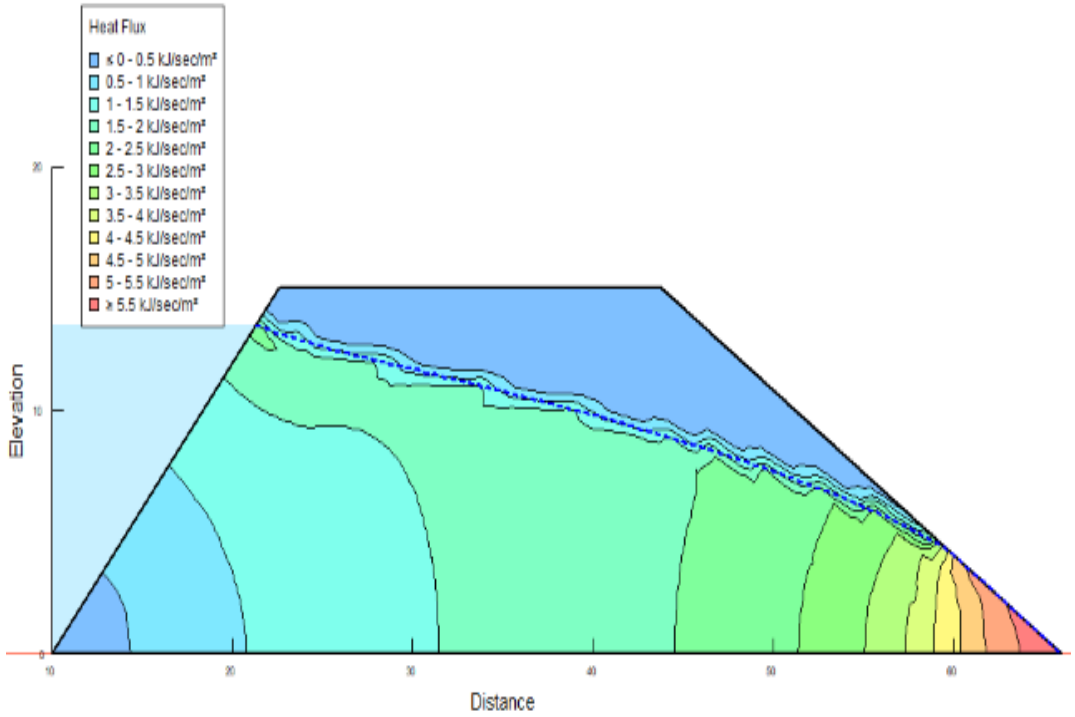

Figure 5.117: Heat flux in M5

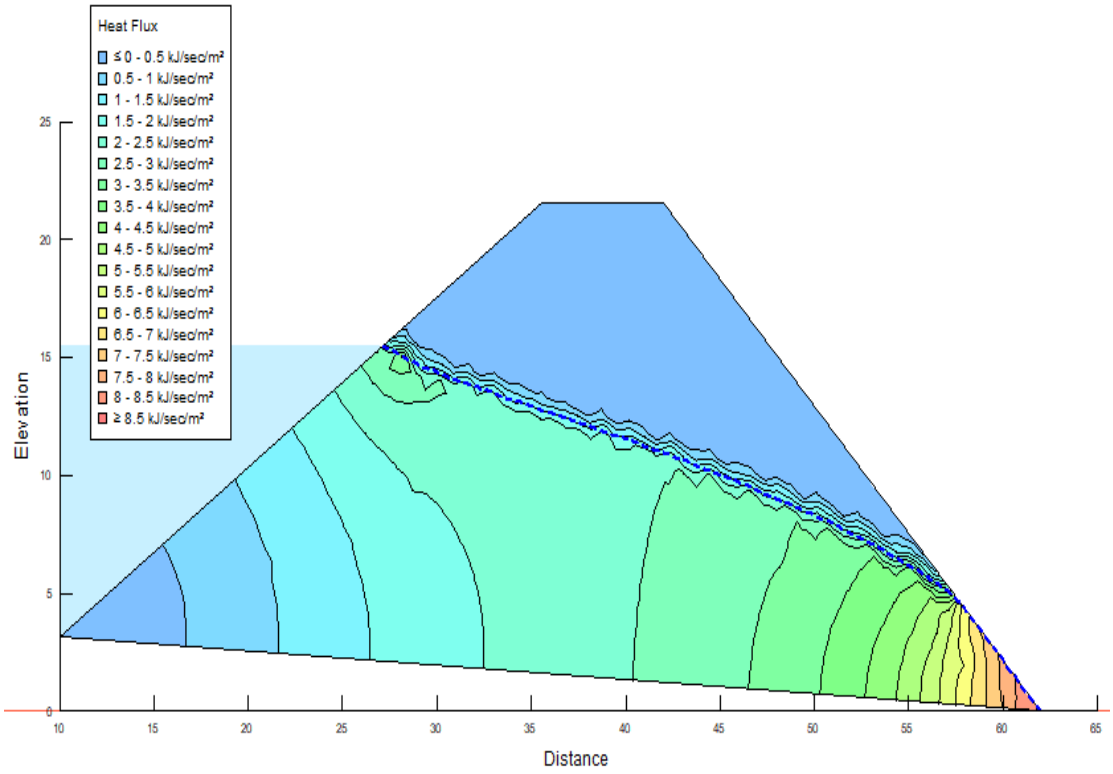

Figure 5.118: Heat flux in M6

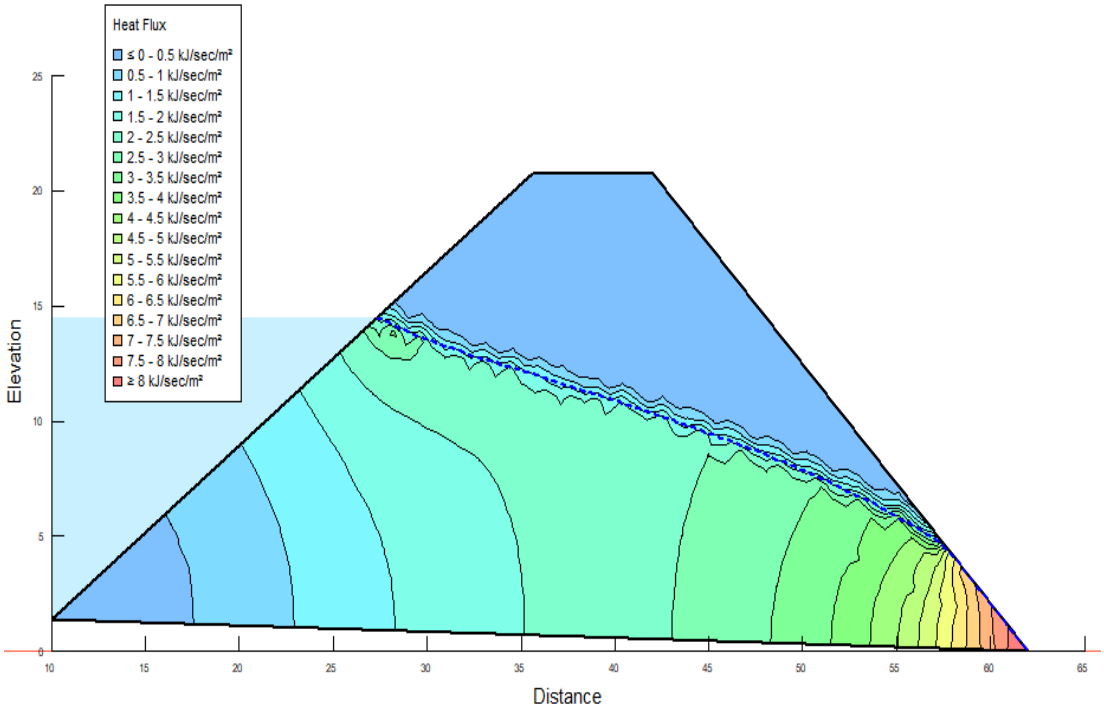

Figure 5.119: Heat flux in M7

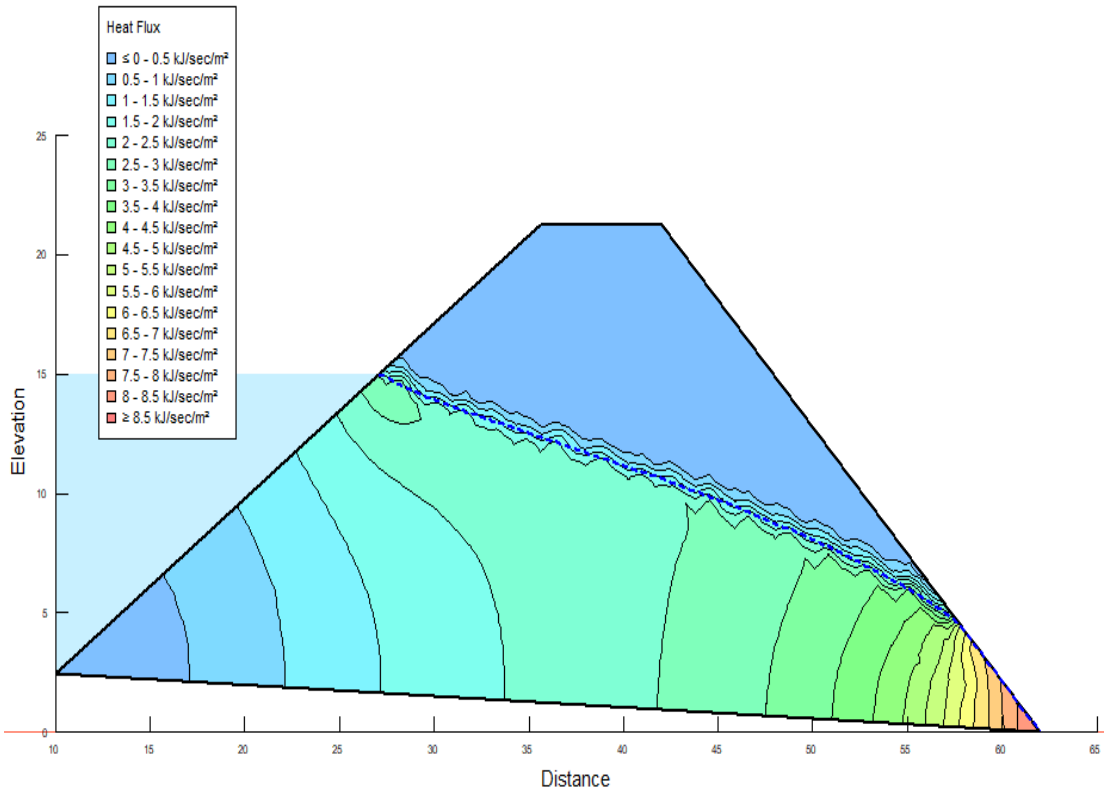

Figure 5.120: Heat flux in M8

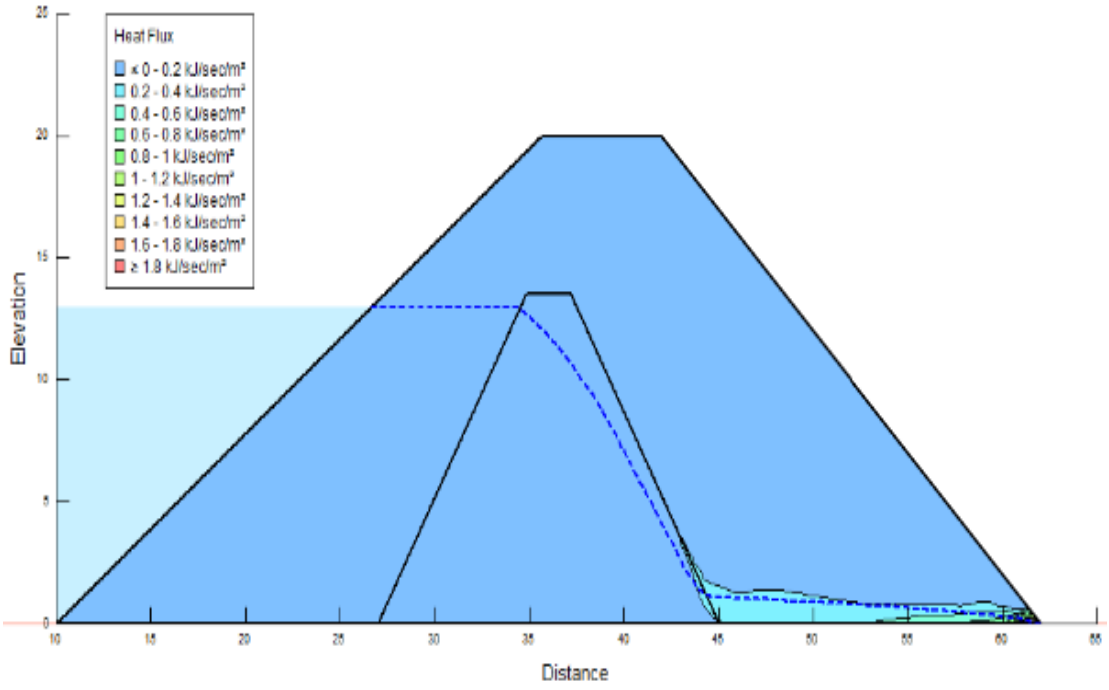

Figure 5.121: Heat flux in M9

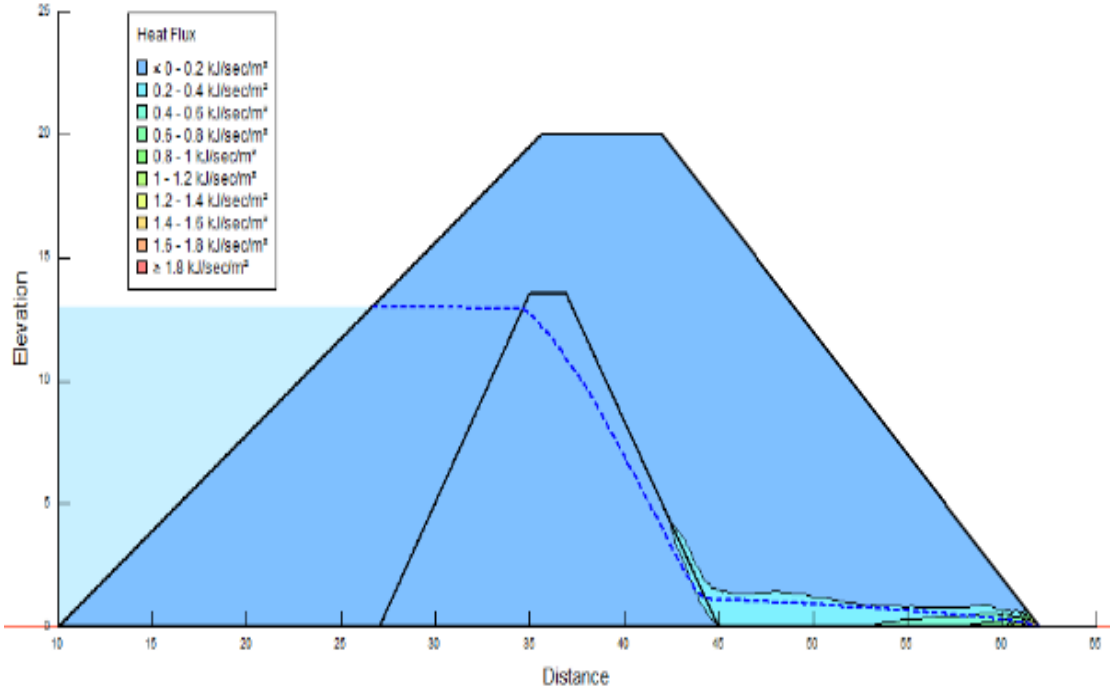

Figure 5.122: Heat flux in M10

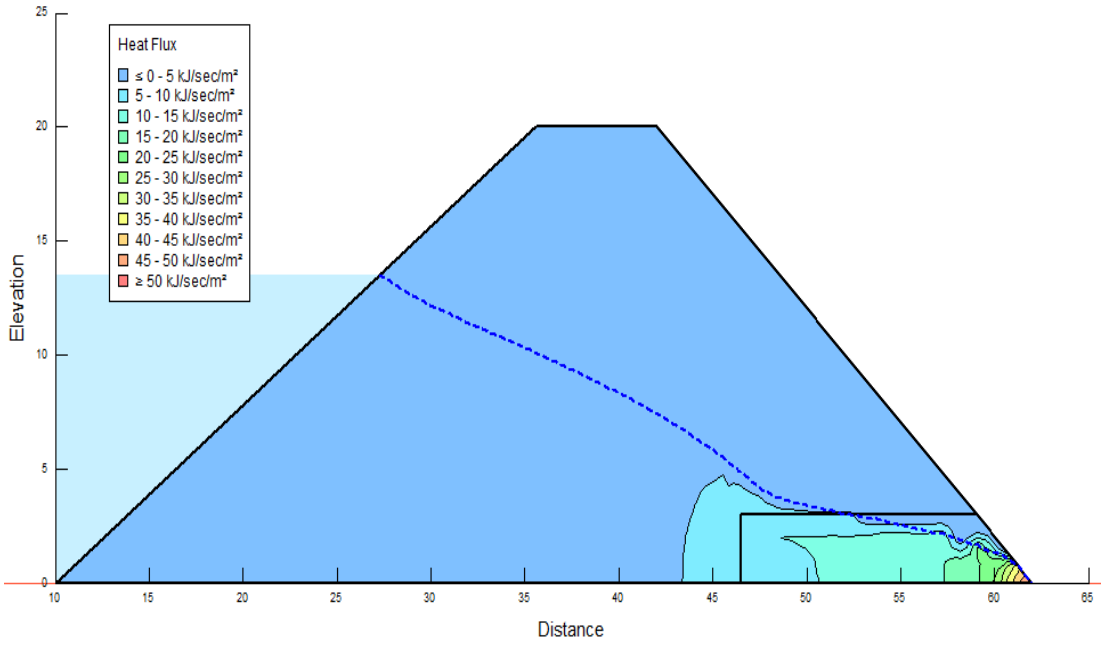

Figure 5.123: Heat flux in M13

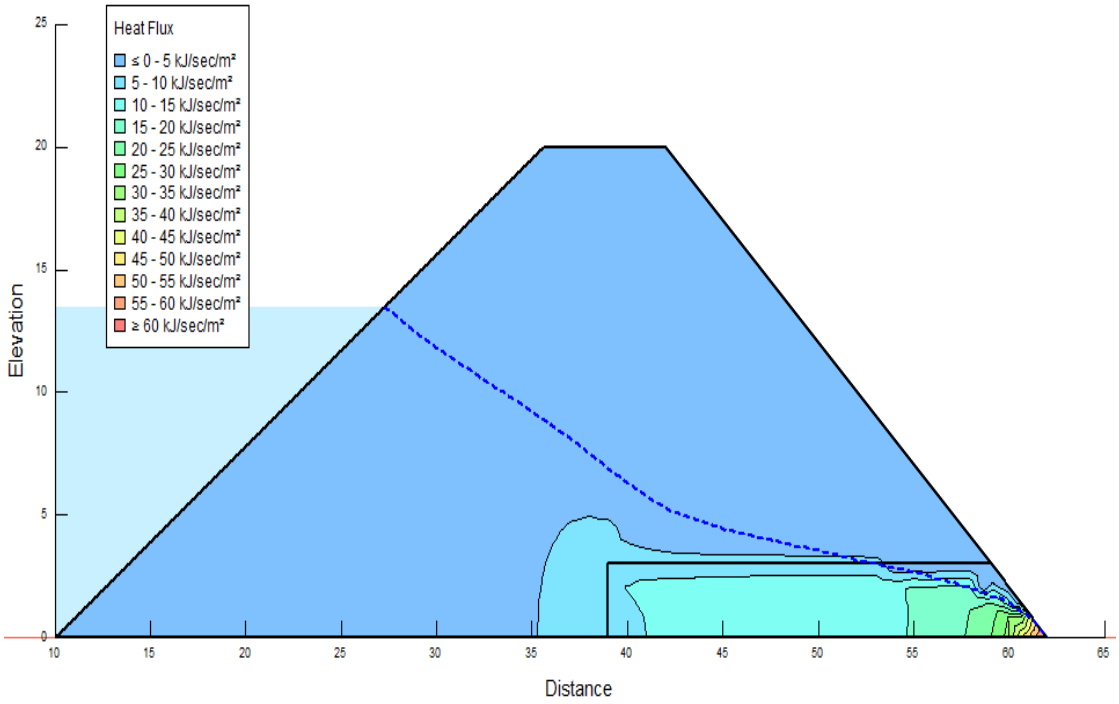

Figure 5.124: Heat flux in M14

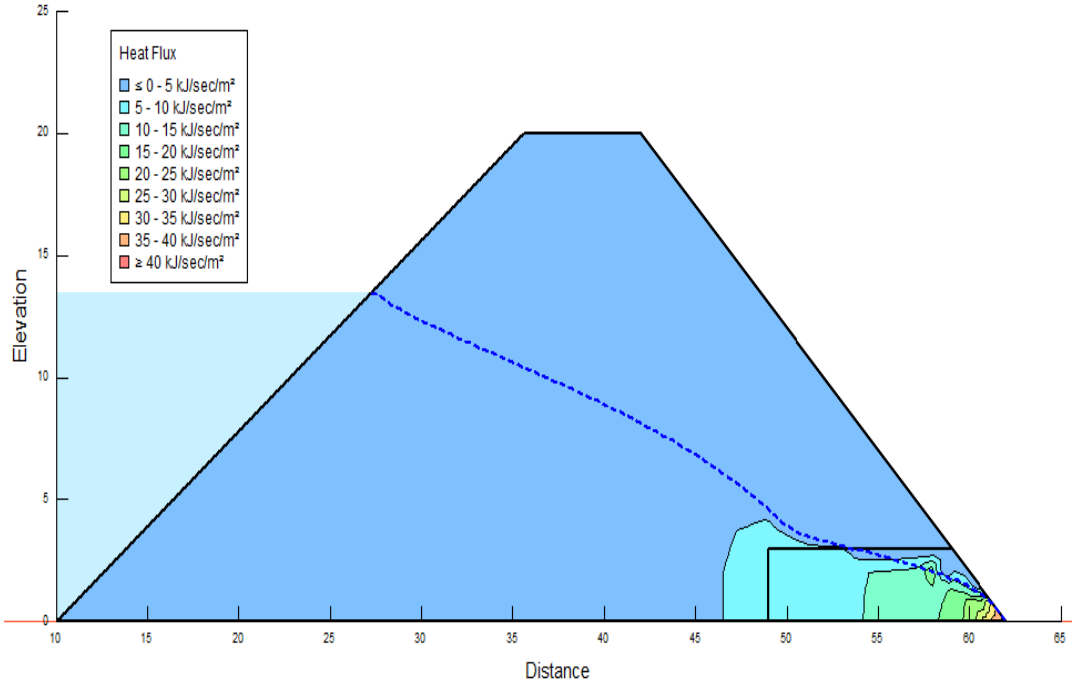

Figure 5.125: Heat flux in M15

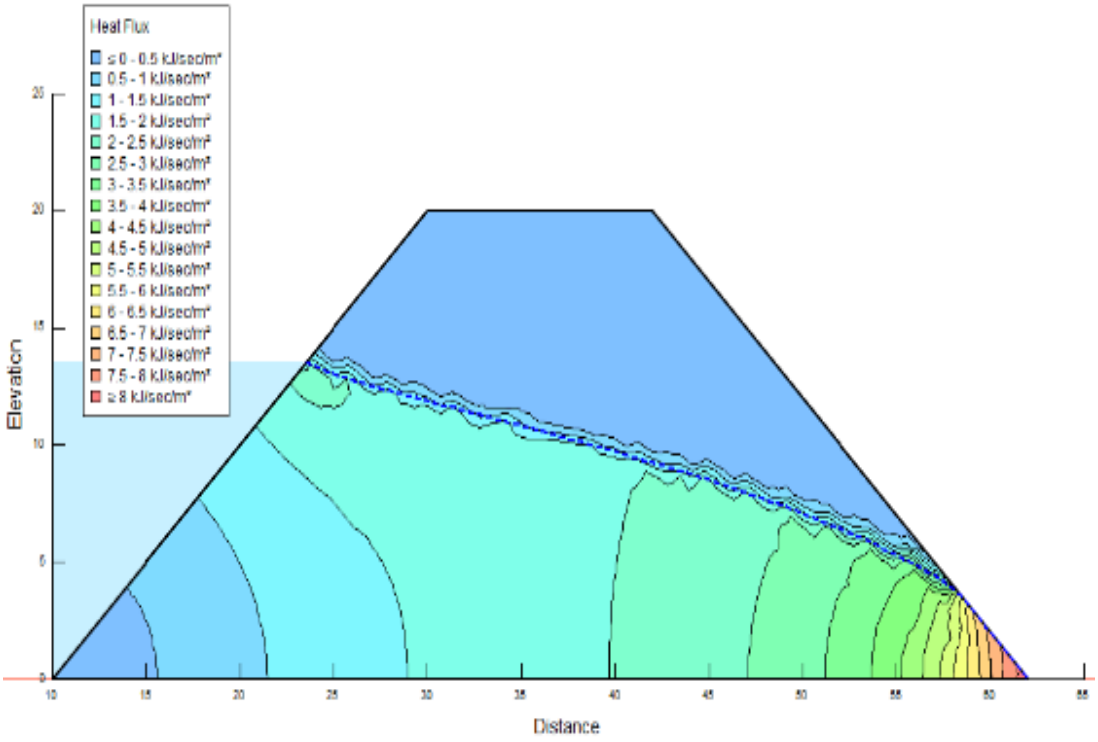

Figure 5.126: Heat flux in M18

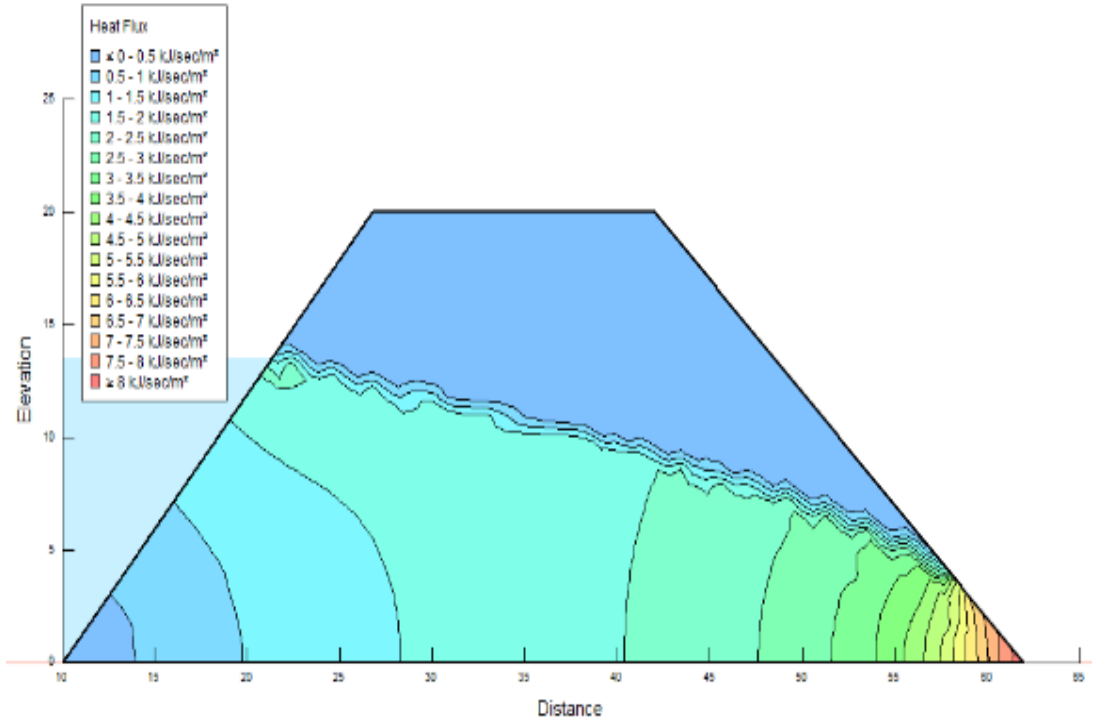

Figure 5.127: Heat flux in M19

5.2.2 Contours of water flux

The contours of water flux in $m^3/sec/m^2$ are shown in figure 5.128 to figure 5.142 for models- M1 to M10, M13, M14, M15, M18, and M19, respectively. The water flux variation for the location is shown. The elevation of the dam was shown in metres on the y-axis, while the distance from the upstream heel was in metres on the x-axis. The phreatic line of the earth dam model is likewise represented in its corresponding figure, indicated with a dotted line.

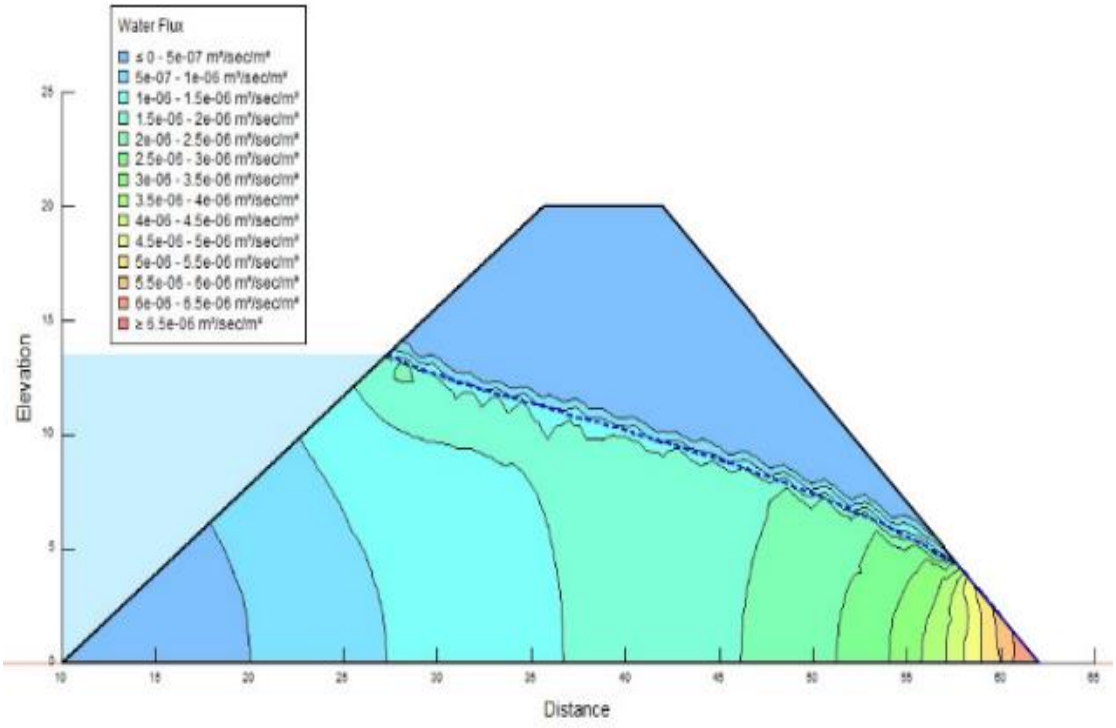

Figure 5.128: Water flux in M1

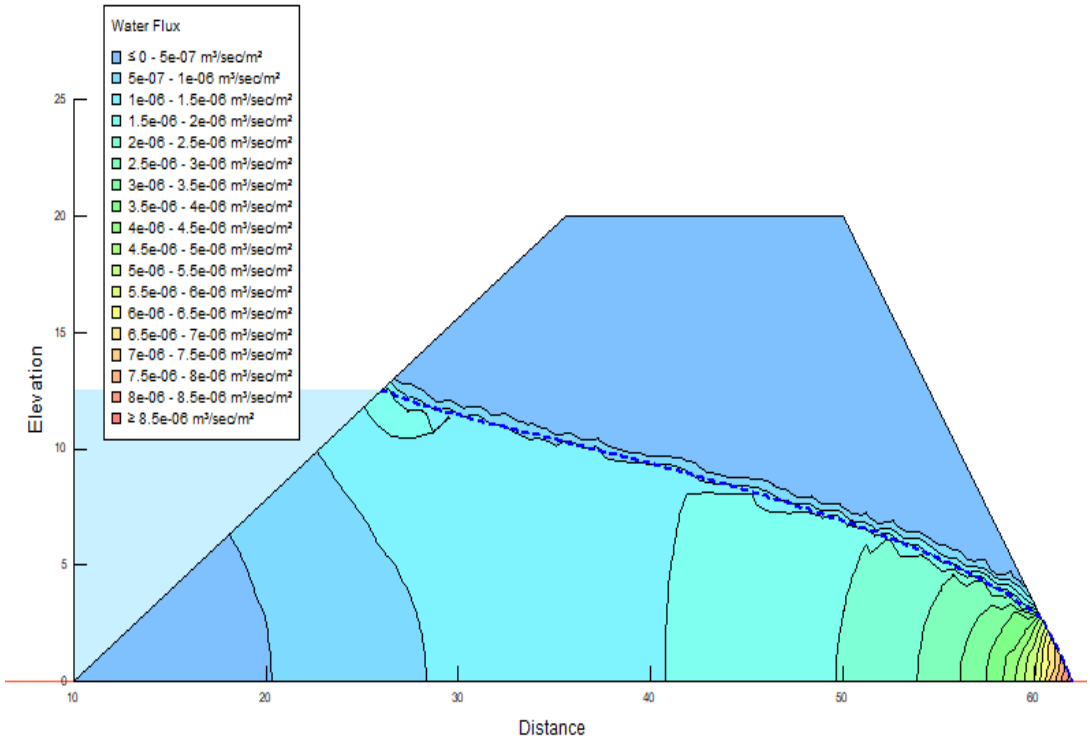

Figure 5.129: Water flux in M2

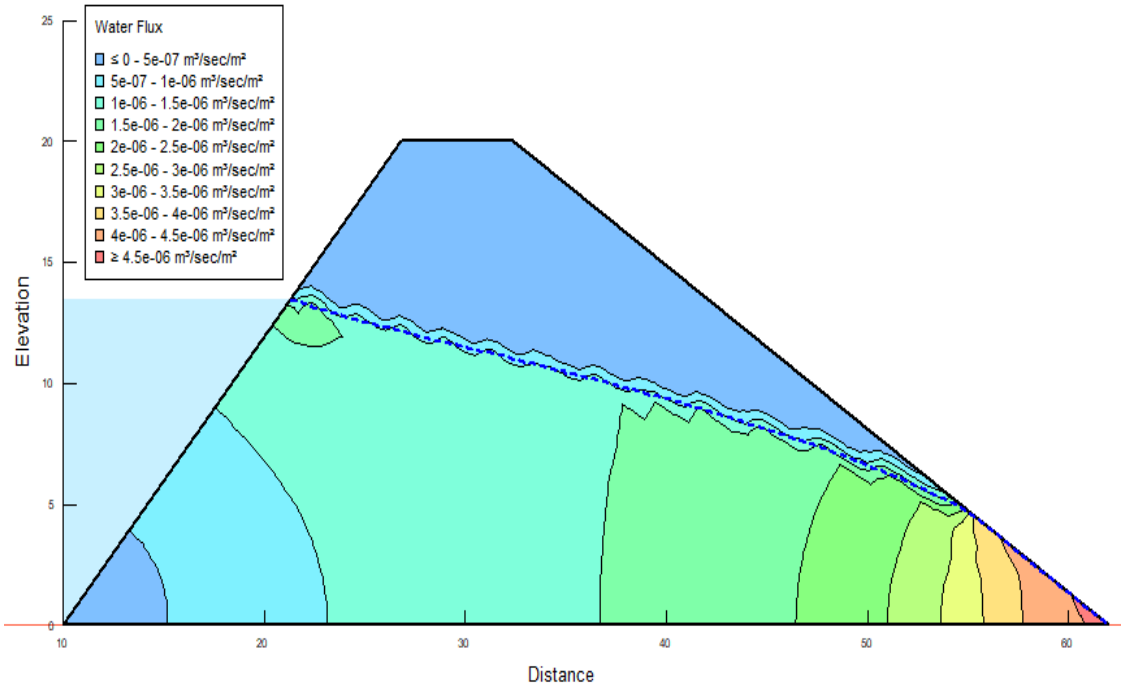

Figure 5.130: Water flux in M3

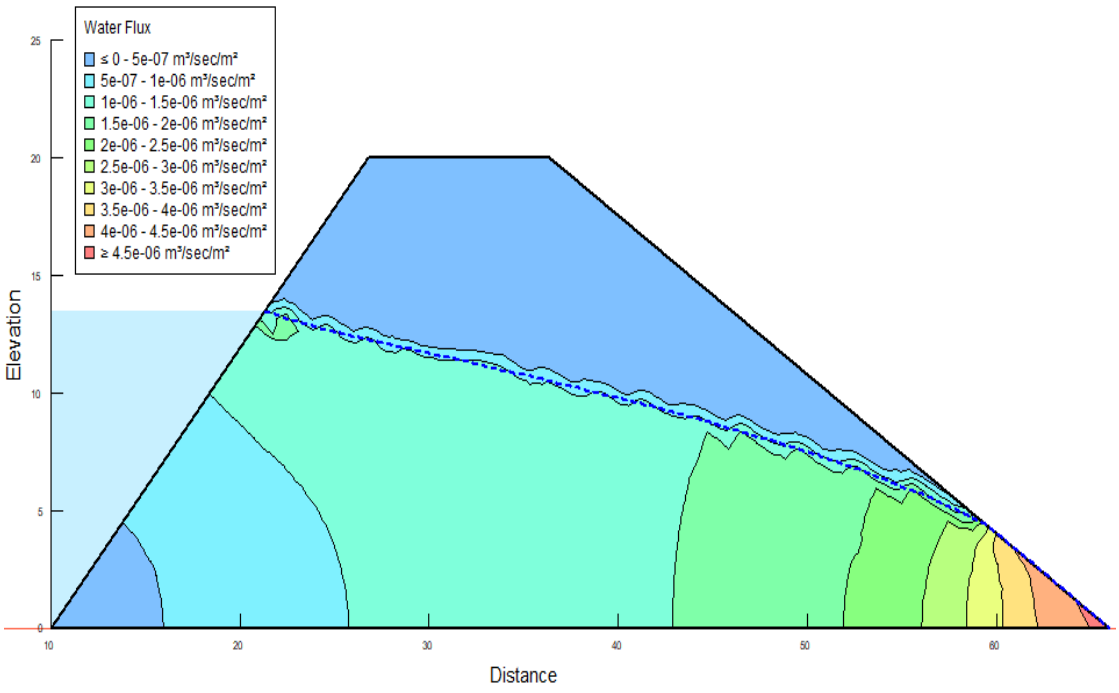

Figure 5.131: Water flux in M4

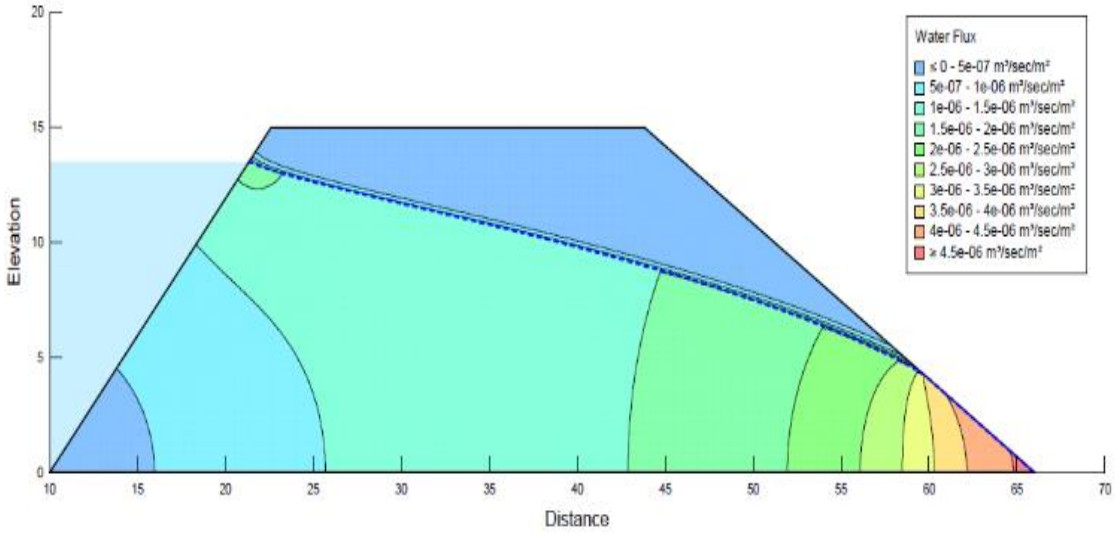

Figure 5.132: Water flux in M5

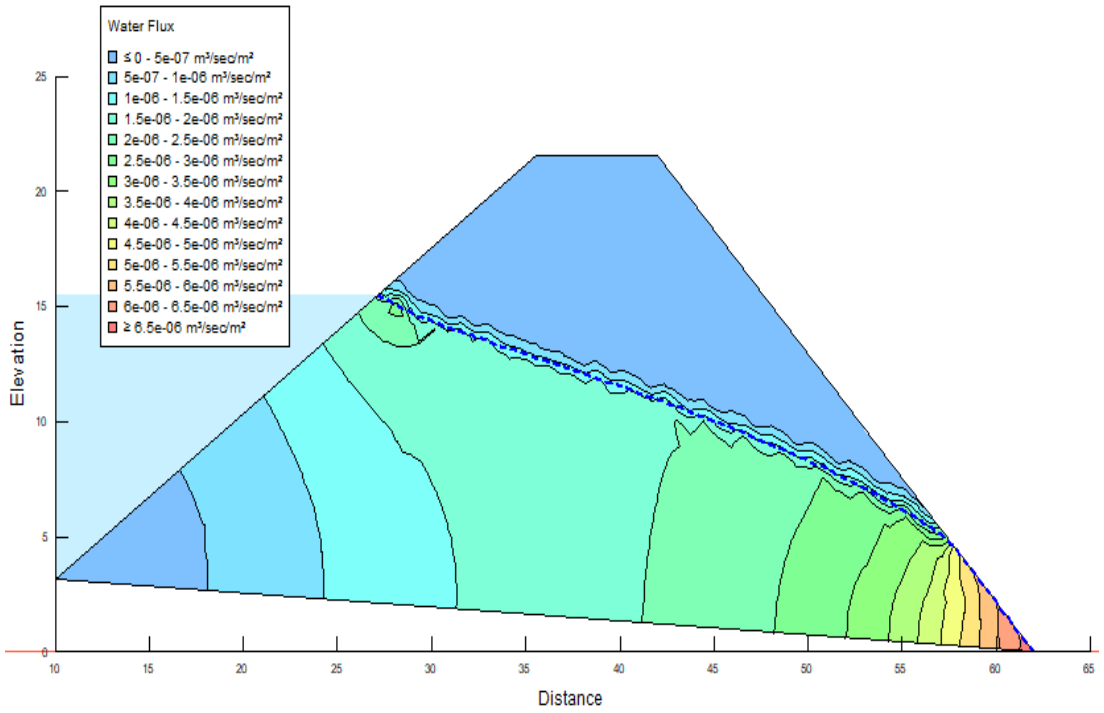

Figure 5.133: Water flux in M6

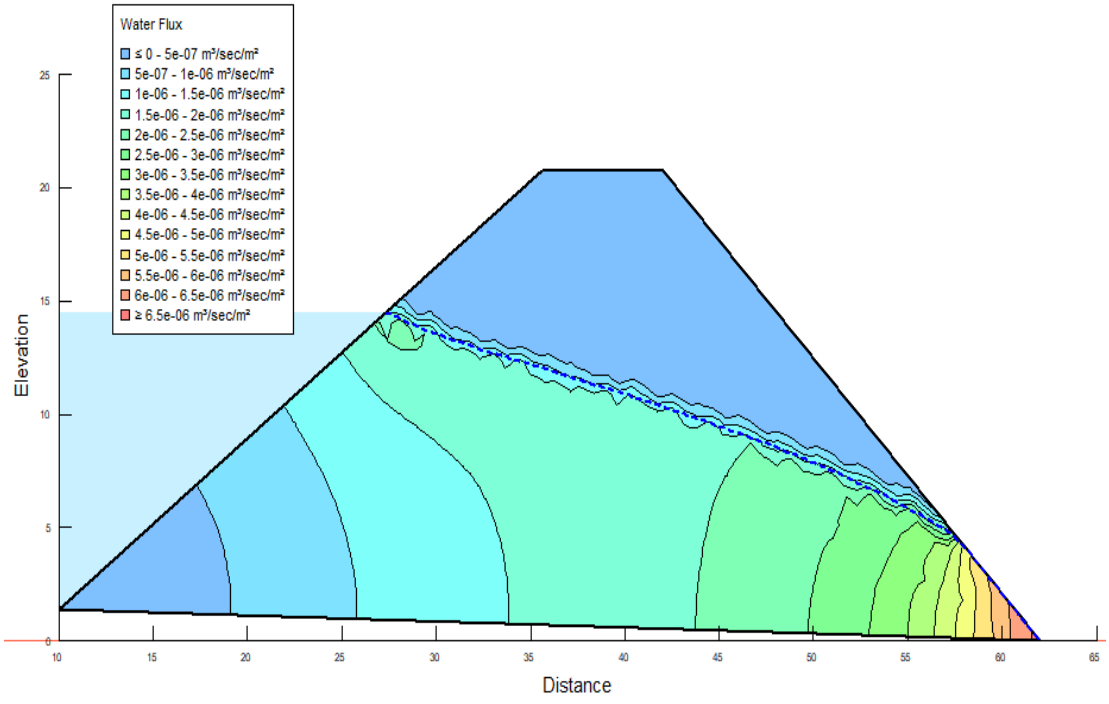

Figure 5.134: Water flux in M7

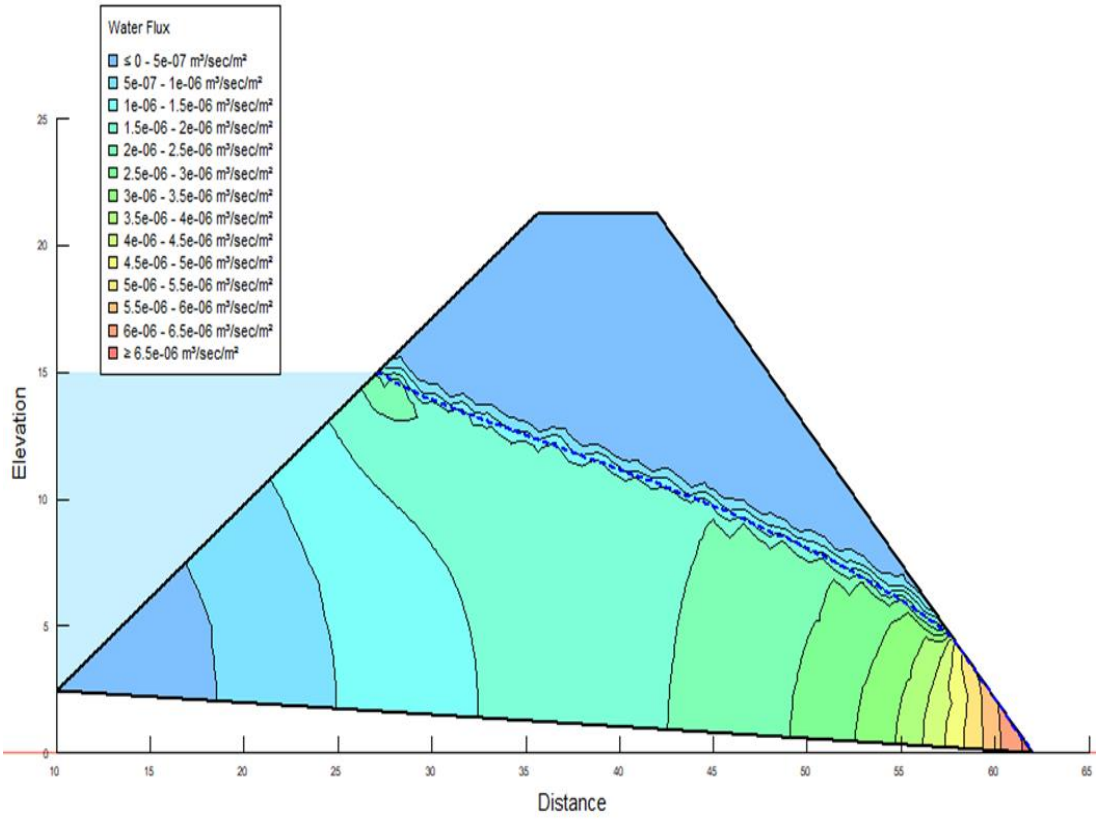

Figure 5.135: Water flux in M8

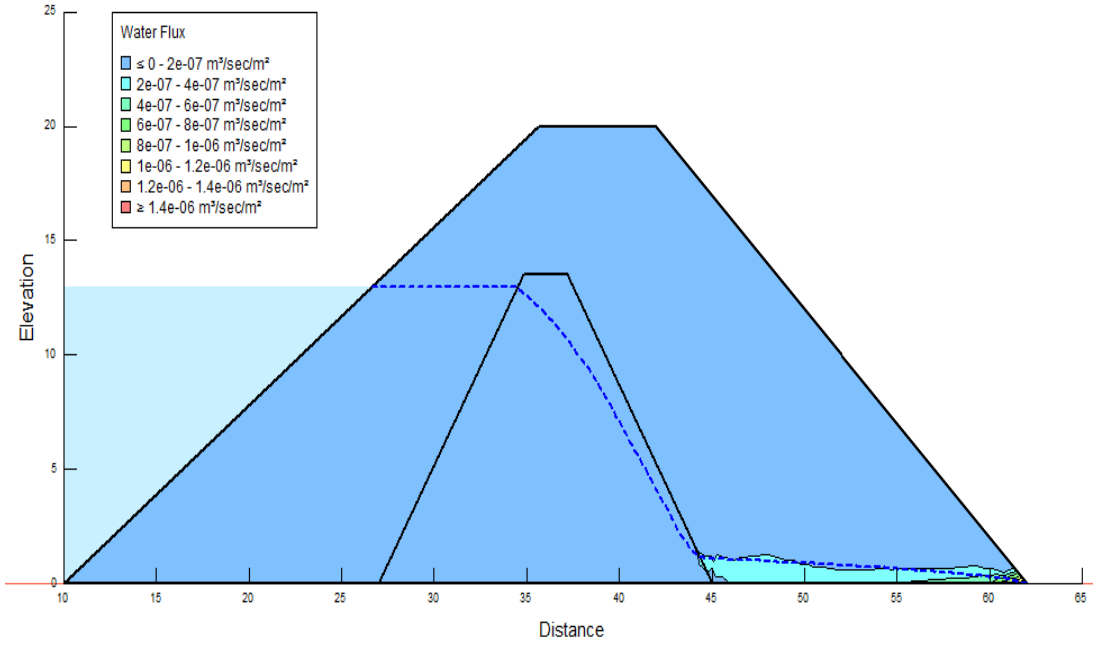

Figure 5.136: Water flux in M9

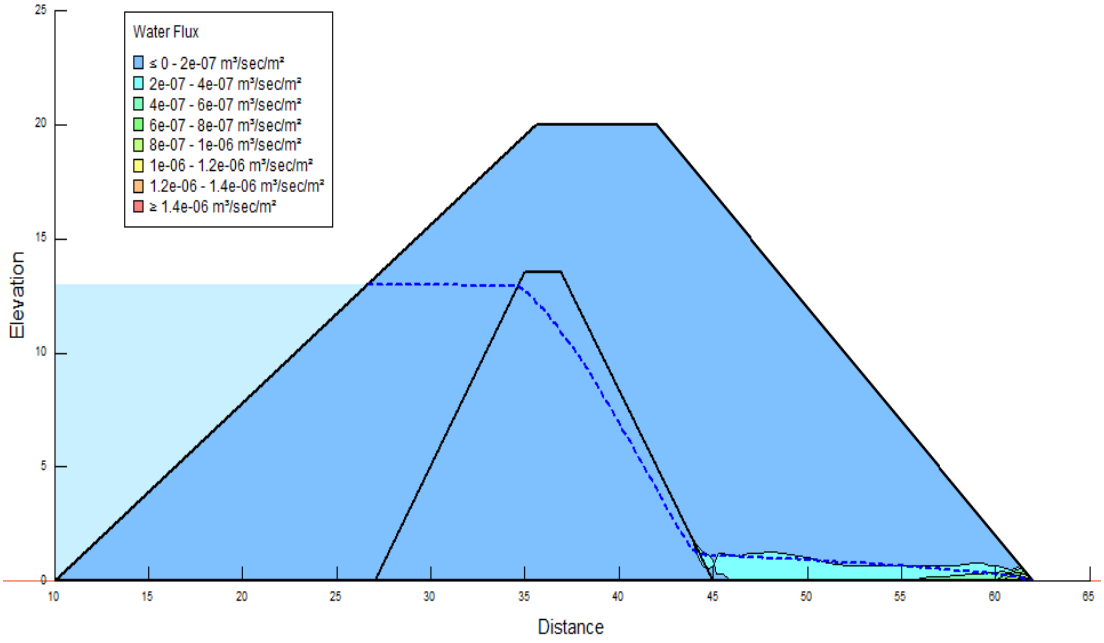

Figure 5.137: Water flux in M10

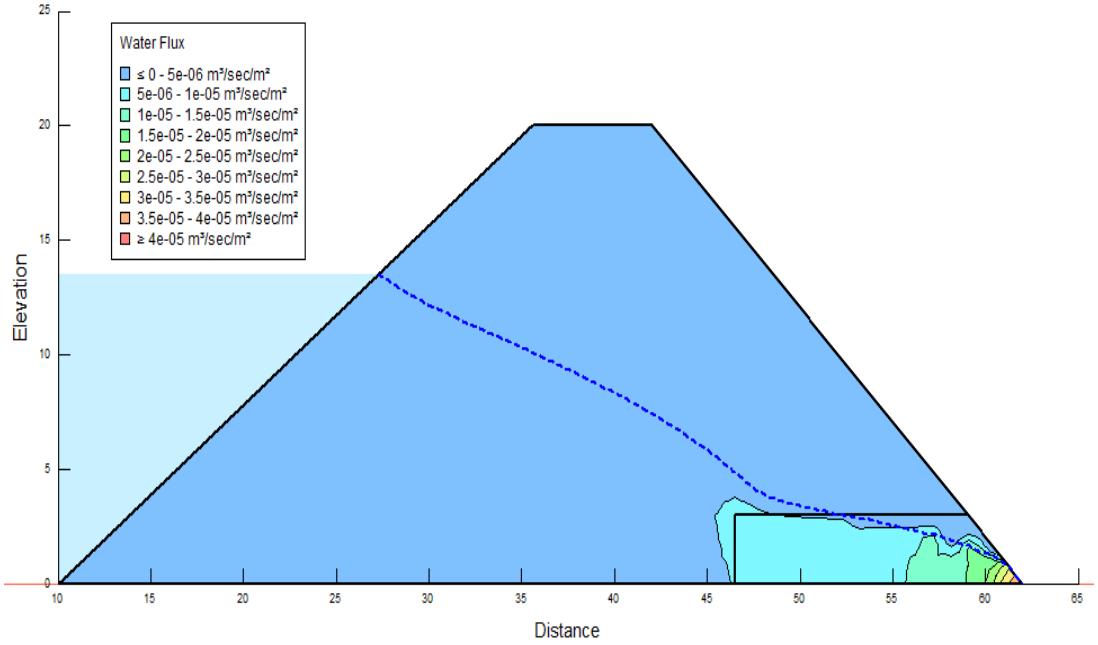

Figure 5.138: Water flux in M13

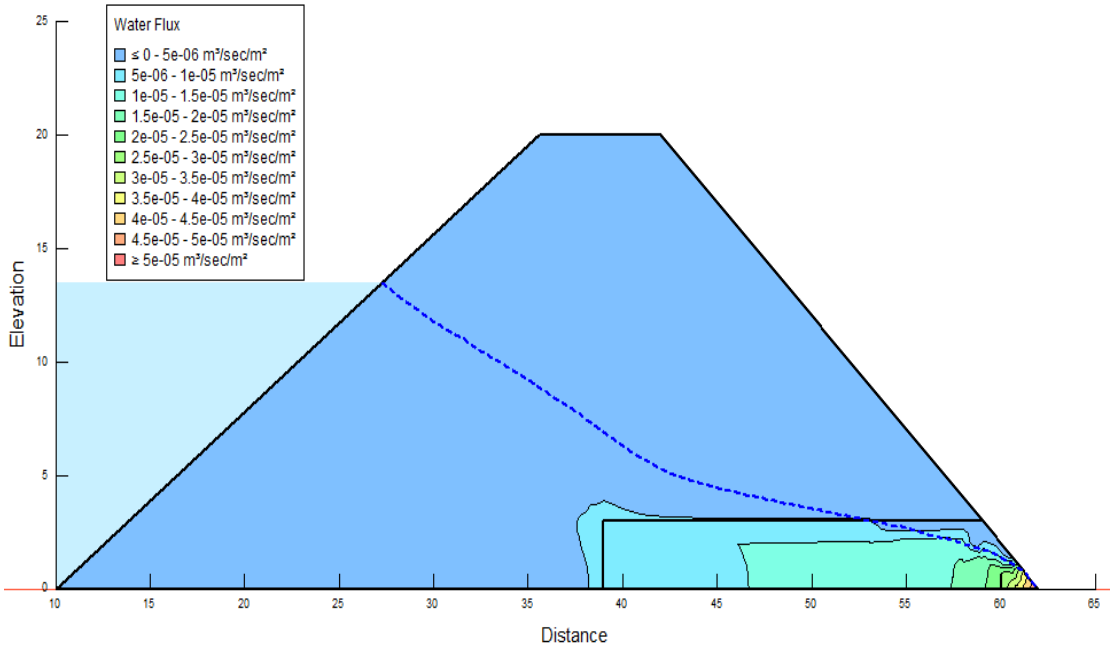

Figure 5.139: Water flux in M14

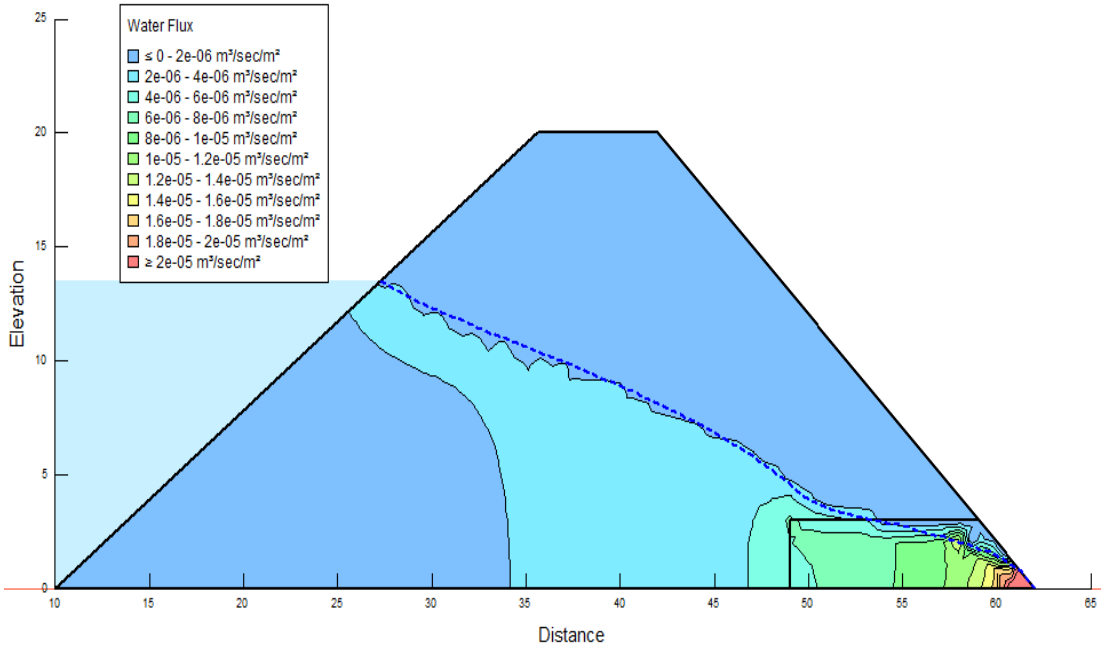

Figure 5.140: Water flux in M15

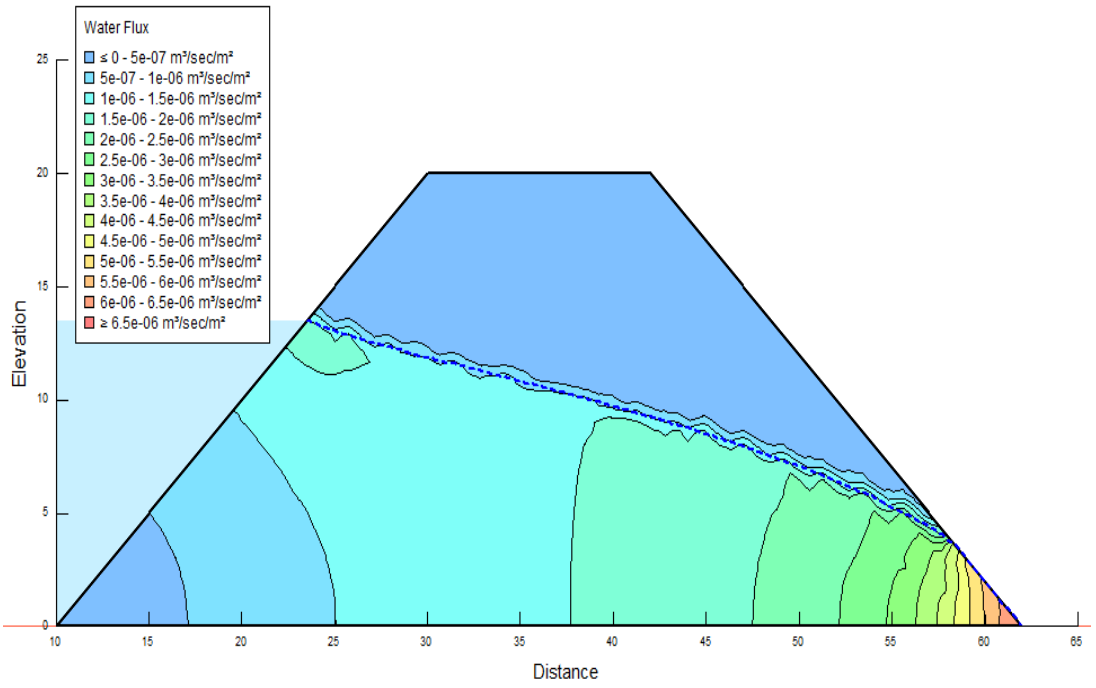

Figure 5.141: Water flux in M18

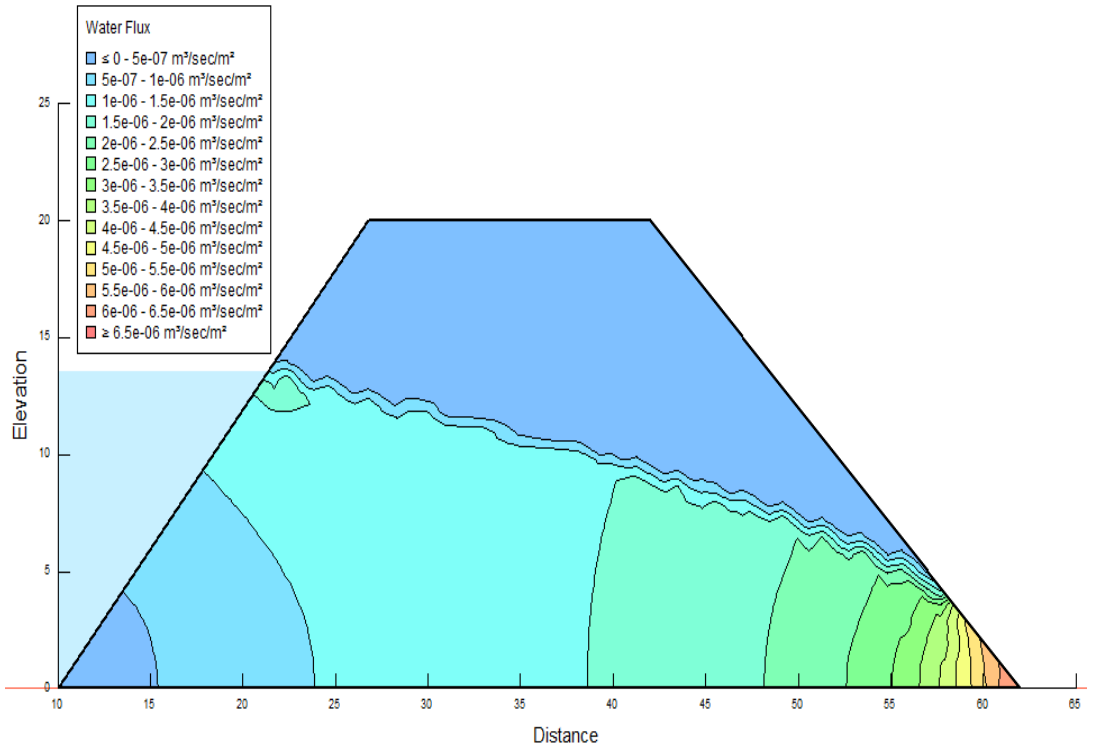

Figure 5.142: Water flux in M19

5.2.3 Contours of Temperature

The contours of temperature in ºC obtained using Temp/w are shown in figure 5.143 to figure 5.157 for models M1 to M10, M13, M14, M15, M18, and M19, respectively. The elevation of the dam is shown in metres on the y-axis, while the distance from the upstream heel is in metres on the x-axis.

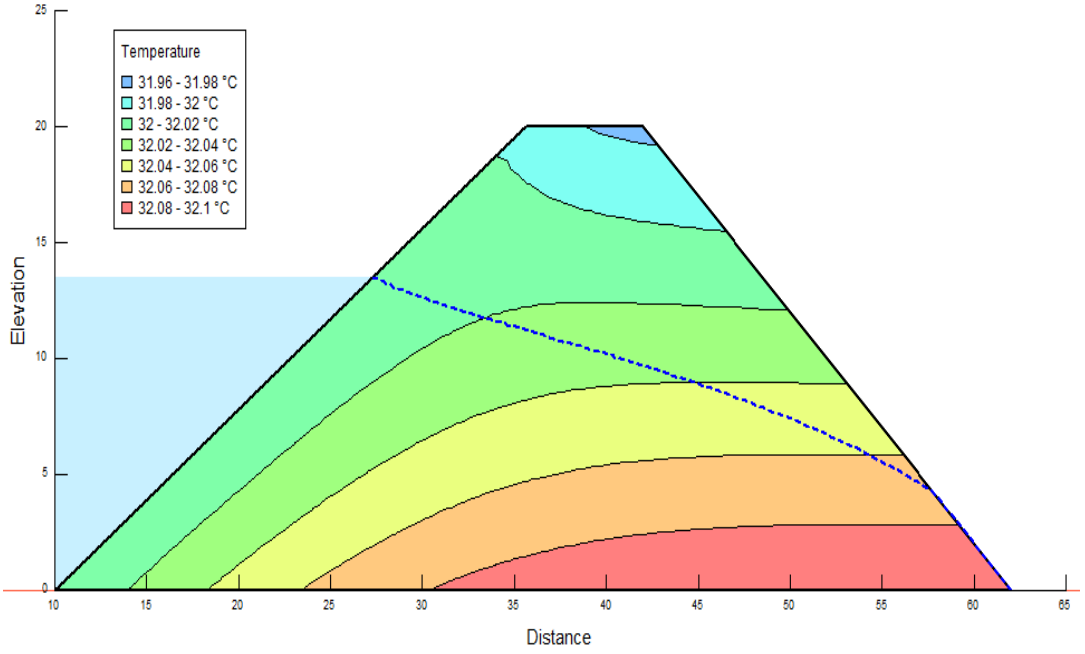

Figure 5.143: Temperature in M1

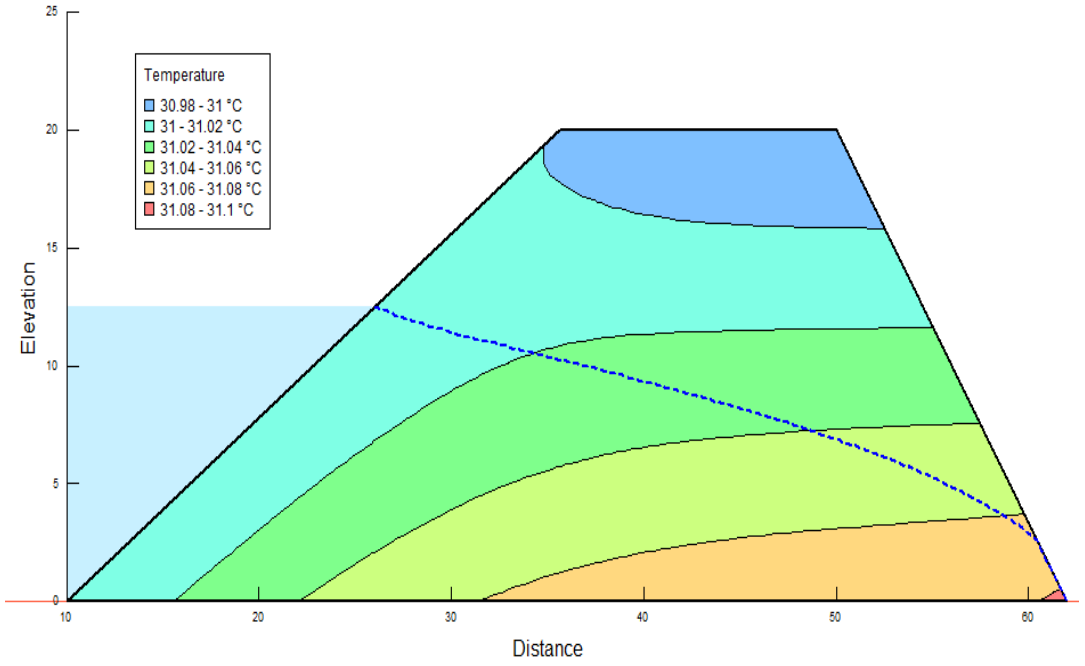

Figure 5.144: Temperature in M2

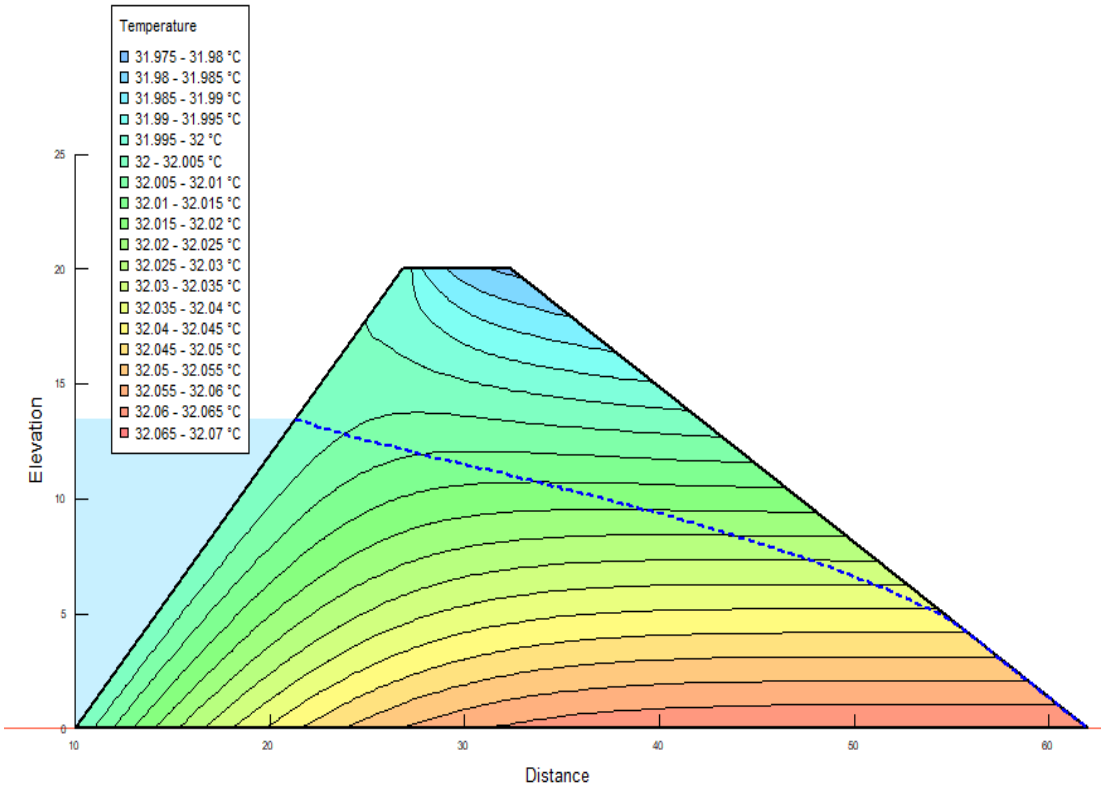

Figure 5.145: Temperature in M3

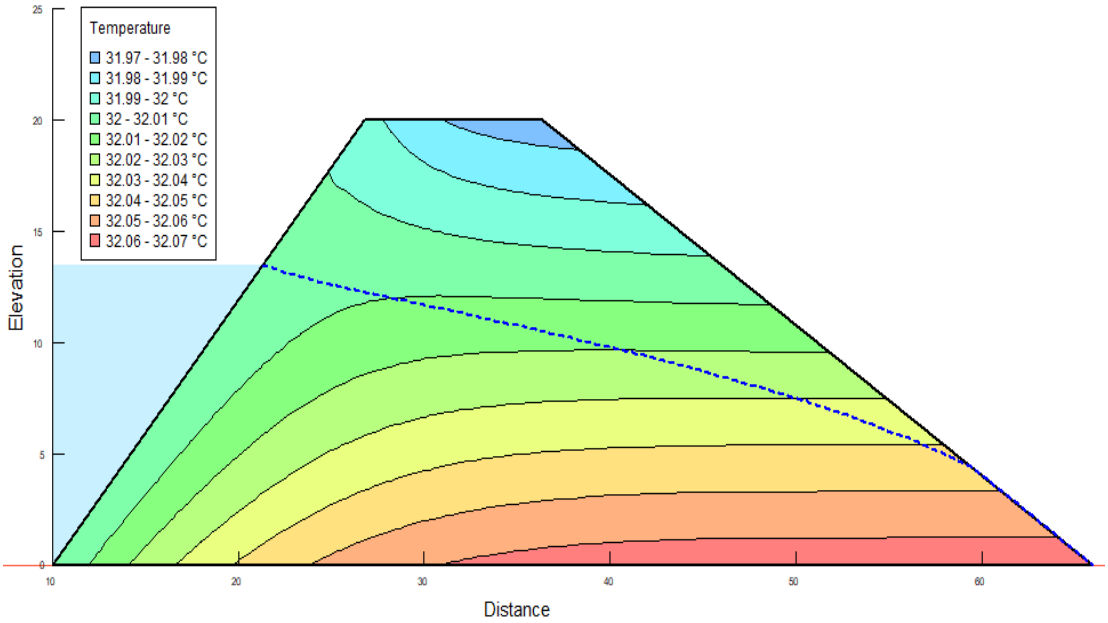

Figure 5.146: Temperature in M4

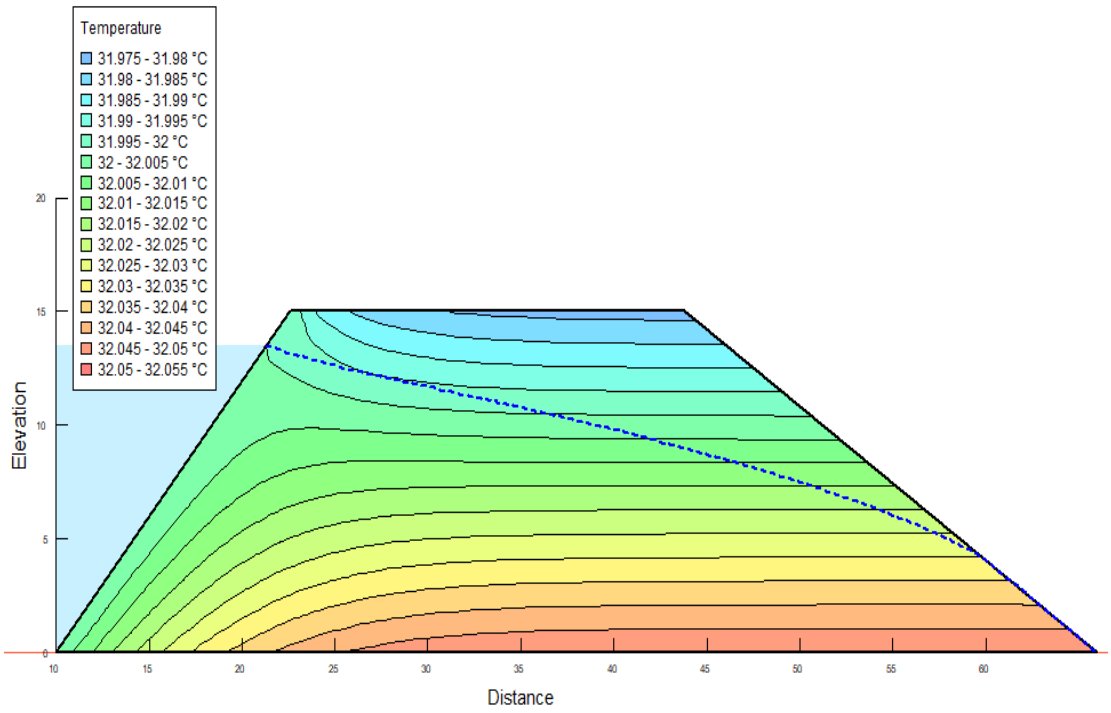

Figure 5.147: Temperature in M5

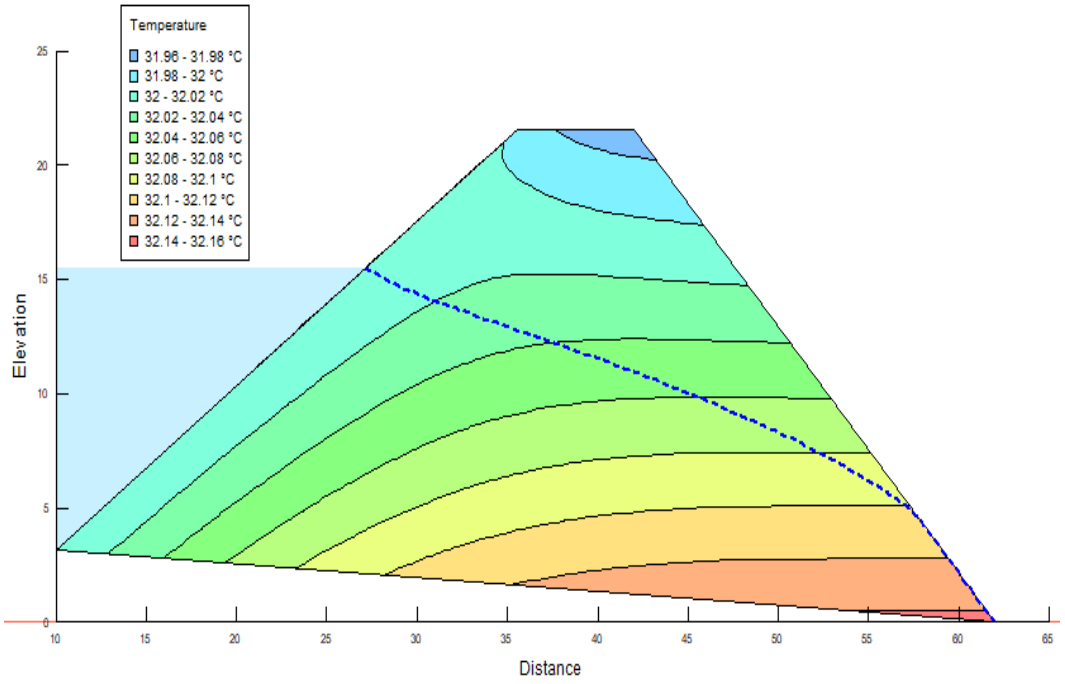

Figure 5.148: Temperature in M6

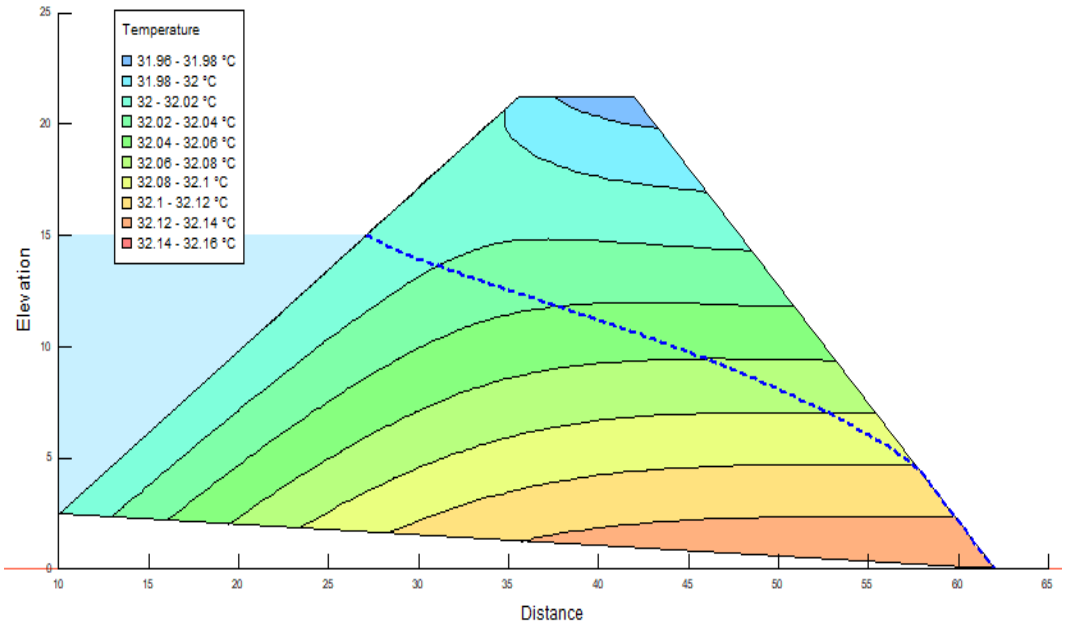

Figure 5.149: Temperature in M7

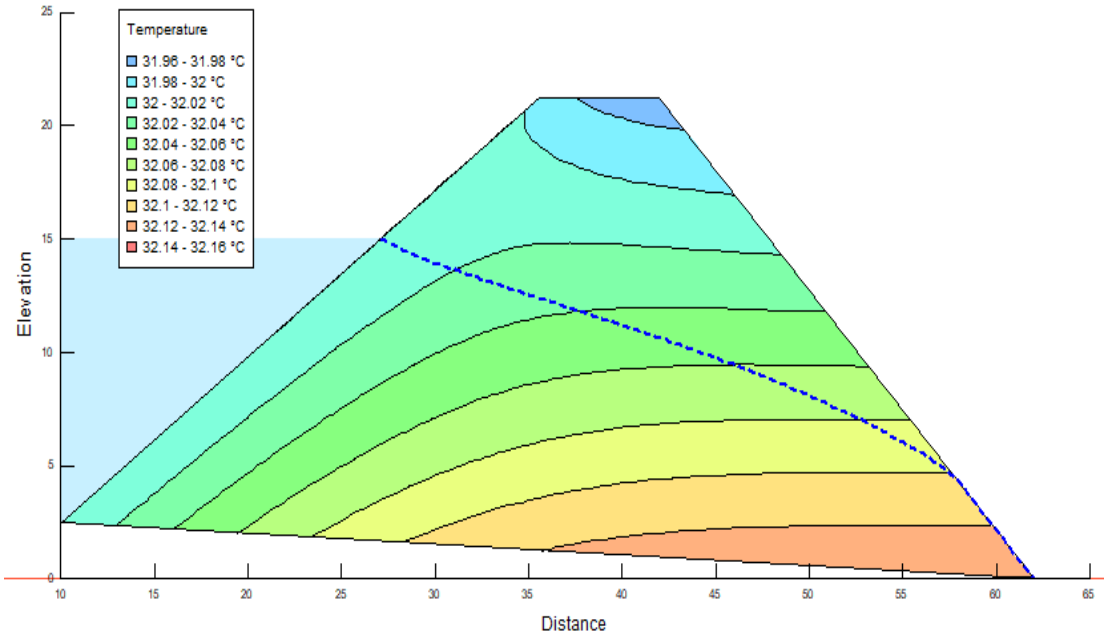

Figure 5.150: Temperature in M8

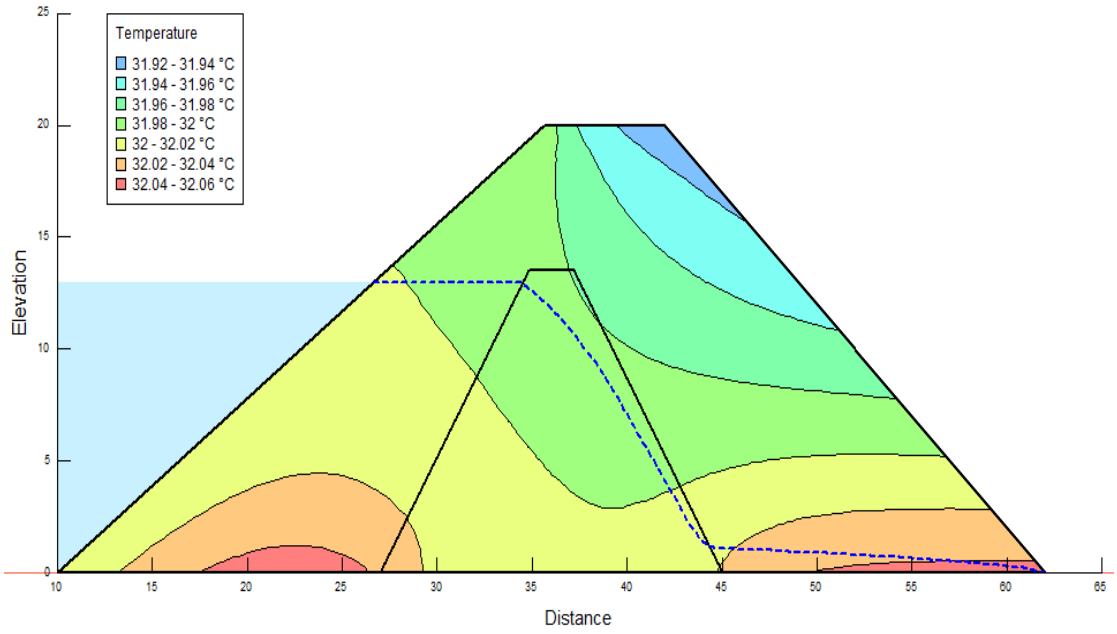

Figure 5.151: Temperature in M9

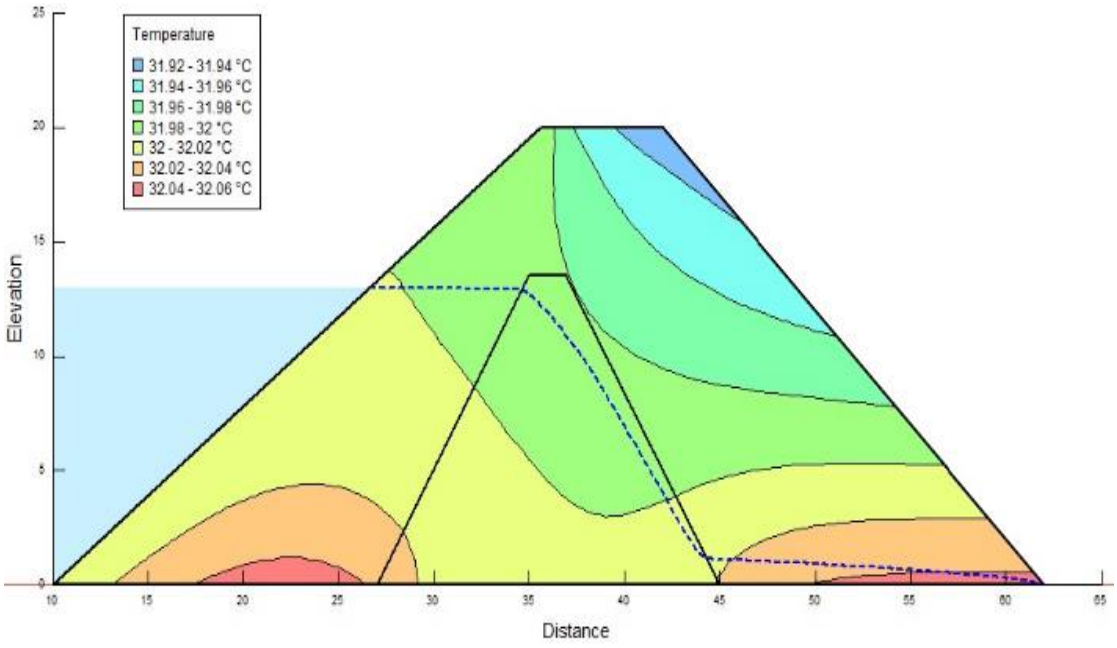

Figure 5.152: Temperature in M10

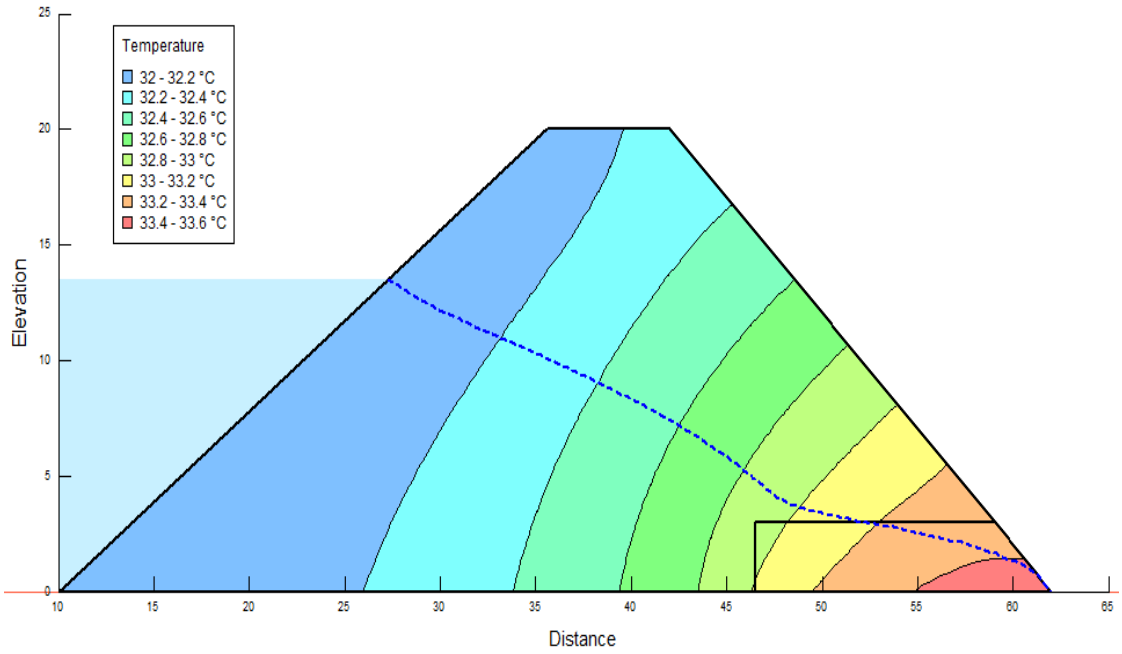

Figure 5.153: Temperature in M13

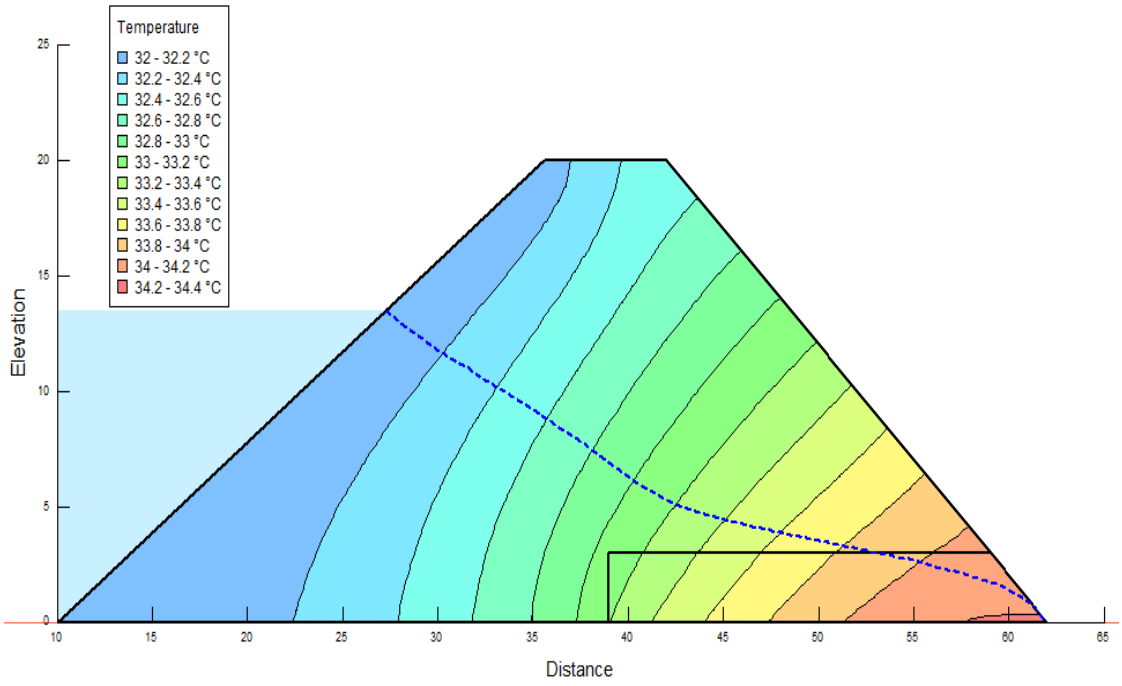

Figure 5.154: Temperature in M14

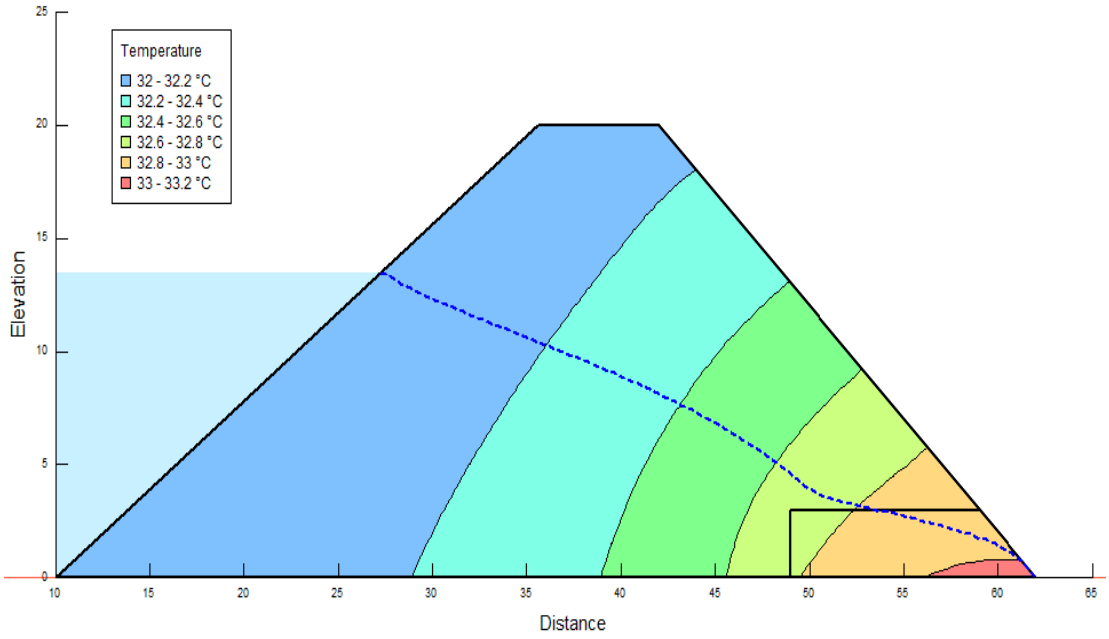

Figure 5.155: Temperature in M15

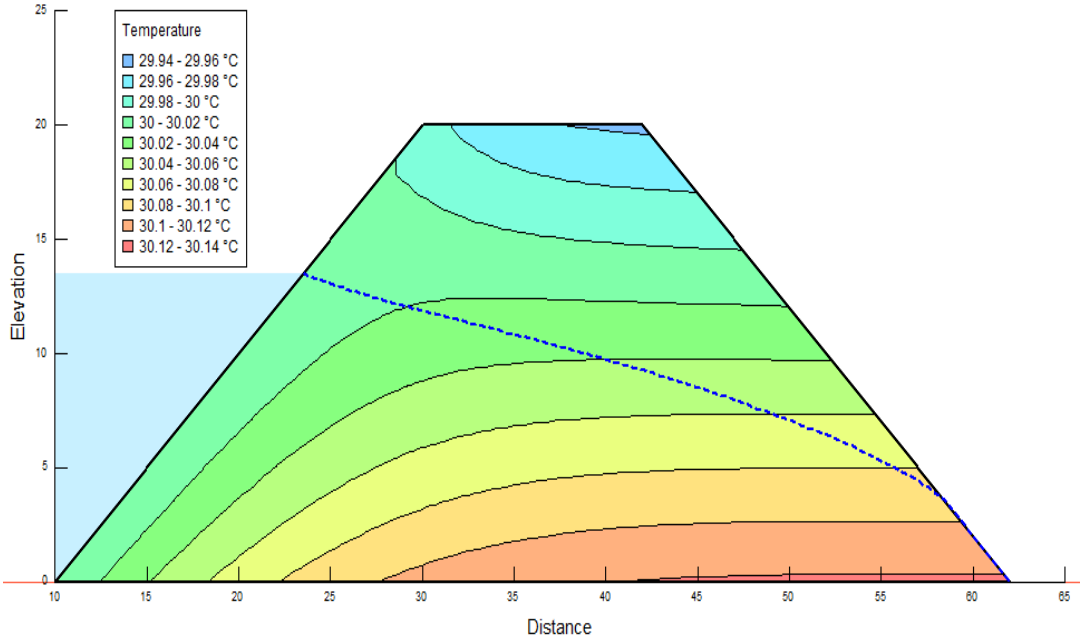

Figure 5.156: Temperature in M18

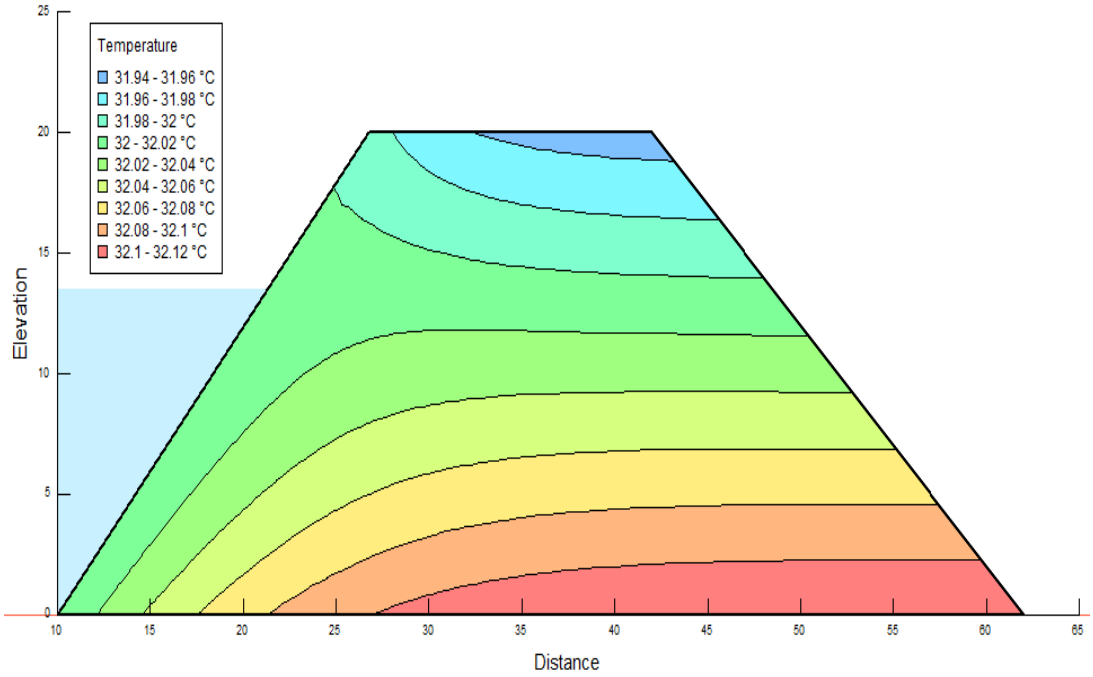

Figure 5.157: Temperature in M19

5.2.4 Discussion of temperature and flux modelling

Table 5.13 lists the heat and water fluxes for each model, whereas Figure 5.158 depicts a heat flux graph with the x-axis indicating the number of earth dam models and the y-axis indicating heat flux in kJ/sec/m^2. Figure 5.159 depicts a water flux graph with the number of earth dam models on the x-axis and water flux in m^3/sec/m^2 on the y-axis. Figure 5.160 shows a semi-logarithmic flux graph on the y-axis on a log scale to compare heat flux and water flux with the respective model on the x-axis.

On increasing the downstream slope of an earth dam from 45 degrees (in M1) to 59 degrees (in M2), the water flux and heat flux increased by 34.81% and 34.37%. While increasing the downstream slope from 34 degrees (in M3) to 45 degrees (in M19), the water and heat flux increased by 42.36%. On increasing longitudinal slope by 2.28% (in M1 to M7), water flux and heat flux increased by 1.33%, increasing longitudinal gradient by 4% (in M1 and M8), water flux and heat flux increased by 2.01% and 2.06%, respectively. While increasing slope by 6.07% (from M1 to M6), water flux and heat flux increased by 2.55%. With the increase in the downstream filter of length 13m in M15, 15.5m in M13, and 23m in M14, water flux increased by 414.23%, 533.38%, and 666.51%, respectively; at the same time, heat flux increased by 414.23%, 533.38%, and 666.75%, respectively. This increase in heat flux is due to an increase in water flow

and hence an increase in heat convection in the earth dam. Similar results were seen by Alekseevich and Sergeevich (2017), Badruddin et al. (2020), Cuong et al. (2017), Narasimhan (2016), and Radzicki and Bonelli (2010).

Table 5.13 Comparison of results of heat flux and water flux

Model No.	Water Flux ($m^3/sec/m^2$)	Heat flux ($kJ/sec/m^2$)
M1	6.549×10^{-06}	08.365
M2	8.829×10^{-06}	11.241
M3	4.576×10^{-06}	05.846
M4	4.575×10^{-06}	05.844
M5	4.575×10^{-06}	05.844
M6	6.716×10^{-06}	08.579
M7	6.636×10^{-06}	08.477
M8	6.681×10^{-06}	08.538
M9	1.410×10^{-06}	01.801
M10	1.459×10^{-06}	01.863
M13	4.148×10^{-05}	52.989
M14	5.020×10^{-05}	64.126
M15	3.367×10^{-05}	43.020
M18	6.526×10^{-06}	08.282
M19	6.515×10^{-06}	08.322

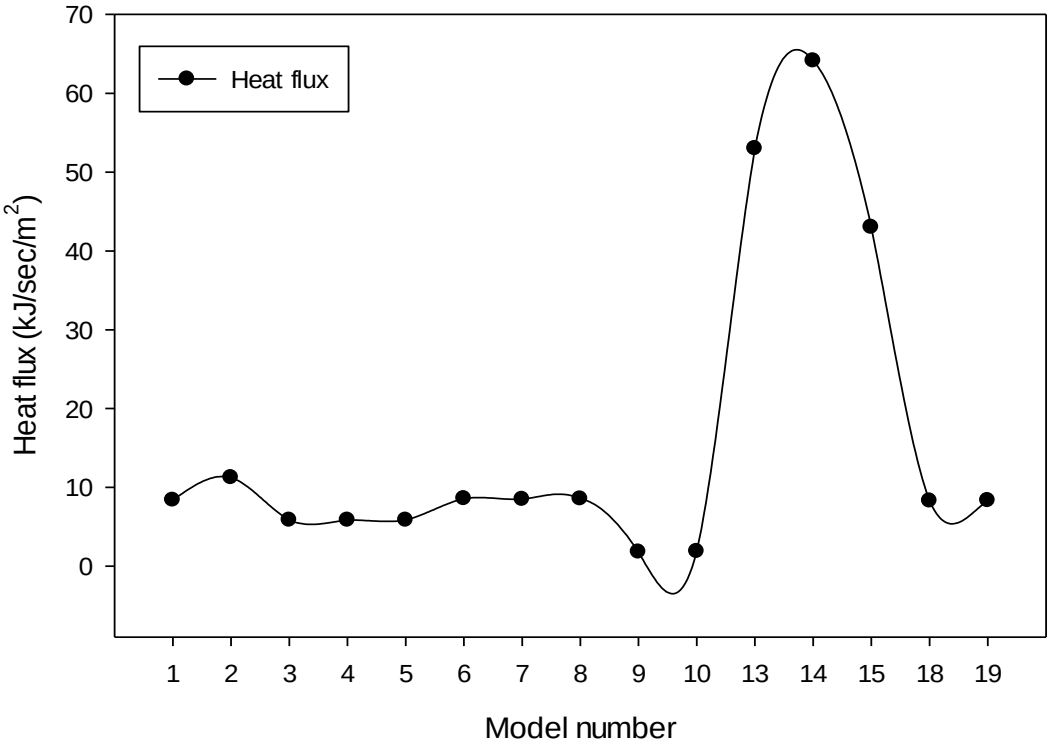

Figure 5.158: Heat flux in different models of an earth dam

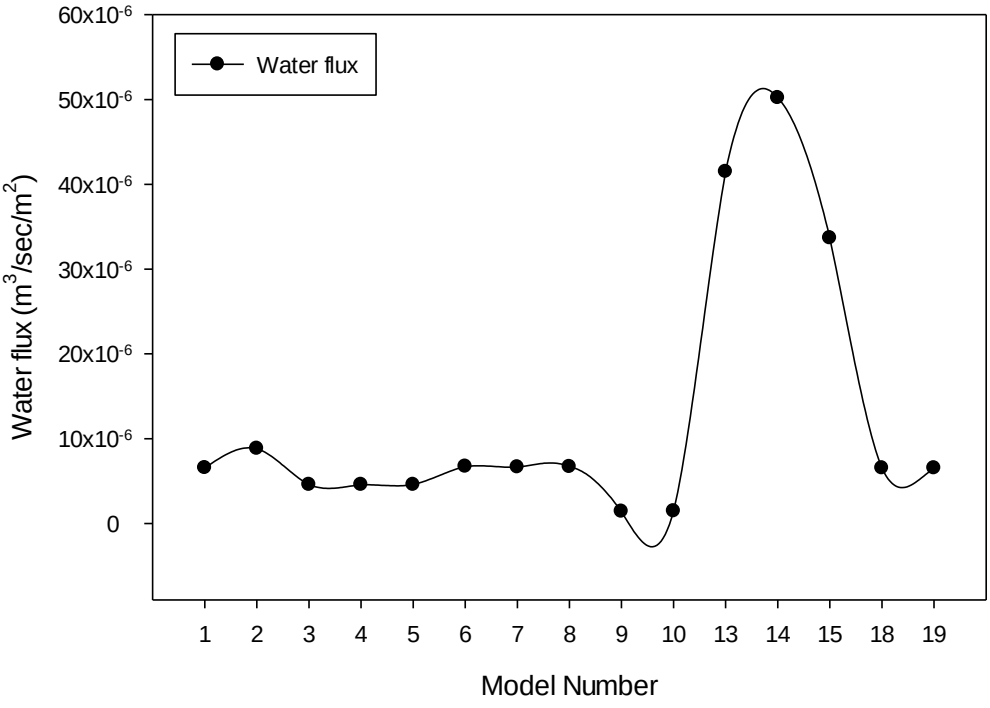

Figure 5.159: Water flux in different models of an earth dam

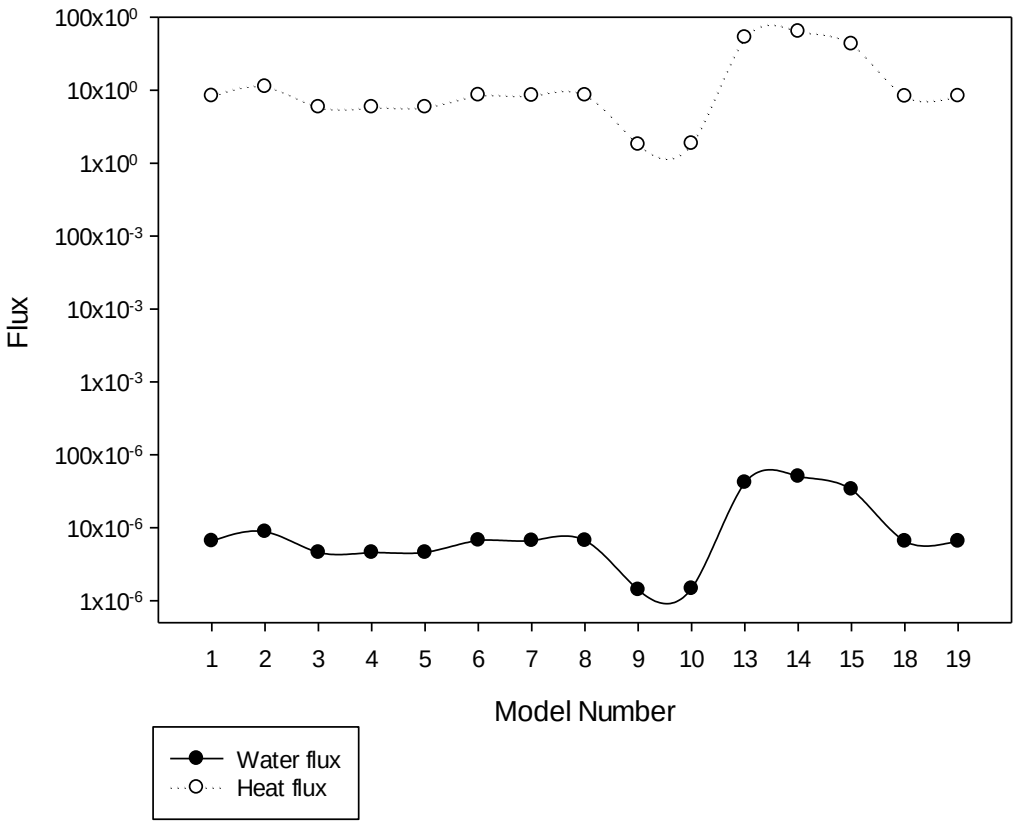

Figure 5.160: Water and heat flux comparison in different models of an earth dam

On increasing upstream slope from 38 degrees (in M1) to 45 degrees (in M18), i.e., 18.42%, the water flux and heat flux decrease by 0.34% and 0.99%, respectively. While increasing the slope from 38 degrees (in M1) to 50 degrees (in M19), i.e., 31.57%, water flux and heat flux decreased by 0.51%. Comparing fluxes in a homogeneous dam model (M1) with the clay core model (M9) with a top width of 2.4 m and bottom width of 18m in M9, both water flux and heat flux were reduced by 78.46%. While comparing M1 with M10, with a bottom core width of 18m and a top core width of 1.9 m, both water flux and heat flux were reduced by 77.72%. Hence, an increase in the clay core's width leads to a reduction of water flux and heat flux and vice-versa, with a decrease in the top width of the clay core by 20.83% in the model M9 to M10, the water and heat flux increased by 3.44%. The reduction in heat flux is due to the reduction of water flow in the earth dam, which results in the reduction of the heat flow due to convection. Similar

results were seen by Alekseevich and Sergeevich (2017), Badruddin et al. (2020), Cuong et al. (2017), Narasimhan (2016), and Radzicki and Bonelli (2010).

Increasing the earth dam's height for the same upstream head by 33.33%, i.e., 15 m (in M5) to 20 m (in M4), the water flux and heat flux remain unchanged. On increasing the dam's length from 52m (in M3) to 56m (in M4), i.e., by 7.69%, both the water flux and heat flux had an insignificant reduction of 0.02%. An insignificant reduction in heat flux and water flux is due to a slight reduction in seepage discharge which causes a reduction in heat convection and a slight increase in heat conduction as at low seepage area conduction predominates convection. Similar results were seen by Alekseevich and Sergeevich (2017), Badruddin et al. (2020), Cuong et al. (2017), and Narasimhan (2016).

On increasing the downstream slope of an earth dam by 31.11%, i.e., from 45 degrees (in M1) to 59 degrees (in M2), the maximum temperature due to convection changed from 32.1 ºC to 31.1ºC, while increasing downstream slope from 34 degrees (in M3) to 45 degrees (in M19), i.e., by 32.35%, the temperature increased from 32.07 ºC to 32.12 ºC. It was found that temperature increases on increasing downstream slope till 45-degree slope then this effect is reversed because water flow doesn't increase beyond this point. It shows a direct relationship between temperature rise due to convection and the downstream slope of the dam. Similar results for seepage were seen by Chahar (2004). With the introduction of a downstream filter of length 7.8m in M18 from the downstream end, the temperature increased to 32.85 ºC from the maximum temperature of 32.10 ºC in a homogeneous dam M1. While with the filter of length 13m in M13, 15.5 m in M13, and 23m in M14, the temperature increased to 33.20 ºC, 33.60 ºC, 34.40 ºC, respectively. On increasing the longitudinal slope by 2.28% (in M1 to M7), the temperature increased from 32.10 ºC to 32.16 ºC. Increasing the longitudinal gradient by 4% (in M1 and M8) and increasing the slope by 6.07% (from M1 to M6), the temperature increased from 32.10 ºC to 32.16 ºC in both cases. Increasing the earth dam's height for the same upstream head by 33.33%, i.e., 15 m in M5 to 20m in M4, the temperature due to convection increased from 32.05 ºC to 32.07 ºC. The temperature relation with seepage flow was seen by Badruddin et al. (2020), Bobkob (1973), Cuong et al. (2017), Johansson and Sjödahl (2004), Kappelmeyer (1957), Radzicki and Bonelli (2010), Yousefi et al. (2013).

On increasing upstream slope, from 38 degrees (in M1) to 45 degrees (in M18), i.e., 18.42%, the temperature decreases from 32.1 ºC to 30.14 ºC. It shows that the dam's upstream slope and the convective heat transfer decreased due to the reduced water flow in the soil's pores. While on an increasing upstream slope, from 45 degrees (in M18) to 50 degrees (in M19), i.e., 11.11% and increasing slope, from 38 degrees (in M1) to 50 degrees (in M19), i.e., 31.57%; the temperature was negligibly increased from 32.10 ºC to 32.12 ºC and 32.10 ºC to 32.12 ºC respectively. This increase in temperature was due to an increase in conduction, i.e. transfer of heat from the soil to soil particle, while convection remained almost invariable. Increasing the dam's length from 52m (in M3) to 56m (in M4), i.e., by 7.69%, the temperature variation remains unchanged. It was observed that with an increase in upstream slope and increase in dam's length, the seepage in the earth dam reduced, which causes in reduction of temperature in the dam due to a reduction in convection. While in the model hence similar results were seen by Bobkob (1973), Cuong et al. (2017), Johansson and Sjödahl (2004), and Kappelmeyer (1957), Radzicki and Bonelli (2010), Yousefi et al. (2013).

Comparing temperature in a homogeneous dam to earth dam (M1) with clay core with the upstream and downstream angle of 60 degrees and bottom width of 18m in M9, temperature reduced from 32.10 ºC to 32.06 ºC. While in M10, with bottom core width of 18m and top core width of 1.9m, the temperature reduced to 32.06 from 32.10ºC in M1. It was also observed that temperature variation doesn't significantly change with a decrease of the top width of M9 to M10. The introduction of an impervious core in the dam causes a temperature sink due to the reduced water flow. Similar results were seen by Bobkob (1973), Cuong et al. (2017), Johansson and Sjödahl (2004), Kappelmeyer (1957), Radzicki and Bonelli (2010), Yousefi et al. (2013).

CHAPTER 6

CONCLUSIONS

6.1 SEEPAGE MODELLING

Twenty-four earth dam models were constructed in the hydraulic flume to study seepage flow by varying upstream, downstream slope, longitudinal slope, the dam's height, the viscosity of upstream water, and upstream head of water. The models were also studied for the effect of the downstream filter with its homogeneous earth dam model. The variation in downstream filter length was also carried out. The seepage variation in the earth dam was studied with and without a central impervious clay core and by varying central core width. Earth dam models were also studied for change in the property of constructing material by using silty sand, clay, silty sand containing fifteen per cent clay content, and silty sand containing thirty per cent clay content. The slope stability was done using Slope/w software in Geostudio 2020, while seepage analysis was done using Seep/w software in Geostudio 2020 using finite element analysis. Following conclusions were drawn based on the result analysis of the earth dam models.

- The factor of safety of upstream and downstream slope at full reservoir conditions was found safe.

- The phreatic line was compared between the experimental and numerical model in Seep/w; it was found to be in good agreement with each other. Pavlovsky's equation was also used to determine the phreatic line in a homogeneous earth dam model, and it was in parity with the phreatic line obtained in experimental models. The phreatic line obtained from Seep/w models in Geostudio was a little higher than the respective experimental models.
- Seepage obtained from experimental work was found to be in good agreement with Seep/w software. It was then validated with the analytical solutions obtained from Casagrande's, Dupuit's, Pavlovsky's, and Schaffernak's solutions.
- It was observed that with the increased longitudinal slope, there was an increase in seepage discharge, and the phreatic line was lowered.

- It was observed that with the flattening of the upstream slope, the discharge is increased. While with the flattening of the downstream slope, the discharge decreases.
- With increasing the length of the earth dam, the seepage discharge got reduced.
- Dam with clay core reduces the seepage significantly. The thickness effect of the clay core effect was also studied, and it was observed that with the increase in thickness of the clay core, the seepage reduces.
- With the introduction of a downstream filter, the phreatic line was prevented from cutting the downstream face of the earth dam. But increased the seepage drastically after the length of the filter reached 30% of the total length of the dam from the downstream end. With the increase in thickness of the filter, the seepage reduced, but that change was almost negligible. Hence, the thickness of filters on seepage doesn't have much effect.
- With the increase in the height of the dam or freeboard, the seepage discharge increased slightly.
- With an increase in clay content in the soil, seepage discharge decreases.
- Discharge obtained from numerical models was found to be slightly higher than the discharge obtained from experimental results. It may be due to evaporation losses in the physical model.

6.2 HEAT AND WATER FLUX MODELLING

Fifteen earth dam models were taken to compare the water flux due to seepage and heat flux due to the convective heat transfer in the respective earth dam model. The water temperature was higher than the earth dam, and the surrounding air acted as a thermal loading source. The dam's heat flux and water flux were studied by varying several parameters, including an upstream slope, downstream slope, longitudinal slope, and the dam's height. Earth dam with and without a downstream filter was studied. Earth dam with and without central impervious core was studied along with the variation in central impervious clay core width on seepage discharge was also considered for the study. Temperature measurements were done in the earth dam model placed in a hydraulic flume using digital thermometers to determine the heat flux compared with the

simulation result of Temp/w in Geostudio 2020. The following conclusions were drawn based on the result analysis of the earth dam models.

- Water flux obtained from experimental work was found to be in good agreement with Seep/w software.
- It was observed that with the increased longitudinal slope, there is an increase in the heat and water flux.
- It was that with an increase in the upstream slope, the heat and water flux decreased.
- On increasing the earth dam's length, the heat had an insignificantly low reduction due to an insignificant increase in water flux, and hence flux remained almost the same.
- The thickness effect of the clay core on flux variation was also studied, and it was observed that with the increase in thickness of the clay core, the heat and water flux reduced. Hence, a dam with a clay core reduces the heat and water flux significantly.
- With the increase in the dam's height with the same upstream water head, the heat and water flux remained unchanged.
- A Correlation between heat flux and water flux exists in all the fifteen models of the earth embankment dam.
- Heat flux obtained was a practical alternative in detecting seepage and water flux in an earth dam. As temperature sensors are cheaper than the discharge and water flow measuring devices, it helps detect water at a reduced cost than conventional devices.

6.3 TEMPERATURE VARIATION MODELING

The temperature variation with the water flow due to the convective heat transfer in porous media was studied in fifteen earth dam models. The water temperature was higher than the earth dam, and the surrounding air acted as a thermal loading source. Temperature measurements were done in the earth dam model placed in a hydraulic flume using digital thermometers and compared with the simulation result of Temp/w in Geostudio 2020. The following conclusions were drawn based on the result analysis of the earth dam models.

- It was observed that near the walls of a hydraulic flume, the soil pores of the dam were of larger volume, resulting in an increased local water flow. Regional flow variation due to wall channelling led to enhanced convection heat transfer, hence increasing the temperature.
- It was observed that with the increased longitudinal slope, there is an increase in water flow which led to an increase in the temperature variation in the earth dam due to increased convection.
- It was that with an increase in the upstream slope, the temperature in the earth dam reduced. While with an increase in the downstream slope, the temperature increased.
- With increasing the length of the earth dam, the temperature in the earth dam remained almost the same due to negligible variation in the flow of water.
- With the introduction of the impervious central core in the earth dam, the temperature inside the dam reduced significantly due to the reduced flow rate of water. By increasing the width of the core effect, the temperature variation remains unchanged.
- With the introduction of a downstream filter, the phreatic line was prevented from cutting the downstream face of the earth dam. With the increase in the length of the horizontal filter and the thickness of the filter, the temperature was increased drastically due to the increased water flow rate.
- With the increase in the height of the dam or the freeboard, the temperature due to convection increased due to the increased water flow rate; hence convection increased inside the earth dam.
- Temperature measurement was a practical alternative in detecting seepage in an earth dam as it helps detect seepage using lesser price sensors compared to conventional devices.

6.4 SCOPE FOR FURTHER STUDIES

Several factors or variations that can be further taken into consideration for the study of seepage in porous media such as earth dams are as follows

- Chemicals transport modelling due to seepage
- Effect of coir fibre as a preventive measure for seepage control

- Stability of earth dam during earthquake events
- The convective effect in freezing conditions
- Use of fly ash and other materials to minimise seepage

LIST OF PUBLICATIONS

- Sushant Kumar, Anil Kumar Sahu, and Munendra Kumar (2022) "Modeling the effect of central impervious core and downstream filter geometry on seepage through earth dams", Ain Shams Engineering Journal, Elsevier, Volume 13, Issue 1, pp. 1-11. (SCIE)
- Sushant Kumar, Anil Kumar Sahu, and Munendra Kumar (2021) "Heat and water flux modeling in an earth dam", Water Science & Technology, IWA Publishing, Vol 84 No 10-11, pp. 2760-2779. (SCIE)
- Sushant, Anil Kumar Sahu, and Munendra Kumar (2023) "Temperature analysis modeling to detect the seepage flow variation in an earth dam" J. Environmental Protection and Ecology, SciBulCom Ltd., Vol 24, Book1, (Article accepted and under Publication). (SCIE)
- Sushant Kumar, Anil Kumar Sahu, and Munendra Kumar, "Effect of seepage through an earth dam on its water quality: A review", 2nd ASCE India Conference on challenges of resilient and sustainable infrastructure development in emerging economies (CRSIDE-2020), March 2020 held at Kolkata, ISBN-978-93-5396-500-6.
- Sushant Kumar, Anil Kumar Sahu, and Munendra Kumar, "Simulation of solute mass flux in an earth dam", "3rd International Conference on Advances in Engineering, Science and Technology – 2021", ICAEST-21 Dehradun, ISBN 978-93-5473-534-9.

REFERENCES

1. Abdul Alim M., Ahmed F., and Islam M.S. (2017) “Seepage analysis of Mahananda earthen embankment at Chapai Nawabganj in Bangladesh” J. American Journal of Engineering and Technology Management, Vol 2, No 1, pp. 1-6.
2. Abu-Hamdeh N. (2014) "Specific heat and volumetric heat capacity of granular materials as affected by moisture and density" J. Applied mechanics and material, vol 575, pp. 103-107.
3. Abu-Hamdeh N. (2003) "Thermal properties of soils as affected by density and water content" J. Biosystems engineering (2003), 86 (1), 97-102.
4. Ahmed A.A. (2009) “Stochastic analysis of free surface flow through earth dam” J. Computers and Geotechnics, Vol 36, pp. 1186-1190.
5. Akyüz A. and Merdun H. (2003) “Seepage through an earth dam on impervious base with Hele-Shaw viscous liquid physical model” J. EJGE, pp. 1-17.
6. Alekseevich A.N. and Sergeevich A.A. (2017) "Numerical modelling on tailings dam thermal-seepage regime considering phase transitions" J. Modelling and simulation in engineering, Vol. 2017, pp. 1-10.
7. Al-Mansori N.J.H., Al-Fatlawi T.J.M., Othman N.Y., and Al-Zubaidi L.S.A. (2020) “Numerical analysis of seepage in earth-fill dams” Civ Eng Journal, Vol. 6, pp. 1336–1348. https://doi.org/10.28991/cej-2020-03091552.
8. Amanifard N., Borji M., and Haghi A.K. (2007) "Heat transfer in porous media" J. Brazilian journal of chemical engineering, vol 24, No.02, pp. 223-232.
9. Andreea C. (2015) “Unsaturated slope stability and seepage analysis of a dam” J. Energy Procedia 85 (2016), pp. 93-98.
10. Aniskin N.A., Rasskazov L.N. and Yadgorov E.Kh. (2016) “Seepage and pore pressure in the core of earth and rockfill dam” J.Power Technology and Engineering, Vol 50, No 4, pp. 378-384.
11. ASTM D1558-10, Standard Test Method for Moisture Content Penetration Resistance Relationships of Fine-Grained Soils
12. Athani S., Sivamanth, Solanki C.H. and Dodagoudar G.R. (2015) “Seepage and stability analysis of earth dam using finite element method” J. International Conference on Water Resources, Coastal and Ocean Engineering (ICWRCOE 2015), pp. 887-883.

13. Badruddin I.A., Azeem, Yunus Khan T.M., and Baig M.A.A (2020) "Heat transfer in porous media: A mini Review" Proc. Materials Today: Proceedings 24(2020), pp. 1318-1321.
14. Bardet J. and Tobita T. (2002) “A practical method for solving free-surface seepage problems” J. Computer and geotechnics 29, pp. 451-475.
15. Bobkob K.A. (1973), "Use of temperature observations in the maintenance of earth dams" Rationalization and exchange of experience, translated from Gidrotekhnicheskoe Stroitel'stvo, pp. 497-502.
16. Buntebarth G. (2020) "Thermal properties of sand and mineral flours" J. SN Applied Sciences (2020) 2:396.
17. Bureau of Indian Standard code IS 1448-2018 (part 25), Methods of test for petroleum and its products; transparent and opaque liquid section 1; Determination of dynamic viscosity.
18. Bureau of Indian Standard code, IS 2720-1983 (part 1), “Preparation of dry soil samples for various tests”.
19. Bureau of Indian Standard code, IS 10635-1993, Freeboard requirements in embankment dams- Guidelines.
20. Bureau of Indian Standard code, IS 2720-1973 (part 2), “Determination of water content”.
21. Bureau of Indian Standard code, IS 2720-1980 (part 3), “Determination of specific gravity”.
22. Bureau of Indian Standard code, IS 2720-1985 (part 4), “Methods of test for soils- Grain size analysis”.
23. Bureau of Indian Standard code, IS 2720-1985 (part 5), “Determination of liquid and plastic limit”.
24. Bureau of Indian Standard code, IS 2720-1972 (part 6), “Determination of shrinkage factors”.
25. Bureau of Indian Standard code, IS 2720-1980 (part 7), “Determination of water content-dry density relation using light compaction “
26. Bureau of Indian Standard code, IS 2720-1981 (part 12), “Determination of shear strength parameters of soil from consolidated undrained tri-axial compression test with measurement of pore water pressure”.

27. Bureau of Indian Standard code, IS 2720-1986 (part 13), “Methods of test for soils- Direct Shear Test”.
28. Bureau of Indian Standard code, IS 2720-1986 (part “15), “Determination of Consolidation Properties”.
29. Bureau of Indian Standard code, IS 2720-1986 (part 17), “Methods of test for soils- laboratory determination of permeability”.
30. Bureau of Indian Standard code, IS 7894-1975, Code of practice for stability analysis of earth dams
31. Bureau of Indian Standard code, IS 8237-1985, Code of practice for protection of slope for reservoir embankment.
32. Bureau of Indian Standard code, IS 8826-1978, Guidelines for design of large earth and rockfill dams.
33. Chahar B.R. (2004) “Determination of length of a horizontal drain in homogeneous earth dam”, J. of Irrigation and Drainage Engineering, Vol 130, no 6, pp. 530-536.
34. Chen Y., Hu R., Zhou C., Li D., Rong G., and Jiang Q. (2010) “A new classification of seepage control mechanism in geotechnical engineering” J. of Rock Mechanics and Geotechnical Engineering, 2(3), pp. 209-222.
35. Chen Y., Zhou C., and Jing L. (2009), "Modeling coupled THM processes of geological porous media with multiphase flow: Theory and validation against laboratory and field scale experiments" Journal of Computers and Geotechnics, Vol 36, pp. 1308-1329.
36. Cho S. E. (2012) “Probabilistic analysis of seepage that considers the spatial variability of permeability for an embankment on soil foundation” J. Engineering Geology, 133-134, pp. 30-39.
37. Chuvilin E. and Bukhanov B. (2019) "Thermal conductivity of frozen sediments containing self-preserved pore gas hydrates at atmospheric pressure: An experimental study" J. Geosciences, 9,65.
38. Cuong B.Q., Thai N.C., Yihong Z., and Chunju Z. (2017) "Estimating seepage in embankment dams based on temperature measurement: A review paper" J. International journal of engineering research and technology (IJERT), Vol 6 Issue 01, pp. 106-113.

39. Das BM. (2014) “Advanced Soil Mechanics” 4th edition, CRC Press, Taylor and Francis Group, pp.241-301.
40. Del Piero G. (2020) "A mechanical model for heat conduction" J. Continuum Mech. Thermodyn., 32, pp.1159-1172.
41. Djehiche A., Rekia A., and Mostafa G. (2014) “The seepage the rough the earthen dam with a vertical drain: An experimental study” Journal of Environmental Research and Development, Vol 8, Issue 3, pp. 471-476.
42. Dvinoff A.H. (1987) “Unsteady state phreatic surface in earth dams” J. ASCE, Vol 113 (6), pp. 686-687.
43. El Molla DA. (2019) “Seepage through homogeneous earth dams provided with a vertical sheet pile and formed on impervious foundation” J. Ain Shams Engineering Journals, Vol. 10, pp.529–539. https://doi.org/10.1016/j.asej.2018.12.008.
44. Engineering ToolBox, (2003). Specific Heat of some common Substances. [online] Available at: https://www.engineeringtoolbox.com/specific-heat-capacity-d_391.html [1/7/2021]
45. Engineering ToolBox, (2004). Water- Specific Heat. [online] Available at: https://www.engineeringtoolbox.com/specific-heat-capacity-water-d_660.html [10/28/2020]
46. Fakhari A. and Ghanbari A. (2013) “A simple method for calculating the seepage from earth dam with clay core” J. of Geo. Engineering, Vol 8, pp. 27-32.
47. Farzampour A., Salmasi F., and Mansuri B. (2014) “Optimum size of clay core of Alavian earth dam by numerical simulation” J. Iranica Journal of Energy & Environment, 5(3), pp. 240-246.
48. Fazelabdolabadi B., and Golestan M.H. (2020) “Towards Bayesian Quantification of Permeability in Micro-scale Porous Structures – The Database of Micro Networks” J. HighTech Innov Journal,Vol 1, pp. 148–160. https://doi.org/10.28991/hij-2020-01-04-02.
49. Foster M., Fell M., and Spannagle M. (2020) “The statistics of embankment dam failures and accidents” J. Canadian Geotech. Journal, 37, pp. 1000-1024.
50. Fu J. and Jin S. (2009) “A study on unsteady seepage flow through dam” J. of Hydrodynamics, Vol- 21, issue 4, pp. 499-504.

51. Indraratna B., Trani L.D., and Khabbaz H. (2008) “A critical review on granular dam filter behaviour- from particle sizes to construction-based design criteria” J. Geomechanics and geoengineering: An International journal, Vol 3, No.4, pp. 279-290.
52. Irzooki R.H. and Jamel A.A. (2012) “Experimental study of characteristics of top seepage line through homogenous earth dam using HELE-SHAW model” Journal of International Review of Civil Engineering, Vol 3, no 6., pp. 430-440.
53. Ižvolt L. and Dobeš P. (2014) "Test procedure for the value of specific heat capacity and thermal conductivity coefficient" XXIII R-S-P seminar, Theoretical Foundation of Civil Engineering (23 RSP) (TFoCE 2014), J. Procedia engineering, 91(2014), pp. 453-458.
54. Jiang Q.H., Deng S.S., Zhou C.B, and Lu W.B. (2010) “Modeling unconfined seepage flow using 3-D numerical manifold method” Journal of Hydrodynamics, Vol 22, issue 4, pp. 554-561.
55. Jhanwar A., Babua R. and Mehta R. (2016) “Analysis of seepage through an earthen dam” Project report in Water Resources Engineering, VIT University, Chennai, India.
56. Johansson S. and Sjödahl P. (2004) "Downstream seepage detection using temperature measurements and visual inspection-monitoring experience from Røsvatn field test dam and large embankment dams in Sweden" Proc. Intl. Seminar on stability and breaching of embankment dams, 21.
57. Kacimov A.R. (1996) “Explicit solution for seepage infiltration into a porous earth dam due to precipitation” J. International Journal for numerical and analytical methods in geomechanics, Vol 20, pp. 715-723.
58. Kamanbedast A. and Delvari A. (2012) “Analysis of earth dam: Seepage and stability using Ansys and Geo- Studio software” J. World Applied Science Journal, Vol 17, issue 9, pp. 1087-1094.
59. Kamanbedast A. and Shahosseini M. (2011) “Determination of seepage and analysis of earth dams (Case study: Karkheh dam)” J. Iranica journal of energy & environment, 2(3), pp. 201-207.
60. Kanarskii V.F. (1987), “Effect of seepage on earth dams” J. Link. Springer, pp. 19-21.
61. Kanchana H.J. and Prasanna H.S. (2015) “Adequacy of seepage analysis in core section of earthen dam with different mix, proportions” J. International

Conference on Water Resources, Coastal and Ocean Engineering (ICWRCOE 2015), pp. 868-875.

62. Kappelmeyer O. (1957) "The use of near surface temperature measurements for discovering anomalies due to cause at depths" J. Geophysical prospecting, vol 5, Issue 3, pp. 239-258.
63. Kazemzadeh-Parsi M.J. and Daneshmand F (2012) “Unconfined seepage analysis in earth dam using smoothed fixed grid finite element method” J. International Journal for Numerical and Analytical Methods in Geomechanics, Vol 36, pp. 780-797.
64. Kodešová R., Vlasáková M., Fér M., Teplá D., Jakšík O., Neuberger P., and Adamovský (2013) “Thermal properties of representative soils of the Czech Republic” J. Soil & Water Res., 8 (4), pp. 141-150.
65. Kosky P., Balmer R., Keat W., and Wise G. (2012) “Exploring Engineering” Third Edition, Elsevier, pp. 259-264.
66. Kratochvil J. and Bachorec T. (2004) “Numerical modelling of nonstationary free surface flow in embankment dams” Ansys conference 2004, pp. 1-4.
67. Kumar A and Mohan A. (2017) “A study on seepage through earthen dams by using analytical methods” J. International Journal of Mechanical, Civil, Automobile and Structural Engineering, Vol-1, issue 2.
68. Kumar S., Sahu A.K., and Kumar M. (2020) “Effect of seepage through an earth dam on its water quality: A review”, 2nd ASCE India Conference on challenges of resilient and sustainable infrastructure development in emerging economies (CRSIDE-2020), March 2020 held at Kolkata, ISBN-978-93-5396-500-6.
69. Kumar S., Sahu A.K., and Kumar M. (2021) “Heat and water flux modeling in an earth dam”, Water Science & Technology, IWA Publishing, Vol 84 No 10-11, pp. 2760-2779.
70. Kumar S., Sahu A.K., and Kumar M. (2021) “Modeling the effect of central impervious core and downstream filter geometry on seepage through earth dams”, Ain Shams Engineering Journal, Elsevier, pp. 1-11.
71. Kumar S., Sahu A.K., and Kumar M. (2021) “Simulation of solute mass flux in an earth dam”, “3rd International Conference on Advances in Engineering, Science and Technology – 2021”, ICAEST-21 Dehradun, ISBN 978-93-5473-534-9.

72. Kumar S., Sahu A.K., and Kumar M. (2023) “Temperature analysis modeling to detect the seepage flow variation in an earth dam” J. Environmental Protection and Ecology, SciBulCom Ltd., Vol 24, Book1, Article under Publication.
73. Kurz D., Alfaro M., and Graham J. (2017) "Thermal conductivities of frozen and unfrozen soils at three project sites in northern Manitoba" J. Cold regions science and technology 140, pp. 30-38.
74. Lam L., Fredlund D.G. and Barbour S.L. (1987) “Transient seepage model for saturated -unsaturated soil system: a geotechnical engineering approach.” J. Canadian geotechnical journal, Vol 24 (4), pp. 565-580.
75. Li G.C. and Desai C.S. (1983) “Stress and seepage Analysis of earth dam” J. Geotech. Eng., Vol 109, issue 7, pp. 946-960.
76. Malekpour A., Farsadizadeh D., Dalir A.H. and Sadrekarimi J. (2011) “Effect of horizontal drain size on the stability of an embankment dam in steady and transient seepage conditions” J. Turkish Journal Eng. Env. Sci., Vol 36, pp. 139-152.
77. Martin J.L, McCutcheon, and Steven C. (1999) “Hydrodynamics and transport for water quality modelling” Taylor and Francis, pp. 165-166.
78. Mauriya V. (2010) “Geotechnical instrumentation in earth and rock-fill dams” J. Indian Geotechnical Conference-2010, GEOtrendz, IGS Mumbai, pp. 1027-1030.
79. Miao X., Chu J., Qiao J., and Zhang L. (2012) “Predicting seepage of earth dam using neural network and genetic algorithm” J. Advanced materials research, Vol 403, Issue 408, pp. 3081-3085.
80. Misra A., Becker B.R., and Fricke B.A (1995) "A theoretical model of the thermal conductivity of idealized soil” J. HVAC&R Research, 1:1, pp. 81-96.
81. Narasimhan A. (2016) “Essentials of Heat and Fluid Flow in Porous Media” 1st edition, second reprint, Ane Books Pvt. Ltd., New Delhi, pp. 1-187.
82. Omofunmi O.E., Kolo J.G., Oladipo A.S., Diabana P.D., and Ojo A.S. (2017) “A review on effects and control of seepage through earth-fill dam” J. current Journal of Applied Science and Technology, Vol 22, issue 5, pp. 1-11.

83. Ouzaid I, Benmebarek N, and Benmebarek S. (2020) “FEM optimisation of seepage control system used for base stability of excavation” J. Civ Eng Journal; Vol. 6, pp. 1739–1751. https://doi.org/10.28991/cej-2020-03091579.
84. Pingyu Z., Thévanaz, Yuanbao L., and Yang Z. (2007) “Design of simulator for seepage detection in an embankment based on distributed optic fibre sensing technology” J. Chinese journal of scientific instrument, vol 28, No. 3, pp. 431-436.
85. Radzicki K. and Bonelli S. (2010) "Thermal Seepage monitoring in the earth dams with impulse response function analysis model" Proc. 8th ICOLD European Club Symposium, Innsbruck, Austria, pp. 624-629.
86. Refaiy A.R., Aboulatta N.M., Saad N.Y., and El-molla D.A. (2021) “Modeling the effect of downstream drain geometry on seepage through earth dams” J. Ain Shams Eng Journal., pp. 1-21. https://doi.org/10.1016/j.asej.2021.02.011.
87. Rerak M. (2017) "Selected soil thermal conductivity models" J. E3S Web of conferences 13, 02003 WTiUE, pp. 1-4.
88. Rezk M. and Senoon A.A. (2012) “Analytical solution of earth dam with upstream blanket” J. Alexandria Engineering Journal, Vol. 51, pp. 45-51.
89. Rinehart A., Lācis U., and Bagheri S. (2021) “The Brinkman viscosity for porous media exposed to a free flow” Article in press, Cornell University, pp.0-21. https://doi.org/10.48550/arXiv.2106.01879.
90. Roushangar K., Garekhani S., and Alizadeh F. (2016) “Forecasting daily seepage discharge of an earth dam using wavelet-mutual information- Gaussian process regression approaches” J. Geotech. Geol. Engineering, Vol 34, pp. 1313-1326.
91. Sachpazis C.I. (2014) “Experimental conceptualisation of flownet system construction inside the body of homogeneous earth embankment dams” Journal. EJGE, Vol -19, pp. 2113-2136.
92. Salmasi F. and Jafari F. (2016) “Validity of Schaffernak’s and Casagrande’s analytical solutions for seepage through a homogeneous earth dams” J. SAJCEE, Vol 2(1), pp. 15-28.
93. Salmasi F. and Mansuri B. (2014) “Effect of homogeneous earth dam hydraulic conductivity ratio (k_x/k_y) with horizontal drain on seepage” J. Indian Geotech. Journal, Vol 44, issue 3, pp. 322-328.

94. Sarstedt M. and Mooi E. (2014) “Regression Analysis” A Concise Guide to Market Research. The Process, Data, and Methods Using IBM SPSS Statistics - 3rd Edition, Chapter 7, pp.193-233.
95. Shrivastava A.K., Jain A., Kansal D., and Gupta S. (2015) “Modification on the Casagrande’s equation of phreatic line” J. International journal of civil engineering and technology (IJCIET), Vol 6, Issue 6, pp. 1-13
96. Sivakumar Babu G. and Srivastava A. (2007) “A procedure for the design of protective filters” J. Canadian Geotech. Journal, vol 44, 490-495.
97. Sivakumar Babu G. and Vasudevan A.K. (2008) “Seepage velocity and piping resistance of coir fiber mixed soils” J. of Irrigation and Drainage engineering, ASCE, Vol 134, Issue 4, pp. 485-492.
98. Srivastava A. and Sivakumar Babu G. (2015) “System reliability analysis of granular filter for protection against piping in dams” J. International symposium on geohazards and geomechanics, 26 (2015), pp. 1-12.
99. Starov V.M. and Zhdanov V.G. (2001) “Effective viscosity and permeability of porous media” J. Colloids and Surfaces, Elsevier, pp. 363-375.
100. Tokoro T., Ishikawa T., Shirai S., and Nakamura T. (2016) "Estimation methods for thermal conductivity of sandy soil with electrical characteristics" J. Soil and foundation, The Japanese Geotechnical Society, 56(5), pp. 927-936.
101. Vogt W.P. and Johnson R.B. (2015) “Dictionary of Statistics and Methodology: A Nontechnical Guide for the Social Sciences 5th Edition” SAGE Publications, Inc; 5th edition, ISBN-10: 9781483381763, pp. 1-522.
102. Wang Q., Shi A., and Shah F. (2019) “18 - Rheology instruments for food quality evaluation” J. Evaluation Technologies for Food Quality, Woodhead Publishing Series in Food Science, Technology and Nutrition, pp. 465-490.
103. Wood D.M. (2004) “Geotechnical modelling”, Applied Geotechnics, CRC Press; 1st Edition, Volume 1, pp.181-308.
104. Xiao J., Ku C., Liu C., Fan C., and Yeih W. (2017) “On solving free surface problems in layered soil using the method of fundamental solutions” J. Engineering analysis with boundary elements, vol 83, pp. 96-106.
105. Yousefi S., Ghiassi R., Noorzad A., Ghaemian M., and Kharaghani S. (2013) "Application of temperature simulation for seepage inspection in earth-fill dams" J. Gradevinar, 65 (9), pp. 825-832

106. Zhu P.Y., Zhou Y., Thévenaz L., and Jiang G.L. (2008) "Seepage and settlement monitoring for each embankment dams using fully distributed sensing along optical fibers" 2008 International Conference on Optical Instruments and Technology: Optoelectronic Measurement Technology and Application, Vol 7160, pp. 1-7.
107. Zadeh Touri R.A., Pourbakhshian S., and Pouraminian M. (2015) "Experimental and numerical study of effect of PET recycling admixtures on pore water pressure and output discharge in homogeneous earth dam" J. of Civil Engineering and Urbanisation, Vol 5 (1), pp. 31-34.